2008

Cryopreservation of Adipose Derived Adult Stem Cells and Multidimensional Cell Sheets

Sreedhar Thirumala
Louisiana State University and Agricultural and Mechanical College

CRYOPRESERVATION OF ADIPOSE DERIVED ADULT STEM CELLS AND MULTIDIMENSIONAL STEM CELL SHEETS

A Dissertation

Submitted to the Graduate Faculty of the
Louisiana State University and
Agricultural and Mechanical College
In partial fulfillment of the
requirements for the degree of
Doctor of Philosophy
in
The Department of Mechanical Engineering

by
Sreedhar Thirumala
B.Tech, Jawaharlal Nehru Technological University, Jan 2000
M.S, Louisiana State University, May 2004
May, 2009

DEDICATION

TO MY PARENTS

ACKNOWLEDGEMENTS

It is a pleasure to thank the many people who made this dissertation possible. First and foremost, I would like to thank my advisor, Dr. Ram Devireddy, for lending his valuable time to teach and guide me, without whom this work would not have been possible. I would sincerely thank him for his technical insight and patience in motivating and nurturing me throughout this work.

Next, I would like to sincerely express my gratitude to Dr. Jeffrey Gimble for his invaluable guidance and support throughout my study at LSU. His gentle nature and moral support during my difficult times was more than what I needed and I am ever grateful to him. His depth of knowledge and ability to achieve perfection will always be my inspiration. My sincere thanks also go to my committee members, Dr. Charalampopoulos, Dr. Michael Murphy, and Dr. Todd Monroe who have been helpful and generous with their time and expertise to evaluate my dissertation. I would like to thank Dean's representative Dr. Robb Brumfield for being in my committee and for his suggestions during my proposal defense.

I would like to have this opportunity to thank Dr. Richard Rogers and Dr. Gerlinda Hermann for their guidance and support with ASCs calcium study. Thanks are also due to Dr. Proyag Datta for introducing me to a new horizon in bio-microfluidic research. I highly appreciate Dr. Sungook Park suggestions with cell sheet engineering study.

I also thank all my friends and colleagues in the Bioengineering Laboratory and Stem Cell Laboratory for providing me with an environment and support for my work. I extend my sincere gratitude to Dr. Xiying Wu, Sudheer, Brian Goh, Gang Yu, Dinesh and

Taehyun Park for their valuable suggestions and for the fruitful discussions we had during my course and research work. I am thankful to all my friends and well wishers, especially Rupesh, Sachin, Vamsi and Raghava for their support in terms of providing congenial surroundings and making my stay at LSU memorable and enjoyable. I wish to specially thank my friends Muniraju, Prashanth Nookala, Brahma, Keerthi and Deepika for helping me get through the difficult times, and for their support, amity and thoughts they provided which motivated towards my work. There are countless other people whose names and faces pass through my mind as I ruminate about this period at LSU. So, I would have to include all of them saying that it was really a pleasure knowing them and that aspect, as much as anything else, made this whole journey worthwhile.

Finally, and most importantly, I would like to thank my wife 'Sunitha' for her support, encouragement, quiet patience and unwavering love were undeniably the bedrock upon which the past several years of my life have been built. My final acknowledgement is due to my parents and family members back in India, who were always behind me with their prayers, love and blessings, encouraged me and provided tremendous support throughout my life. Without their help, I wouldn't have been here. I would like to dedicate this work to my beloved parents SaraswathammaThirumala and Sada Nandam Thirumala.

TABLE OF CONTENTS

LIST OF TABLES

LIST OF FIGURES

ABSTRACT

Human adipose tissue provides a uniquely abundant and accessible source of adult stem cells. In response to chemical, hormonal or structural stimuli, these human adipose-derived adult stem (ASCs) cells can differentiate along multiple lineage pathways, including adipocytes, chondrocytes, myocytes, neurons and osteoblasts. Successful cryopreservation of scientifically and commercially important ASCs would revolutionize the tissue engineering and regenerative medicine industry. In this research, we have investigated the water transport phenomenon during freezing of several passages of adipose derived adult stem cells and generated the membrane permeability parameters in the presence and absence of cryoprotective agents. These measured permeability parameters were then used to find the optimal cooling rates for freezing ASCs. We have also analyzed the individual and interaction effects of four important thermal parameters (cooling rate, hold time, thawing rate and end temperature) on the post-thaw viability of all passages (passage 0 to passage 4) of ASCs. We have then studied the effect of nanoparticles on the water transport response and apoptotic behavior of biological systems during a cryopreservation process. Further, we have investigated the maintenance of differentiation potential of post-freeze huASCs through histochemical staining. In an attempt to eliminate the usage of chemical CPAs (DMSO/glycerol) during cryopreservation, studies were conducted to investigate the possibility of using non toxic polymers, such as PVP, as cryoprotective agents. Flow cytometry analysis was employed to assess the post-thaw viability and apoptotic response of P1 ASCs frozen stored for more than two weeks in different concentrations of PVP. The results suggest that PVP in fact posses' cryoprotective properties

and produced reasonable good viability when compared to the most routinely used cryopreservation media involving DMSO and serum. In another study, cell sheet engineering approach has been applied to generate multi-dimensional cell sheets for tissue engineering using ASCs.

CHAPTER 1
INTRODUCTION AND REVIEW

1.1 CRYOBIOLOGY

Cryobiology is that branch of science, which deals with the effects of reduced temperatures on living organisms, their constituent parts, and their products. One important goal of the field of cryobiology is to preserve and store viable biological systems in the frozen state for extended periods of time in order to ensure reproducible results and continuity in research and biomedical processes. One such technique to preserve and genetically stabilize the biological systems is the “cryopreservation” process. Cryopreservation refers to the storage of a living organism at ultra- low-temperature in suspended animation for longer periods of time, such that it can be revived and restored to the same living state as before it was stored. Advances in cryopreservation technology have made it possible to develop new methods that allow low temperature maintenance of a variety of cell and tissue systems.

Cryopreservation techniques are developed for the preservation of various biological systems such as, microorganisms, isolated tissue cells, small multicellular organisms and even more complex organisms such as embryos. These techniques have been successfully applied to a variety of mammalian systems such as red blood cells, lymphocytes, platelets, granulocytes, gametes and embryos, hepatocytes, bone marrow stem cells, cornea and skin, pancreatic tissue, heart and kidney, etc. as reviewed by Mazur (1984) and McGrath (1975). Other viewpoints of applied cryobiology that are of significance include the preservation of human and non-human mammalian oocytes (Bernard and Fuller 1996), food freezing, tissue engineered equivalents (Oegema et al., 1999), human and animal stem cells (Richards et al.,

2004; Thirumala et al., 2005; Thirumala et al., 2005; Fleming and Hubel 2006), protozoa and parasites, insects, fish, microorganisms and plats, including algae (Walsh). Other applications include cryopreservation of rat and human liver slices (Day et al., 1999), fish gametes and aquatic species and spermatozoa from variety of species, including human sperm (Devireddy et al., 1998; Devireddy et al.,2002 Thirumala et al., 2006; Thirumala et al., 2007; Alapati et al., 2008). Successful cryopreservation of biological cells and tissues will impact a wide range of human endeavors, including assisted reproductive techniques, cancer recovery and rehabilitation procedures, organ storage and transplantation processes and conservation of endangered species.

1.2 CRYOPROTECTIVE AGENTS

In general, freezing storage requires the addition of a class of chemicals denoted as cryoprotective agents (CPAs) and their extensive use is based on the serendipitous observation by Polge and co-workers (Polge et al., 1949) that sperm cells were able to survive freezing in the presence of a chemical (glycerol) and did not survive the freezing process in its absence. There is considerable divergence across the classes of organic molecules that possess some CPA activity ranging from low molecular weight solutes like DMSO, glycerol, and sucrose (Fuller 2004; Lovelock, 1954) to high molecular weight polymers like PVP and hydroxyl ethyl starch (Fuller 2004; Connor and Ashwood-Smith 1973). There are several hypotheses that have attempted to explain the protective action of CPAs, but none of them are widely accepted and well established (Lovelock 1954; Karrow 1974; Conner and Ashwood-Smith 1973). On the other hand there is a significant amount of evidence suggesting that cryoprotective agents, albeit their benefits, can actually play a direct role in producing cryoinjury (Fahy 1986; Fuller 2004).

Detrimental effects of cryoprotectants are almost as relevant to cryobiology as are their cryoprotective effects (Fahy 1986).

Studies related to cryoprotectant action goes back to 1950s when Lovelock (1954) demonstrated that the hemolysis of red blood cells depends on the permeability of the neutral solutes and proposed partially permeable solutes offer only partial protection and high molecular weight solutes to which the cell is impermeable offers little or no protection. A more detailed attempt was made by Nash (1966) to explain the cryoprotectant action on a combination of parameters based on the property of forming strong and numerous hydrogen bonds, interaction with water molecules, and the volume occupied by a molecule of solute. If hydroxyl radicals are the most likely reactive oxygen species to be produced at low temperatures then oxygen free radical scavenging capacities of cryoprotectants (such as DMSO) will make a significant contribution to their colligative and osmotic properties (Benson and Bremner 2004). Anchordoguy et al., (1987) suggested additional modes of action of CPAs such as electrostatic interaction of CPAs (such as Glycerol, Trehalose and Sucrose) with polar head groups of phospholipids and the efficacy of CPAs depend on the strength of these interactions. Arakawa, Timasheff and colleagues have shown that the effect of solute on the stability of proteins derives from the balance between stabilizing and destabilizing effects of solute either by preferential binding or preferential exclusion from the protein surface (reviewed by Crowe et al., 1990). The disaccharide sugar, such as trehalose, has been shown preserving membrane structure and function by interacting with polar head groups of phospholipids at hypertonic exposures during freezing (Fuller 2004; Rudolph and Crowe 1985).

A systematic study on the use of polymers such as hydroxyl ethyl starch (HES) in erythrocyte freezing has been conducted my Sputtek and colleagues (Fuller 2004; Sputtek and Sputtek 2004). Conner and Ashwood-Smith (1973) proposed that the high molecular weight CPAs which are found to be most effective with red blood cell cryopreservation, in fact possess inadequate activity for nucleated cells when they used as only CPA. However they may make significant contribution to success of freezing when used in combination with other permeating CPAs such as DMSO, glycerol (Sputtek and Sputtek 2004). Farrant (1969) advocated that a polymer such as polyvinylepyrrolidone (PVP) may exhibit enhanced colligative properties at higher concentrations and may protect cells by lowering the external salt concentrations in a manner similar to low molecular cryoprotectants. Mazur (1960) proposed that polymeric CPAs avoid denaturing of the membranes by strong salt solutions at low temperatures either by preventing seeding of the supercooled water inside the cells or by coating the sensitive plasma membranes. In another study Williams (1983) suggested that the cryoprotective efficiency of polymers reside in their ability to alter the physical properties of solutions during freezing rather than in direct effects on cell membranes.

1.3 CRYOPRESERVATION OF BIOLOGICAL SYSTEMS

The freezing process involves complex phenomenon that, even after decades of research, are not fully understood. Ice tends to form at different rates during a freezing process. The generally accepted theory is based on Mazur's Law which states that the probability of an ice crystal to form at any temperature is a function of volume. The extracellular space is much larger than the intracellular space. For this reason ice tends to form first in the extracellular space and whereas intracellular solution becomes supercooled. Due to

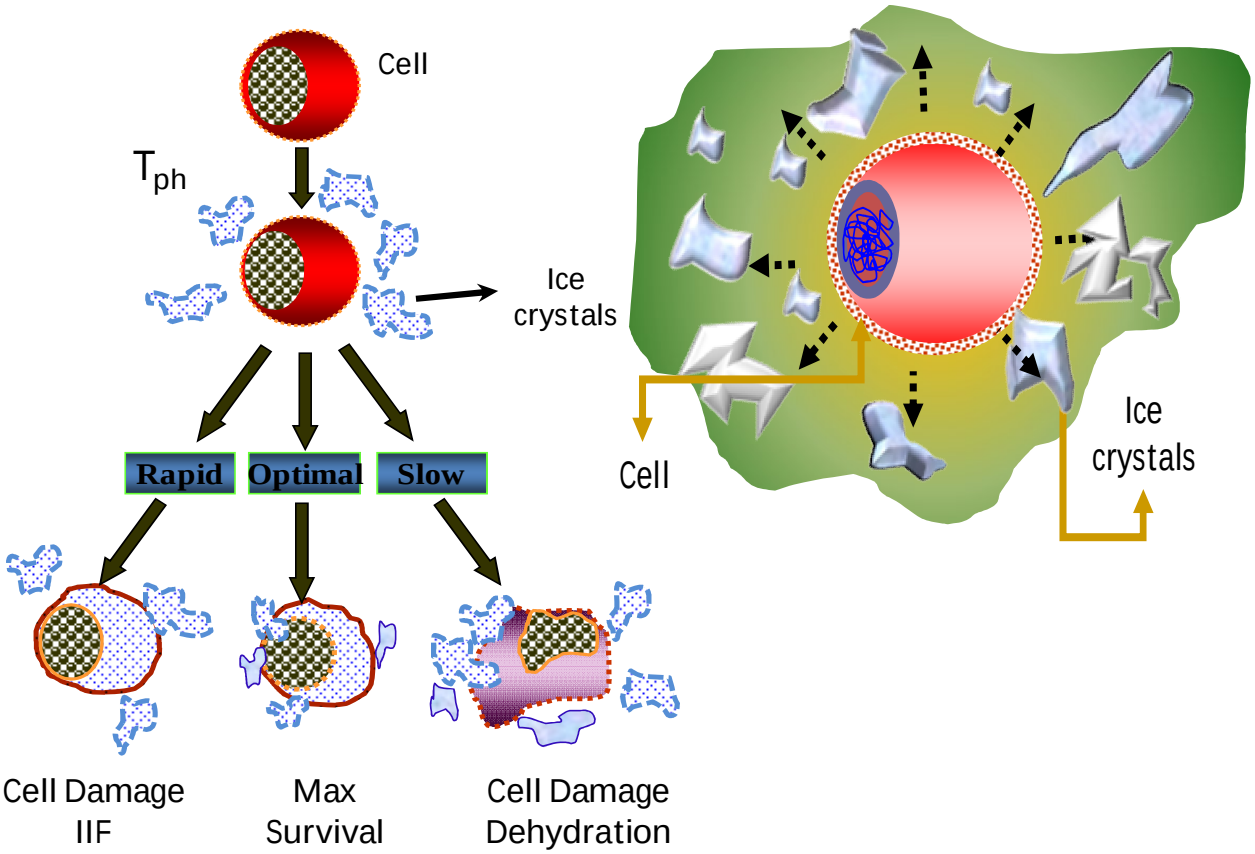

Figure 1.1: Biophysical response of single cells to freezing stress. The mass transport process (water loss) occurs due to the chemical potential difference between intracellular and extracellular regions.

the fact that the partially frozen extracellular solution has a lower chemical potential than the unfrozen super cooled intracellular solution, a chemical potential difference is established across the cell membrane (Mazur 1970). This results in a thermodynamically non-equilibrium state that provides a driving force for the two biophysical processes during freezing, cellular dehydration or the loss of intracellular water and the formation of intracellular ice (Mazur 1984) (see Fig 1.1). At low cooling rates cellular dehydration is the dominant mechanism while at very rapid cooling rates intracellular ice formation (IIF) is the dominant mechanism (Mazur 1963). Both cellular dehydration and IIF have been shown to be deleterious to the post-thaw

survival of biological systems (Lovelock 1953; Mazur et al., 1972). The rate of cooling has a dramatic effect on these two biophysical processes. If the cooling velocity is sufficiently slow, there will be sufficient time for the cell water to leave the cell and join the extracellular space. The result is the cell loses water rapidly by exmosis to concentrate the intracellular liquid sufficiently enough to eliminate super cooling and maintain chemical potential of intracellular water in equilibrium with that of extracellular water (Fig 1.1). The resulting changes in the extracellular region, such as changes in pH, changes in ionic concentration cause the tertiary structure of proteins to unfold, so that some of its original properties, especially its biological activity, are diminished or eliminated. This denaturation of cell proteins may be lethal to cell survival (Lovelock 1953). In addition, mechanical interaction between extracellular ice crystals and cells can also lead to the deformation of cells and rupture of cell membranes (Ishiguro and Rubinsky 1994; Ishiguro and Rubinsky 1994). On the other hand if the cell is cooled too rapidly it is not able to lose water fast enough to reach equilibrium; it becomes increasingly super cooled and eventually attains equilibrium by freezing intracellularly.

Intracellular ice formation (IIF) is generally lethal as it causes injury to cellular membranes and intracellular structures. So, cooling rates which are either “too slow” or “too fast” can and do reduce the post thaw survival of the cells, therefore, a cooling rate for maximum cell cryosurvival should and does exist between the "high" and "low" rates (McGrath 1988). This has been confirmed experimentally for a variety of cells and the curve of cell survival plotted as a function of the cooling rate, has a characteristic U-shape as shown in Fig 1.2 (Mazur et al., 1972). Permeability of the membrane shows how fast the water can leave the cell at a given cooling rate. More the permeability of the membrane, more the water transport

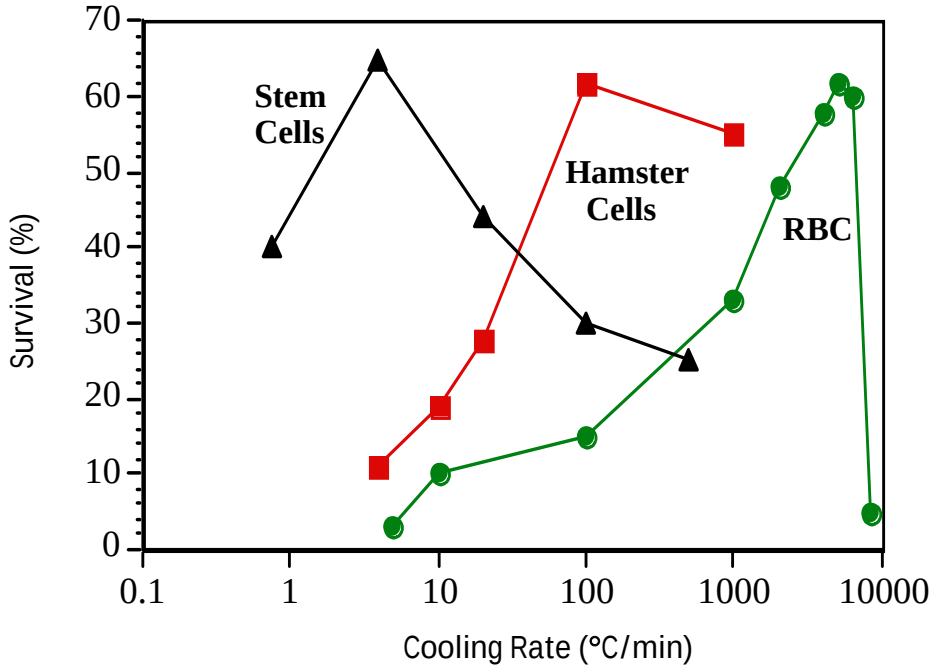

Figure 1.2: Relation (inverted "U" shape) between percentage of survival and cooling rate in three types of cells. Stem cells refer to mouse bone marrow stem cells, and hamster cells refer to hamster oocytes. RBC refers to human red blood cells.

across the cell membrane in a given time and vice versa. Therefore, whether a prescribed cooling rate is too ‘‘slow ’’or too ‘‘fast,’’ is a function of cell membrane permeability to water and the probability that any water remaining trapped within the cell at a given subzero temperature will nucleate and turn to ice. The difference in membrane permeability to water and probability of IIF results in different optimal cooling rates for different cells. Therefore, to find out the optimal cooling rate for maximum cell survival and to optimize a cryopreservation protocol, it is important to measure the cell membrane’s permeability to water. Clearly, the quantitative understanding of the water transport across the cell membrane during a cryopreservation is critical for the success of the respective protocol.

Water transport during freezing has been extensively studied by using various methods. One such method is measurement of water transport in single spherical cells by using cryomicroscopy technique (Diller and Cravalho 1970; McGrath 1988). Cryomicroscopy involves the application of cryogenic temperatures to cellular systems mounted under a light microscope to study the biophysical response of cells to freezing. The quantitative measurement of water transport during freezing of a tissue system were efficiently performed by using directional solidification device and two-step freezing technique (Pazhayannur and Bischof 1997). A shape independent Differential Scanning Calorimeter (DSC) technique has recently been applied to measure the membrane permeability parameters in both cell and tissue systems (Devireddy et al., 1998, Thirumala et al., 2006, Thirumala et al., 2007).

1.4 ADIPOSE DERIVED ADULT STEM CELLS (ASC)

Stem cells are essentially building blocks of multicellular organisms and provide a wonderful tool for the study of cellular and developmental processes. Harnessing the potential of stem cells to differentiate into multi-lineage pathways and produce more specialized cells of the body would provide a tool to study the early human embryonic development and also to develop novel strategies of organ regeneration and transplantation (Thomson and Odorico 2000). The stem cell research field has been transformed in the past few years by successes achieved in culturing early human embryonic stem cells (Thomson et al., 1998), human embryonic germ cells (Michael et al., 1998) and in manipulating their differentiation *in vitro*. More recently, excitement has been fuelled by the evidence that adult stem cells have a much higher degree of developmental potential and are more plastic, versatile and capable of transferring into many different types of cells than previously imagined. Though embryonic

stem cell potential is enormous, the legal and ethical issues associated with embryonic stem cells and their tendency to form multi-lineage tumors called teratomas after injection into animal models (Wakitani et al., 2003; Brickman and Thomas 2002) forced the scientists to focus more onto adult derived stem cells.

Of the many different types of adult stem cells, the most widely known and best studied are the bone marrow stem cells. Besides hematopoietic stem cells that produce red blood cells, a cell type termed mesenchymal also exists in marrow. These bone marrow derived mesenchymal stem cells have been successfully differentiated into various cell lineages including neuronal cells (Woodbury et al., 2000; Sanchez-Ramos et al., 2000), as well as cartilage, bone, tendon, muscle, and fat lineages (Pittenger et al., 1999). Two groups showed that neuronal stem cells can differentiate and produce not only neuronal cells but also other tissues, including blood and muscle (Bjornson 1999; Clarke et al., 2000; Galli et al., 2000), whereas others showed that mesenchymal stem cells transplanted into mice can differentiate into astrocytes, neurons, and oligodendrocytes (Kopen et al., 1999; Vogel 2000). Also, evidence now exists that liver stem cells can be converted, in vitro, into insulin-secreting pancreatic cells (Horb et al., 2003; Yang et al., 2002). Until recently the major source of the adult stem cells was the bone marrow. But extracting bone marrow is a very invasive and painful procedure. Also use of stem cells from bone marrow is limited because bone marrow yields a very small quantity of stem cells.

New research has demonstrated that adult stem cells similar to the mesenchymal stem cells are plentiful in human fat, specifically fat obtained via liposuction (Halvorsen et al., 2001; Sen et al., 2001; Zuk et al., 2002; Gimble and Guilak 2003). Termed Adipose Derived Adult Stem

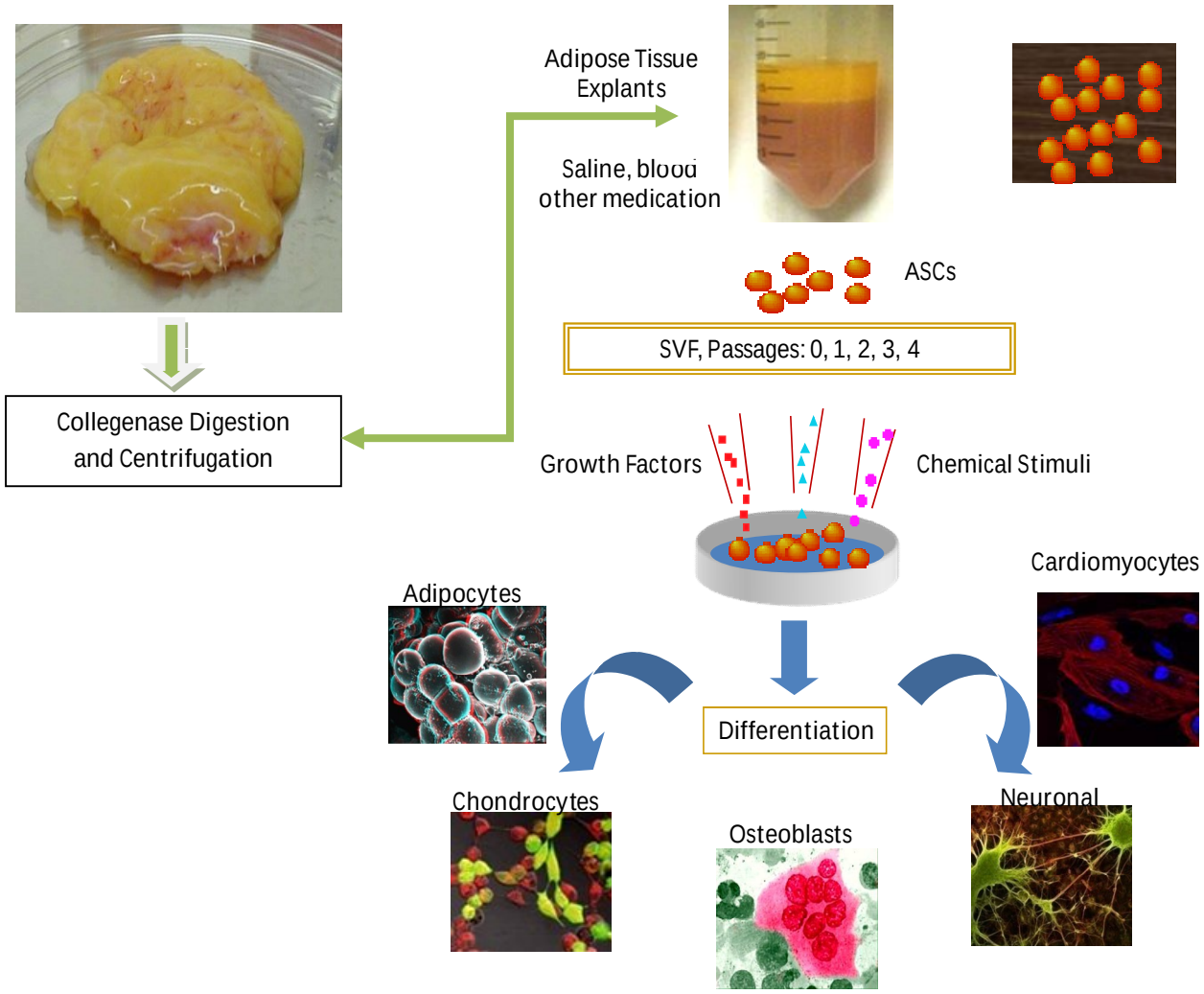

Figure 1.3: Processing and differentiation ability of adipose derived adults stem cells (ASCs). The fat tissue (adipose tissue) obtained through liposuction is used as a source for ASCs. Collagenase digestion and differential centrifugation of adipose tissue results in the formation of two distinct fractions: the floating mature fat cells, and the sedimented stromal vascular cells. The stromal vascular fraction is the source of ASCs and also contains fibroblasts, endothelial cells, and a high proportion of blood cells.

(ASCs) cells, these progenitor cells exhibit multi-lineage potential and differentiate in vitro toward fat (18), cartilage (Zuk et al., 2001), muscle (Mizuno et al., 2001; Awad et al., 2004; Wickham et al., 2003), bone (Halvorsen et al., 2001; Gimble and Nuttall 2004) and nerve cells (Safford et al., 2002; Ashjian et al., 2003; Safford et al., 2004). A Recent study by Gimble and his

colleagues (2004) showed that the ASCs cells are capable to form osteoid in vivo once implanted subcutaneously into mice. In another study, successful use of fat-derived stem cells to treat a damaged region in a skull was reported (Lendeckel et al., 2004).

Using potential benefits of ASCs cells to develop future tissue engineering strategies and cell-based therapies requires efficient cryopreservation of these cells for longer periods of time without losing their multipotentiality. Studying the cryobiological properties of ASCs cells would enhance our understanding of freezing response of these cells which will further help to design and develop methods to freeze complex tissues, intact organs and possibly entire multicellular organisms.

Bone marrow has been successfully cryopreserved since 1955 (Barnes and Loutit 1955). Cryopreservation of peripheral blood stem cells was first reported in 1975 when Dr. Epstein and his graduate student successfully isolated the blood stem cells, cryopreserved and then later used for transplantation (Debelak-Fehir and Epstein 1975; Debelak-Fehir et al., 1975). Subsequently, a simplified freezing technique called 'statistically controlled freezing' was developed for cryopreservation of canine hematopoietic cells (English et al., 1979) which was later developed and implemented by several investigators to preserve bone marrow cells (Stiff et al., 1987) and peripheral blood derived stem cells (Jackson et al., 1992). Slow-rate cooling methods using dimethylsulfoxide (DMSO) as a cryoprotectant were effective for a wide variety of cell lines, including mouse embryonic stem cell lines (Robertson 1987) and Porcine Primordial Germ Cells (Shim et al., 1997). Vitrification procedure was effectively used to preserve human embryonic stem cells (Reubinoff 2001) and primate embryonic stem cells (Fujioka 2004). In a recent study, to eliminate the toxic characteristics of high concentrations of DMSO for

treatment of stem cells for clinical use, an optimal cryopreservation method was developed for the cryopreservation of hematopoietic progenitor stem cells using low concentrations of trehalose (Buchanan 2004). A recent study also reports that apoptosis in murine neural precursor cells post-freeze can be limited by the addition of caspase inhibitor zVAD-fmk (Milosevic et al., 2005). Despite recent progress in ASCs research the possibility of cryopreservation of adipose stem cells to clinical standards has not been explored. The successful cryopreservation of scientifically and commercially important ASCs using relatively simple methods would revolutionize the tissue engineering and regenerative medicine industry. Therefore, this research essentially aims to rectify this lack of cryobiological knowledge in adipose stem cells (ASCs).

1.5 CELL SHEET ENGINEERING

Organ transplantation has been restricted by two major obstacles; first, a critical shortage of donors and second, the high risk of graft rejection. To overcome these major limitations, Professor Langer, a chemical engineer, and Drs. Joseph and Charles Vacanti, two medical doctors, proposed the concept of tissue engineering (Langer and Vacanti 2003; Vacanti and Vacanti 2000). Traditional tissue engineering methods have generally focused on one of two strategies: either the injection of isolated cell suspensions or the use of biodegradable scaffolds to support tissue generation. There has been considerable progress in developing cellularized scaffolds to regenerate various tissues including bone, cartilage, blood vessel, nerve, liver, myocardium and many other tissues (Sittinger et al., 1996; Sikavitsas et al., 2002). However, most of the conventional scaffolds do not allow sufficient cell migration to establish adequate cell–extracellular matrix (ECM) and cell–cell interaction. Cell seeding plays a

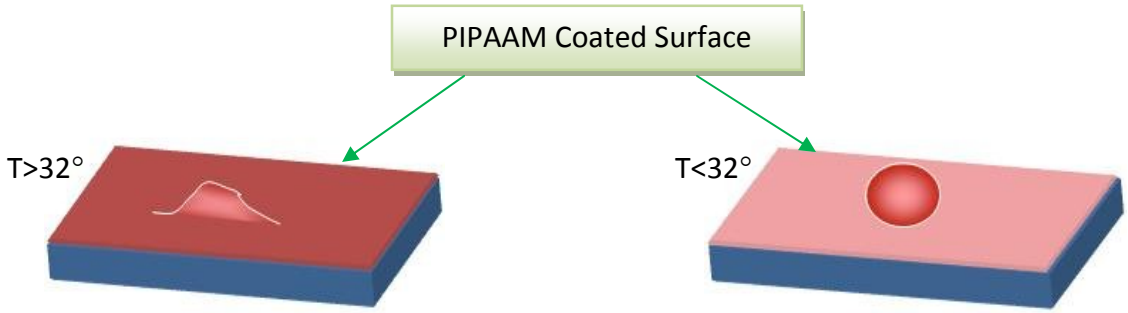

A: Temperature dependent wettability changes of PIPAAM coated surface

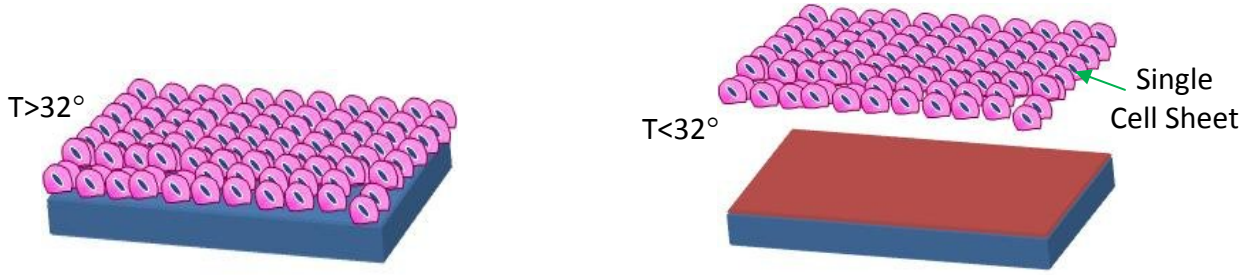

B: Cell sheet recovery from PIPAAM coated surface by reducing the temperature below 32 °C.

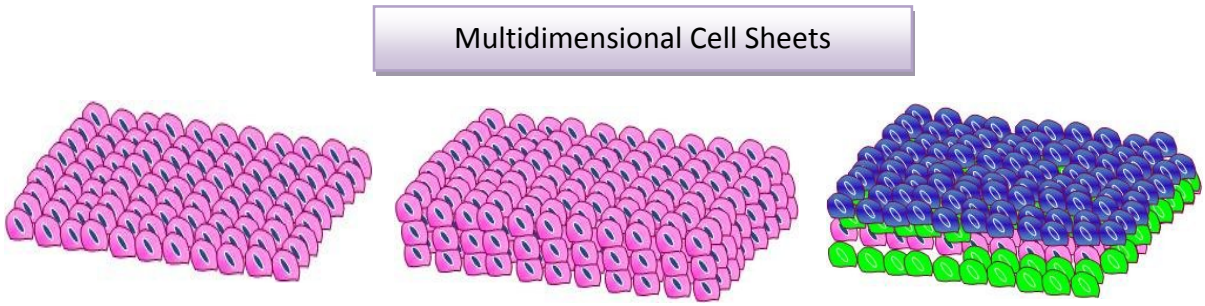

C: Single and multidimensional cell sheets using homogeneous or heterogeneous cell sheets

Figure 1.4: Concept of cell sheet engineering proposed by Okano and his colleagues. A thermoresponsive polymer PIPAAm is covalently grafted to TCPS dish and a sheet of cells was subsequently generated by simply reducing the culture temperature below 32 °C.

crucial role in determining the progression of tissue formation to establish 3D cell culture. High density cell seeding in static and dynamic cultures inside bioreactors are methods to improve cell seeding in scaffolds (Sistino 2003; Martin et al., 2004). Since the cells located in the interior of the scaffold rely on diffusion for solute transport, the current methods of seeding are compromised by the depletion of nutrients.

To overcome some of the drawbacks associated with traditional scaffold based tissue engineering, cell sheet engineering has been developed as an alternative approach for tissue engineering (Yamada et al., 1990; Okano et al., 1993; Matsuda et al., 2007; Yanga et al., 2007, Nagase et al., 2009). Cell sheet engineering has the advantage of eliminating the use of biodegradable scaffolds (see Fig 1.4). Using temperature-responsive poly (N-isopropylacrylamide) (PIPAAm) coated TCPS dishes, cultured cells were successfully harvested as intact sheets by simple temperature changes, thereby avoiding the use of proteolytic enzymes (Yamada et al., 1990; Okano et al.,., 1993; Matsuda et al., 2007; Yanga et al., 2007, Nagase et al., 2009).

PIPAAm shows remarkable changes in aqueous swelling with changes of temperature and shows full-hydrated and extended conformation at low temperature. Over 32 ^{o}C, however, PIPAAm extensively dehydrates and changes to compact chain conformations. When PIPAAm is grafted on the surface of a cell culture substrate, the modified surface will be hydrophobic in nature at temperatures higher than 32 ^{o}C, but becomes hydrophilic as the temperature falls (Fig 1.4). Cells can attach and grow more easily on hydrophobic surfaces than on hydrophilic surfaces. Cell attachment and adherence are prevented by the difficulty of displacing adsorbed water molecules on highly hydrated hydrophilic surfaces allowing for their spontaneous detachment without the need of trypsinization (Yamada et al., 1990; Okano et al., 1993; Matsuda et al., 2007; Yanga et al., 2007, Nagase et al., 2009). By avoiding proteolytic treatment, critical cell surface proteins such as ion channels, growth factor receptors and cell-to-cell junction proteins remain intact, and cells can be noninvasively harvested as intact sheets along with their deposited extracellular matrix (ECM) (Okano et al., 1993; Matsuda et al., 2007; Yanga

et al., 2007, Nagase et al., 2009). As ECM remains present on the basal surface of the cell sheets, they can be directly transplanted to tissue beds or even layered to create three-dimensional (3-D) tissue-like structures (Fig 1.4). This approach therefore apparently provides several advantages over traditional tissue reconstruction with biodegradable scaffolds. With the use of single cell suspensions, there is often a significant loss of cells, with only a small percentage of cells remaining at the site of interest. In addition, in cases of damaged tissues, injected cells are often unable to attach at sites where the host architecture is destroyed. In contrast, cell sheets via their deposited ECM, can be attached to host tissues and even wound sites, with minimal cell loss. However, the grafting process used to coat PIPAAm onto TCPS dishes was relatively complicated and time consuming involving complex irradiation procedures.

In a more recent study, a novel method, using a thermoresponsive hydrogel coated on TCPS dishes, was developed for harvesting living cell sheets (Chen et al., 2006). The hydrogel system was prepared by coating aqueous methylcellulose mixed with distinct salts on TCPS dishes at room temperature and subsequently gelled at 37 ˚C for cell culture. Methyl Cellulose (MC) with a viscosity of 4000cP at 2% solution was used to form gels at physiologically relevant temperatures (Chen et al., 2006). However, the procedure described was unreliable and cumbersome as MC was too viscous to be manipulated easily. In addition, the procedure described results in a non-uniform coating and is not practicable in a standard cell culture facility. Further, the MC systems generated were not consistently stable as the time of culture is increased. Therefore, this research aims to modify and characterize the MC hydrogel system

developed by Chen and his colleagues for off-the-shelf supply of stable thermo-responsive TCPS dishes for ASCs tissue engineering applications.

1.6 OUTLINE OF DISSERTATION

Research is divided into 5 independent chapters. Each chapter focuses on an important aspect of this project. Information regarding the published citation of each chapter is listed below. Two published journal papers were used to prepare chapter 2. All chapters were either published in peer reviewed journals or are currently under review.

- CHAPTER 2: S. Thirumala, J.M. Gimble and R.V. Devireddy. Transport Phenomena During Freezing of Adipose Tissue Derived Adult Stem Cells. Biotechnology & Bioengineering, 92: 372-383 (2005)

  R. V. Devireddy, S. Thirumala and J.M. Gimble. Cellular Response of Adipose Derived Passage-4 Adult Stem Cells to Freezing Stress. ASME Journal of Biomechanical Engineering, 127: 1081-1086 (2005).

- CHAPTER 3: S. Thirumala, S. Zvonic, E. Floyd, J.M. Gimble and R.V. Devireddy. The Effect of Various Freezing Parameters on the Immediate Post-Thaw Membrane Integrity of Adipose Tissue Derived Adult Stem Cells. Biotechnology Progress, 21: 1511-1524 (2005).

- CHAPTER 4: S. Thirumala, J.M Forman, W.T. Monroe and R.V. Devireddy. Freezing and Post-Thaw Apoptotic Behavior of Cells in The Presence of Palmitoyl Nanogold Particles. Nanotechnology. 18: 195104 (2007).

- CHAPTER 5: S. Thirumala, J.M. Gimble and R.V. Devireddy. Evaluation of Polyvinylpyrollidone (PVP) as a Cryoprotectant for Adipose Derived Adult Stem Cells (ASCs). Tissue Engineering.

- CHAPTER 6: S. Thirumala, J.M. Gimble and R.V. Devireddy. Characterization of a Thermally Reversible Methylcellulose Hydrogel System for Adult Stem Cell Sheets. Biomaterials.

Apart from these five chapters, Chapter 1 gives introduction to the research and review of the literature.

CHAPTER 2
TRANSPORT PHENOMENA DURING FREEZING OF ADIPOSE TISSUE DERIVED ADULT STEM CELLS (ASCs)[1]

2.1 INTRODUCTION

Rational design and optimization of a cryopreservation process requires a quantitative understanding of the two biophysical responses in the target cell or tissue during freezing, namely water transport and intracellular ice formation (IIF). Water transport during freezing in cell suspensions has been extensively studied using cryomicroscopy (Devireddy et al., 1998; Diller 2005) and calorimetric (Devireddy et al., 1998) techniques. Differences in membrane permeability to water and the probability of IIF result in different "optimal" cooling rates for different cells (Mazur et al., 1972). Therefore, to optimize a cryopreservation protocol it is important to measure the cell membrane's permeability to water. This project set out to establish the water transport (and consequently the membrane permeability parameters) of stromal vascular fraction (SVF) cells, passage (P0), passage 2 (P2) and passage 4 (P4) ASCs during freezing using a calorimetric technique at a cooling rate of 20 ˚C/min in three different media: culture medium without cryoprotectants; culture medium with 10% glycerol; and culture medium with 10% DMSO. The adipose derived cells were modeled as spheres of 50μm diameter with an osmotically inactive volume (V_b) of $0.6V_o$, where V_o is the isotonic cell volume. By fitting a model of water transport to the experimentally obtained volumetric shrinkage data, the "best-fit" membrane permeability parameters (reference membrane permeability to water,

1 This chapter was published in the following citations. 1] S. Thirumala, J.M. Gimble and R.V. Devireddy. This chapter was published in the following citations: Transport Phenomena During Freezing of Adipose Tissue Derived Adult Stem Cells. Biotechnology & Bioengineering, 92: 372-383 (2005). 2] R.V. Devireddy, S. Thirumala and J.M. Gimble. Cellular Response of Adipose Derived Passage-4 Adult Stem Cells to Freezing Stress. ASME Journal of Biomechanical Engineering, 127: 1081-1086 (2005).

L_{pg} or $L_{pg}[cpa]$ and the activation energy, E_{Lp} or $E_{Lp}[cpa]$) were determined. The experimentally determined ASC membrane permeability parameters are used to numerically predict the loss of intracellular water under a variety of cooling rates (5–100 ˚C/min). The numerical predictions are analyzed to predict the amount of water left in the ASCs upon the cessation of water transport, in the absence of IIF and to determine the ‘‘optimal cooling rates’’ for freezing adipose derived cells.

2.2 MATERIALS AND METHODS

2.2.1: Isolation, Collection and Culture of ASCs

All the human protocols were reviewed and approved by the Pennington Biomedical Research Center Institutional Review Board. Subcutaneous adipose tissue liposuction aspirates were provided by plastic surgeons in Baton Rouge, LA. All procedures were conducted under aseptic conditions according to a modification of methods outlined in Halvorsen et al., (2001) and Sen et al., (2001). Tissue samples (100 to 200 ml) were washed 3-4 times in phosphate buffered saline (PBS) prewarmed to 37 ˚C, suspended in PBS supplemented with 1% bovine serum albumin and 0.1% collagenase (Type I, Worthington Biochemicals, Lakewood, NJ), and digested with gentle rocking for 45-60 min at 37 ˚C. The digests were centrifuged for 5 min at 1200 rpm (300Xg) at room temperature, resuspended, and the centrifugation step repeated. The supernatant was aspirated and the pellet re-suspended in culture medium (DMEM high glucose, 10% fetal bovine serum, 100 units penicillin/ml, 100 mcg streptomycin/ml, and 25mcg amphotericin/ml). The resulting pellet was defined as the stromal vascular fraction (SVF).

The cell suspension was plated at a density equivalent to 0.156 ml of liposuction tissue per sq cm of surface area, using a 35 ml volume of culture medium per T225 flask. Cells were

cultured for 48 hrs in a 5% CO_2, humidified, 37 ˚C incubator. At that time, the adherent cells were rinsed once with pre-warmed PBS and the cells fed with fresh culture medium. The cells were fed with fresh culture medium every 2-3 days until they reached approximately 75-80% confluence. At this time, the medium was aspirated, the cells were rinsed with prewarmed PBS, and harvested by digestion with 0.05% trypsin solution (5-8 ml per T225 flask) for 3 to 5 min at 37 ˚C. The cells were suspended in culture medium, centrifuged for 5 min at 1200 rpm (300 X g), the pellet resuspended in a volume of 10 ml of culture medium, and the cell count determined by trypan blue exclusion. These cells were identified as Passage 0 (P0). An aliquot of cells was reserved for cryopreservation studies. The remaining cells were seeded in T225 flasks at a density of 5 X 10^3 cells per sq cm. The cells were maintained in culture and passaged as described through successive Passages 0 to 4 (P0, P1, P2, P3 and P4). In this study stromal vascular fraction (SVF), P0, P2 and P4 ASCs were used to evaluate the membrane permeability parameters and consequently optimal cooling rates for freezing ASCs.

2.2.2: Differential Scanning Calorimeter (DSC) Experiments

DSC experiments were carried out both in the absence and presence of CPAs on adipose derived cells. For both SVF and ASCs (P0, P2 and P4), six separate DSC experiments were conducted in the absence of any CPAs and in the presence of two permeating CPAs, glycerol (10%, v/v), and dimethylsulfoxide (DMSO; 10%, v/v)[2]. The ASCs were equilibrated in the freezing media for ~10 minutes before the freezing experiments were performed. A simple

[2]Although, both the choice of the chemicals and their concentration is rather arbitrary, it is important to note that both chemicals are routinely used in cryobiology in the selected concentration and in the interest of commonality and universality we chose to use a similar combination of these chemicals in the present study, as well.

analysis of the coupled CPA and water transport out of the ASCs using the model of Kedem and Katchalsky (1958) showed that the equilibration time or time required for the CPA to permeate into the ASC is ~2 to 5 minutes. Thus, it is presumed that the CPA has permeated into the ASCs before the freezing process. In addition, a two step addition of CPAs was performed, to ensure the volumetric excursions (shrink-swell) response (and the associated osmotic injury) of the cells were minimized (Devireddy et al. 1999; Devireddy et al., 2000). Approximately 10 μL of the ASC suspension was loaded in the DSC standard aluminum sample pan (Perkin Elmer Corporation, Norwalk, CT, USA) with ~0.5mg of Pseudomonas syringe (ATCC, Rockville, MD, USA), a naturally occurring ice nucleating agent.

The DSC dynamic cooling protocol used to measure the water transport out of the ASC suspensions was the same as that reported in earlier studies on other cell systems (Devireddy et al., 1998; Devireddy et al., 2000; Diller, 2005; Thirumala et al., 2003; Yuan and Diller, 2001; Thirumala et al., 2005) and will only be briefly stated here. In the DSC technique, heat releases from the same cell suspension are measured: (i) during freezing of osmotically active (live) cells in media and; (ii) during freezing of osmotically inactive (dead) cells in media. The difference in heat release measured between the two cooling runs was correlated to water transport and was denoted as Δq_{dsc} (See Fig 2.1). This has been demonstrated in a variety of cellular systems (Devireddy and Bischof, 2003; Thirumala et al., 2003) and independently verified by Yuan and Diller (2001) and Diller (2005). Should the cells be osmotically inactive or lysed prior to the start of the experiment, the DSC cooling protocol will measure no difference in heat release, as describe in earlier studies (Devireddy et al., 1998; Devireddy et al., 2002; Thirumala et al., 2003,

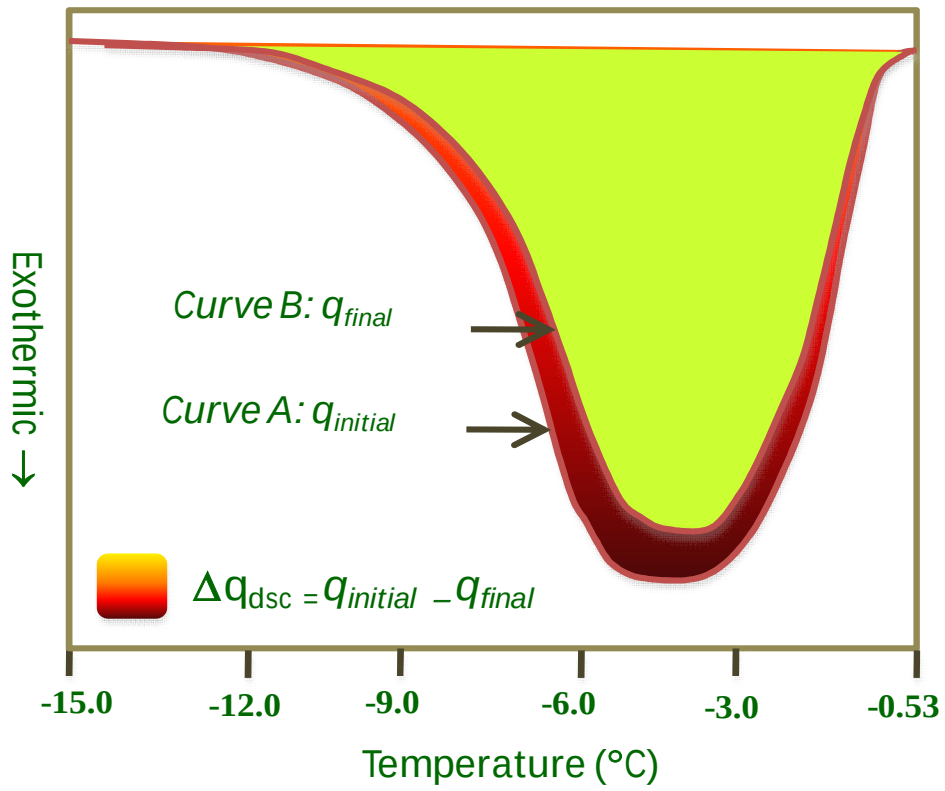

Figure 2.1: Superimposed heat flow thermograms during freezing of osmotically active (Curve A) and inactive cells (Curve B). The heat flow thermogram is integrated to calculate the total heat released during freezing of osmotically active cells and inactive cells. Heat flow (mW/mg) is plotted along the y-axis and subzero temperatures (°C) are plotted along x-axis

He et al., 2004; Thirumala et al., 2005; Thirumala and Devireddy 2005; Devireddy et al., 2005; Li et al., 2006; Thirumala et al., 2006; Thirumala et al., 2007; Alapati et al., 2008).

2.2.3: Translation of DSC Heat Release Data to Water Transport Data

The heat release measurements of interest were Δq_{dsc} and $\Delta q(T)_{dsc}$ which are the total and fractional difference between the heat releases measured by integration of the heat flows during freezing of osmotically active (live) cells in media, $q_{initial}$ and during freezing of osmotically inactive (dead) cells in media, q_{final} (i.e. $\Delta q_{dsc} = q_{initial} - q_{final}$; $\Delta q(T)_{dsc} = q(T)_{initial} - q(T)_{final}$).

As defined in a series of earlier studies by Devireddy and colleagues, this difference in heat release has been shown to be related to cell volume changes in several biological systems (Devireddy et al., 1998; Devireddy et al., 2002; Thirumala et al., 2003, He et al., 2004; Thirumala et al., 2005; Thirumala and Devireddy 2005; Devireddy et al., 2005; Li et al., 2006; Thirumala et al., 2006; Thirumala et al., 2007; Alapati et al., 2008) as:

$$V(T) = V_i - \frac{\Delta q(T)_{dsc}}{\Delta q_{dsc}} \cdot (V_i - V_e) \quad (1)$$

The unknowns needed in Eqn. (1) apart from the DSC heat release readings are V_i (the initial cell volume) and V_e (the end or the final cell volume). The initial volumes (V_i) of the adipose derived (SVF, P0, P2 and P4) cells in the medium with no CPAs was assumed to be the initial isotonic cell volume, V_o. Similarly, the end volume in the medium with no CPAs was assumed to be the osmotically inactive cell volume, V_b (=0.6V_i). To ensure the accuracy and repeatability of the experimental data, a set of calibration and control experiments were performed as detailed previously for a DSC-7 (Perkin Elmer Corporation, Norwalk, CT) machine (Devireddy et al., 1998).

2.2.4: Water Transport Model and Numerical Methods

Once the volumetric shrinkage data has been determined from the calorimetric experiments, a well established model of water transport was used to determine the membrane permeability parameters. This model of water and CPA transport in response to chemical potential gradients was developed by Kedem and Katchalsky (1958) and is based on irreversible thermodynamics. If the flux of CPA is negligible in comparison to the water flux, then the Kedem-Katchalsky model reduces to a model of water transport alone as proposed by

Mazur (1963) and later modified by Levin et al. (1976). The water transport model of Mazur represents the volumetric shrinkage response of cells during freezing in the presence of CPAs as,

$$\frac{dV}{dT} = -\frac{L_p A_c RT}{B v_w}\left[ln\frac{(V_o - V_b - n_{cpa}v_{cpa})/v_w}{(V_o - V_b - n_{cpa}v_{cpa})/v_w + (\varphi_s n_s + n_{cpa})} - \frac{\Delta H_f v_w \rho}{R}\left(\frac{1}{T_R} - \frac{1}{T}\right)\right] \quad (2)$$

with L_p, the ASC membrane permeability to water defined by Levin et al. (1976) as,

$$L_p = L_{pg}[cpa]\ exp\left(-\frac{E_{Lp}[cpa]}{R}\left(\frac{1}{T} - \frac{1}{T_R}\right)\right) \quad (3)$$

where, $L_{pg}[cpa]$ is the reference membrane permeability at a reference temperature, T_R (= 273.15 K); $E_{Lp}[cpa]$ is the apparent activation energy (kJ/mol) or the temperature dependence of the cell membrane permeability; V is the ASC volume at temperature, T(K); A_c is the effective membrane surface area for water transport, assumed to be constant during the freezing process; V_o and V_b are the isotonic (initial) and osmotically inactive ASC volumes, respectively; As stated earlier all the adipose derived cells were modeled as a spheres of radius (r_o) of 25µm; R is the universal gas constant; B is the constant cooling rate (K/min); n_{cpa} is the number of moles of salt; v_{cpa} is the molar volume of CPA; v_w is the molar volume of water; ⍰S is the disassociation constant for salt; n_s is the number of osmoles of salt (=C_i•(V_o - V_b), where C_i is the initial cell osmolality); ΔH_f is the latent heat of fusion of water; ⍰⍰ is the density of water. Note that when n_{cpa} is zero (i.e. no CPA is present), Eqns. (2) and (3) reduce to a model of water transport only and L_p is an Arrhenius function of L_{pg} and E_{Lp}. The two unknown membrane permeability parameters of the model either $L_{pg}[cpa]$ and $E_{Lp}[cpa]$ in the presence of CPA or L_{pg}

and E_{Lp} in the absence of CPA, are determined by curve-fitting the water transport model to experimentally obtained volumetric shrinkage data during freezing. The various assumptions made in the development of Mazur's model of water transport are discussed in detail elsewhere (Levin et al., 1976; Mazur et al., 1963; McGrath et al., 1988; Smith et al., 1998; Toner, 1993) and are beyond the scope of this paper.

2.2.5: Numerical Methods

A nonlinear least squares curve fitting technique was implemented using a computer program to calculate the membrane permeability parameters that best fit the volumetric shrinkage data as previously described by Bevington and Robinson (1992). The optimal fit of Eqn. (2) to the experimental data was obtained by selecting a set of parameters which minimized the residual variance, χ^2, and maximized a goodness of fit parameter, R^2 (Montgomery and Runger, 1994). All the curve fitting results presented have an R^2 value greater than or equal to 0.99 indicating that there was a good agreement between the experimental data points and the fit calculated using the estimated membrane permeability parameters. To simulate the biophysical response of a ASC under a variety of cooling rates, the best fit parameters were substituted in the water transport equation which was then numerically solved using a 4th order Runge-Kutta method using a custom written FORTRAN code on a Mac Powerbook G4 (Apple Computer Inc, Cupertino, CA) workstation.

2.3 RESULTS AND DISCUSSION

2.3.1: Dynamic Cooling Response and Membrane Permeability Parameters

Fig. 2.2 shows the water transport data and simulation for SVF cells using the best fit parameters in Eqn. (2) at a cooling rate of 20 ˚C/min in culture medium with no CPAs (Fig. 2.2A),

in culture medium with 10% glycerol (Fig. 2.2B) and in culture medium with 10% DMSO (Fig. 2.2C). The dynamic portion of the cooling curve (region where the initial and final heat release thermograms are distinct and separate) is found to be between -0.6 ˚C to -14˚C in medium with no CPAs, between -3.1 and -30 ˚C in medium with 10% glycerol and between -3.2 and -30 ˚C in medium with 10% DMSO for SVF cells. The SVF cell membrane permeability parameter values that best fit the 20 ˚C/min water transport data in the absence and presence of CPAs are shown in Table 2.1 and Table 2.2. The model simulated equilibrium cooling response (equilibrium is achieved at each temperature when the internal and external osmotic pressures are equal) is also shown as reference as dotted line (------). The equilibrium cooling response represents the volumetric shrinkage response of an ASC cooled infinitely slowly and is significantly different (greater than 99% confidence level using the student's t-test) from the dynamic water transport data obtained at 20 ˚C/min.

Fig. 2.3 shows the water transport data and simulation for P0 ASCs using the best fit parameters in Eqn. (2) at a cooling rate of 20 ˚C/min with no CPAs (Fig. 2.3A), with 10% glycerol (Fig. 2.3B) and with 10% DMSO (Fig. 2.3C). Similar data is shown for P2 ASCs in Fig. 2.4 for cells cooled with no CPA (Fig. 2.4A), with glycerol (Fig 2.4B) and with 10%DMSO (Fig 2.4C). For both P0 and P2 ASCs, the dynamic portion of the cooling curve is found to be between -0.6 ˚C to -10˚C in medium with no CPAs, between -3.1 and -30 ˚C in medium with 10% glycerol and between -3.2 and -30 ˚C in medium with 10% DMSO. The best fit permeability parameters are shown in Table 2.1 and Table 2.2 while the model simulated equilibrium cooling response is shown as a dotted line (------) in all the figures.

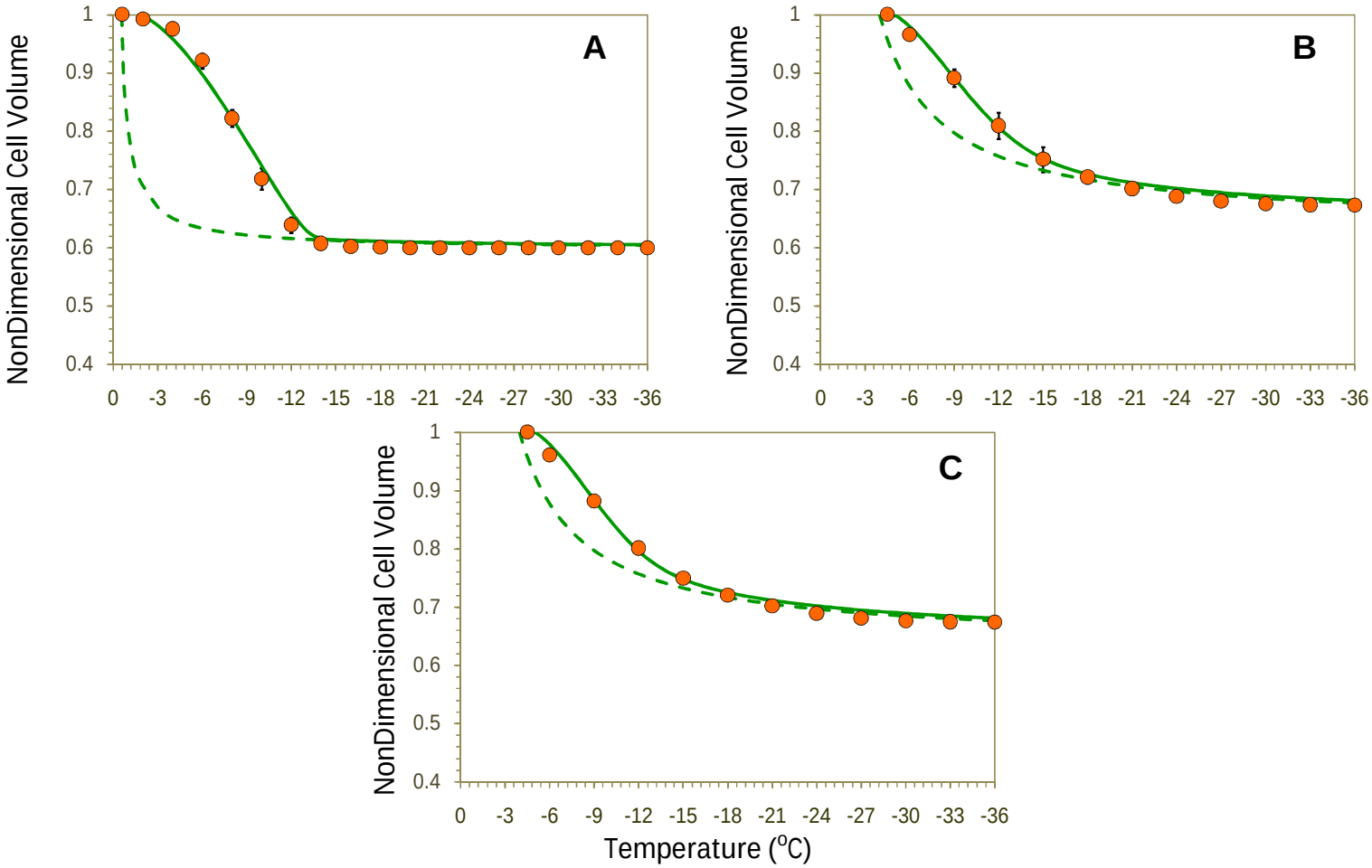

Figure 2.2: Volumetric response of SVF cells as a function of subzero temperatures obtained using the DSC technique in the presence of extracellular ice (Fig. 2.2A), in the presence of extracellular ice and glycerol (Fig. 2.2B), and in the presence of extracellular ice and DMSO (Fig. 2.2C). The filled circles represent the experimentally obtained water transport (volumetric shrinkage) at a cooling rate of 20 ˚C/min. The model-simulated dynamic cooling response at 20 ˚C/min is shown as a solid line and was obtained by using the best-fit membrane permeability parameters (L_{pg} *and* E_{Lp} *or* L_{pg}*[cpa] and* E_{Lp}*[cpa]*) (Table 2.1) in the water transport equation (equations 2 and 3). The model-simulated equilibrium cooling response obtained is shown as a dotted line in all the figures. The error bars represent the standard deviation for the mean values of six separate DSC experiments (*n=6*)

Table 2.1: Predicted sub zero membrane permeability parameters and the model predicted optimal rates of freezing for SVF and P0 ASCs for an assumed inactive cell volume of $V_b=0.6V_o$.

Cell Type	*Freezing Media*	L_{pg} *or* L_{pg}*[cpa] x* 10^{15} m^3*/Ns (μm/min-atm)*	E_{Lp} *or* E_{Lp}*[cpa] kJ/mol (kcal/mole)*	R^2 *Value*	B_{opt} *(Simulation)* ^oC*/min*
SVF	*No CPA*	23.1 (0.135)	43.4 (9.66)	0.992	59.2
	10% Glycerol	56.4 (0.330)	63.3 (15.25)	0.994	25.8
	10.0% DMSO	59.0 (0.345)	57.4 (13.40)	0.994	33.5
P0	*No CPA*	41.0 (0.24)	43.1 (10.30)	0.997	96.7
	10% Glycerol	53.7 (0.314)	64.0 (15.3)	0.994	25.3
	10.0% DMSO	55.1 (0.322)	58.9 (14.1)	0.994	30.2

Table 2.2: Predicted sub zero membrane permeability parameters and the model predicted optimal rates of freezing for P2 and P4 ASCs for an assumed inactive cell volume of $V_b=0.6V_o$.

Cell Type	*Freezing Media*	L_{pg} *or* L_{pg}*[cpa] x* 10^{15} m^3*/Ns (μm/min-atm)*	E_{Lp} *or* E_{Lp}*[cpa] kJ/mol (kcal/mole)*	R^2 *Value*	B_{opt} *(Simulation)* ^oC*/min*
P2	*No CPA*	111.5 (0.652)	168.8 (40.37)	0.995	22.1
	10% Glycerol	50.5 (0.295)	64.6 (15.45)	0.993	23.3
	10.0% DMSO	51.3 (0.300)	61.1 (14.61)	0.994	24.2
P4	*No CPA*	1.20 (0.7)	177.8 (42.5)	0.993	21.0
	10% Glycerol	0.39 (0.23)	51.0 (12.2)	0.995	29.0
	10% DMSO	0.50 (0.29)	61.5 (14.7)	0.996	22.0

Fig. 2.5 shows the water transport data and simulation for P4 ASCs using the best fit parameters in Eqn. (1) at a cooling rate of 20 ˚C/min in culture medium with no CPAs (Fig. 2.5A), in culture medium with 10% glycerol (Fig. 2.5B) and in culture medium with 10% DMSO (Fig. 2.5C). The dynamic portion of the cooling curve (region where the initial and final heat release thermograms are distinct and separate) is found to be between -0.6 ˚C to -14˚C in medium with no CPAs, between -3.1 and -24 ˚C with either 10% glycerol or 10% DMSO. The P4 ASC membrane permeability parameter values that best fit the water transport data in the absence and presence of CPAs are shown in Table 2.2. The model simulated equilibrium cooling response (equilibrium is achieved at each temperature when the internal and external osmotic pressures are equal) is also shown as reference as dotted line (------). The equilibrium cooling response represents the volumetric shrinkage response of an ASC cooled infinitely slowly and is significantly different (>99% confidence level using the student's t-test) from the dynamic water transport data obtained at 20 ˚C/min.

2.3.2: Membrane Permeability Parametric Space

To assess the variability of the parametric space that best fit the measured water transport data the goodness of fit parameter, R^2 was generated for a wide range of L_{pg} and E_{Lp} (or $L_{pg}[cpa]$ and $E_{Lp}[cpa]$) values. To summarize the results of this analysis a series of contour plots are shown in Figs. 2.6. Any combination of L_{pg} and E_{Lp} (or $L_{pg}[cpa]$ and $E_{Lp}[cpa]$) shown to be within the contour in the Figs. 2.5 will "fit" the water transport data in that media with an R^2 value greater than 0.99. Figs. 2.6A, 2.6B, 2.6C and 2.6D represent contour plots of the goodness of fit parameter, R^2 (= 0.99) in the L_{pg} and E_{Lp} (or $L_{pg}[cpa]$ and $E_{Lp}[cpa]$) space that corresponds to the water transport data (or volume change data) of SVF, P0, P2 and P4 cells, respectively.

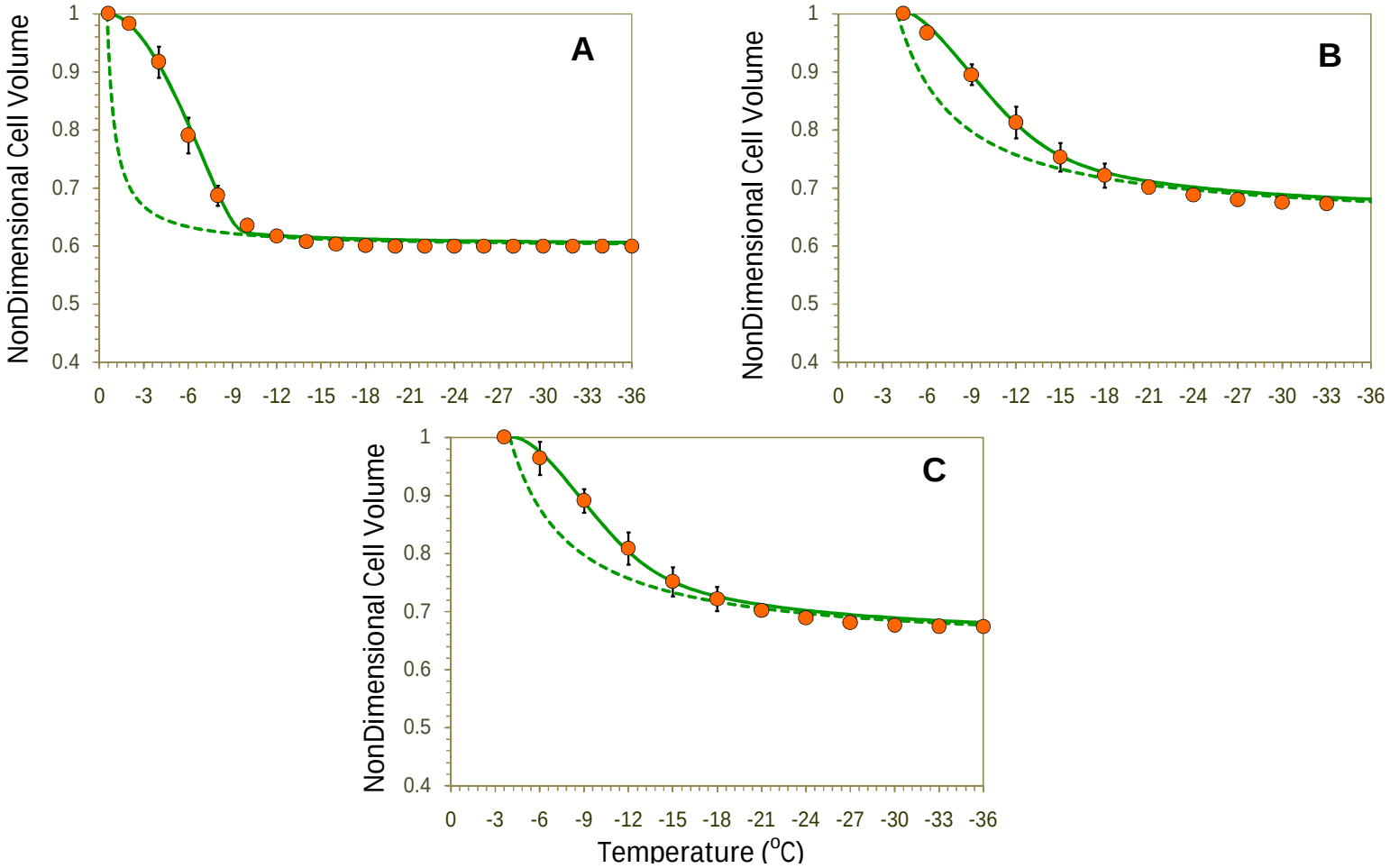

Figure 2.3: Volumetric response of P0 ASCs as a function of subzero temperatures in the presence of extracellular ice (Fig. 2.3A), in the presence of extracellular ice and glycerol (Fig. 2.3B), and in the presence of extracellular ice and DMSO (Fig. 2.3C). The filled circles represent the experimentally obtained water transport at a cooling rate of 20 ˚C/min. The model-simulated dynamic cooling response at 20 ˚C/min is shown as a solid line and the model-simulated equilibrium cooling response obtained is shown as a dotted line in all the figures. The error bars represent the standard deviation for the mean values of six separate DSC experiments (*n=6*)

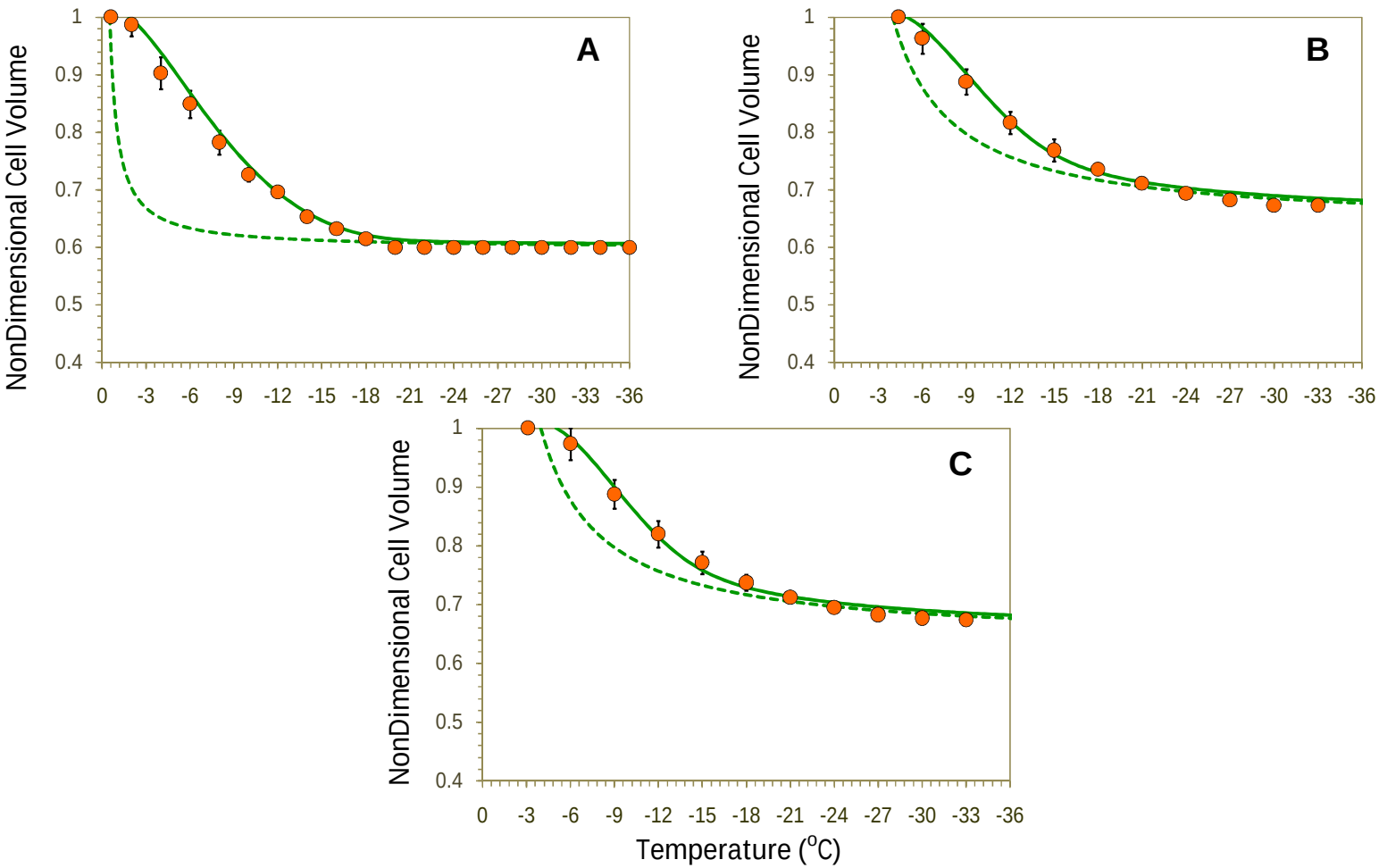

Figure 2.4: Volumetric response of P2 ASCs as a function of subzero temperatures in the presence of extracellular ice (Fig. 2.4A), in the presence of extracellular ice and glycerol (Fig. 2.4B), and in the presence of extracellular ice and DMSO (Fig. 2.4C). The filled circles represent the experimentally obtained water transport at a cooling rate of 20 ˚C/min. The model-simulated dynamic cooling response at 20 ˚C/min is shown as a solid line and the model-simulated equilibrium cooling response obtained is shown as a dotted line in all the figures. The error bars represent the standard deviation for the mean values of six separate DSC experiments (*n=6*)

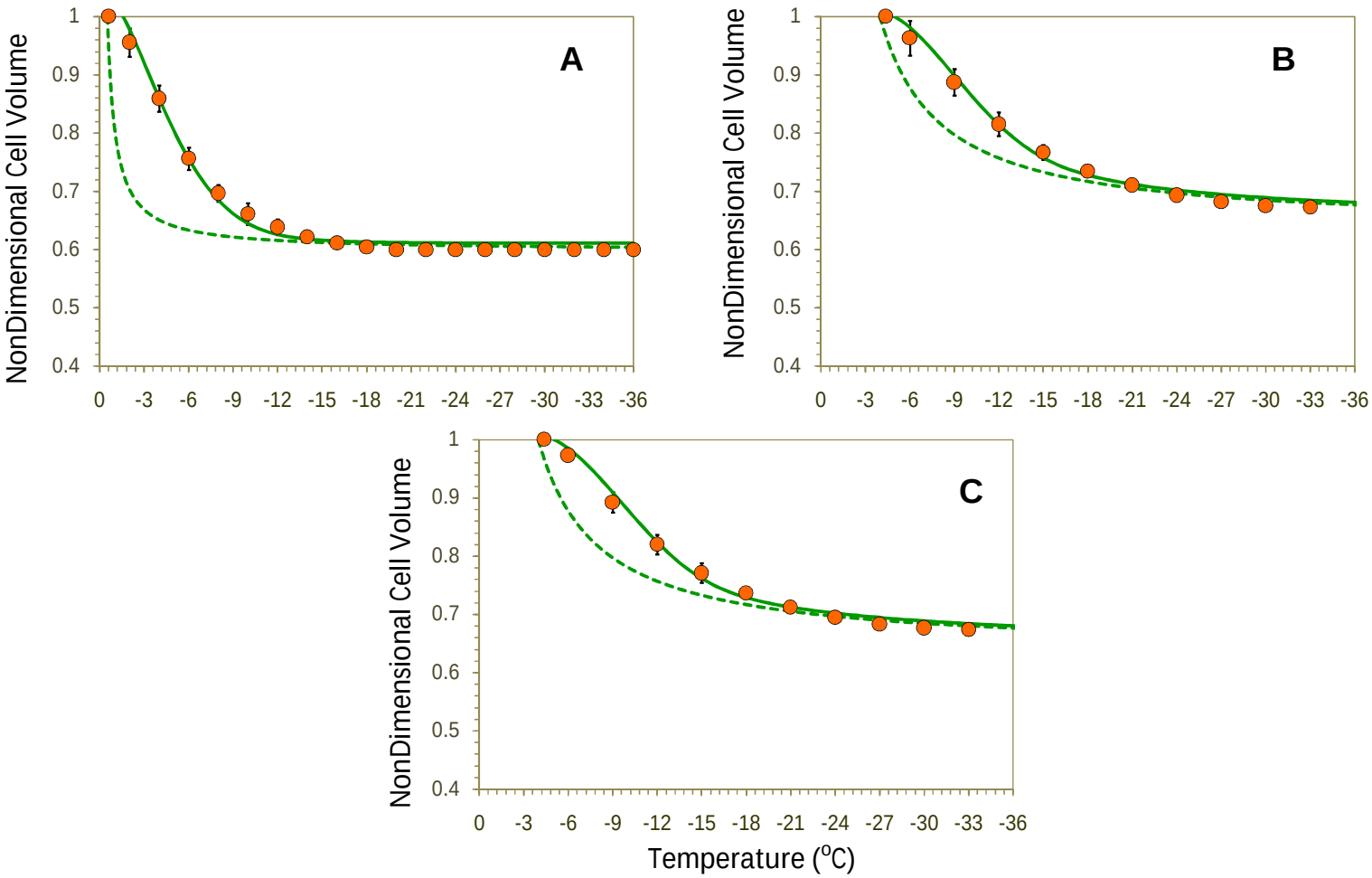

Figure 2.5: Volumetric response of P4 ASCs as a function of subzero temperatures in the presence of extracellular ice (Fig. 2.5A), in the presence of extracellular ice and glycerol (Fig. 2.5B), and in the presence of extracellular ice and DMSO (Fig. 2.5C). The filled circles represent the experimentally obtained water transport at a cooling rate of 20 ˚C/min. The model-simulated dynamic cooling response at 20 ˚C/min is shown as a solid line and the model-simulated equilibrium cooling response obtained is shown as a dotted line in all the figures. The error bars represent the standard deviation for the mean values of six separate DSC experiments (*n=6*)

The three contours within each figure (Figs. 2.6A, 2.6B, 2.6C and 2.6D) represent the three different media investigated, namely culture medium with no CPAs, culture media with 10% glycerol and culture medium with 10% DMSO. Note that, for all the adipose derived cells studied the contour for the media containing 10% glycerol is almost completely within the contour corresponding to 10% DMSO. This suggests that the membrane permeability parameters obtained in the presence of 10% DMSO could predict the volumetric response of the adipose derived (SVF, P0, P2 and P4) cells in the presence of 10% glycerol quite accurately, while the converse is not true.

For using V_b of $0.6V_o$, the values of E_{Lp} or $E_{Lp}[cpa]$ are not significantly different and are within ± 10% of each other. The only exception being the value of $E_{Lp}[cpa]$ with 10% DMSO at an assumed V_b value of $0.8V_o$ (Table 2.5 and Table 2.6). Despite the differences in the predicted permeability (L_{pg} and $L_{pg}[cpa]$) values of SVF cells for different V_b values, a very similar value (±20%) is obtained for the predicted optimal cooling rate (Tables 2.1, 2.2, 2.3, 2.4, 2.5 and 2.6). This suggests that the variation in the value of V_b does not significantly alter our model predicted optimal rates of freezing SVF cells (Tables 2.1, 2.2, 2.3, 2.4, 2.5 and 2.6). A similar result (significant difference in L_{pg} values and negligible difference in E_{Lp} values for V_b = 0.4, 0.6 and $0.8V_o$) was also observed with P0 and P2 ASCs. The sole P4 cells, note that the contour for the media containing 10% glycerol and 10% DMSO are almost identical. This suggests that the membrane permeability parameters obtained in the presence of 10% DMSO could predict the volumetric response of the adipose derived(P4) cells in the presence

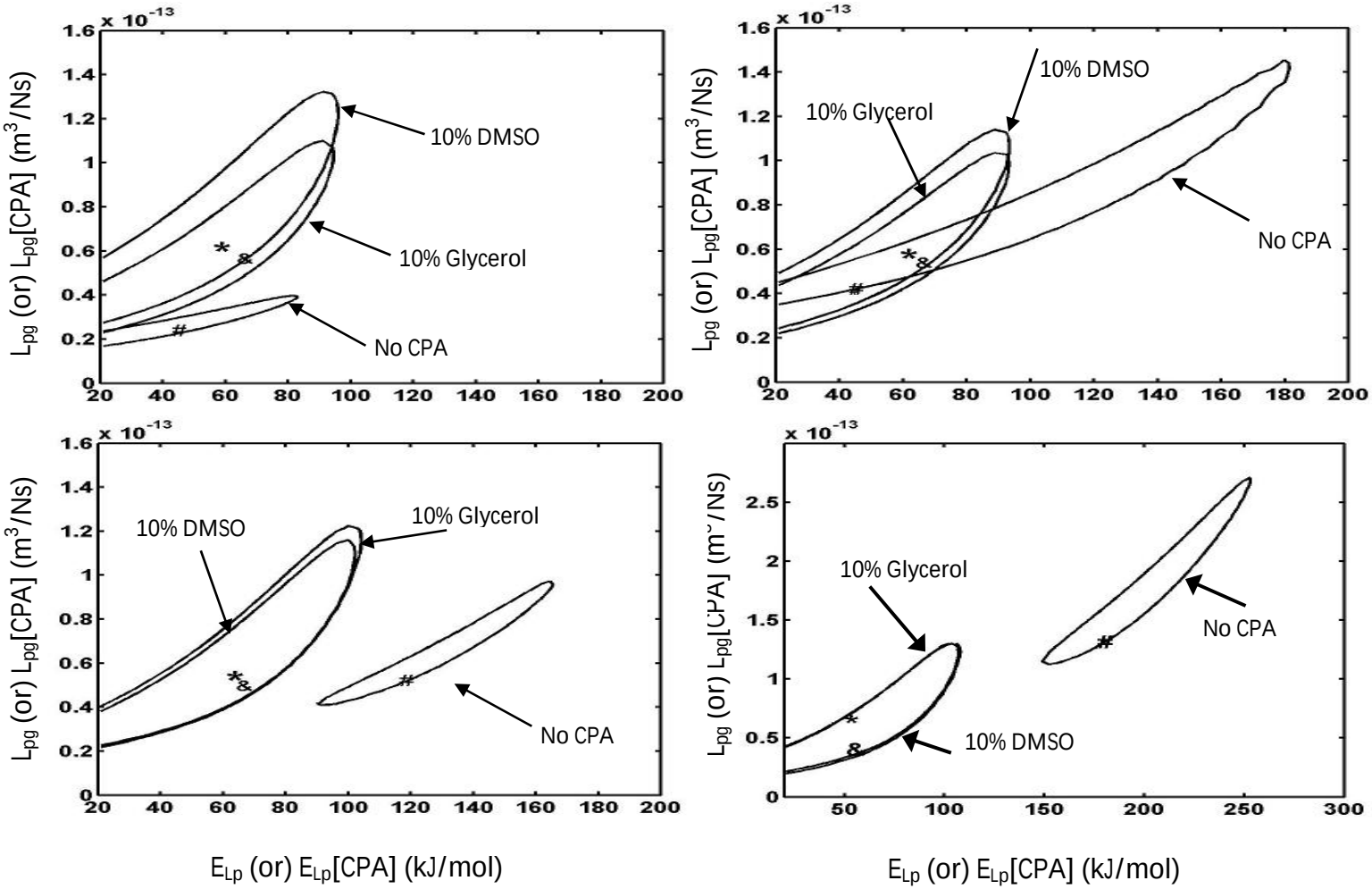

Figure 2.6: Contour plots of the goodness of fit parameter R2 (=0.99) for water transport response in SVF (Fig. 2.6A), P0 (Fig. 2.6B), P2 (Fig. 2.6C) and P4 (Fig. 2.6D) ASCs in medium with no CPAs, in medium with 10% glycerol and in medium with 10% DMSO. The enclosed region corresponds to the range of parameters that best fit the water transport data at a cooling rate of 20 ˚C/min with R2 = 0.99. Note that the best-fit parameters (Table 2.1 and Table 2.2) are represented within the contours by a "#" (absence of CPA), "&" (10% glycerol) and "*" (with 10% DMSO)

of 10% glycerol quite accurately and vice-versa. The reasons for the similarity in the water transport response (and consequently the membrane permeability parameters) in the presence of DMSO and glycerol for P4 ASCs are beyond the scope of this study and cannot be fully answered unless a mechanistic model describing the interactions and modifications caused by different chemicals on different cell membranes can be developed (such models are currently unavailable). Also note that the parameters obtained in the absence of CPAs are significantly different than those obtained in their presence (the contour plot corresponding to 0% of CPAs has no overlap with the contours obtained with 10% glycerol or 10% DMSO).

2.3.3: Water Transport Simulations

Water transport simulations obtained using the best fit parameters (shown in Table 2.1 and Table 2.2) in Eqn. (2) are shown for a variety of cooling rates (5 - 100 ˚C/min) in Fig 2.7 and Fig 2.8). From these water transport simulations, the amount of trapped water (or a lower bound on the intracellular ice volume or IIV) was computed as a ratio of the volume of the water trapped inside the ASCs at a temperature, T (~-30 ˚C) relative to the initial ASC water volume, a strategy previously applied in several cell system (Devireddy et al, 2000; Devireddy et al., 2002 Thirumala et al., 2003). Hence IIV is represented as $(V- V_e)/(V_i - V_e)$ where V is the end volume after water transport ceases (at ~ -30 ˚C), and V_i and V_e are the initial (isotonic) and final (osmotically inactive) ASC volumes, respectively. For SVF cells in the absence of CPAs, for cooling rates less than or equal to 40˚C/min, 60˚C/min and 100˚C/min, the IIV was less than or equal to

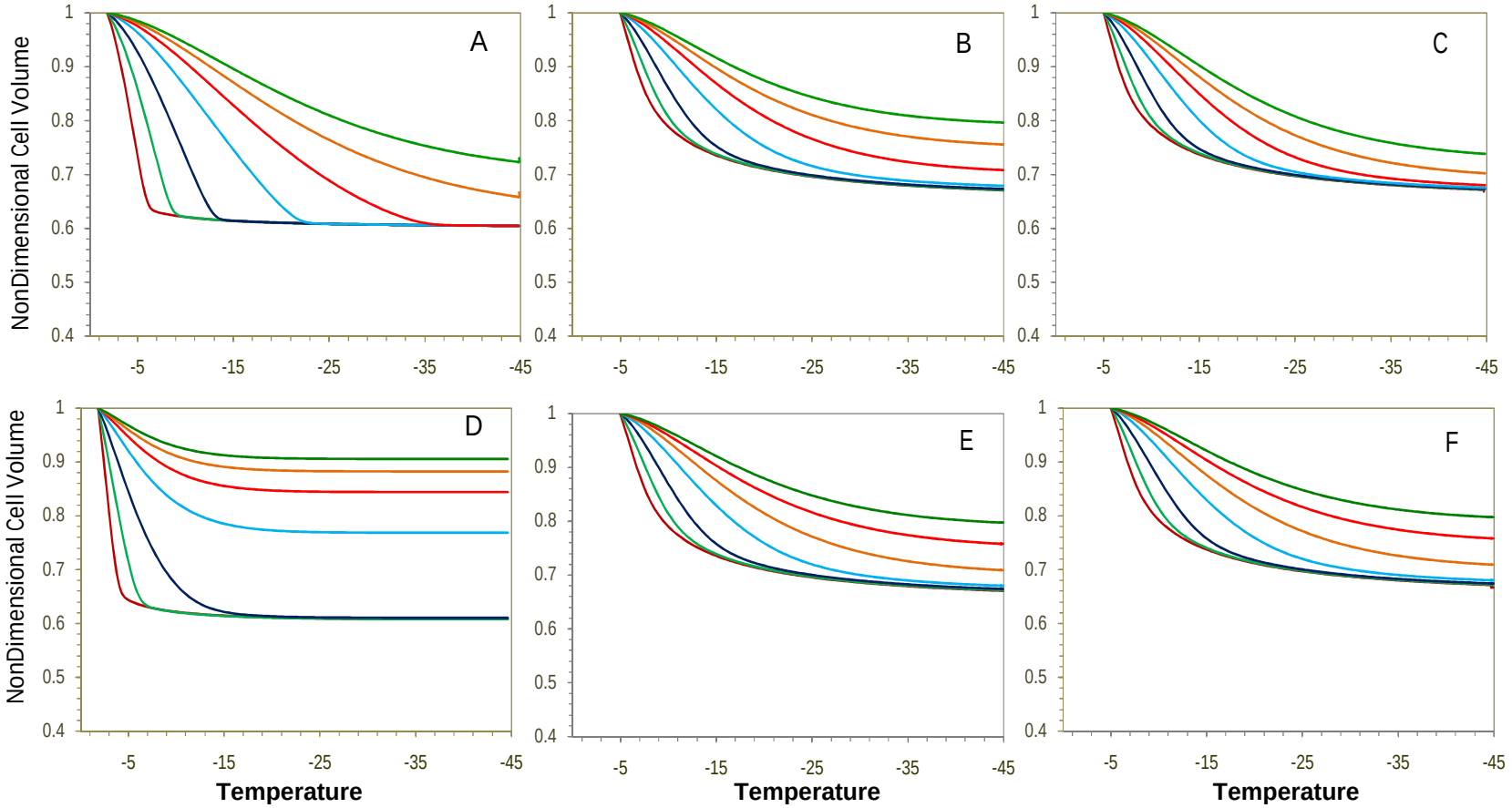

Figure 2.7: Volumetric response of adipose derived (SVF and P0) cells at various cooling rates as a function of subzero temperatures using the best-fit membrane permeability parameters (shown in Table 2.1). The water transport curves (solid lines) represent the model-simulated response for different cooling rates (from left to right: 5, 10, 20, 40, 60, 80 and 100 ˚C/min). The subzero temperatures are shown along the x-axis while the nondimensional volume is plotted along the y-axis. The changes in the normalized cell volume (V/V_o) are shown as a function of temperature for different cooling rates in SVF cell suspensions without CPA (Fig. 2.7A), with 10% Glycerol (Fig. 2.7B) and with 10% DMSO (Fig. 2.7C). For P0 ASCs, the changes in the V/V_o are shown as a function of temperature for different cooling rates in cell suspensions without CPA (Fig. 2.7D), with 10% Glycerol (Fig. 2.7E) and with 10% DMSO (Fig. 2.7F).

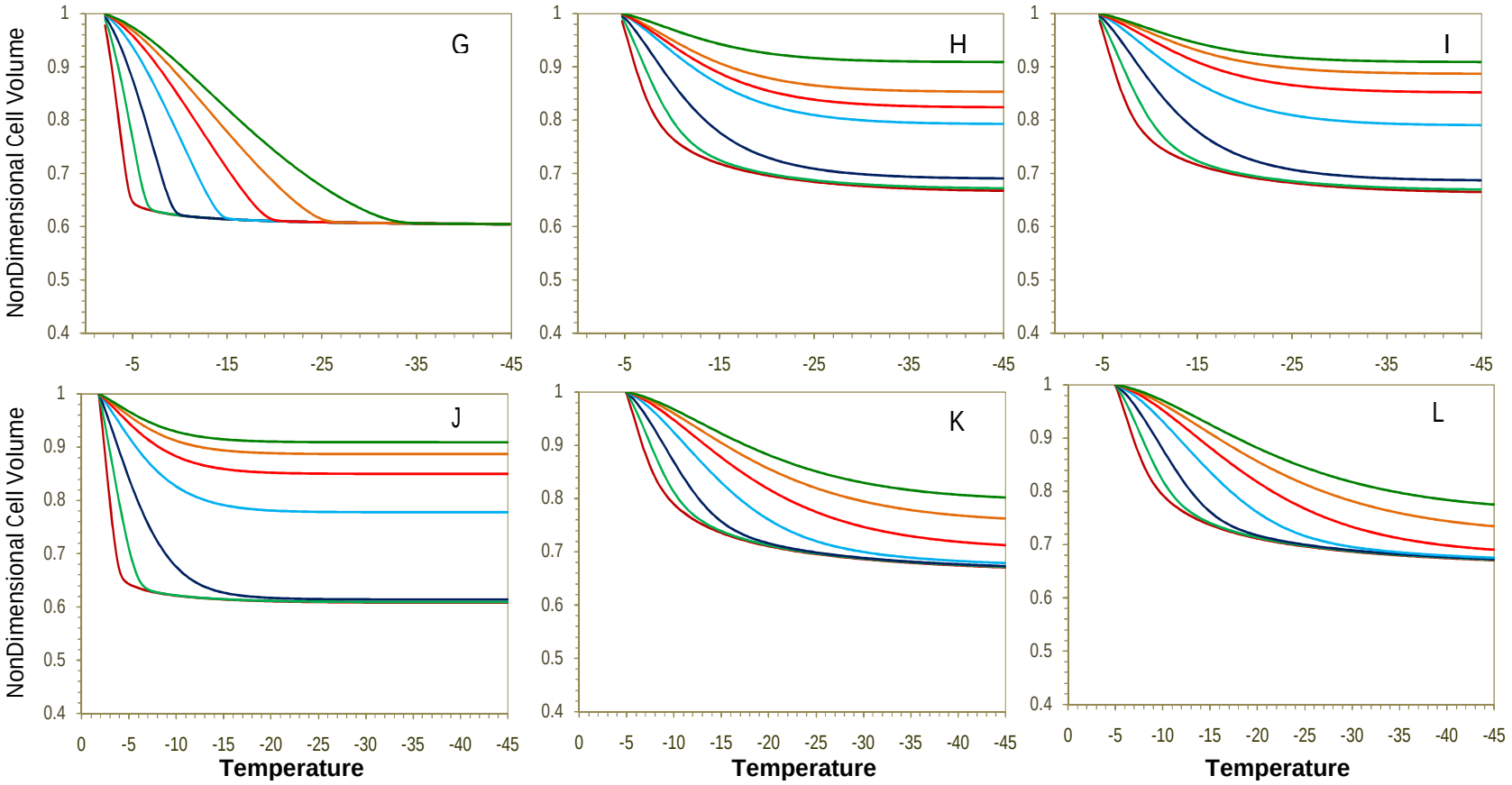

Figure 2.8: Volumetric response of adipose derived (P2 and P4) cells at various cooling rates as a function of subzero temperatures using the best-fit membrane permeability parameters (shown in Table 2). The water transport curves (solid lines) represent the model-simulated response for different cooling rates (from left to right: 5, 10, 20, 40, 60, 80 and 100 ˚C/min). The subzero temperatures are shown along the x-axis while the nondimensional volume is plotted along the y-axis. The changes in the normalized cell volume (V/V_o) are shown as a function of temperature for different cooling rates in P2 cell suspensions without CPA (Fig. 2.8G), with 10% Glycerol (Fig. 2.8H) and with 10% DMSO (Fig. 2.8I). For P4 ASCs, the changes in the V/V_o are shown as a function of temperature for different cooling rates in cell suspensions without CPA (Fig. 2.8J), with 10% Glycerol (Fig. 2.8K) and with 10% DMSO (Fig. 2.8L).

1.8%, 10.3%, and 44.8% of the initial osmotically active water volume, respectively, and the corresponding end volumes were less than or equal to $0.61V_i$, and $0.64V_i$, and $0.781V_i$, respectively (Fig. 2.7A).

Similarly for SVF cells in the presence of 10% glycerol, for cooling rates less than or equal to 20 ˚C/min, 40 ˚C/min, 60 ˚C/min, 80 ˚C/min and 100 ˚C/min, the IIV was less than or equal to 4.8%, 7.6%, 20.2%, 34.6%, and 45.6% of the initial osmotically active water volume, respectively, and the corresponding end volumes were less than or equal to $0.69V_i$, $0.70V_i$, $0.74V_i$, $0.79V_i$, and $0.82V_i$, respectively (Fig. 2.7B). And finally for SVF cells in the presence of 10% DMSO, for cooling rates of less than or equal to 20 ˚C/min, 40 ˚C/min, 60 ˚C/min, 80 ˚C/min and 100 ˚C/min,, the IIV was less than or equal to 4.5%, 5.4%, 9.8%, 20.7% and 32.0% of the initial osmotically active water volume, respectively, and the corresponding end volumes were less than or equal to $0.69V_i$, $0.69V_i$, $0.71V_i$, $0.74V_i$, and $0.78V_i$, respectively (Fig. 2. 7C). Similar calculations were performed for P0, P2 and P4 ASCs from the simulations shown in Figs. 2.7D, 2.7E, 2.7F and 2.8G, 2.8H, 2.8I, 2.8J, 2.8K and 2.8L (data not shown, in the interest of brevity).

As described earlier (see Introduction), the cooling rate which optimizes the freeze/thaw response of any cellular system can be defined as the fastest cooling rate in a given media without forming damaging intracellular ice formation, IIF. Mazur (1990) defines IIF as damaging and lethal if it is greater than 10-15% of the initial intracellular water is involved. We defined, for all the adipose derived cells studied, the “optimal cooling rate” as the cooling rate at which 5% of the initial osmotically active water volume (or 5% IIV) is trapped inside the cells at temperature, T ~ -30°C. This assumption of 5% IIV being optimal was recently validated by comparing the model predicted optimal cooling rates with experimentally (empirically)

determined optimal rates of freezing for a variety of cells by Thirumala and Devireddy (2005). Thus, we are reasonably confident that a choice of 5% IIV is optimal for ASCs in suspension as well.

For SVF cells, the simulations (shown in Figs. 2. 7A to 2. 7C) suggest the following cooling rates as optimal in the three media investigated: 59.2 °C/min with no CPAs, 25.8 °C/min with 10% glycerol as the CPA and 33.5 °C/min with 10% DMSO as the CPA (as shown in Table 2.1 and Table 2.2). Similarly for P0 ASCs the simulations show an optimal cooling rate of 96.7 °C/min (no CPAs), 25.3 °C/min (10% glycerol) and 30.2 °C/min (10% DMSO). For P2 ASCs the simulations suggest an optimal cooling rate of 22.1°C/min (no CPAs), 23.3 °C/min (10% glycerol) and 24.2 °C/min (10% DMSO).

Finally for P4 cells, the simulations (shown in Figs. 2. 8J to 2. 8L) suggest the following cooling rates as optimal in the three media investigated: 21 ˚C/min with no CPAs, 29 ˚C/min with 10% glycerol as the CPA and 22 ˚C/min with 10% DMSO as the CPA (as shown in Table 2.1 and Table 2.2). Note, that if intracellular ice formation (IIF) occurs by a heterogeneous or a surface catalyzed nucleation mechanism (Toner, 1993), generally between -5 and -20 °C for a variety of single cells, which our model does not predict, then potentially even more water will be trapped in the ASCs than predicted by water transport alone (i.e. the lower bound of intracellular ice discussed above). Thus, the “optimal cooling rates” (stated above) based on the lower bound of intracellular ice are probably over estimated. Future empirical studies that determine the viability of ASCs as a function of the imposed cooling rates are clearly needed (and are currently in progress) to independently confirm the predicted optimal rates of ASC freezing obtained in the present study.

2.3.4: Parameter Sensitivity Analysis - Effect of Varying V_b

There are no prior experimental studies that report the osmotically inactive cell volume fraction (V_b) of adipose derived adult stem (ADAS) cells. Thus, we assigned a value of $0.6V_o$ as the inactive cell volume, a value that is commonly used for most mammalian cells (Devireddy et al., 1998; He et al., 2004; Mazur et al., 1972; McGrath, 1988; Smith et al., 1998; Thirumala et al., 2003; Toner, 1993). To further study the effect of varying the V_b on measured membrane permeability parameters (L_{pg} and E_{Lp}) and consequently on the predicted optimal cooling rates, the value of V_b was increased to $0.8V_o$ and decreased to $0.4V_o$. The DSC data was correspondingly modified (using Eqn. 1) and the modified DSC water transport data was curve fitted to the water transport model (Eqns. 2 and 3) using the nonlinear least squares curve fitting technique as previously described. The predicted values of the membrane permeability

Table 2.3: Predicted sub zero membrane permeability parameters and optimal rates of freezing for adipose derived SVF and P0 ASCs for an assumed inactive cell volume of $V_b=0.4V_o$.

Cell Type	*Freezing Media*	L_{pg} *or* L_{pg}*[cpa]* *x* 10^{15} m^3/Ns *(μm/min-atm)*	E_{Lp} *or* E_{Lp}*[cpa]* *kJ/mol (kcal/mole)*	R^2 *Value*	B_{opt} *(Simulation)* $^oC/min$
SVF	*No CPA*	34.3 (0.201)	39.9 (9.54)	0.992	59.0
	10% Glycerol	85.3 (0.499)	60.7 (14.51)	0.994	29.7
	10.0% DMSO	93.9 (0.549)	57.0 (13.64)	0.994	33.9
P0	*No CPA*	65.5 (0.383)	48.6 (11.62)	0.997	88.0
	10% Glycerol	80.5 (0.471)	60.5 (14.47)	0.994	28.0
	10.0% DMSO	77.1 (0.451)	55.2 (13.21)	0.994	30.1

parameters (L_{pg} and E_{Lp}) for adipose derived cells using a value of $0.4V_o$ and $0.8V_o$ as the osmotically inactive cell volume are shown in Tables 2.3, 2.4 and Table 2.5, 2.6 respectively.

For SVF cells, although the predicted L_{pg} and $L_{pg}[cpa]$ values using $V_b = 0.4V_o$ and $0.8V_o$ are significantly different from each other and from the values obtained earlier using V_b of $0.6V_o$, the values of E_{Lp} or $E_{Lp}[cpa]$ are not significantly different and are within ± 10% of each other. The only exception being the value of $E_{Lp}[cpa]$ with 10% DMSO at an assumed V_b value of $0.8V_o$ (Table 2.5 and Table 2.6). Despite the differences in the predicted permeability (L_{pg} and $L_{pg}[cpa]$) values of SVF cells for different V_b values, a very similar value (±20%) is obtained for the predicted optimal cooling rate (Tables 2.1, 2.2, 2.3, 2.4, 2.5 and 2.6). This suggests that the variation in the value of V_b does not significantly alter our model predicted optimal rates of freezing SVF cells (Tables 2.1, 2.2, 2.3, 2.4, 2.5 and 2.6).

Table 2.4: Predicted sub zero membrane permeability parameters and optimal rates of freezing for adipose derived P2 and P4 ASCs for an assumed inactive cell volume of $V_b=0.4V_o$.

Cell Type	*Freezing Media*	L_{pg} *or* $L_{pg}[cpa]$ *x* 10^{15} m^3/Ns *(μm/min-atm)*	E_{Lp} *or* $E_{Lp}[cpa]$ *kJ/mol (kcal/mole)*	R^2 *Value*	B_{opt} *(Simulation)* $^oC/min$
P2	*No CPA*	177.7 (1.039)	177.7 (42.50)	0.997	27.7
	10% Glycerol	75.1 (0.439)	64.0 (15.31)	0.994	22.0
	10.0% DMSO	71.0 (0.415)	58.7 (14.05)	0.994	23.4
P4	*No CPA*	1.86 (1.09)	180.4 (43.2)	0.994	21.0
	10% Glycerol	0.74 (0.43)	61.0 (14.6)	0.955	25.0
	10.0% DMSO	0.68 (0.40)	57.7 (13.8)	0.994	24.0

Table 2.5: Predicted sub zero membrane permeability parameters and optimal rates of freezing for adipose derived SVF and P0 ASCs for an assumed inactive cell volume of $V_b=0.8V_o$.

Cell Type	*Freezing Media*	L_{pg} *or* L_{pg}*[cpa] x* 10^{15} m^3*/Ns (µm/min-atm)*	E_{Lp} *or* E_{Lp}*[cpa] kJ/mol (kcal/mole)*	R^2 *Value*	B_{opt} *(Simulation)* ^oC*/min*
SVF	*No CPA*	10.3 (0.06)	38.9 (9.3)	0.992	54.3
	10% Glycerol	25.7 (0.15)	62.7 (15.0)	0.994	24.0
	10.0% DMSO	20.5 (0.12)	41.8 (10.0)	0.994	39.2
P0	*No CPA*	30.1 (0.176)	92.0 (22.0)	0.996	43.4
	10% Glycerol	27.4 (0.16)	61.9 (14.8)	0.994	24.9
	10.0% DMSO	20.5 (0.12)	45.6 (10.9)	0.994	34.2

A similar result (significant difference in L_{pg} values and negligible difference in E_{Lp} values for V_b = 0.4, 0.6 and 0.8V_o) was also observed with P0 and P2 ASCs. The sole exception being the permeability values obtained for P0 cells with no CPAs using an assumed V_b value of 0.8V_o (Tables 2.1, 2.2, 2.3, 2.4, 2.5 and 2.6). For P0 ASCs frozen in the absence of CPAs, varying the assumed value of V_b from 0.6V_o to 0.8V_o had a significant effect (~50% lower) on the predicted optimal cooling rate while lowering the value of V_b from 0.6V_o to 0.4V_o had essentially no effect (~10% lower). Intriguingly, no such effect is seen in P2 ASCs frozen in the absence of CPAs (Tables 2.1, 2.2, 2.3, 2.4, 2.5 and 2.6). And finally, for P0 and P2 ASCs frozen in the presence of CPAs, lowering or increasing the assumed value of V_b from 0.4V_o to 0.8V_o had some effect

Table 2.6: Predicted sub zero membrane permeability parameters and optimal rates of freezing for adipose derived P2 and P4 ASCs for an assumed inactive cell volume of V_b=0.4V_o.

Cell Type	*Freezing Media*	L_{pg} *or* L_{pg}*[cpa] x* 10^{15} m^3*/Ns (µm/min-atm)*	E_{Lp} *or* E_{Lp}*[cpa] kJ/mol (kcal/mole)*	R^2 *Value*	B_{opt} *(Simulation)* ^oC*/min*
P2	*No CPA*	54.9 (0.321)	159.2 (38.09)	0.996	24.9
	10% Glycerol	27.4 (0.16)	69.7 (16.67)	0.993	19.6
	10.0% DMSO	24.0 (0.14)	63.0 (15.07)	0.994	19.1
P4	*No CPA*	0.56 (0.33)	171.4 (41.0)	0.991	22.0
	10% Glycerol	0.27 (0.16)	62.7 (15.0)	0.993	24.0
	10.0% DMSO	0.26 (0.15)	62.8 (15.0)	0.996	19.0

(±25%) variation in the predicted optimal cooling rates; although the magnitudes are within ± 6 ˚C/min of each other for corresponding freezing media).

In case of P4 cells (Table 2.2, 2.4 and 2.6) as the assumed value of V_b increases the model predicted values of L_{pg} decreases in all the media. However, for P4 cells the behavior of E_{Lp} is more complex, without CPAs, it decreases as V_b increases. In the presence of 10% DMSO, E_{Lp} increases as V_b increases. While in the presence of 10% glycerol, E_{Lp} has a minimum at an assumed V_b value of 0.6 V_o and increases as the value of V_b is varied, irrespective of whether it is lowered to 0.4 V_o or increased to 0.8 V_o. The exact reason for this anomalous behavior of P4 ASCs in the presence of glycerol is unclear and warrants further study. Despite the differences in the predicted permeability (L_{pg} and L_{pg}*[cpa]*) values of P4 ASCs for different V_b values, a similar value (±20%) is obtained for the predicted optimal cooling rate

(Tables 2.1, 2.2, 2.3, 2.4, 2.5 and 2.6). Thus, the results for all adipose derived cells (except P0 with no CPA) showed that the variation in the value of V_b does not significantly alter the model predicted optimal rates of freezing and further studies are clearly needed to understand this lack of sensitivity in the value of predicted optimal cooling rates for adipose derived cells to the assumed value of V_b.

This relative insensitivity of the predicted optimal cooling rate to the assumed value of V_b has been reported earlier for a variety of biological systems (Devireddy et al., 1998; Devireddy et al., 1999; Thirumala et al., 2003; Thirumala and Devireddy 2005). A possible explanation for the independence of the predicted optimal cooling rate from V_b could be due the following concatenation of events: i) assuming V_b decreases (or the initial water volume increases), the ratio of surface area available for water transport (A) to the initial water volume (V_o - V_b) decreases; ii) a simple analysis of equation (1), shows that as the ratio of A and (V_o - V_b) decreases, L_{pg} has to increase (this trend of increasing L_{pg} with decreasing V_b is clear from the data shown (Tables 2.1, 2.2, 2.3, 2.4, 2.5 and 2.6). The effect of varying V_b on E_{Lp} is not quite as straight forward due to the exponential (arrhenius) relationship between L_p and E_{Lp}, as described earlier in equation (2); iii) and if we realize, as revealed in a recent study by Thirumala and Devireddy (2005), that the optimal cooling rate is a direct and linear function of L_{pg} and the ratio A/(V_o - V_b) we conclude that changes in V_b will effect the value of L_{pg} but should not dramatically alter the optimal cooling rate (as is clear from the data shown in Tables 2.1, 2.2, 2.3, 2.4, 2.5 and 2.6). And finally, it is important to note that the effect of E_{Lp} on the predicted optimal cooling rate is not linear and in fact decreases exponentially as it increases (Thirumala and Devireddy 2005). In essence, the most significant measurements that determine

the optimal cooling rate are the water transport (volumetric shrinkage) response and the ratio of the cell surface area available for water transport to the initial amount of water present in the cell.

2.3.5: Effect of Varying Assumed Cell Diameter (or Surface Area to Volume Ratio)

To account for any errors and uncertainties in the measured cell diameter of the adipose derived cells, we also investigated the effect of varying the surface area to volume ratio (S:V) by ±50%, from 0.12 to 0.06 and 0.18. The geometric model was suitably modified in the water transport model (Eqns. 2 and 3) and the corresponding best-fit permeability parameters (L_{pg} or $L_{pg}[cpa]$ and E_{Lp} or $E_{Lp}[cpa]$) were obtained using the nonlinear least squares curve fitting technique as previously described (data not shown in the interest of brevity). As expected the membrane permeability parameters obtained, by increasing the S:V ratio are lower than those shown in Tables 2.1, 2.2, 2.3, 2.4, 2.5 and 2.6). Similarly, the membrane permeability parameters obtained by decreasing the S:V ratio, are higher than those shown in Tables 2.1, 2.2 2.3, 2.4, 2.5 and 2.6. This inverse relationship between S:V ratio and the predicted membrane permeability parameters (L_{pg} or $L_{pg}[cpa]$ and E_{Lp} or $E_{Lp}[cpa]$) is not surprising, since Eqn. (2) shows that the change in the volume of the adipose derived cells as a function of temperature (dV/dT) is proportional to the product of L_p and A_C. Thus, for a given change in the ASC volume as a function of temperature (dV/dT), an increase in A_c (or S:V ratio) will cause a corresponding decrease in the predicted value of L_p, where $L_p = f(L_{pg}, E_{Lp})$ as shown in Eqn. (3) and vice-versa. Thus any changes to the geometrical model of the adipose derived cells (specifically membrane surface area, A_C) will manifest themselves with corresponding changes to the model predicted membrane permeability parameters (L_{pg} or $L_{pg}[cpa]$ and E_{Lp} or $E_{Lp}[cpa]$).

Additional numerical simulations were also performed assuming the new S:V ratio's by varying the assumed diameter of the cell and the corresponding water transport parameters in the water transport model (Eqns. 2 and 3). The simulations were analyzed to predict the "optimal cooling rate" as described earlier, i.e. the cooling rate at which 5% of the initial osmotically active water volume is trapped inside the cells at temperature, T ~ -30˚C. As expected, water transport simulations using the new S:V ratios suggest a range of optimal cooling rates (data not shown) that are quite close to the values obtained earlier with a S:V ratio of 0.12 (cooling rates are shown in Tables 2.1, 2.2, 2.3, 2.4, 2.5 and 2.6).

2.3.6: Effect of Cryoprotective Agents on Membrane Permeability Parameters

There is a significant increase in the measured values of reference membrane permeability, L_{pg} (or $L_{pg}[cpa]$) (~100-170%) and the activation energy, E_{Lp} (or E_{Lp} $[cpa]$) (~8 to 65%) values for SVF cells obtained in the presence of CPAs when compared to values obtained in their absence, for all the assumed values of V_b. Similarly for P0 ASCs there is an increase in the measured values of L_{pg} (or $L_{pg}[cpa]$) (~18 to 34%) and the activation energy, E_{Lp} (or E_{Lp} $[cpa]$) (~15 to 50%) in the presence of CPAs when compared to the values obtained in the absence of CPA for an assumed value of V_b of either $0.6V_o$ or $0.4V_o$. However, when the assumed value of V_b is increased to $0.8V_o$, the converse is found to be true for P0 ASCs, i.e., adding either glycerol or DMSO significantly decreased the measured values of the activation energy, E_{Lp} (or E_{Lp} $[cpa]$) (~33-50%) and the reference membrane permeability, L_{pg} (or L_{pg} $[cpa]$) (~9 to 32%) when compared to values obtained in their absence (Table 2.5 and Table 2.6).

Contrary to the above discussed ASCs (SVF, P0, [except P0 at $V_b=0.8V_o$]), P2 ASCs showed a significant decrease in measured values of L_{pg} (or $L_{pg}[cpa]$) (~50 to 60%) and the

activation energy, E_{Lp} (or E_{Lp} *[cpa]*) (~56 to 67%) for all V_b values when compared to values obtained in the absence of CPAs (Tables 2.1, 2.2, 2.3, 2.4, 2.5 and 2.6). Similar to P2 cells, for P4 cells there is a significant decrease in the measured values of reference membrane permeability, L_{pg} (or L_{pg}*[cpa]*) (~50-70%) and the activation energy, E_{Lp} (or E_{Lp} *[cpa]*) (~60-70%) obtained in the presence of CPAs when compared to values obtained in their absence, for all the assumed values of V_b. Clearly, the relative effects of the composition of the freezing media and the assumed value of the inactive cell volume had different effects on the predicted permeability parameters for different ASCs.

2.3.7: Effect of Cryoprotective Agents on the Predicted Optimal Cooling Rates

For SVF and P0 ASCs at $V_b = 0.6V_o$ (as shown in Table 2.1 and Table 2.2), the optimal cooling rates in the presence of either 10% glycerol or 10% DMSO are significantly smaller (~43 to 74%) than the predicted optimal values in their absence. Interestingly, at $V_b = 0.6V_o$ the addition of CPAs increases the optimal freezing rates by ~5 to 10% for P2 ASCs. At $V_b = 0.4V_o$, the presence of CPAs significantly decreased the optimal cooling rates by ~42 to 50% (for SVF cells), ~ ~66 to 68% (for P0 ASCs) and by ~15 to 18% (P2 ASCs), whereas at $V_b = 0.8V_o$, the presence of CPAs the optimal cooling rates were reduced by ~30 to 50% (for SVF cells), ~20 to 40% (for P0 ASCs) and by ~21 to 23% (P2 ASCs). The significant decrease in the predicted optimal cooling rates for adipose derived cells (except for P2 ASCs at $V_b = 0.6V_o$) in the presence of CPAs is surprising as the presence of CPAs is expected to increase the ability of the cell membrane to dehydrate at faster cooling rates as shown for several mammalian cells (Devireddy et al., 1999; Devireddy et al., 2000; Smith et al., 1998). However, a similar decrease in the predicted optimal cooling rates in the presence of CPAs was observed for other biological

cell systems (Devireddy et al., 2002; Thirumala et al., 2003; Devireddy et al., 2005) as well. For P4 cells the presence of CPAs (either glycerol or DMSO) did not significantly alter the predicted optimal cooling rates at all V_b values. Further studies are needed to elucidate the precise mechanism by which CPAs alter the ASC membranes during and after a freeze-thaw process (Pinisetty et al., 2005).

2.4 CONCLUSIONS

The water transport phenomena (volumetric shrinkage) during freezing of adipose derived adult stem (ASCs) cells in the presence of extracellular ice and CPAs (glycerol and DMSO) was obtained in this study using a DSC technique at a cooling rate 20 ˚C/min. Volumetric shrinkage during freezing of adipose derived cells was obtained in the presence of extracellular ice and CPAs (10% DMSO and 10% glycerol). The measured water transport data in the presence and absence of CPAs was curve fitted to a model of water transport (Eqns. 2 and 3), to predict the membrane permeability parameters L_{pg} or $L_{pg}[cpa]$ and E_{Lp} or $E_{Lp}[cpa]$ of adipose derived cells. The permeability parameters obtained in this study predict an optimal rate of freezing for SVF cells ranging from 25 to 60 ˚C/min, for P0 ASCs from 25 to 100 ˚C/min, for P2 ASCs from 20 to 25 ˚C/min and for P4 ASCs from 19 to 22 ˚C/min. The water permeability parameters presented in this study will help to establish cryopreservation of adipose derived cells on a firm biophysical basis. Future studies should make direct comparisons of the optimal cooling rates predicted using the water transport models developed here with experimentally determined optimal cooling rate values for adipose derived cells.

CHAPTER 3
THE EFFECT OF VARIOUS FREEZING PARAMETERS ON THE IMMEDIATE POST-THAW MEMBRANE INTEGRITY OF ADIPOSE TISSUE DERIVED ADULT STEM CELLS[1]

3.1 INTRODUCTION

In a typical cryopreservation process, the membrane integrity of any biological cell depends upon the thermal history it experiences, i.e., cooling rate (CR), end temperature (ET), hold time or the time spent at the end temperature (HT) and warming or thawing rate (TR) (Mazur 1984). Depending on whether the CR is ''slow'' or ''fast,'' the intracellular water permeates across the cell membrane and joins the extracellular ice phase or freezes and forms ice inside the cell, respectively (Mazur 1963; Mazur 1984). In most cases, cells undergoing ice formation inside the cells or intracellular ice formation (IIF) are rendered osmotically inactive (lysed), due to the loss of cell membrane integrity (Mazu 1970; Meryman 1966). Similarly cells, which experience a severe loss of intracellular water, are also rendered osmotically inactive (Lovelock 1953). The deleterious effect of lowering the ET and increasing the HT on cell membrane integrity was observed with human prostate cancer cells (Tatsutani et al., 1996), rat prostate cancer cells (Smith et al., 1999) and ELT-3 uterine leiomyoma tumor cells (Bischof et al., 2001). Finally, the beneficial effect of increasing TR on cell membrane integrity is assumed at least in part to be due to minimization of recrystallization injury (Mazur 1984).

A detailed study assessing the effect of varying all these four parameters within a practically relevant range would help to evaluate which parameter would impact the post-thaw

[1] This work was published in the following citations: S. Thirumala, S. Zvonic, E. Floyd, J.M. Gimble and R.V. Devireddy. The Effect of Various Freezing Parameters on the Immediate Post-Thaw Membrane Integrity of Adipose Tissue Derived Adult Stem Cells. Biotechnology Progress, 21: 1511-1524 (2005).

membrane integrity most adversely and establish optimal thermal conditions for ASCs cell freezing storage. A two-level, four-parameter (2^4) full factorial design was implemented to calculate the individual and interaction effects of all thermal parameters (Box et al., 1978; Hynsjo et al., 1995; Smith et al., 1999; Moffat 1985; Moore and McCabe 1993; Guilak et al., 2005). ASCs cell suspensions were frozen in the presence of dimethylsulfoxide (DMSO), arguably the most commonly used chemical as a cryoprotective agent (CPA). Individual parameter effect values represent which parameters most significantly affect the post thaw membrane integrity, where as parameter interaction values reveal any coaction effect among all the parameters in determining the post thaw membrane integrity of ASCs cells at various passages. These observed results could be used as a basis for developing rational freezing storage of ASCs cells.

3.2 MATERIALS AND METHODS

3.2.1: Isolation, Collection and Culture of Adult Stem Cells

The isolation and culture of the ASCs were given in the chapter 2. Note that there is extensive data suggesting that these adherent ASCs exhibit multiple lineages when culture *in vitro* (Zuk et al., 2001; Zuk et al., 2002; Gimble and Guilak 2003; Awad et al., 2004; Mizuno et al., 2001; Gimble and Nuttall 2004; Safford et al., 2002; Hicok et al., 2004). A recent study by Guilak et al., (2005) shows with the aid of histological and biochemical analyses that pools of human ASCs cells can exhibit multiple differentiated phenotypes under appropriate *in vitro* culture conditions (briefly, 52% of the ASCs cells clones differentiated into two or more lineages; with more clones expressing osteoblasts, chondrocytes and neuron-like cells than adipocytes). Thus, there is clear evidence that the adherent cells cultured from stromal

vascular fraction exhibit “stem cell” behavior, and are termed as human adipose derived adult stem (ASCs) cells, in the present study.

3.2.2: Freeze/Thaw Experiments

All freezing protocols were carried out on all passages of ASCs cells using a programmable controlled rate-freezing (CRF) machine (Planer Series Kryo 560-16, TS Scientific, Perkasie, PA). The samples were loaded into a 6-well cell culture cluster (Corning Incorporated, Corning, USA). Before freezing, the cell suspensions were gently mixed with 10% DMSO as a cryoprotective solution (CPA), i.e. a one-step addition of CPA. The samples were equilibrated in the cryoprotective solution for ~10min before the freezing experiments were performed. The cluster was then loaded into the cryo-machine (which was precooled to 4 ^{o}C) and kept for 1 min for equilibration. The samples were then cooled at a predetermined CR to a predetermined ET and HT. Extracellular ice nucleation was observed visually and almost always occurred in the sample solution at ≥ -6 ^{o}C (i.e. the supercooling was always sufficient to drive ice nucleation). In the rare instance that ice nucleation did not occur spontaneously, a chilled metallic needle at -196 ^{o}C was inserted into the supercooled sample solution to facilitate the formation of extracellular ice. As the CRF machine we used was limited to a controlled thawing/warming rate of 40 ^{o}C/min, the thawing rate 200 ^{o}C/min was obtained by removing the 6-well cluster from the CRF machine and quickly bringing the bottom of the cluster into contact with a warm water bath maintained at 37 ^{o}C.

The accuracy of the CRF (and the thawing rate obtained by placing the cluster in a warm water bath) was verified by measuring the temperature in the well plates, using type-T hypodermic needle thermocouples (Omega Technologies, Stamford, CT, USA). Thermocouple

voltages were read by a precision temperature data logger (Veriteq Instruments Inc, Richmond, BC, Canada) and transferred to a personal computer for further reduction and data analysis. The cooling rates imposed by the CRF was within 5% for cooling rates of ≤ 10 ^{o}C/min and within 10% for the highest cooling rates of 40 ^{o}C/min. Similarly, we found that the thawing rate obtained by placing the cluster in the warm water bath was within 5% of 200˚C/min.

3.2.3: Cell Membrane Integrity Measurements

The membrane integrity assay was based on cell membrane integrity of post-thaw ASCs cells. This type of assay takes advantage of the ability of healthy cells with uncompromised cytoplasmic membrane integrity to exclude dyes such as trypan blue (English et al., 1979; Jackson et al., 1992). The control and frozen/thawed samples were incubated for 15 min and then stained with trypan blue solution (Sigma Chemical Co., St. Louis, MO, USA). After staining, the samples were placed on a microslide, coverslipped, and analyzed under a light microscope (Nikon Instruments Inc. Melville, NY, USA) at 10X magnification.

3.2.4: Statistical Analysis

As stated earlier, we proposed to implement a two-level, full factorial design to compare the individual and interaction effects of four different thermal parameters (CR, ET, HT and TR) on the post thaw membrane integrity of ASCs cells. A two-level, full factorial design consists of 2^k experiments where k is the number of factors each with a high and low value. In this context a factor is an experimental variable, and a result is the quantitative measure of the parameter of interest. In this approach, the effect of each parameter on the overall post thaw membrane integrity of ASCs cells during a freezing process can be individually identified. The relevant statistical effects of each parameter were estimated by comparing the results from all the

Table 3.1: High and low values of each parameter used to define the experimental matrix of freeze/thaw protocol.

Parameter	*Low Value*	*High Value*
Cooling rate (CR)	1 ^{o}C/min	40 ^{o}C/min
End temperature (ET)	-80 ^{o}C	-20 ^{o}C
Hold time (HT)	1 min	15 min
Thawing rate (TR)	10 ^{o}C/min	200 ^{o}C/min

experiments with the high value of a parameter to the results of all the experiments with the low value. Any synergy between two, three or more parameters in determining membrane integrity outcome was revealed through calculation of interaction effects. Detailed explanation of these calculations will be given in the 'data analysis' section. The two levels (lower and higher level) of the four parameters (CR, ET, HT and TR) were chosen in such a way that they enclosed all parameter values possible in a typical freezing process obtainable in a commercially available controlled rate freezer (Table 3.1). Note that the actual magnitude for the high and low values selected for these parameters in the present study is somewhat subjective (for example, the CRF is capable of obtaining controlled cooling rates as low as 0.1 ˚C/min and thawing rates as low as 0.1 ˚C/min). However, choosing a lower limit on the cooling rate than 1 ˚C/min would have meant cooling ASCs cells for an inordinate amount of time (to get to –80 ˚C while cooling at 0.1 ˚C/min would have meant allocating over 13 hours and to get to –160 ˚C would have taken longer than a day). Additionally we tried to include in our range of parameters with some practical considerations in mind (for example we chose –80 ˚C as the

high ET as this is the temperature that is most commonly used in clinical settings and our choice of 40 ˚C/min as the high cooling rate is based on the engineering approximation of this being the highest value achievable in a large scale industrial setting while freezing samples that are in multiples of milliliters, i.e. reasonably large sized samples). For three parameter ranges the design can be represented, graphically, by a three-dimensional observation space as shown in Fig 3.1 (Smith et al., 1999). As we have four parameter ranges in our experimental design, the three parameters CR, ET and HT were depicted in a three dimensional space where as the variation in fourth parameter TR was shown as two separate three dimensional spaces, one for low value of TR and other for high value of TR as shown in Fig 3.1.

Each corner of the parameter space represents the mean of the experimental results of each combination of factors. There are a total of $2^4 = 16$ experimental protocols each of which is one point in the design matrix. A center point protocol (average of high and low values) was also included in the design matrix to determine the nonlinearity of the membrane integrity dependence on four parameter ranges studied. The statistical effects were found by comparing the different corners of the space. These effects include the relative effects of individual parameters on ASCs cell membrane integrity and as well as two factor interaction effects and higher order interaction effects (three and four parameter interactions) among various parameters on ASCs cell membrane integrity. The ASCs cells were exposed to all freeze/thaw conditions described by each of these corner points and after each experiment the cell membrane integrity was measured under microscope and the mean membrane integrity values were then used to determine the various effects of all four thermal parameters studied.

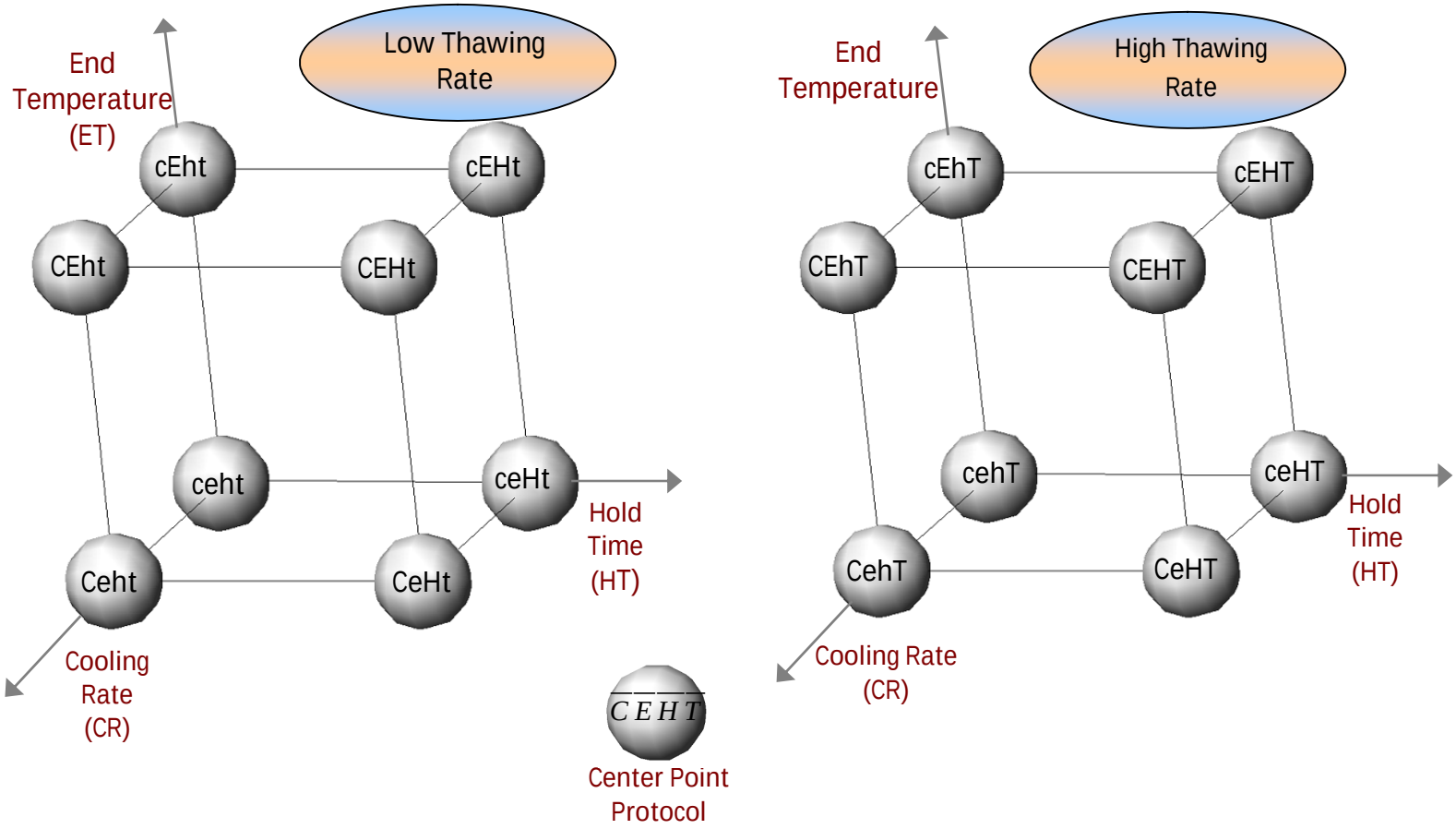

Figure 3.1: Diagram of the three dimensional experimental matrix for ASCs membrane integrity over high and low values of four thermal parameters, namely cooling rate (CR), end temperature (ET), hold time (HT) and thawing rate (TR). Variation in three parameters (CR, ET and HT) is shown in three-dimensional space whereas the variation in the fourth parameter, TR, is shown as a separate three-dimensional space for each level of TR. Each parameter is indicated using the first letter of its designation and the high and low values of each parameter are designated by upper and lower case letters respectively. The overscore bar on each parameter in the center point protocol represents average of high and low values of that parameter.

3.2.5: Data Analysis

By using the formulation described in Box et al., (1978), and procedures used by Smith et al., (1999), all the parameter effects were calculated using the membrane integrity data from all experimental protocols. The statistical effects of each parameter were found by comparing the results from all of the experiments with the high value of a parameter to the results of all of the experiments with the low value. The main effect of each parameter was calculated from the mean of the membrane integrity data obtained from eight experimental protocols in which high value of that parameter was used minus mean of the membrane integrity data obtained from eight protocols in which low value of that parameter was used. The main effect of a parameter determines the average effect of that parameter over all conditions of the other variables. As an example, calculation of CR effect is shown in Equation 1 and is geometrically represented in Fig 3.2A.

$$E_{CR} = \frac{1}{8}(Ceht + CEht + CehT + CeHt + CEhT + CeHT + CEHt + CEHT) - \frac{1}{8}(ceht + cEht + cehT + ceHt + cEhT + ceHT + cEHt + cEHT) \quad (1)$$

where E_{CR} represents the average effect of cooling rate (Smitha et al., 1999). Each four letter combination of (*c or C)*, *(e or E)*, *(h or H)*, and (*t or T)* represents one of the 16 average membrane integrity measurements in the experimental matrix. Note that the high and low values of parameters are distinguished by the use of capital and lower case letters respectively. For example, the term '*CehT*' represents the average membrane integrity for cells exposed to the high CR (40 ^{o}C/min), low ET (-80 ^{o}C), low HT (1 min), and high TR (200 ^{o}C/min). All other remaining individual parameter effect values were also determined in a similar manner.

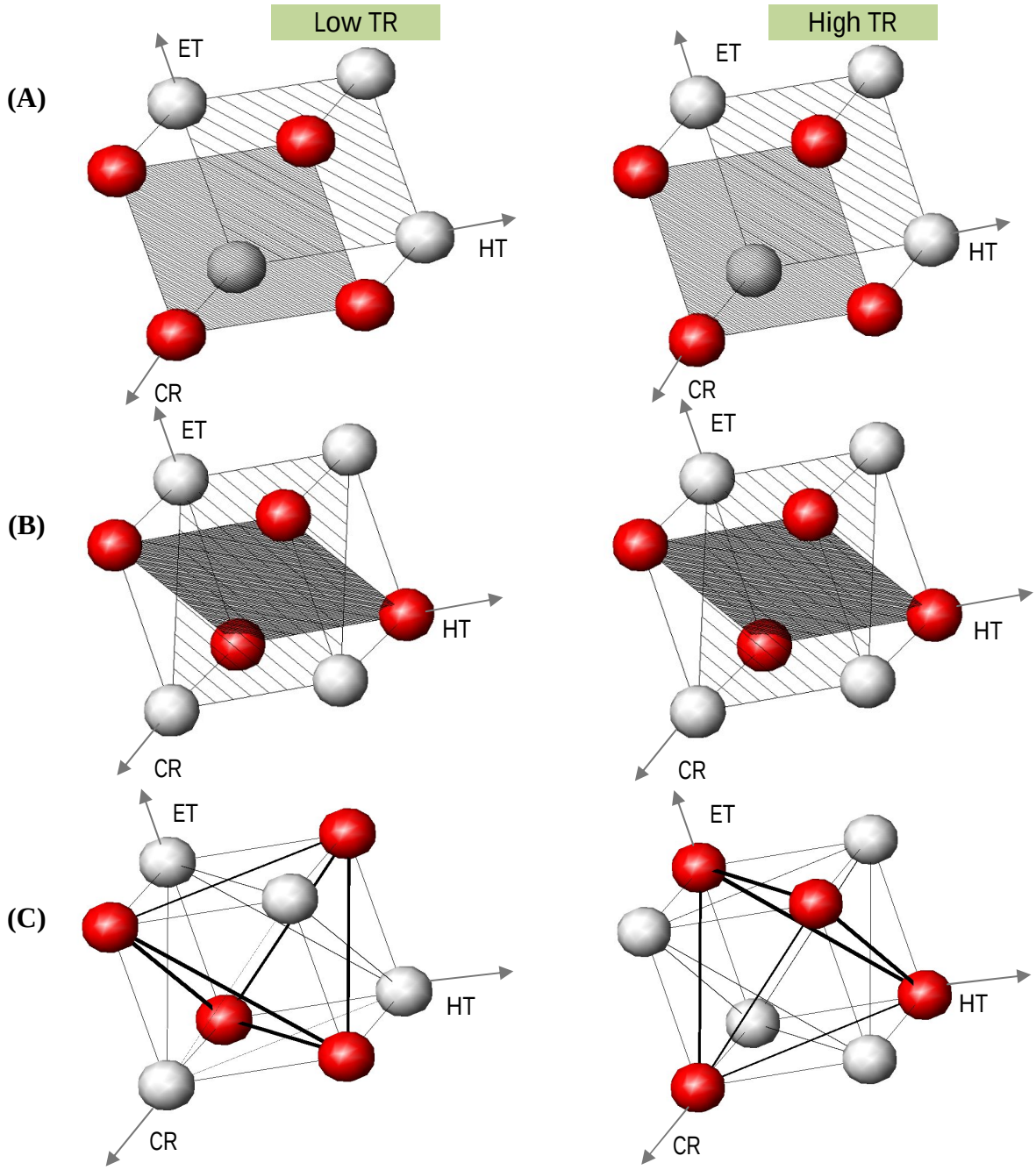

Figure 3.2: Geometric representation of main effects and two and three interactions effects. Main effects are represented as a contrast between results on parallel faces (Fig 3.2A), 2 parameter interactions as a contrast between results on diagonal faces (Fig 3.2B) and finally the 3 parameter interactions are represented as a contrast between results on two tetrahedral in each three dimensional space (Fig 3.2C). The effects can be computed as the difference between two averages of eight experimental membrane integrity values: (1/8)*$\sum$ ● values - (1/8)*$\sum$O values. Calculation of the 'cooling rate' effect (E_{CR}) is shown in (Fig 3.2A), 'cooling rate - end temperature' interaction effect (I_{CR-ET}) is shown in (Fig 3.2B) and the 'cooling rate-end temperature -hold time' interaction effect ($I_{CR-ET-HT}$) is shown in (Fig 3.2C).

Following Box et al., (1978), two or more parameter interaction effects were also determined. The two parameter interaction effect is the average difference between the effect of one parameter at the high and low level of a second parameter; for example the interaction between CR and TR is the average difference between the effect of CR at the high level of TR and the effect of CR at the low level of TR. Therefore, like the main effect the interaction effect is also a difference between two averages. An example, calculation of CR and TR effect is shown in Eq 2 and is geometrically represented in Fig 3.2B.

$$I_{CR-TR} = \frac{1}{8}(CehT + CeHT + CEHT + CEhT + cEHt + cEht + ceHt + ceht) - \frac{1}{8}(Ceht + CeHt + CEHt + CEht + cEHT + cEhT + cehT + ceHT) \quad (2)$$

where I_{CR-TR} represents the cooling rate-thawing rate interaction value. In a similar manner higher order interaction can also be determined (Box et al., 1978). Note that all interaction effect values are symmetric, i.e. $I_{CR-TR} = I_{TR-CR}$. Thus for a 4 parameter experimental model there are 6 distinct parameter interactions (as listed in Table 3.3). The relative magnitude of interaction effects show which parameter most significantly affects the cell membrane integrity in the parameter range investigated.

The three parameter interaction effect is the average difference between the interaction effect of any two parameters at the high and low level of a third parameter; for example the interaction between CR, ET and HT is the average difference between the effect of CR-ET interaction (I_{CR-ET}) at high and low levels of HT. As an example, calculation of CR-ET-HT interaction effect is shown in Equation 3 and is geometrically represented in Fig 3.2C.

$$I_{CR-ET-HT} = \frac{1}{8}(Ceht + cEht + ceHt + CEHt + CehT + cEhT + ceHT + CEHT) - \frac{1}{8}(CeHT + CeHt + CEhT + CEht + cEHT + cEHt + ceht + cehT) \quad (3)$$

where '$I_{CR-ET-HT}$' represents the cooling rate-end temperature-hold time interaction value. As before the three parameter interaction effects are also symmetric in all the variables. Finally, the four-parameter interaction effect can be determined in a similar manner explained above. The interaction between four parameters CR-ET-HT-TR is the average difference between the effect of CR-ET-HT interaction ($I_{CR-ET-HT}$) at the high and low values of TR and is given by the following equation as:

$$I_{CR-ET-HT-TR} = \frac{1}{8}(ceht + CEht + CeHt + cEHt + CehT + cEhT + ceHT + CEHT) - \frac{1}{8}(Ceht + cEht + ceHt + cehT + CEHt + CEhT + CeHT + cEHT) \quad (4)$$

where '$I_{CR-ET-HT-TR}$' represents the cooling rate-end temperature-hold time-thawing rate interaction value.

As experiments inherently have errors, e.g., due to instrumentation, data acquisition limitations, and facility and environmental effects, it is necessary to estimate the variations in the membrane integrity data due to these experimental errors, which are referred to as uncertainties. The variations in the membrane integrity data to these experimental uncertainties were determined with the calculation of minimum significant parameter effect. Any individual or interaction effect value must be greater than this minimum value to be considered as significant parameter effect value. The minimum significant parameter effect can be calculated using the formula (Smith et al., 1999; Moffat 1988; Moore 1993),

$$\mu_E = ts\sqrt{\frac{2}{mk}} \tag{5}$$

where, μ_E is the minimum significant parameter value, t is the t-statistic for a given confidence interval from Student's t-distribution as specified by giving the number degrees of freedom (as described below), s is the pooled standard deviation for all the experimental protocols, m is the number of levels of each parameter raised to the power of number of parameters minus 1 and is equal to $2^{4-1} = 8$, and k is the number of repeated experiments for each protocol and is equal to 3.

The total number of degrees of freedom for the whole set of experimental protocols in design matrix is the degrees of freedom for each protocol times total number of protocols in the parametric design. The total number of protocols was 17 (16 experimental protocols from all combinations of four thermal parameters with a high and low value plus one center point protocol) and the degrees of freedom for each protocol was 2. Thus, the number of degrees of freedom for the whole set of experimental protocols was 34. Note that the t value also depends upon the chosen confidence level (either 99%, 95% or 90%). It is to be noted that, the minimum significant parameter interaction values μ_I are same as μ_E, because both values are computed using the same membrane integrity values (Moffat 1985).

Non-linear dependence of cell membrane integrity on thermal history was assessed with the calculation of of curvature (CV) as described in Moore and McCabe (1993) and Smith et al., 1999. The curvature (CV) was computed by the following equation:

$$CV = \frac{1}{16}\begin{pmatrix} ceht + CEht + CeHt + cEHt + CehT + cEhT + \\ ceHT + CEHT + Ceht + cEht + ceHt + cehT + \\ CEHt + CEhT + CeHT + cEHT \end{pmatrix} - \overline{CEHT} \tag{6}$$

where 'CV' is the curvature value and $\overline{C}\,\overline{E}\,\overline{H}\,\overline{T}$ is the membrane integrity value for the center point protocol. The minimum significant curvature values can be calculated using student's t-distribution in a similar way described earlier for the calculation of μ_E. The minimum significant curvature value, μ_C is computed by using the formula:

$$\mu_C = ts\sqrt{\frac{1}{mk}+\frac{1}{z}} \tag{7}$$

The parameters t, s, m, k are same as for equation 5 and 'z' is the number of repeated experiments (z=3) for the center point protocol. If the value of CV is not equal to μ_C then there is a nonlinear dependence between post-thaw membrane integrity of ASCs and the thermal parameters. The μ_E (or μ_I) along with the curvature (CV) for all passages of ASCs as computed from the post-thaw membrane integrity data is given in Table 3.5.

3.3 RESULTS AND DISCUSSION

The results of the post thaw membrane integrity of P0 cells are summarized in a three-dimensional space arrangement as explained in the previous section (Fig 3.1) and are shown in Fig 3.3. The membrane integrity data at each corner points of the parameter space is normalized to the percentage of initial (or unfrozen control) membrane integrity of the suspended ASCs. The results, within the range of parameters studied, showed a variation in percentage membrane integrity of P0 cells from a minimum of 47.1% at the high CR of 40 ^{o}C/min and at low values of the other three parameters ET, HT and TR (i.e. for the protocol *Ceht*) to a maximum of 97% at the slow CR of 1 ^{o}C/min and at the high ET, high HT and low TR (i.e. for the protocol *cEHt*). Although, the difference in membrane integrity between *cEHt* and *ceht* is statistically not significant (97% vs. 96.3%). A close observation of the data reveals that

as long as the cooling rate is at its lower value, other parameters have little effect ($< \pm$ 8%) on post thaw membrane integrity of P0 ASCs cells.

Individual parameter effect (E) values for P0 cells are calculated from Eq 1 (as described under Materials and Methods) and are given in Table 3.2 and Fig 3.8. The parameter effect represents the average effect of that parameter over all conditions of the other variables. Note that a high positive value of E indicates a strong correlation between increased post-thaw membrane integrity and an increase in the parameter while a low negative value indicates a decrease in post-thaw membrane integrity while the value of the parameter is increased (for example: The E_{CR} value of –18.3% in Table 3.1 for P0 cells indicates that there is a decrease in post-thaw membrane integrity of 18.3% of the cells while the CR increases from 1 to 40 ˚C/min; similarly E_{ET} of 15.72% implies that the average membrane integrity of P0 cells increases by 15.72% when the ET is increased from –80 ˚C to –20 ˚C).

The minimum significant parameter effect (μ_E) values for P0 cells at various confidence levels, CLs (99.0%, 95.0% and 90.0%) are calculated from Equation 5 and are given in Table 3.5. At 99% CL the μ_E for P0 cells was 3.4%, which indicates a possible variation of 3.4% in membrane integrity outcome between any two freezing protocols could be solely because of experimental uncertainties. So any parameter effect less than this value cannot be considered as statistically significant parameter with 99% CL. Of all the parameter effect values for P0 cells only CR (E_{CR} = -18.27%) and ET (E_{ET} = 15.72%) have significant effect (with 99% CL) on P0 ASCs membrane integrity as their values

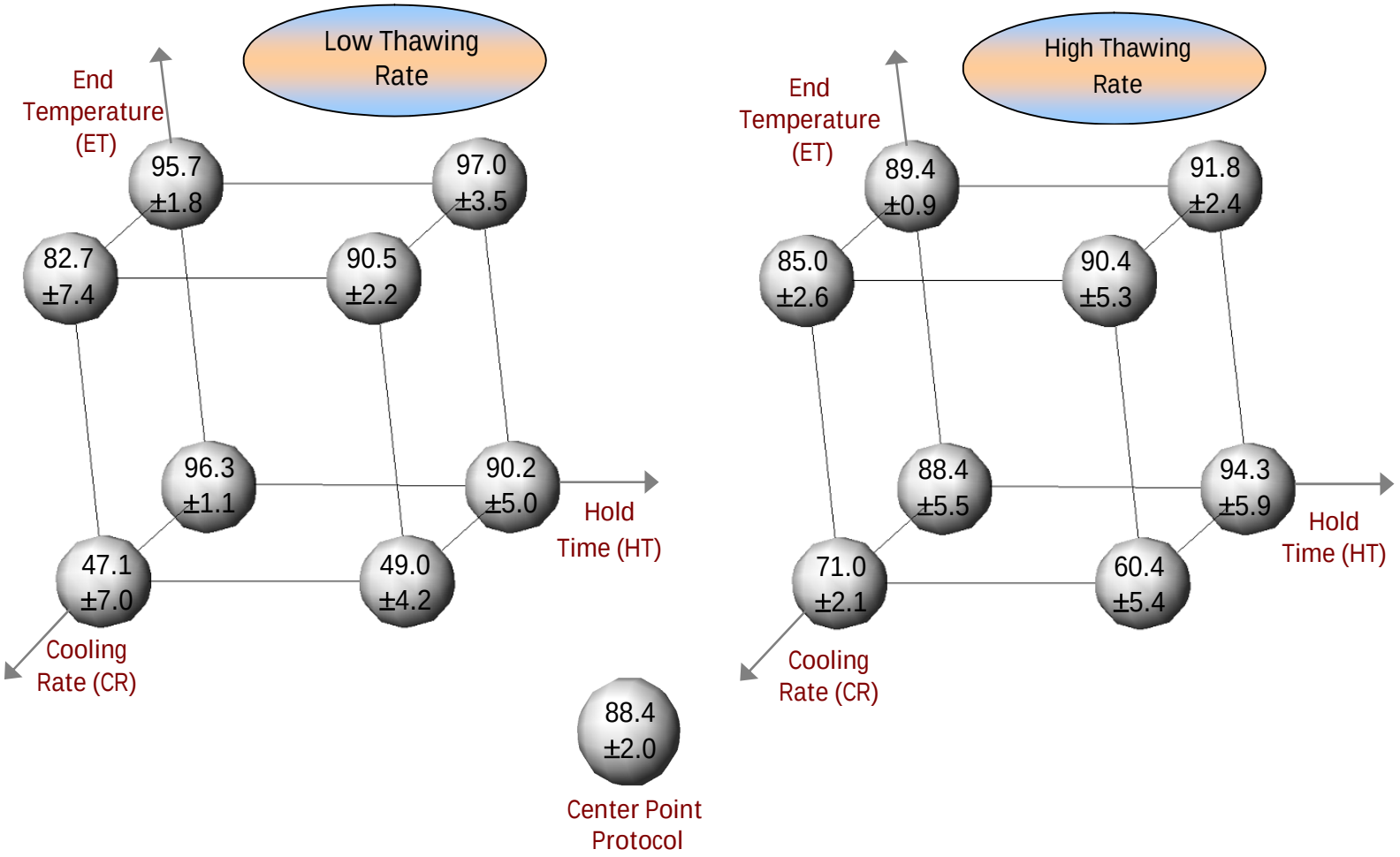

Figure 3.3: Membrane integrity data of Passage 0 (P0) of ASCs exposed to all the freezing protocols in the experimental matrix. Post-thaw membrane integrity values are normalized to control (or unfrozen) cell membrane integrity. The average and standard deviation are given for each protocol in the design matrix.

Table 3.2: Parameter effects and total curvature values calculated from the membrane integrity results and by using equations (1) and (6).

Cell Type	*Cooling Rate Effect (E_{CR})*	*End. Temp. Effect (E_{ET})*	*Hold Time Effect (E_{HT})*	*Thawing Rate Effect (E_{TR})*	*Curvature (CV)*
P0	-18.27% [a]	+15.72% [a]	0.99%	2.75% [b]	-5.9%
P1	-9.56% [a]	+10.00% [a]	0.90%	2.37% [c]	2.3%
P2	-9.64% [a]	+13.87% [a]	-2.74% [c]	3.60% [b]	2.0%
P3	-16.73% [a]	+12.10% [a]	-4.18% [a]	-3.18% [a]	-4.9%
P4	-8.86% [a]	+9.96% [a]	-4.07% [b]	-18.11% [a]	-1.2%

Table 3.3: Two parameter interaction effects calculated from the membrane integrity results and by using equation (2).

Cell Type	I_{CR-ET}	I_{ET-HT}	I_{CR-HT}	I_{ET-TR}	I_{CR-TR}	I_{HT-TR}
P0	14.55% [a]	3.24% [b]	0.14%	-5.09% [a]	6.60% [a]	-0.23%
P1	10.02% [a]	-2.0%	3.20% [b]	1.75%	2.54% [b]	-8.34% [a]
P2	9.40% [a]	2.34% [c]	-0.04%	-1.41%	8.30% [a]	-2.04%
P3	11.68% [a]	2.12% [c]	-0.68%	-4.83% [a]	7.42% [a]	-4.06% [a]
P4	13.95% [a]	-3.48% [c]	2.81%	-4.68% [b]	2.06%	1.30%

For Tables 3.2 and 3.3

- [a]: Significant at 99.0% confidence level
- [b]: Significant at 95.0% confidence level
- [c]: Significant at 90.0% confidence level

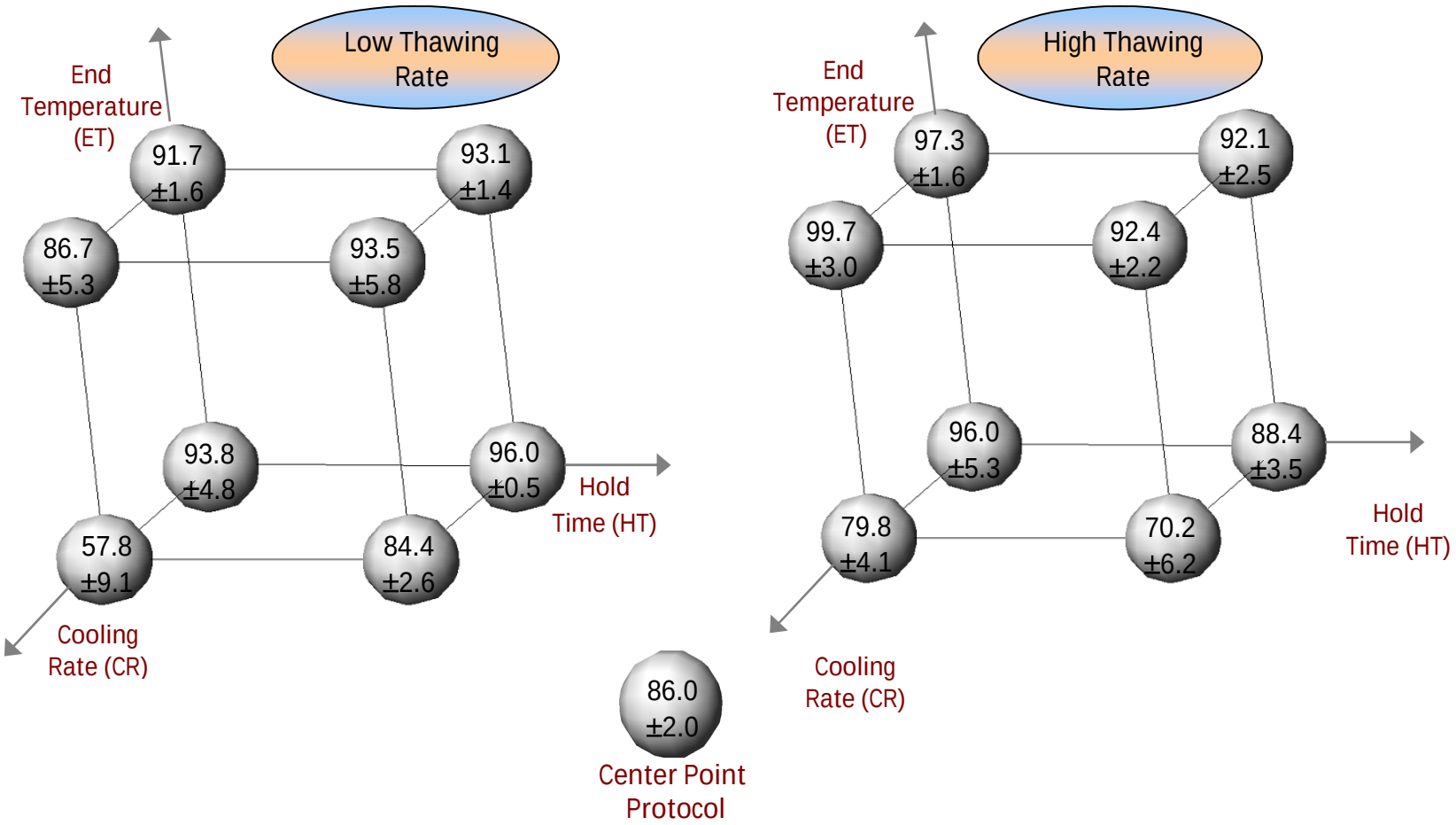

Figure 3.4: Membrane integrity data of Passage 1 (P1) of ASCs exposed to all the freezing protocols in the experimental matrix. Post-thaw membrane integrity values are normalized to control (or unfrozen) cell membrane integrity. The average and standard deviation of the membrane integrity results are given for each protocol in the design matrix.

are greater than μ_E (μ_E for 99% CL is 3.4%) – as shown in Fig. 3.8 and Table 3.2. The E_{TR} is significant at only 95% CL while E_{HT} is not significant even at a confidence level of 90% (see Table 3.2).

The multi-parameter interaction effect (I) values for P0 cells are calculated using Equations 2, 3, and 4 respectively and are given in Tables 3.3 & 3.4 (and Figs. 3.9 and 10). The value of each interaction between any two parameters is defined as the average difference in effect of one parameter due to a change in other parameter. For example, $I_{CR\text{-}ET}$ value of 14.55% implies that, the average change in P0 ASCs cell membrane integrity caused by reducing CR is further increased by 14.55% if the ET is increased from its lower value to higher value. Similarly, $I_{CR\text{-}ET\text{-}HT}$ value of 2.25% implies that the average change in membrane integrity caused by $I_{CR\text{-}ET}$ is further increased by 2.25% if HT is increased from 1 to 15 min. As stated earlier, $\mu_I = \mu_E$ for all confidence levels and any interaction effect below this value is statistically insignificant and can be disregarded. Among the six two parameter interactions, three interactions CR-ET ($I_{CR\text{-}ET}$ =14.55%), ET-TR ($I_{ET\text{-}TR}$ = -5.1%) and CR-TR ($I_{CR\text{-}TR}$ = 6.6%) have a significant impact on P0 ASCs cell membrane integrity with 99% CL (μ_I = 3.4%). The interaction effect between ET-HT ($I_{ET\text{-}HT}$ = 3.2%), is significant at 95% CL (μ_I = 2.5%). The remaining two interactions CR-HT ($I_{CR\text{-}HT}$ = 0.1%) and HT-TR ($I_{HT\text{-}TR}$ = 0.2%) are not significant even at a confidence level of 90% (μ_I = 2.1%) and can be accounted for experimental uncertainties. Similarly, from the data shown in Table 3.4 it is clear that with the exception of CR-HT-TR ($I_{CR\text{-}HT\text{-}TR}$ = 3.53%) all other three and four parameter interactions are statistically not significant at 99% CL for P0 ASCs cells (μ_I = 3.4%). However, the interactions between CR-ET-TR ($I_{CR\text{-}ET\text{-}TR}$ = 3.15%) and CR-ET-HT-TR ($I_{CR\text{-}ET\text{-}HT\text{-}TR}$ = 2.6%) are significant at 95% CL for P0 ASCs cells (μ_I = 2.5%). And finally among the remaining

Table 3.4: Three and four parameter interaction effects calculated from the membrane integrity results and by using equations (3) and (4)

Cell Type	*Three Parameter Interactions*				*Four parameter Interaction*
	$I_{CR\text{-}ET\text{-}HT}$	$I_{CR\text{-}ET\text{-}TR}$	$I_{CR\text{-}HT\text{-}TR}$	$I_{ET\text{-}HT\text{-}TR}$	$I_{CR\text{-}ET\text{-}HT\text{-}TR}$
P0	2.25%[c]	-3.15%[b]	-3.53%[a]	-0.11%	2.60%[b]
P1	-2.38%[c]	-0.75%	-4.23%[a]	3.15%[b]	2.37%[c]
P2	-2.25%	-6.63%[a]	2.81%[b]	1.81%	-0.98%
P3	2.77%[b]	-7.38%[a]	-6.11%[a]	0.07%	2.02%[c]
P4	1.83%	3.11%[c]	2.82%	-8.89%[a]	-0.33%

- [a]: Significant at 99.0% confidence level
- [b]: Significant at 95.0% confidence level
- [c]: Significant at 90.0% confidence level

multi-parameter interactions CR-ET-HT is significant at 90% CL while the interaction between ET-HT-TR is not significant even at 90% CL.

The curvature (CV) in the membrane integrity results of P0 cells was calculated by using Equation 6 and is equal to -5.9% (Table 3.2) which is lower than the calculated minimum significant curvature value (μ_C) of P0 ASCs cells at all CLs (Table 3.5). This suggests a nonlinear dependence of membrane integrity results on thermal history. This difference between CV and and μ_C indicates that measured membrane integrity of cells exposed to a thermal history defined by the midpoint protocol ($\overline{CEHT}$) deviates by ~5.9% from the predicted value

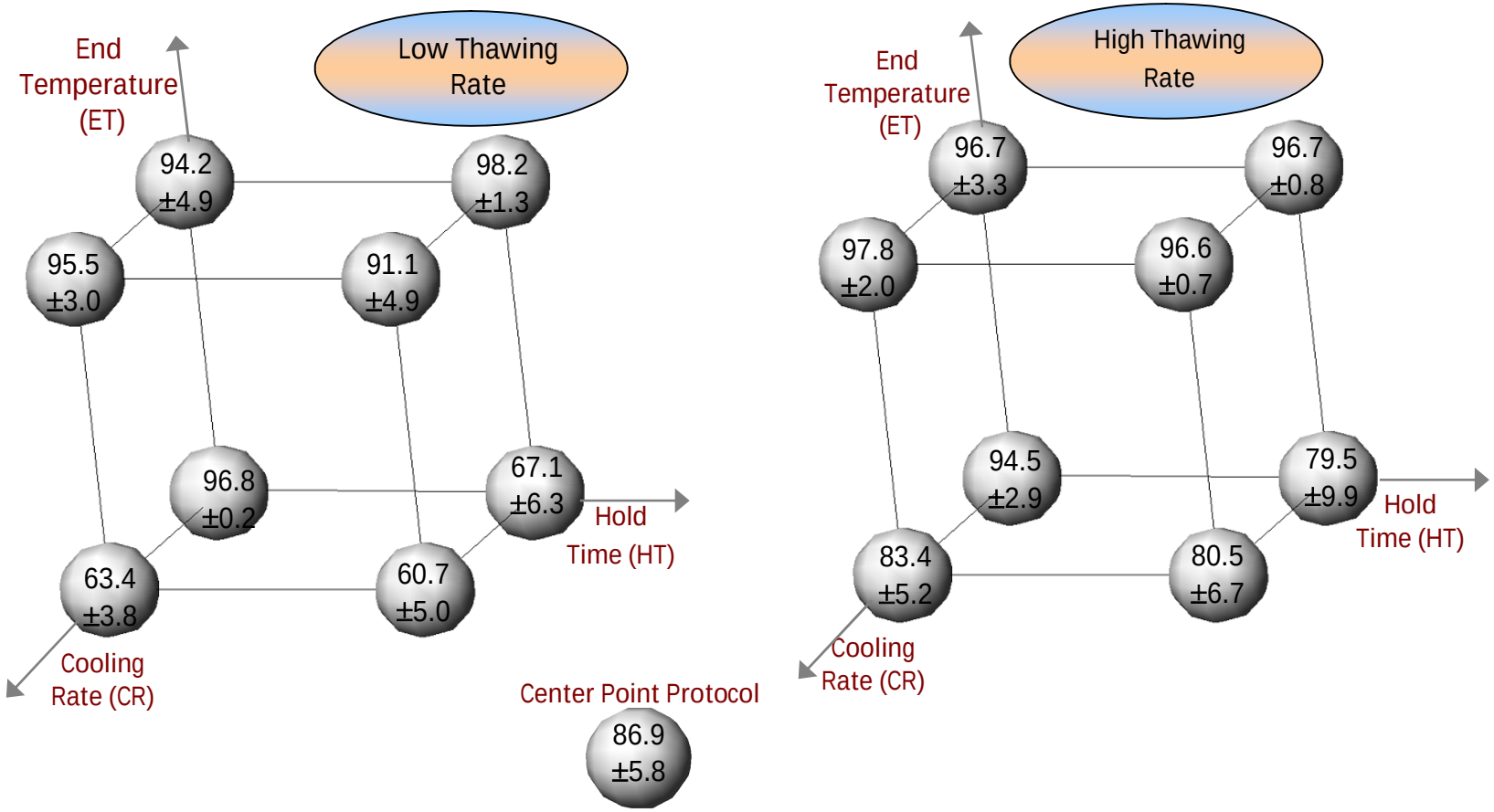

Figure 3.5: Membrane integrity data of Passage 2 (P2) of ASCs exposed to all the freezing protocols in the experimental matrix. Membrane integrity values are normalized to control (or unfrozen) cell membrane integrity. The average and standard deviation of the membrane integrity results are given for each protocol in the design matrix

obtained by a linear interpolation of all the other membrane integrity results for P0 ASCs (Smith et al., 2007).

The results of the post thaw membrane integrity of P1 cells are summarized in a three-dimensional space arrangement as shown in Fig 3.4. The results showed a variation in percentage membrane integrity of P1 cells from a minimum of 57.8% at high CR of 40 ^{o}C/min and at lower values of other three parameters (*Ceht*) to a maximum of 99.7% at high CR and at high ET, low HT and high TR (*CEhT*). A very similar membrane integrity outcome of 97.3% is observed at low CR, high ET, low HT and high TR (*cEhT*). The corresponding E and μ_E (or μ_I) values for P1 cells are given in Table 3.2 and Table 3.5 respectively. At 99% CL the μ_E for P1 cells was 3.3%. Of all the individual parameter effect values for P1 cells, only CR (E_{CR} = -9.56%) and ET

Table 3.5: Minimum significant parameter values and minimum significant curvature values calculated from the membrane integrity results and by using equations (5) and (6) for several confidence levels (CLs)

Cell Type	*Minimum Significant Parameter Value (μ_E or μ_I)*			*Minimum Significant Curvature Value (μ_C)*		
	99.0%	*95.0%*	*90.0%*	*99.0%*	*95.0%*	*90.0%*
P0	3.4%	2.5%	2.1%	7.1%	5.3%	4.4%
P1	3.3%	2.5%	2.1%	7.0%	5.2%	4.4%
P2	3.7%	2.8%	2.3%	7.9%	5.9%	4.9%
P3	3.0%	2.2%	1.9%	6.3%	4.7%	3.9%
P4	4.9%	3.6%	3.0%	10.3%	7.7%	6.4%

(E_{ET} = 10.0%) have significant effect with 99% CL (as shown in Fig. 3.8) while TR is in effect with only 90% confidence level and HT is statistically not significant even at a confidence level of 90%. For P1 cells, only CR-ET ($I_{CR\text{-}ET}$ =10.02%), and HT-TR ($I_{HT\text{-}TR}$ =-8.34%) are statistically significant with 99% CL (μ_I = 3.3%). All other interactions, with the exception CR-TR and CR-HT at a confidence level of 95%, are not statistically significant and have no effect on P1 ASCs cell membrane integrity (Table 3.3).

Similarly, with exception of the multi-parameter interaction between CR-HT-TR, all the other higher order interactions are not significant at a confidence level of 99% CL (Table 3.4 and Fig. 3.10). Although, by lowering the confidence level to 95%, we find that the interaction between ET-HT-TR is significant and by lowering the confidence level further to 90% we find that the interactions between CR-ET-HT and CR-ET-HT-TR are significant as well. And finally, the curvature (CV) in the membrane integrity results of P1 ASCs cells is equal to 2.3% (Table 3.2) and is lower than 'μ_C' of P1 cells at all CLs. Thus, suggesting a nonlinear dependence of membrane integrity results of P1 cells on the four thermal parameters within the experimental range.

Figs 3.5 and 3.6 show the membrane integrity data of P2 and P3 ASCs cells, respectively. Within the range of the themal parameters investigated, the variation in the percentage membrane integrity of P2 ASCs cells is from a minimum of 60.7% for the protocol *CeHt* to a maximum of 97.8% for the protocol *CEhT*, whereas the membrane integrity of P3 ASCs cells is from a minimum of 48.6% for the protocol *Ceht* to a maximum of 97.4% for the protocol *ceht*. A very similar membrane integrity outcome of P2 ASCs cells is also observed for protocols *cEhT* (96.7%), *CEHT* (96.6%), *cEHT* (96.7%) and *ceht* (96.8%). The corresponding E and

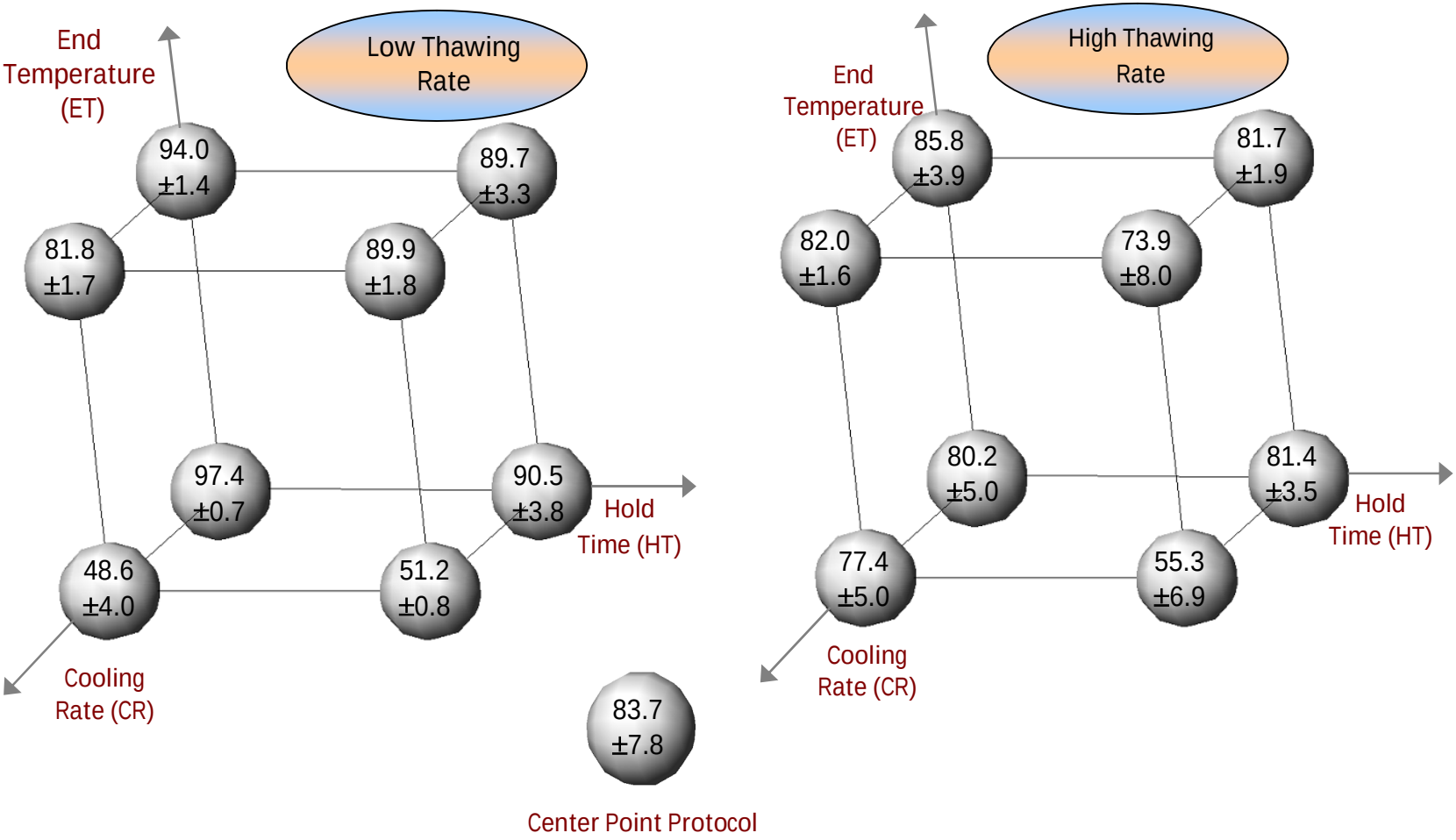

Figure 3.6: Membrane integrity data of Passage 3 (P3) of ASCs exposed to all the freezing protocols in the experimental matrix. Post-thaw membrane integrity values are normalized to control (or unfrozen) cell membrane integrity. The average and standard deviation of the membrane integrity results are given for each protocol in the design matrix.

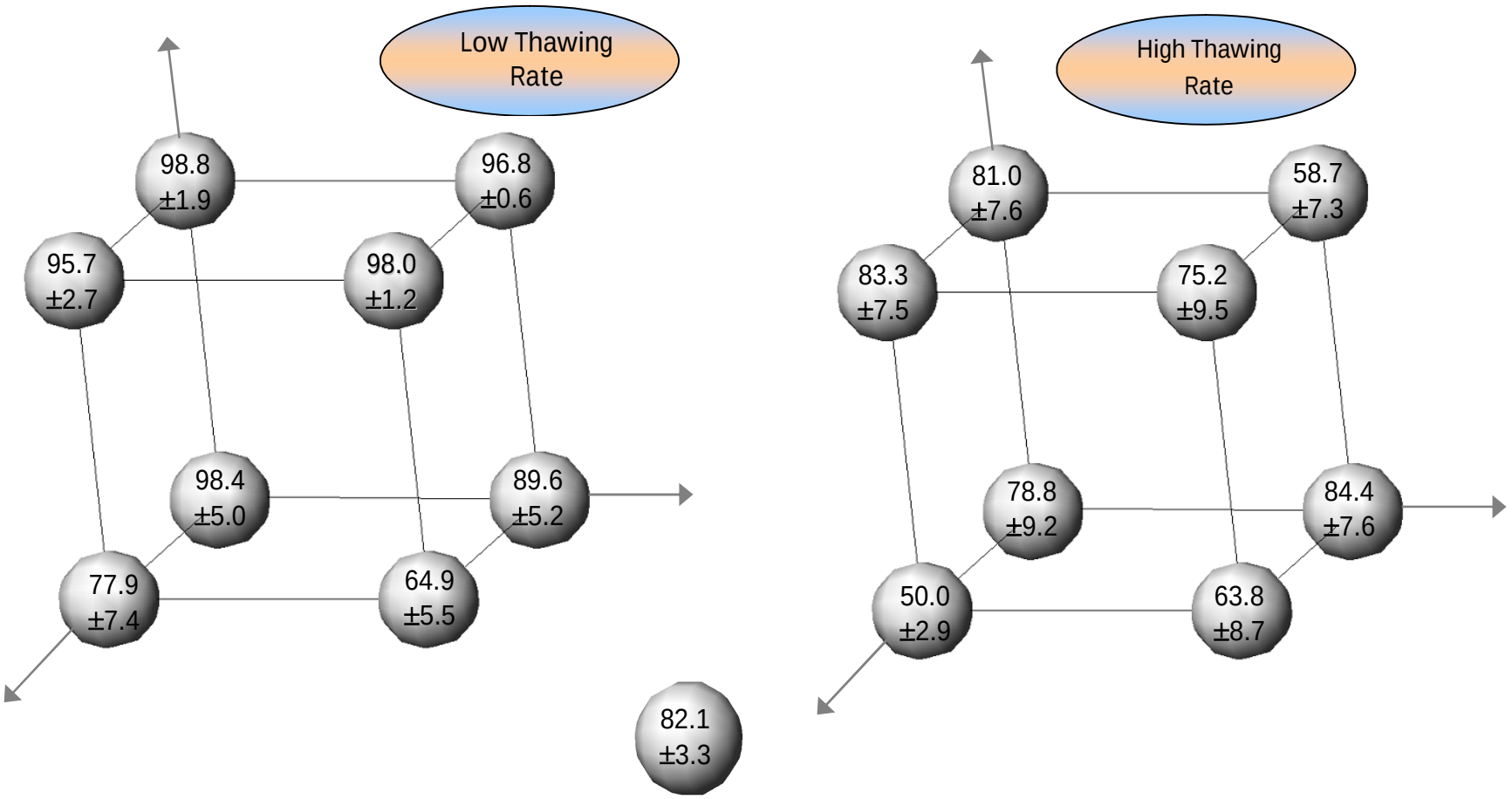

Figure 3.7: Membrane integrity data of Passage 4 (P4) of ASCs exposed to all the freezing protocols in the experimental matrix. Post-thaw membrane integrity values are normalized to control (or unfrozen) cell membrane integrity. The average and standard deviation of the membrane integrity results are given for each protocol in the design matrix.

μ_E values for P2 and P3 ASCs cells are given in Tables 3.2 and 3.5 respectively. At 99% CL, the μ_E for P2 cells is 3.7% and for P3 cells it is 3.0%. Both CR (E_{CR} = -9.64%) and ET (E_{ET} = 13.87%) have a significant effect on P2 ASCs cell membrane integrity while CR (E_{CR} = -16.73%), ET (E_{ET} = 12.10%), HT (E_{HT} = -4.18%), and TR (E_{TR} = -3.18%), all have a statistically significant effect on P3 ASCs cell membrane integrity (Table 3.2 and Fig. 3.8).

The multi-parameter interaction effect (I) values for both P2 and P3 cells are given in Table 3.3 & 3.4 and the corresponding μ_I values are shown in Table 3.5. For P2 ASCs cells, among the 2 parameter interactions, CR-ET ($I_{CR\text{-}ET}$ =9.4%), and CR-TR ($I_{CR\text{-}TR}$ = 8.3%) are significant at 99% CL while ET-HT is statistically significant with only 90% CL. Among the higher order interactions, $I_{CR\text{-}ET\text{-}TR}$ (with 99% CL) and $I_{CR\text{-}HT\text{-}TR}$ (with 95% CL) are the only ones that show any significant effect on P2 ASCs cell membrane integrity. Whereas in case of P3 cells, four out of the possible six two parameter interactions are significant at 99% CL, CR-ET, ET-TR, CR-TR and HT-TR, as shown in Table 3.2 and Fig. 3.8. While among the higher order interactions, both CR-ET-TR and CR-HT-TR are significant at 99% CL for P3 ASCs cells, as well. The curvature (CV) values of P2 and P3 cells are equal to 2.0% and –4.9% and are lower than their corresponding μ_C values at all CLs. Thus, suggesting a nonlinear dependence of membrane integrity results of P2 and P3 ASCs cells on all the thermal parameters studied.

And finally, the post thaw membrane integrity results of P4 ASCs cells are represented in Fig 3.7. The results showed a variation in membrane integrity from a minimum of 50% for protocol *CehT* to a maximum of 98.8% for protocol *cEht*. Also, membrane integrity with more than 98% is observed with two more protocols in the design, *CEHt* (98.0%) and *ceht* (98.4%). The P4 ASCs cell membrane integrity is significantly impacted by 3 out of the 4 individual

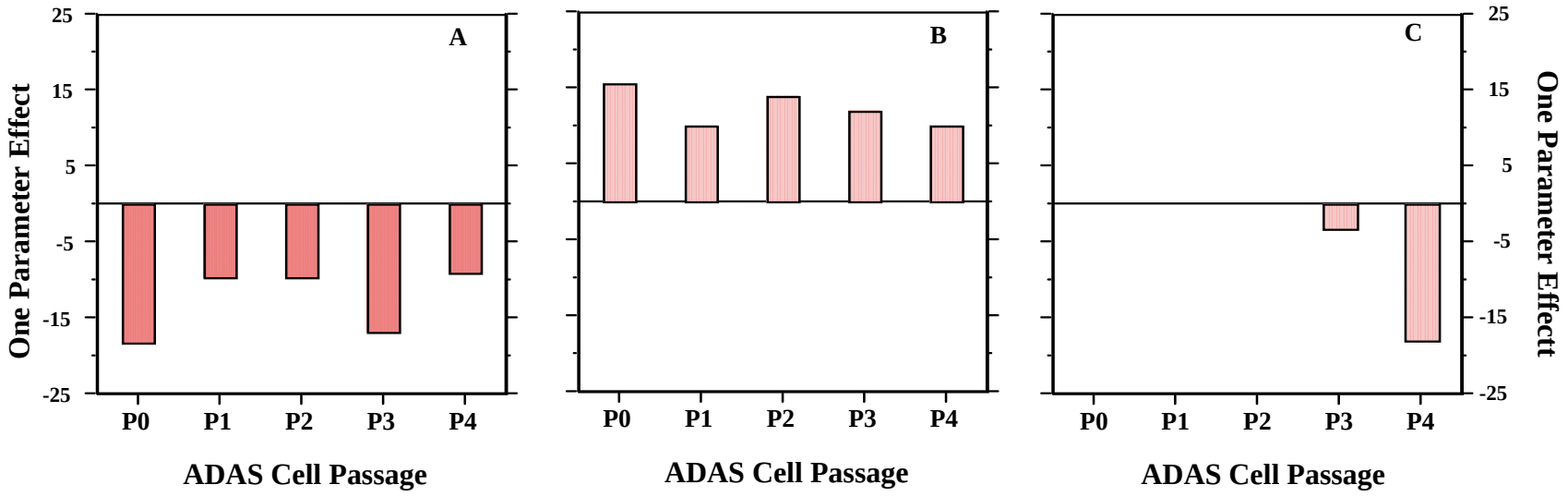

Figure 3.8: A comparison of the single parameter effect for various passages of ASCs (note that the all values shown are significant at a confidence level of 99%). Figs, 3.8AA, 3.8BB and 3.8C correspond to E_{CR}, E_{ET} and E_{TR}, respectively (Equation 1 and Table 2). To simplify the figure, we chose not to represent E_{HT} which is only significant for P3 ADAS cells (see Table 3.2). Also, as shown in Fig. 3.8C, the effect of thawing rate (E_{TR}) is not significant for either P0 or P1 or P2 ADAS cells. The ASCs passage number is shown on the X-axis while the individual parameter effect value is shown on the Y-axis.

parameters, CR, ET and TR with 99% CL (see Table 3.2 and Fig 3.8) while the effect of HT is also significant albeit a lower confidence level of 95% (see Table 3.2). Interestingly, it is observed that TR has a maximum negative effect (E_{TR} = -18.11%) on P4 ASCs cell membrane integrity and while the ET has the maximum positive effect (E_{ET} = 9.96%). Among the higher order interactions, the only significant interactions with 99% CL are the CR-ET (I_{CR-ET} =13.95%) and ET-HT-TR ($I_{ET-HT-TR}$ = -8.89%) – see Tables 3.3 and 3.4 and Figs 3.9 and 3.10. However, the interactions between ET-TR and ET-HT are significant at lower confidence levels of 95% and 90% respectively (Table 3.3). As before, there is a nonlinear dependence of membrane integrity results of P4 ASCs cells on the four thermal parameters investigated (CV is less than μ_C at all confidence levels).

As mentioned earlier, at 99% CL only the parameters CR and ET have significant effect on post thaw membrane integrity of all passages of ASCs cells. For all passages, the increase in CR has a deleterious effect whereas increase in ET has a beneficial effect on post thaw membrane integrity. This observation is further corroborated by the membrane integrity data shown in Figs 3.3 to 3.7, i.e. at the high value of the parameter ET (-20 ^{o}C) the post thaw membrane integrity is “high” at both the high and low values of the parameter CR (1 and 40 ^{o}C/min). While at the low value of ET (-80 ^{o}C) the post thaw membrane integrity is “high” at only the low value CR (1 ^{o}C/min). Also, a “low” post thaw membrane integrity is seen in Figs. 3.3 to 3.7 at high CR and at low ET values suggesting that within the range of parameters investigated, freezing of all ASCs cell passages using rapid cooling rates (40 ^{o}C/min) to lower end temperatures (-80 ^{o}C) is not advantageous.

As seen in Table 3.2 (and Fig. 3.8), the effect of ET and CR on all ASCs cell passages studied are all significant with confidence level (CL) of 99%. However, the effect of TR is significant (at 99% CL) for P3 and P4 ASCs cells while the effect of HT is significant (also at 99% CL) for P3 ASCs cells (Table 3.2 and Fig. 3.8). Even though both HT and TR have a considerable

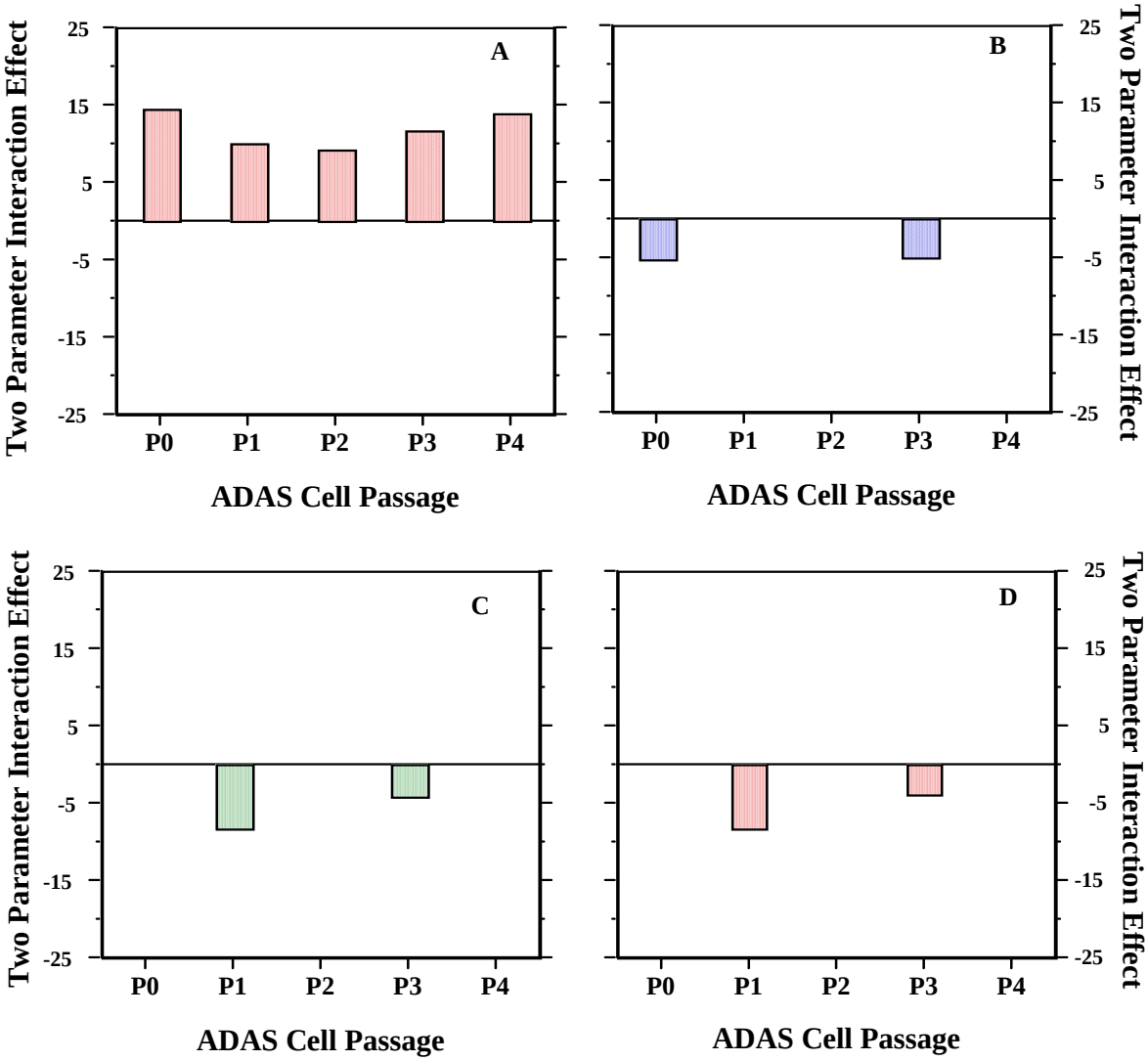

Figure 3.9: A comparison of the two parameter interaction effect for various passages of ASCs (note that the all values shown are significant at a confidence level of 99%). Figs, 3.9A, 3.9B, 3.9C and 3.9D correspond to $I_{CR\text{-}ET}$, $I_{ET\text{-}TR}$, $I_{CR\text{-}TR}$ and $I_{HT\text{-}TR}$ respectively (Equation 2 and Table 3). Note that the other two-parameter interaction effects $I_{ET\text{-}HT}$ and $I_{CR\text{-}HT}$ are not significant at 99% confidence level for any of the ADAS cell passages, investigated (see Table 3.3). The ADAS cell passage number is shown on the X-axis while the individual parameter effect value is shown on the Y-axis.

effect on the post thaw cell membrane integrity of P3 cells, their relative magnitude is small (by a factor of 3 to 4) when compared to the corresponding effect of CR and ET (Fig 3.8). Similarly, it is also quite clear from the data shown in Table 3.2, at 99% CL, that TR and HT have no significant effect on the post thaw membrane integrity of either P0 or P1 or P2 ASCs cells.

The results also showed a significant variation in parameter effects among all passages of ASCs cells (Table 3.2 and Fig 3.8). For example, there is a significant difference in E values between P0 and P1 ASCs cells for CR and ET (decreasing CR for P0 ASCs cells increases the post-thaw cell membrane integrity by ~18% while a similar decrease in CR for P1 ASCs cells only increases the post-thaw cell membrane integrity by ~9%). It is also important to note that the effect of lowering CR seems to have a similar effect on P0 and P3 ASCs cells (E_{CR} being ~16 to 18%) and on P1, P2 and P4 ASCs cells (E_{CR} being ~9 to 10%). However the effect of ET on all the passages of ASCs cells seems to more uniform than CR (E_{CR} varies from ~9 to 18% while E_{ET} varies only from ~10 to ~15% across all passages of the ASCs Cells). Based on the results shown in Table 3.2 and Fig 3.8, it is clear that the most significant increase in post-thaw cell membrane integrity on all the passages of ASCs cells can only be achieved by decreasing CR and increasing ET, with the exception of P4 ASCs cells (P4 cells exhibit the largest decrease in immediate post-thaw cell membrane integrity while TR is increased). This result is intriguing and we are unaware of any prior reporting such a relationship between CR, ET and post-thaw membrane integrity for any cell type. Of course, it is quite possible that the unique nature of our measurement, i.e. immediate post-thaw membrane integrity is responsible for this intriguing relationship. Further studies are clearly warranted to examine if this relationship is

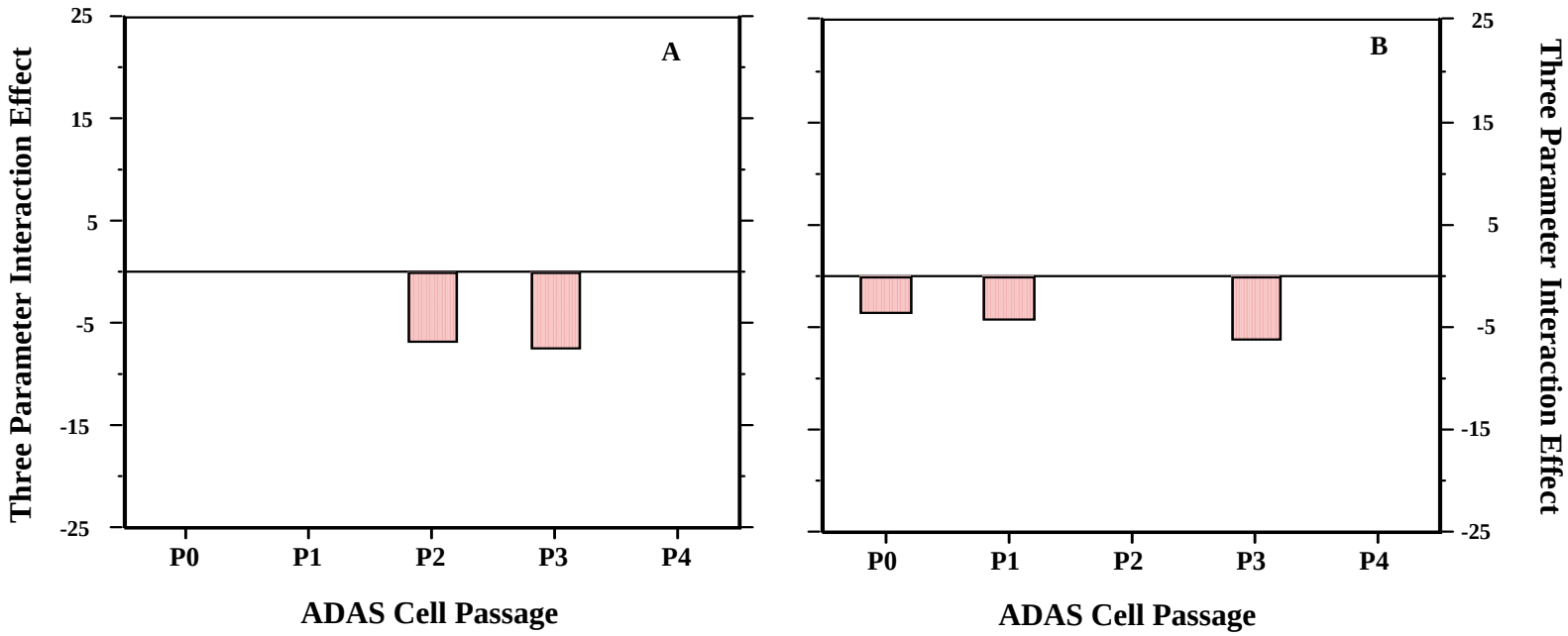

Figure 3.10: A comparison of the three parameter interaction effect for various passages of ASCs (note that the all values shown are significant at a confidence level of 99%). Figs, 3.10A and 3.10B correspond to $I_{CR\text{-}ET\text{-}TR}$ and $I_{CR\text{-}HT\text{-}TR}$ (Equation 3 and Table 4). Note that the other two three-parameter interaction effects $I_{CR\text{-}ET\text{-}HT}$ and $I_{ET\text{-}HT\text{-}TR}$ are not significant at 99% confidence level for any of the ADAS cell passages, investigated (Table 3.4) and neither is the four-parameter interaction effect, $I_{CR\text{-}ET\text{-}HT\text{-}TR}$ (Table 4). The ASCs passage number is shown on the X-axis while the individual parameter effect value is shown on the Y-axis.

unique to ASCs cells or a more general relationship for all cell types. Another observation that merits further study is the effect of TR on post thaw ASCs cell membrane integrity. It is typically accepted in the literature that increasing TR decreases recrystallization injury and hence increases post thaw cell membrane integrity (Mazur 1984). While this assertion is found to be valid for P0, P1 and P2 ASCs cells, both P3 and P4 cells show a decrease in post thaw membrane integrity with increasing TR. This result needs to be further investigated and suggests a) the TR required to minimize recrystallization or thawing injury in P3 and P4 ASCs cells is larger than the high TR (200 ˚C/min) chosen in the present study or b) P3 and P4 ASCs experience, contrary to accepted wisdom, increasing recrystallization injury with increasing TR.

The significant interaction effects between CR and ET for all ASCs cell passages shown in Table 3.3 (and Fig 3.9), further support the argument that CR and ET are the critical parameters in determining the post thaw membrane integrity of ASCs cells. As shown in Table 3.3, the average change in post thaw membrane integrity caused by reducing CR is further increased by 9 to 15% for all ASCs cell passages if ET is increased from –80 to –20 ˚C, i.e. the parameter $I_{CR\text{-}ET}$ varies from ~9% to 15%. At 99% CL, the increase in TR has a damaging interaction with decrease in ET for P0, and P3 ASCs cells and a beneficial interaction with decrease in CR for P0, P2 and P3 ASCs cells (Table 3.3). An increase in TR coupled with a decrease of HT is also found to decrease the post thaw cell membrane integrity of P1 and P3 ASCs cells. Thus, a complex interaction is present between post thaw cell membrane integrity and the 4 thermal parameters.

To further delineate the complex interactions among CR, ET, HT and TR on the post thaw cell membrane integrity of ASCs cells, the multi-parameter interaction shown in Table 3.4

need to be analyzed. As shown in Table 3.4 (and Fig 3.10), the interaction among the 4 parameters is not significant even at 90% CL for P2 and P4 ASCs cells, while it is significant at 90% CL for P1 and P3 ASCs cells and significant at 95% CL or P0 ASCs cells. At 99% CL, the interactions among CR, ET and TR are significant only for P2 and P3 cells, while the interactions among CR, HT and TR are important for P0, P1 and P3 cells (note that no other multi-parameters interactions are significant at 99% CL, i.e. only 6 interactions are significant out of the 25 shown in Table 3.4). Although, reducing the confidence level to 90% does increase the number of significant multi-parameters interactions to 16 out of 25 (as shown in Table 3.4).

An examination of the multi-parameter interactions shown in Table 3.4 (Fig 3.10) reveals that each passage has only one significant interaction at 99% CL (with the exception of P3 ASCs cells) – for P0 and P1 this interaction is among CR-HT-TR, while for P2 this interaction is among CR-ET-TR, while for P3 this interaction is among CR-ET-TR and CR-HT-TR and finally for P4 cells this interaction is among ET-HT-TR. Note that the interaction effect among CR-ET-HT is not significant at 99% CL for any of the cell passages (the only 3 parameter interaction that is not significant for even one passage of ASCs cells). This result is quite intriguing, as the effect of CR-ET was found to be significant for all cell passages (Table 3.3) and suggests that HT seems to be the least significant of the 4 thermal parameters investigated in the present study (in the range chosen for each parameter). It is possible that increasing HT from 15 min to hours or even days might result in a decrease in post thaw cell membrane integrity for P2, P3 and P4 cells (note that these cells have a negative E_{HT}; see Table 3.2) and an increase in the post thaw cell membrane integrity of P0 and P1 cells (note these cells have a positive E_{HT}; see Table 3.2). However, further studies are clearly needed. It is also important to note that the results in the

present study are obtained during freezing of ASCs cells in the presence of 10% DMSO as a cryoprotectant (CPA). Future studies are clearly needed to understand the effect of choice and concentration of CPAs (for example, glycerol, methanol are other commonly used CPAs) on the post thaw cell membrane integrity of ASCs cells as well as extending the hold time to days or weeks (from the 15 minutes used in the present study).

3.4 CONCLUSIONS

In conclusion, this study is a first attempt to understand and delineate the various complex interactions between thermal parameters during a freezing process and post thaw cell membrane integrity of ASCs cells at various passages. Depending on the passage of ASCs cells, different thermal parameters are found to significantly impact the measured post-thaw cell membrane integrity. The results obtained in the present study will form the basis for a rigorous and rational design of optimal freezing protocols for ASCs cells, in

CHAPTER 4
FREEZING AND POST-THAW APOPTOTIC BEHAVIOR OF CELLS IN THE PRESENCE OF PALMITOYL NANOGOLD PARTICLES[1]

4.1 INTRODUCTION

Successful cryo-therapeutic procedures for biological cells and tissues will impact a wide range of human endeavors, including assisted reproductive techniques, cancer recovery and rehabilitation procedures, organ storage and transplantation processes and conservation of endangered species.

The aim of the present study is to examine the potential cryobiological applications of commercially available nanoparticles, NPs (Palmitoyl Nanogold®, Nanoprobes, Yaphank, NY). Gold NPs have been widely used for analytical and biomedical applications for many years. For an excellent review of gold nanoparticles and their applications, the interested reader is referred to Daniel and Astruc (Daniel and Astruc 2004). Palmitoyl gold nanoparticles have been used to label and visualize lipid vesicles and cell membranes (Brewer et al., 2004) yet their direct effect on membrane permeability and thus cryostability remains unknown. The palmitate functionality on these nanoparticles may serve as an anchor to membranes similar to the fatty acylated domains of amphitrophic proteins that regulate membrane function (Resh 1999). In addition to specific chemistries, the heat conducting aspects of metallic nanoparticles have been shown to influence targeted freezing in cryosurgical procedures (Yu et al., 2005). Because the modes of cryoprotectant action can vary from alteration of physical properties of

[1] This chapter was published in the following citation: S. Thirumala, J.M Forman, W.T. Monroe and R.V. Devireddy. Freezing and Post-Thaw Apoptotic Behavior of Cells in The Presence of Palmitoyl Nanogold Particles. Nanotechnology. 18: 195104 (2007). IOP Publishers (www.iop.org/journals/nano)

the freezing media to the direct changes in the cell membrane properties, we presumed that NPs could act as benign replacement for toxic organically based CPAs.

During freezing of cells in suspensions, ice forms initially in the extra-cellular space. Depending on the imposed cooling rate, the two main biophysical processes during freezing will then occur: i.) cellular dehydration associated with the loss of intracellular water, or ii.) intracellular ice formation (IIF) associated with the nucleation of ice crystals within the intracellular space. Water transport has been extensively investigated in single cells using standard cellular microscopy (Diller 2005) and more recently, a differential scanning calorimetric (DSC) technique (Devireddy et al., 1998; Thirumala et al., 2003; Thirumala et al., 2005).

In the present study, we utilized the DSC technique to assess the water transport response during freezing of HeLa and Jurkat cells with and without NPs. These two cell lines were chosen as examples of an adherent (HeLa) and a suspension (Jurkat) cell, each of which is well-characterized, widely used, and commonly frozen in various laboratories. In the interest of completeness, we also present water transport responses during freezing of these cells in the presence of DMSO, a commonly used CPA. By fitting a well established model of water transport to the measured water transport response we determined the membrane permeability (water transport) parameters during freezing of HeLa and Jurkat cells in the absence of CPAs, in the presence of DMSO and in the presence of NPs. The experimentally determined membrane permeability parameters were incorporated into a recently developed generic optimal cooling rate equation (Thirumala and Devireddy 2005) and used to predict the optimal cooling rates for cryopreservation of the two cell types studied. Based on the predicted

optimal cooling rates, three cooling rates were chosen to investigate the post-thaw behavior of HeLa and Jurkat cells frozen and thawed in the presence and absence of DMSO and NPs.

There exists substantial evidence in literature that 'apoptosis' could be a possible contributing factor in cryopreservation failure. For example, it has been reported that apoptotic cell death occurs in cells exposed to subfreezing temperatures (Mathew 1997; Hollister 1998). Therefore, in addition to analyzing the immediate post-thaw survival, we have also analyzed the post-freeze apoptotic response of the HeLa cells (for reasons, described later, Jurkat cells were not used in these apoptotic studies). Post thaw experiments were based on propidium iodide (PI)-uptake and the detection of the early apoptosis event, phosphatidylserine (PS) translocation (Koopman 1994) using a flow cytometric annexin V apoptosis assay (Pena et al., 2003).

4.2 THEORETICAL BACKGROUND

A model for water and solute transport in response to chemical potential gradients based on irreversible thermodynamics has been proposed by Kedem and Katchalsky that consist**s** of two differential equations which describe the water and CPA flux across the membrane (Kedem and Katchalsky 1958). If the flux of CPA is negligible in comparison to the flux of water**,** and assuming that water is essentially the only species transported at subzero temperatures, the Kedem-Katachalsky model reduces to a water transport model, as proposed by Mazur (Mazur 1963) and later modified by Levin et al. (Levin et al., 1976). The water transport model of Mazur can be further modified to incorporate the presence of CPAs as:

$$\frac{dV_w}{dT} = -\frac{L_p ART}{Bv_w}\left[\ln\left(\frac{(V_{cell}-V_b)-(n_s v_s + n_{cpa}v_{cpa})}{(V_{cell}-V_b)-(n_s v_s + n_{cpa}v_{cpa})+v_w(\psi_s n_s + n_{cpa})}\right)-\frac{\Delta H_f}{R}\left(\frac{1}{T_R}-\frac{1}{T}\right)\right] \quad (1)$$

where R is the universal gas constant; V_{cell} is the cell volume; V_b is the osmotically inactive cell volume; A is the constant cell surface area; T is the absolute temperature; T_R is the reference temperature (273.15 K); B is the cooling rate (°C/min); v_w is the molar specific volume of water; v_{cpa} is the specific molar volume of CPA; n_{cpa} is the number of moles of CPA; ψ_s is the dissociation constant for salt in water (=2); n_s is the number of moles of salt initially inside the cell; ΔH_f is the latent heat of fusion of water; L_p is the permeability of the plasma membrane to water. The permeability of the plasma membrane to water, L_p, is assumed to be a function of temperature and concentration of solute, CPA and water, and is given as (Levin 1976):

$$L_p = L_{pg}(cpa)\exp\left(-\frac{E_{Lp}(cpa)}{R}\left(\frac{1}{T}-\frac{1}{T_R}\right)\right) \quad (2)$$

where $L_{pg}(cpa)$ is the permeability of the cell membrane to water at T_R = 273.15K; and $E_{Lp}(cpa)$ is the apparent activation energy for the process. Model assumptions include membrane-limited transport, with negligible temperature and pressure differentials across the plasma membrane, the external solution in equilibrium with extracellular ice, and an approximately ideal internal solution (Devireddy et al., 1998; McGrath 1998, Smith et al., 1998; Toner 1993).

4.3 MATERIALS AND METHODS

4.3.1: Culture and Isolation of HeLa and Jurkat Cells

HeLa cells (human epithelial carcinoma cells, American Type Culture Collection) were maintained in 25-cm^2 flasks (BD Falcon, Franklin Lakes, NJ) with 5 mL of Dulbecco's Modified

Eagle's medium-reduced serum (DMEM-RS) supplemented with 3% fetal bovine serum (FBS) and incubated at 37 ºC in a humidified atmosphere containing 5% CO_2. Jurkat T lymphocyte cells (E6.1, ATCC) were maintained in 25-cm^2 flasks (BD Falcon, Franklin Lakes, NJ) with 5 mL of HyQ® RPMI-1640-reduced serum medium (RPMI-RS) supplemented with 3% fetal bovine serum (FBS) and also incubated at 37 ºC in a humidified atmosphere containing 5% CO_2. HeLa cells were plated at a density of 80,000 cells/cm^2 in 12-well culture plates (BD Falcon, Franklin Lakes, NJ) and were allowed to adhere and grow for 24 hours prior to trypsinization (0.25% trypsin) and resuspension in Opti-MEM® serum-free medium for differential scanning calorimeter (DSC) and controlled rate freezer (CRF) experiments. Opti-MEM was chosen as a reduced protein medium for cell treatments to minimize potential for NP-serum protein interactions that could block potential cryobiological effects. Jurkat cells were resuspended in Opti-MEM to a density of ~1x10^6 cells/mL in 12-well culture plates (BD Falcon, Franklin Lakes, NJ) for treatment prior to being transferred to sterile eppendorf tubes for the DSC and CRF experiments.

Six separate DSC water transport experiments were conducted for HeLa and Jurkat cells in the absence of any CPAs, in the presence of a permeating CPA, dimethylsulfoxide (DMSO; 10%, v/v) and in the presence of NPs (Palmitoyl Nanogold) for incubation times of either 5 min or 180 min. While 180 min is longer than a typical CPA pre-freeze treatment, this extended incubation of nanoparticles and cells was chosen to ensure their complete association, based on typical durations for nanogold labeling procedures (Hainfeld and Powell 2000). All samples used in the experiments had concentration of cells ranging from 0.5 to 1 x 10^6 cells/ml.

For DSC experiments in the absence of CPAs, HeLa cells were washed, harvested by trypsinization, concentrated by centrifugation at 400× g for 5 min, re-suspended to ~20 µl in

Opti-MEM and placed on ice. For DSC experiments in the presence of CPA, cells were treated in an identical manner as above except that the cell pellet was resuspended in stock CPA solution (10% v/v DMSO; Irvine Scientific) and equilibrated for 10 min. Osmolarity of the CPA media was measured to be 1685 mOsm which includes ~1400 mOsm of DMSO (Vapro® Vapor Pressure Osmometer, Wescor Inc). And finally, for DSC experiments in the presence of NPs, 300 nanomoles of nanogold particles (Palmitoyl Nanogold®, Nanoprobes, Yaphank, NY) were first dissolved in 50µl of DMSO as DMSO is a commonly used organic solvent to enhance the solubility of hydrophobic nanoparticles in aqueous solutions (Balakin et al., 2006). The DMSO+NP mixture was then added to 50 ml of Opti–MEM to create a uniform stock solution containing 3.6 x 10^{15} nanoparticles/ml of Opti-MEM. The addition of DMSO to the Nanogold resulted in ~0.001% DMSO concentration in the final Opti-MEM+NPs solution and was presumed to have a negligible effect. For 3-hr NPs treatment, concentrated HeLa cells were re-suspended in the NPs solution and then plated in a 12-well for 3 hr in the incubator before harvesting for the DSC experiments. For the 5 min NPs treatment the concentrated cell pellet was re-suspended in NPs solution for 5 min before being used in the DSC experiments. The osmolarity measurements of the NPs solution ranged from 285 to 290 mOsm (Vapro Vapor Pressure Osmometer) and were essentially similar to the osmolarity measurements of Opti-MEM solution. This suggests that the presence of NPs did not change the osmolarity of the NPs freezing medium.

4.3.2: DSC Experiments

The DSC experiments to measure the water transport in HeLa and Jurkat cells were performed as reported in earlier studies on other cell systems (Diller 2005; Devireddy et al.,

1998; Thirumala et al., 2003; Thirumala et al., 2005a; Yuan and Diller 2001; Devireddy et al., 2004; Thirumala et al., 2006). Briefly, the heat release measurements of interest are Δq_{dsc} and $\Delta q(T)_{dsc}$, which are the total and fractional differences between the heat releases measured by integration of the heat flows during freezing of osmotically active (live) cells in media, $q_{initial}$ and during freezing of osmotically inactive (dead) cells in media, q_{final} (i.e. $\Delta q_{dsc} = q_{initial} - q_{final}$; $\Delta q(T)_{dsc} = q(T)_{initial} - q(T)_{final}$). This difference in heat release has been shown to be related to cell volume changes in several biological systems as:

$$V(T) = V_i - \frac{\Delta q(T)_{dsc}}{\Delta q_{dsc}} \cdot \left(V_i - V_e\right) \qquad (3)$$

The unknowns needed in Eqn. (3) apart from the DSC heat release readings are V_i (the initial cell volume) and V_e (the end or the final cell volume). The cell geometry and the inactive cell volume (V_b) of HeLa and Jurkat cells were determined at constant room temperature by using a light microscope (Nikon Eclipse TS100) equipped with METAVIEW software (see Results and Fig 4.1).

4.3.3: Biophysical Parameter Estimation

The biophysical parameters for water transport were then estimated using a non-linear regression algorithm as previously reported (Thiruamala et al., 2003; Thirumala et al., 2005; Thirumala et al., 2006). The experimentally measured water transport data at 20 ºC/min for both cell types were compared to theoretically predicted curves (Eqns. 1 and 2), and the biophysical parameters of water transport, L_{pg} and E_{Lp} (or $L_{pg}[cpa]$ and $E_{Lp}[cpa]$), were iteratively adjusted until the chi-squared variance, χ^2, was minimized (or a goodness of fit parameter R^2 was maximized: a value of 1 representing a perfect fit while a value of 0

represents a flawed fit) using a gradient search method as described in Bevington and Robinson (Bevington and Robinson 1994). All reported parameters were obtained for curve fits with a variance $\chi^2 < 10^{-3}$ or an $R^2 > 0.99$.

4.3.4: Theoretical Prediction of Optimal Cooling Rates

Thirumala and Devireddy (Thirumala and Devireddy 2005) reported that for a variety of biological systems a comparison of the published experimentally-determined values of B_{opt} (in ˚C/min) agreed quite closely with the value obtained using a Generic Optimal Cooling Rate Equation that defines:

$$B_{opt} = 1009.5 \bullet e^{(-0.0546 \bullet E_{Lp})} \bullet (L_{pg}) \bullet \left(\frac{A_c}{V_o - V_b} \right) \quad (4)$$

In this equation, L_{pg} and E_{Lp} (or $L_{pg}[cpa]$ and $E_{Lp}[cpa]$) represent the membrane permeability parameters (in μm/min-atm and Kcal/mole, respectively), while the last term $\left(\frac{A_c}{V_o - V_b} \right)$ (in μm^{-1}) represents the ratio of the available surface area for water transport (A_C) to the initial volume of intracellular water ($V_o - V_b$). Once the cell level parameters L_{pg} and E_{Lp} (or $L_{pg}[cpa]$ and $E_{Lp}[cpa]$) are determined using the curve-fitting procedure described above, we utilized Eqn. (4) to predict the optimal rates of freezing HeLa cells.

4.3.5: Freeze/Thaw Experiments

All reagents for cell culture were purchased from HyClone Laboratories, Inc. (Logan, UT), unless otherwise stated. Annexin V-FITC/PI kit was purchased from Molecular Probes (Eugene, Oregon). Staurosporine was purchased from CalBiochem (EMD BioSciences, Darmstadt, Germany). HeLa and Jurkat cell culture and treatments for freeze/thaw experiments were

same as mentioned previously for DSC experiments except that, after centrifugation, the cell pellet was resuspended in 0.5 mL of the appropriate cryopreservation or nanoparticle solutions in a 1.5 mL sterile eppendorf tube (USA Scientific, Ocala, FL) and were arranged on to a 1.5 ml tube rack (Stackarack for 1.5 ml tube, USA Scientific). All freezing experiments were carried out using a programmable controlled rate-freezing (CRF) machine (Planer Series Kryo 560-16, TS Scientific, Perkasie, PA). The tube cluster was loaded into the cryo-machine (which was precooled to 4 ºC) and kept for 1 min for equilibration. The samples were then cooled to an end temperature of –80 ºC at three freezing rates: 1 ºC/min, 22 ºC/min, and 34 ºC/min (these cooling rates were chosen based on the predicted optimal rates of cooling**;** see Table 4.1). Using the procedures described earlier by Thirumala et al. (Thirumala et al., 2005), the actual cooling rate imposed by the CRF on the sample was within 5% of 1 ºC/min and within 10% of 22 ºC/min and 34 ºC/min. Because the CRF machine used in this study was limited to a controlled thawing/warming rate of 40 ºC/min, the thawing rate 200 ºC/min was obtained by removing the tube rack from the CRF machine and quickly bringing the tubes into contact with a warm water bath maintained at 37 ºC (Thirumala et al., 2005, Thirumala et al., 2006).

The thawed samples were then centrifuged, re-suspended in appropriate culture media, and seeded in separate wells of a 12-well plate for an 18-hr incubation period at 37 ºC. Unfrozen cell controls of HeLa and Jurkat cells were also carried out for each experimental condition to determine if there were any cellular effects due to the 10% DMSO (10 min), 5-min NP, and 3-hr NP treatments alone. Following the treatment, the cells were resuspended in fresh medium and plated in a 12-well plate. After 18 hr, the unfrozen cell controls and the thawed samples were analyzed by brightfield mircroscopy and flow cytometry.

4.3.6: Brightfield Phase-Contrast Microscopy

Following the 18-hr recovery period, HeLa and Jurkat cells were imaged by brightfield phase-contrast microscopy at 20x magnification. Images were acquired with an inverted Eclipse TS100 Nikon fluorescence microscope and a CoolSnapFX camera (Photometrics, Tucson, AZ). Image processing was performed using MetaVue software (Universal Imaging Corporation, West Chester, PA).

4.3.7: Cell Viability and Apoptosis/Necrosis Assessment

A well-established annexin V apoptosis assay was analyzed by quantitative flow cytometry (Pena et al., 2003). This assessment was carried out only for HeLa cells, as the Jurkat cells treated in similar fashion to the HeLa cells exhibited significant adherence to the cell culture plate (see Results). As a chemically-induced apoptotic control, HeLa cells were incubated in fresh medium enriched with 0.25 μM staurosporine. For a necrotic control, HeLa cells were incubated for 18 hours in fresh medium with 2 mM hydrogen peroxide. The no-treatment control consisted of HeLa cells treated in fresh medium, free from inducing agents. For each treatment, detached and attached cells were pooled, harvested by trypsinization (0.25% trypsin), washed with 200 μL of culture medium, and resuspended in 100 μL of 1X annexin-binding buffer (included in annexin V-FITC/PI kit). 100 μL of HeLa cell suspension was mixed with 5μL of annexin-V-FITC and 1 μL of 100 μg/mL propidium iodide (PI) and incubated in the dark at room temperature for 15 minutes. Liquid volume was removed by centrifugation and aspiration, and the cells were resuspended by gentle vortexing in 300 μL of 1X annexin-binding buffer to be analyzed on the flow cytometer. Apoptosis analyses for HeLa cells were performed on a FACS Caliber flow cytometer (BD Biosciences, San Jose, CA) utilizing 488-nm

laser excitation and fluorescence emission at 530 nm (FL1) and >575nm (FL3). Forward and side scatter measurements were made using linear amplification, and all fluorescence measurements were made with logarithmic amplification. A total of 1,100 to 20,000 cells per sample were acquired using Cell Quest software (BD Biosciences, San Jose, CA), and data samples were analyzed using WinMDI 2.8 software (by Dr. J. Trotter, Scripps Institute, La Jolla, CA).

Apoptosis is characterized by phosphatidylserine (PS) translocation from the inner leaflet to the outer leaflet of the lipid bilayer, while the cell membrane remains intact. Annexin V-positive cells correspond to cells that have experienced PS translocation. PI staining of the cells indicates that the integrity of the cell membrane has been compromised and is used to distinguish living and early apoptotic cells from necrotic cells. The fluorescent dotplots show three cell populations: live (annexin V-FITC-negative/PI-negative), necrotic (annexin V-FITC-positive/PI-positive), and apoptotic (annexin V-FITC-positive/PI-negative). Quadrant analysis was performed on the gated fluorescence dotplot to quantify the percentage of live, necrotic, and apoptotic cell populations. The quadrant was placed according to the no treatment control and 2 mM H_2O_2 necrotic control (the representative reference dotplots with quadrants are shown in the "supplementary data").

4.3.8: Statistical Analysis

All values are indicated as mean ± SEM. Student's t-test was employed, with $p \leq 0.05$ considered to be significant. Each "n" replicate was composed of a single well and treatment in which 1,100 to 20,000 cell events were analyzed and each experiment was conducted in triplicate.

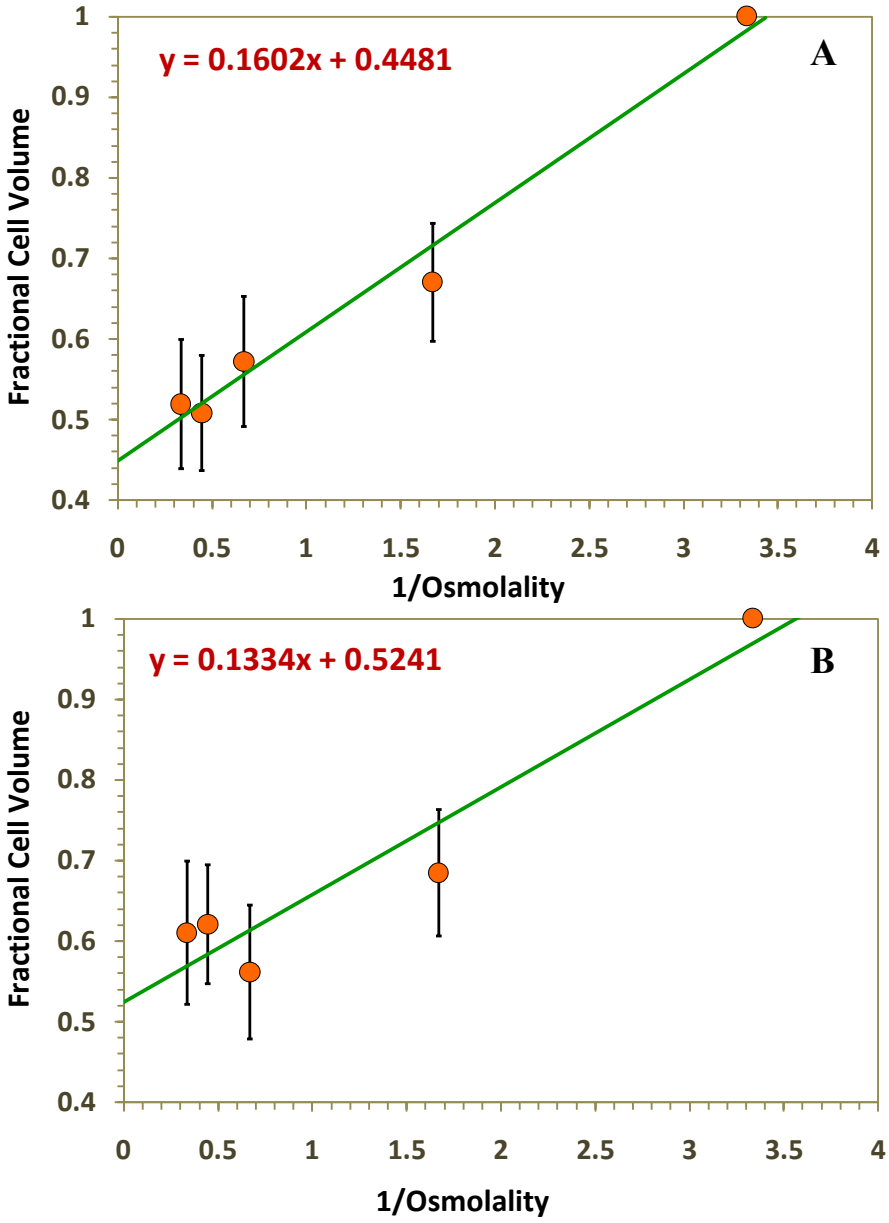

Figure 4.1: The Boyle-van't plot showing the resulting volume changes of the HeLa (Fig 4.1A) and Jurkat cells (Fig 4.1B) when the cells were exposed to several external osmolalities (0.3, 0.6, 1.5, 2.25 and 3.00 Osm/kg) at a constant temperature (~27 ºC). The required osmolalities were achieved by diluting 10x D-PBS (3.00 Osm/kg) with distilled water (~0.0 Osm/kg). The filled circles represent the average volumetric data. The dark line is a linear curve (assumes the cells behave as ideal osmometers) when extrapolated to infinite osmolality, results in an osmotically inactive cell volume, V_b, of $0.45V_o$ for HeLa cells and $0.52V_o$ for Jurkat cells. The inverse of the osmolality is plotted along the x-axis and the normalized volume is plotted along the axis. The error bars represent the standard deviation in the data (for each point n = 60 to 75 cells).

4.4 RESULTS

4.4.1: Cell Geometry and Osmotically Inactive Cell Volume (V_b)

The trypsinized HeLa cells were found to have an initial diameter of 15 $\pm$ 1.5 μm (n = 15), and the Jurkat cell diameter was measured to be 12 $\pm$ 1.1μm (n = 15). The corresponding initial isotonic volume, $V_{o,}$ is ~1767 μm^3 for HeLa cells and 905 μm^3 for Jurkat cells. Osmotically inactive cell volume of HeLa and Jurkat cells was determined by the use of Boyle-van't plot which plots equilibrium cell volume as the dependent variable and the inverse of the external osmolality as the independent variable, see Fig 4.1.

A critical assumption in Boyle van't Hoff analysis is the inhibition or suppression of active compensatory processes by which cells readjust their volume during their passive osmotic water transport (Lucke and McCutcheon 1932; Wehner 2003). In Fig 4.1, the filled circles represent the average cell volume data from the bright field image analysis, and the error bars represent the standard deviations in the measurements. A linear curve was fit to the measured cell volume at various external osmolalities. Extrapolating the linear fit to the vertical axis, corresponding to an infinite external osmolality, resulted in an osmotically inactive cell volume of $0.45V_o$ for HeLa cells and $0.52V_o$ for Jurkat cells. Note that the presence of DMSO in the intracellular compartment increases the osomotically inactive cell volume of HeLa cells to ~$0.53V_i$ and Jurkat cells to ~$0.59V_i$. Based on the HeLa and Jurkat cell dimensions measured, the ratio of $\left(\frac{A_c}{V_o - V_b} \right)$ is 0.727 μm^{-1} for HeLa cells (using $V_b = 0.45V_o$) and 1.04 μm^{-1} for Jurkat cells (using $V_b = 0.52V_o$).

4.4.2: Freezing Response of HeLa Cells

Fig 4.2 shows the water transport data and simulation for HeLa cells using the best fit parameters in Eqn. (1) at a cooling rate of 20 ºC/min in a medium containing no CPAs (Fig 4.2A), DMSO as CPA (Fig 4.2B) and incubated with NPs for 5 min (Fig 4.2C) and 3 hr (Fig 4.2D). The dynamic portion of the cooling curve (region where the initial and final heat release thermograms are distinct and separate) was found to be between –0.6 ºC to –12 ºC with no CPAs or with NPs[2], while it was between –3.1 ºC and –21 ºC with DMSO. The model simulated equilibrium cooling response (equilibrium is achieved at each temperature when the internal and external osmotic pressures are equal) is also shown as reference as dotted line (---------). The HeLa cell membrane permeability values that best fit the water transport data in the absence and presence of DMSO and NPs are shown in Table 4.1. The theoretically predicted optimal cooling rate values obtained using Eq. 4 for freezing HeLa cells are also given in Table 4.1; the optimal cooling rate for HeLa cells in the absence of CPAs is ~31 ºC/min, in the media containing 10% DMSO is ~22 ºC/min and in the media containing NPs is ~21 º/min (for both 5 min and 3 hr incubation times).

The water transport data (see Fig 4.2) obtained in the presence of NPs is significantly different (>99% confidence level using the student's t-test) from the water transport response of HeLa cells in the presence of DMSO. Additionally, the water transport response of HeLa cells obtained in the presence of DMSO is also significantly different than the response obtained in the absence of DMSO, albeit at a lower confidence level of 95%. There is no significant-

[2]As stated earlier we have experimentally verified, using a vapor pressure osmometer, that the presence of NPs does not significantly impact the osmolality of the freezing media (and hence the phase change temperature in the presence of NPs is assumed to be –0.6 ºC).

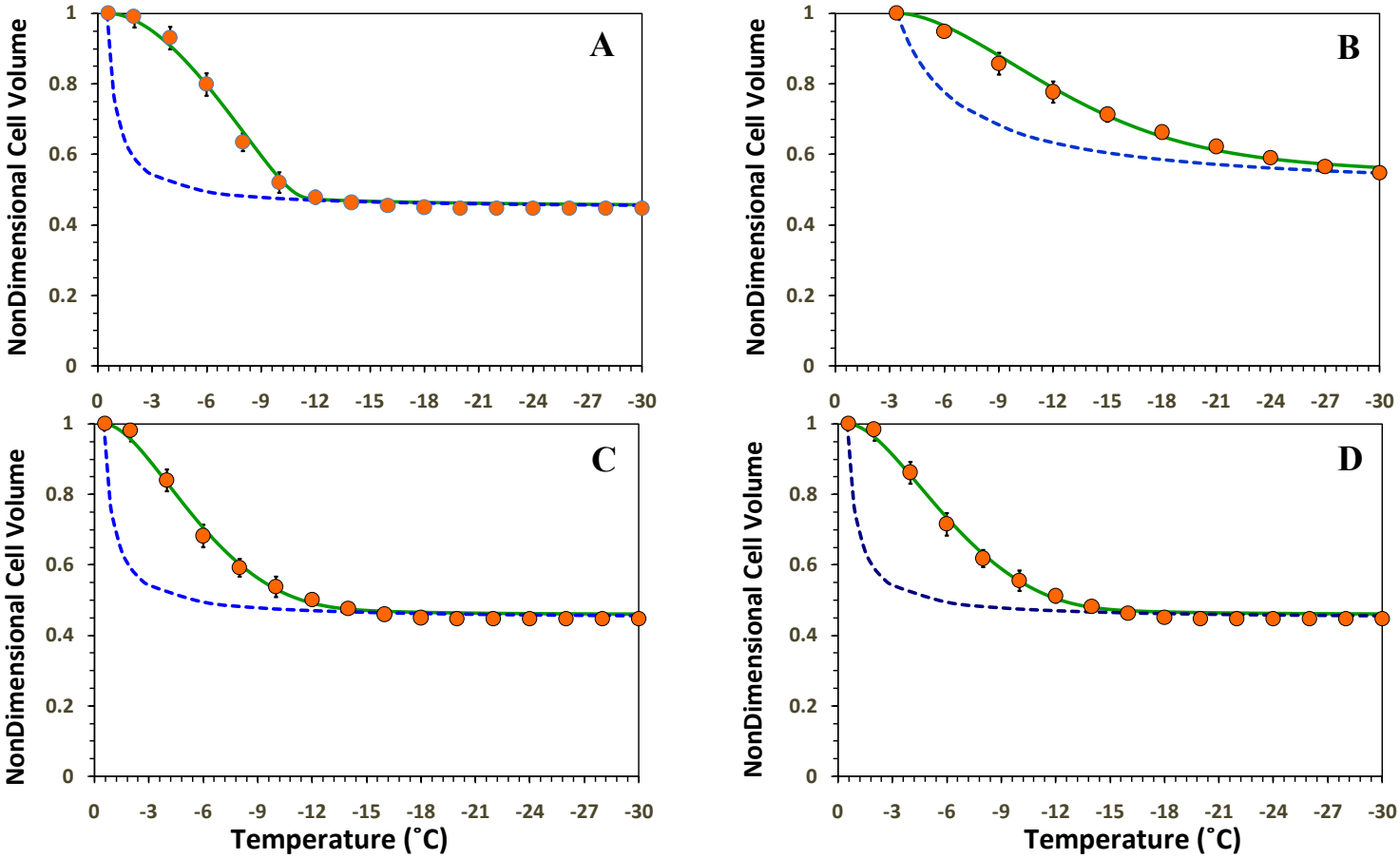

Figure 4.2: Volumetric response of HeLa cells as a function of subzero temperatures obtained using the DSC technique at 20 ºC/min in the absence of CPAs (Fig 4.2A), in the presence of DMSO (Fig 4.2B), in the presence of NPs with 5 min incubation (Fig 2C) and in the presence of NPs with 180 min incubation (Fig 4.2D). The measured volumetric response is shown as filled circles where as the model-simulated dynamic cooling response at 20 ºC/min is shown as a solid line and was obtained by using the best-fit membrane permeability parameters (L_{pg} *and* E_{Lp} *or* L_{pg}*[cpa] and* E_{Lp}*[cpa]*) in the water transport equation (Eqns. 1 and 2). The simulated equilibrium cooling response is also shown, for reference, as a dotted line (---------). The nondimensional volume is plotted along the y-axis while the subzero temperatures are shown along the x-axis. The error bars represent the standard deviation for the mean values of six separate DSC experiments (n = 6).

Table 4.1: Predicted subzero membrane permeability parameters (the reference membrane permeability in the absence and presence of CPAs, L_{pg} or $L_{pg}[cpa]$, and activation energy in the absence and presence of CPAs, E_{Lp} or $E_{Lp}[cpa]$) and optimal rates of freezing for HeLa and Jurkat cells. Note that the goodness of fit, R^2 value was always greater than > 0.99.

Cell Type (V_b)	Freezing Media	L_{pg} or $L_{pg}[cpa]$ (μm/min-atm)	E_{Lp} or $E_{Lp}[cpa]$ (kcal/mole)	B_{opt} (^oC/min)
HeLa cells (0.45Vo)	No CPA	0.08	10.9	30.6
	10% DMSO	0.08	16.7	22.4
	Nanoparticles (5 min incubation)	0.23	37.4	21.0
	Nanoparticles (3 hr incubation)	0.19	33.8	21.1
Jurkat cells ($0.52V_O$)	No CPA	0.05	9.5	33.7
	10% DMSO	0.06	17.4	24.0
	Nanoparticles (5 min incubation)	0.16	35.9	22.3
	Nanoparticles (3 hr incubation	0.13	33.3	20.8

difference between water transport behavior of HeLa cells incubated with NPs for either 5 min versus 3 hr.

4.4.3: Freezing Response of Jurkat Cells

Fig 4.3 shows the water transport data and simulation for Jurkat cells using the best fit parameters in Eqn. (1) at a cooling rate of 20 ºC/min in a medium containing no CPAs (Fig 4.3A), DMSO as CPA (Fig 4.3B) and incubated with NPs for 5 min (Fig 4.3C) and 3 hr (Fig 4.3D). The

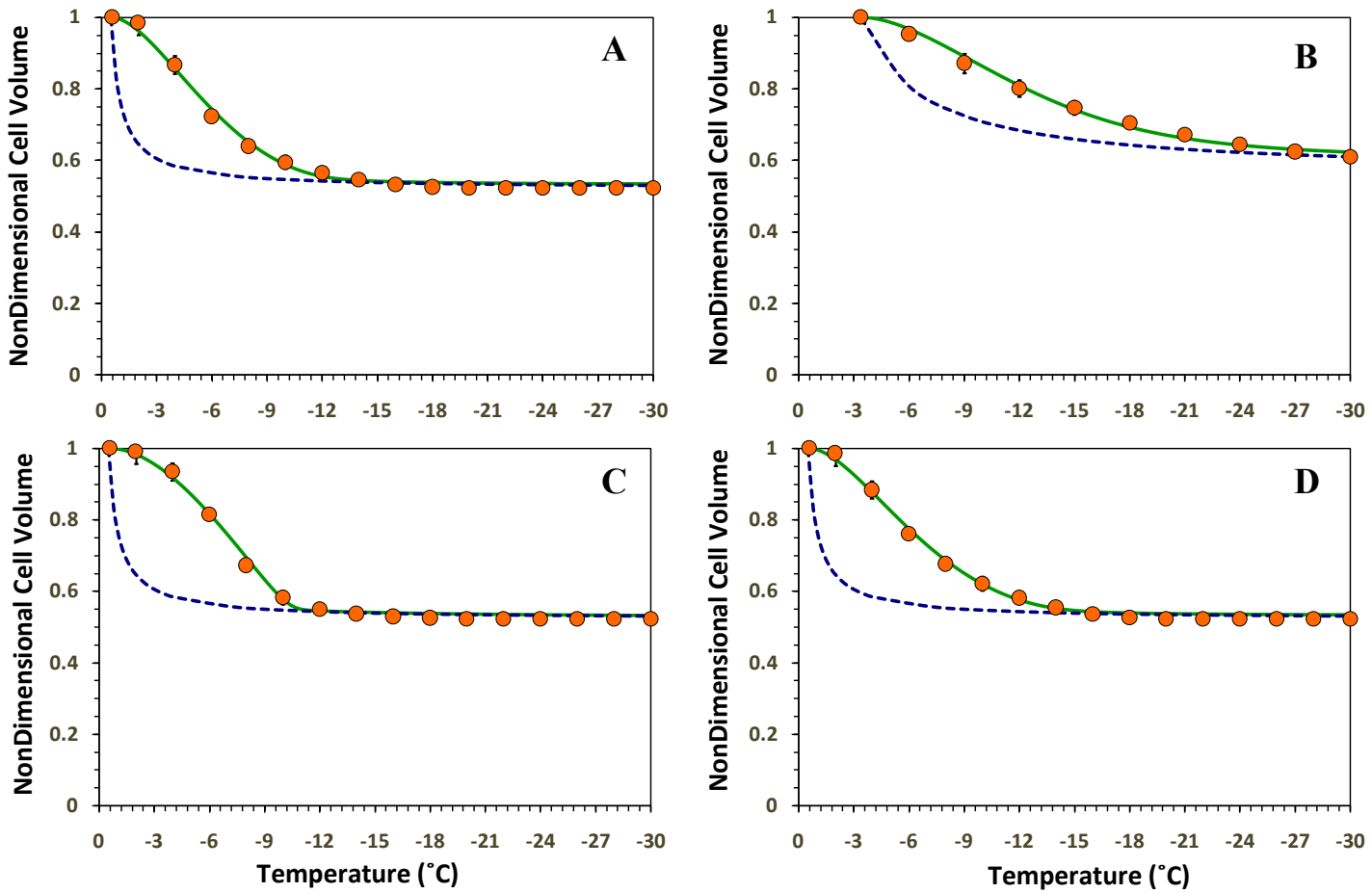

Figure 4.3: Volumetric response of Jurkat cells as a function of subzero temperatures obtained using the DSC technique at 20 ºC/min in the absence of CPAs (Fig 4.3A), in the presence of DMSO (Fig 4.3B), in the presence of NPs with 5 min incubation (Fig 4.3C) and in the presence of NPs with 180 min incubation (Fig 4.3D). The measured volumetric response is shown as filled circles where as the model-simulated dynamic cooling response at 20 ºC/min is shown as a solid line and was obtained by using the best-fit membrane permeability parameters (L_{pg} *and* E_{Lp} *or* L_{pg}*[cpa] and* E_{Lp}*[cpa]*) in the water transport equation (Eqns. 1 and 2). The simulated equilibrium cooling response is also shown, for reference, as a dotted line (---------). The nondimensional volume is plotted along the y-axis while the subzero temperatures are shown along the x-axis. The error bars represent the standard deviation for the mean values of six separate DSC experiments (n = 6).

dynamic portion of the cooling curve was found to be between –0.6 ºC to –10 ºC with no CPAs, –0.6 ºC to –12 ºC with NPs**,** and it was between –3.1 ºC and –21 ºC in the presence of DMSO. The simulated equilibrium cooling response is shown as a dotted line (---------). The Jurkat cell membrane permeability values that best fit the water transport data in the absence and presence of DMSO and NPs are shown in Table 4.1. The theoretically predicted optimal cooling rate values obtained using Eq. 4 for freezing Jurkat cells are given in Table 4.1; the optimal cooling rate for Jurkat cells in the absence of CPAs is ~34 ºC/min, in the media containing 10% DMSO is ~24 ºC/min and in the media containing NPs is ~22 º/min (for both 5 min and 3 hr incubation times).

Similar to the measured water transport response of HeLa cells, the water transport data obtained for Jurkat cells in the presence of NPs was significantly different (>99% confidence level using the student's t-test) from the water transport response in the presence of DMSO. Also, the water transport response of Jurkat cells in the presence of DMSO was significantly different than the response obtained in the absence of DMSO, albeit at a lower confidence level of 95%. No significant difference in water transport response was observed when Jurkat cells were incubated either 5 min or 3 hr, a behavior similar to that observed with HeLa cells. And finally, the equilibrium cooling response or the volumetric shrinkage response of HeLa and Jurkat cells cooled infinitely slowly, was significantly different (>99% confidence level using the student's t-test) from the dynamic water transport data obtained at 20 ºC/min for both cell types (shown in Fig 4.2 and Fig 4.3).

Fig 4.4 shows the contour plots of the goodness of fit parameter (R^2 = 0.96) in the L_{pg} and E_{Lp} (or $L_{pg}[cpa]$ and $E_{Lp}[cpa]$) space that "fit" the measured water transport data for HeLa

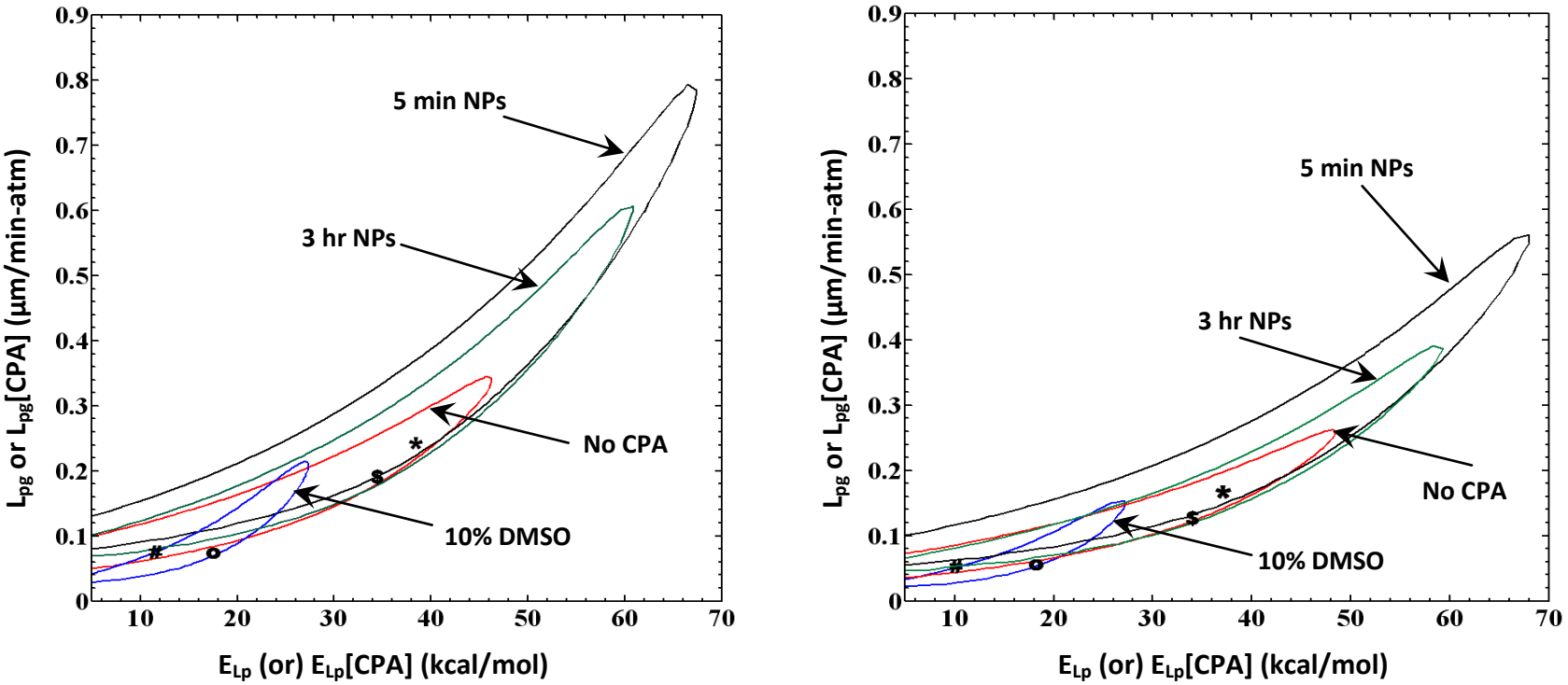

Figure 4.4: Contour plots of the goodness of fit parameter R^2 (= 0.96) for water transport response in HeLa (Fig 4.4A) and Jurkat (Fig 4.4B) cells in the absence of CPAs, in the presence of DMSO and NPs. The common region corresponds to the range of parameters that "fit" the water transport data for different media with $R^2 \geq 0.96$. Note that the "best fit" parameters shown in Table 1 are also shown in both the Figs as either "**#**" (with DMSO), or "**o**" (without DMSO or NPs), or "**$**" (cells incubated with NPs for 3 hr) or "*****" (cells incubated with NPs for 5 min). The membrane permeability at 0 ˚C, L_{pg} (or $L_{pg}[cpa]$) (m^3/Ns) is plotted on the y-axis while the apparent activation energy of the membrane, E_{Lp} (or $E_{Lp}[cpa]$) (kJ/mole) is plotted on the x-axis.

and Jurkat cells in the four media investigated. Any combination of L_{pg} and E_{Lp} (or $L_{pg}[cpa]$ and $E_{Lp}[cpa]$) shown to be within the contour will "fit" the water transport data in the specified freezing media with an R^2 value > 0.96. Note that for both the HeLa and Jurkat cells the best fit parametric space obtained in the absence of DMSO or NPs is almost completely enclosed by that obtained in the presence of NPs. This suggests that the water transport parameters obtained in the absence of DMSO or NPs could predict the water transport response of the HeLa and Jurkat cells in the presence of NPs quite accurately, while the converse is not true.

4.4.4: Post-Thaw Viability and Apoptotic Response

As stated earlier, we have performed several controlled rate freezing (CRF) experiments on different treatments of HeLa and Jurkat cells. As shown in Table 1, the predicted optimal cooling rates for HeLa and Jurkat cells can be broadly classified into two ranges: ~20 to 24 ºC/min in the presence either DMSO or NPs and ~30 to 34 ºC/min in the absence both DMSO and NPs. Thus, for the CRF experiments, we have chosen two cooling rates 22 ºC/min and 33 ºC/min along with an additional slow cooling rate of 1 ºC/min. It was assumed that 22 ºC/min was optimal for both HeLa and Jurkat cells treated with either DMSO or NPs and 33 ºC/min was optimal for cells treated with only Opti-MEM and finally 1 ºC/min was presumed to be a damaging cooling rate for all treatments of HeLa and Jurkat cells.

The controlled rate freezing experiments were performed as detailed earlier in the methods section. Fig 4.5 shows the morphology of the HeLa cells incubated for 18 hours post-thaw and illustrates the state of the cells after freezing in different media. The images are for HeLa cells cooled to -80 ºC at 22 ºC/min and thawed back to 37 ºC at 200 ºC/min and incubated for 18 hours. The unfrozen control (Fig 4.5A) shows attached HeLa cells with normal

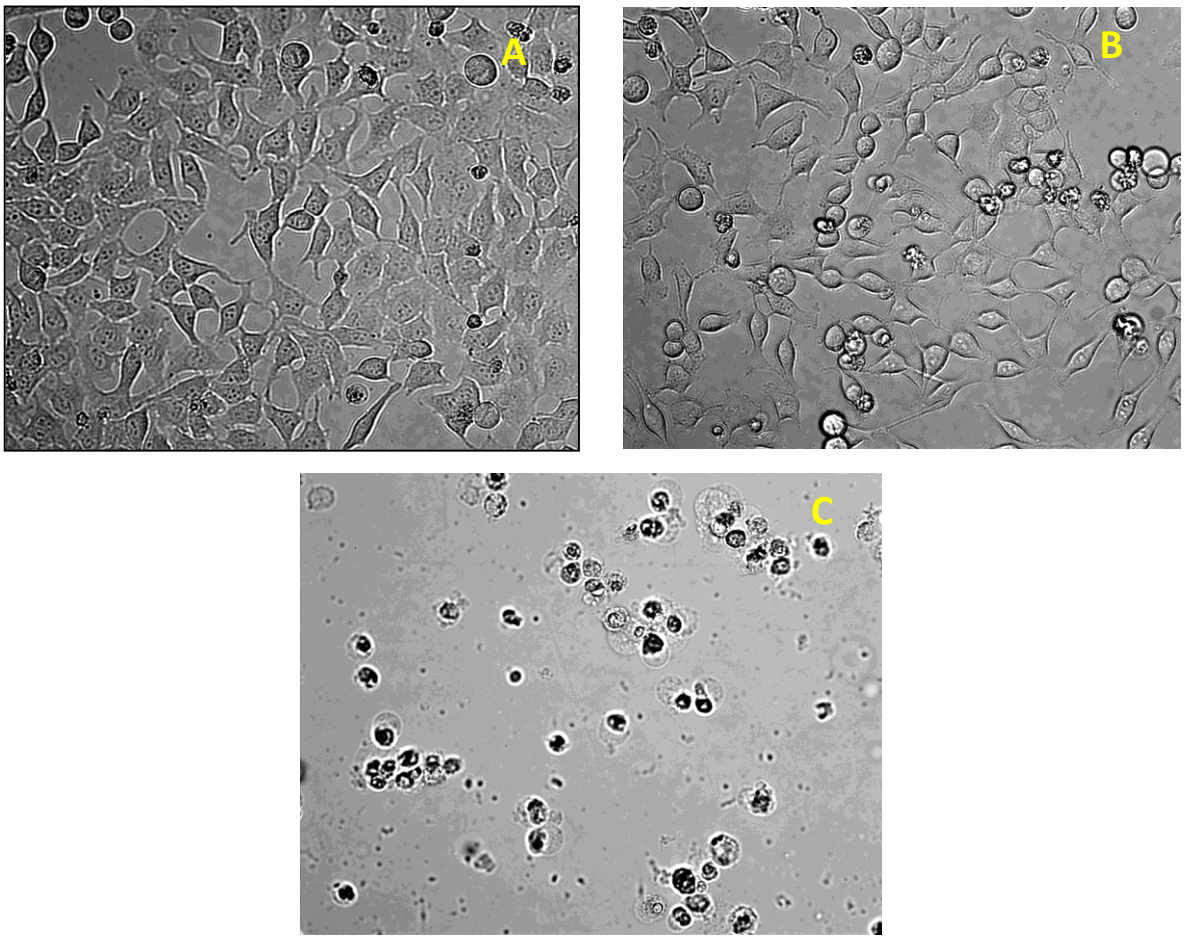

Figure 4.5: 18-hr post-thaw phase-contrast images (20x) of: Fig 4.5A - Control or unfrozen HeLa cells; Fig 4.5B - HeLa cells frozen in 10% DMSO at 22 ºC/min, and Fig 4.5C - HeLa cells incubated with NPs for 5 min and cooled at 22 ºC/min. Scale bar represents 25 µm.

morphology as expected. The image of 10% DMSO-treated HeLa cells (Fig 4.5B) shows that a substantial amount of cells have attached and survived the freeze-thaw protocol while there is only cellular debris and floating necrotic cells in the case of the 5 min NP treatment (Fig 4.5C). When the typically non-adherent Jurkat cells were treated with either no CPA, DMSO, or NPs in Opti-MEM, they adhered to the culture plate. Despite strenuous efforts, we were unable either through enzymatic or mechanical means to disassociate and collect these adherent Jurkat cells. Hence Jurkat cells were not available for analysis of apoptosis through

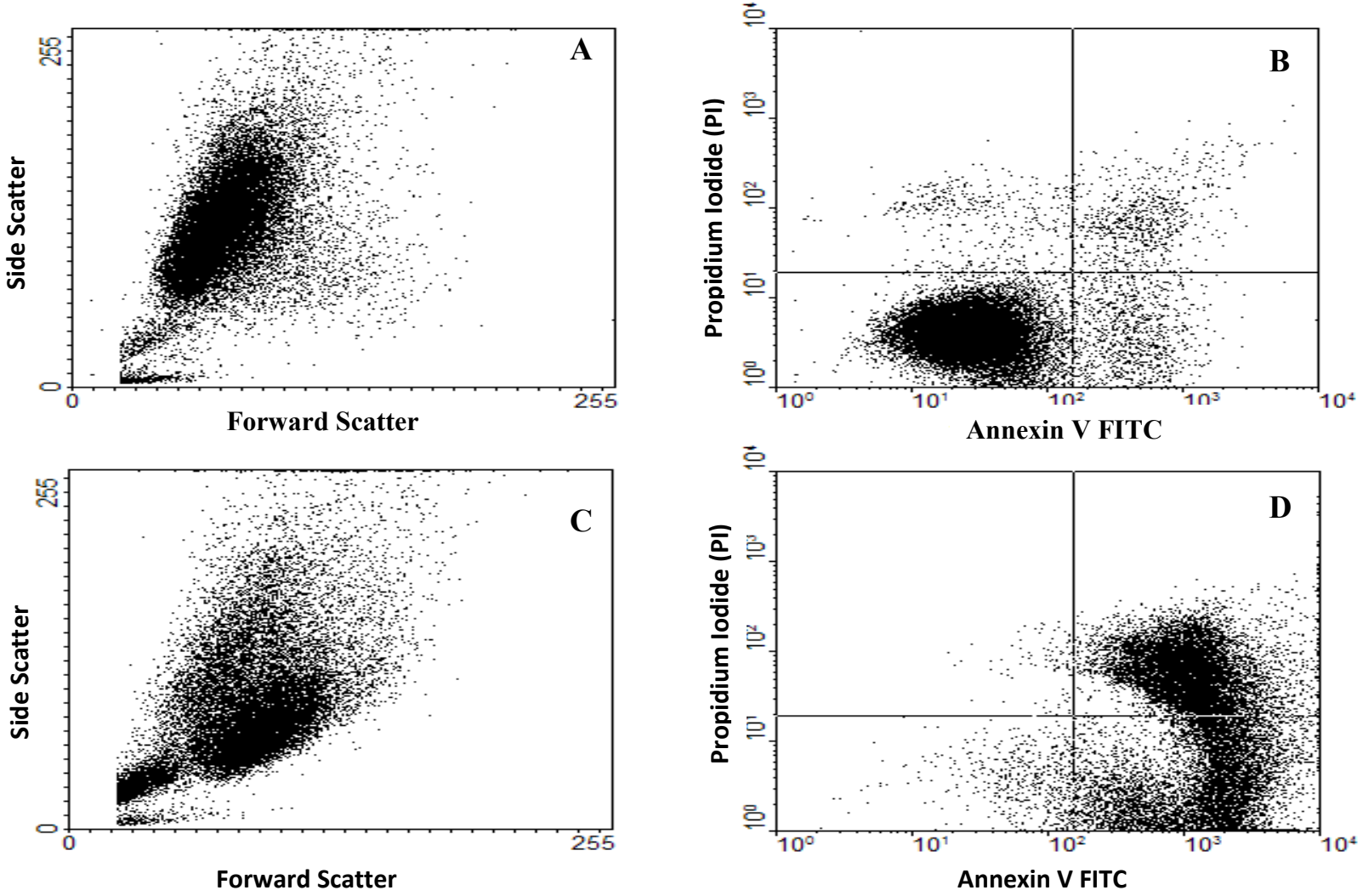

Figure 4.6: Characteristic cytometer scatterplots and fluorescence dotplots showing Fluorescence-activated cell sorting (FACS) analysis of cell death after freezing determined by annexin V staining and PI-uptake for HeLa cells cooled at 22 ºC/min: Fig 4.6A - Scatterplot for HeLa cells frozen in the presence of 10% DMSO; Fig 4.6B - Fluorescence dotplot for HeLa cells frozen in the presence of 10% DMSO; Fig 4.6C - Scatterplot for HeLa cells incubated with NPs for 5 min; and Fig 4.6D - Fluorescence dotplot for HeLa cells incubated with NPs for 5 min.

Table 4.2: Effect of different treatments with non-frozen and assay controls on resulting percentages of necrotic, live, and apoptotic HeLa cells according to the annexin V apoptosis assay protocol. Experiments were performed in triplicate, and data are expressed as mean ± SEM.

Non-frozen Controls	***% Necrotic (± stdev)***	***% Live (± stdev)***	***% Apoptotic (± stdev)***
No CPA	$0.9^{\pm 0.1}$	$89.5^{\pm 1.3}$	$6.0^{\pm 0.9}$
10% DMSO	$2.0^{\pm 0.6}$	$87.6^{\pm 2.2}$	$6.5^{\pm 0.8}$
5min NP	$1.2^{\pm 0.3}$	$87.0^{\pm 3.0}$	$5.9^{\pm 0.8}$
3hr NP	$3.5^{\pm 1.4}$	$81.7^{\pm 4.4}$	$10.23^{\pm 2.7}$
Assay Controls			
Live (Untreated Control)	$1.7^{\pm 0.5}$	$86.9^{\pm 2.3}$	$6.4^{\pm 1.4}$
Necrotic (H_2O_2 Treated)	$51.3^{\pm 10.7}$	$6.2^{\pm 2.3}$	$8.7^{\pm 3.4}$
Apoptotic (Staurosporine Treated)	$10.6^{\pm 2.8}$	$48.9^{\pm 5.7}$	$19.4^{\pm 2.6}$

the flow cytometry assay. Therefore, all post-thaw behavior was assessed only for HeLa cells. Characteristic scatter and fluorescence dotplots are shown in Fig 4.6 for HeLa cells cooled at 22 ˚C/min to –80 ºC. The scatterplot for HeLa cells frozen in the presence of 10% DMSO (Fig 4.6A) reveals a homogenous cell population. The scatterplot for HeLa cells treated with NPs for 5 min and then frozen (Fig 4.6C) reveals an increase in cell fragments as indicated by the appearance of the population with low forward scatter (FSC) and low side scatter (SSC).

Additionally, the increase in internal granularity (increase in SSC) reveals the deteriorating physical condition of HeLa cells frozen with NPs (Fig 4.6C). The fluorescence dotplot for HeLa cells frozen in the presence of 10% DMSO (Fig 4.6B) shows a majority of the cells are in the lower left quadrant (annexin V^-/PI^-), which corresponds with the live cell

population. Conversely, the fluorescence dotplot for HeLa cells treated with NPs for 5 min and then frozen (Fig 4.6D) shows a majority of the cells are either in the lower right quadrant (annexin V^+/PI^-, apoptotic) or in the upper right quadrant (annexin V^+/PI^+, necrotic). This population quadrant analysis was performed on all of the experimental treatments to obtain quantitative information on the condition of the cells following the freeze-thaw protocol described earlier (Fig 4.7).

After the 18-hr incubation period following the freeze-thaw experiment, the percentages of necrotic, live, and apoptotic HeLa cells were determined (Fig 4.7). No significant difference was found among the unfrozen controls (Table 2); indicating that treatment with 10% DMSO or nanoparticles alone was not cytotoxic. The percentage of live, necrotic and apoptotic HeLa cells are shown for the four treatments and the three cooling rates investigated: live (Fig 4.7A), necrotic (Fig 4.7B) and apoptotic (Fig 4.7C). There was no significant difference in the post-thaw survival of 10% DMSO treatments at the three cooling rates studied (Fig 4.7A). This result is not surprising since the HeLa cell line is a robust, widely-used immortalized cell line that laboratories commonly store frozen in liquid nitrogen. McGrath et al. (McGrath, 1975) reported similar data indicating no statistically significant difference in the survival of HeLa cells cooled to –20°C at rates of 5, 20 and 30°C/min.

HeLa cells treated with NPs for 5 min and then cooled at 1 ºC/min had significantly more apoptotic cells (75 ± 1.5%) when compared to apoptotic cells at the faster cooling rates of either 22 ºC/min (44 ± 5.3%) or 33 ºC/min (36 ± 7%). Interestingly, for HeLa cells treated with NPs and then frozen, we observed a significant increase in the percentage of necrotic cells accompanied by a corresponding decrease in the percentage of apoptotic cells, when the

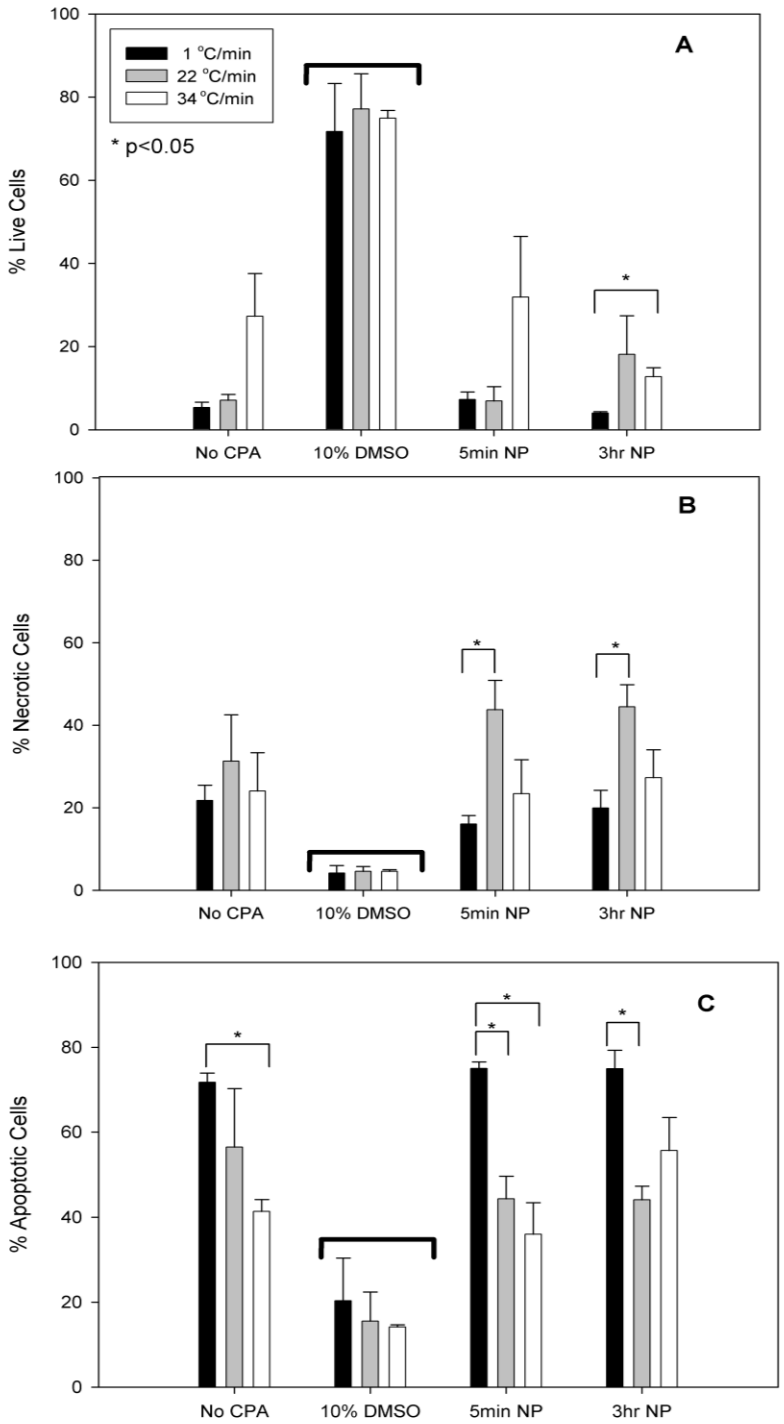

Figure 4.7: 18-hour post-thaw comparison of the percentage of live, necrotic and apoptotic HeLa cells are shown for the four treatments and the three cooling rates investigated: live (Fig 4.7A), necrotic (Fig 4.7B) and apoptotic (Fig 4.7C). The error bars represent the standard error in the data. The horizontal bars denoted with asterisks (*) represent statistically significant differences between similar treatments. The bold horizontal bars above 10% DMSO data in all the panels represents a significant difference from the corresponding data obtained for the other 3 treatments.

cooling rate is increased from 1 to 22 ºC/min. In the absence of cryopreservative agents, the percentage of apoptotic HeLa cells significantly decreases as the cooling rate increases from 1 ºC/min (71 ± 2.1%) to 33 ºC/min (41 ± 2.8%). This suggests that the mechanism of cell death for the slower rate (1 ºC/min) differs from the faster cooling rates in which there is a reduced percentage of apoptotic cells. Conversely, HeLa cells treated with NPs for 3 hr and then frozen, exhibited a significantly higher survival at 34 ºC/min (12 ± 2.1% live) compared to 1 ºC/min (4 ± 0.4%). HeLa cells treated with 10% DMSO and then frozen were found to have significantly higher percentages of surviving cells at all three cooling rates when compared to the other treatments (see Fig 4.7). Although, a cursory examination of Fig 4.7A might suggest an improved post-thaw viability for cells cooled at 34˚C/min in the presence of NPs (5 min incubation) and also in the absence of CPAs. However, a closer examination of the data revealed that this seemingly significant improvement in post-thaw cell viability was actually not statistically significant.

And finally, for the 10% DMSO treatments, 20,000 cell events were collected for all freezing rates; however, in the absence of DMSO and NPs, fewer cell events were collected (ranging from 1,100 to 11,000) which is an indication of cell rupturing and increased cellular debris following the freeze-thaw protocol. Based on the quantitative post-thaw data, there are no significant differences between cells treated with nanoparticles and in the absence of CPAs, which suggests that the nanoparticles do not provide any significant cryoprotective function to HeLa cells at the concentration of NPs used and freeze-thaw rates studied here.

4.5 DISCUSSION

In order to determine the water transport parameters and optimal cooling rates across cellular treatments in this study, cell dimensions and inactive cell volumes of HeLa and Jurkat cells were obtained in this study. The cell diameter values for HeLa (~15 μm) and Jurkat (~12 μm) obtained in the present study are comparable to those reported in the literature; ~14 to 16 μm for HeLa cells (Deman and Bruyneel 1977; Nair 1981) and ~10 to 13 μm for Jurkat cells (Rosenbluth et al., 2006). Conversely, a lower average diameter value of the order of ~ 8μm was reported by Chen et al. (Chen et al., 2004) for Jurkat cells while a higher average diameter of ~20 μm was reported by Morrill and Robbins (Morrill and Robbins 1984) for HeLa cells. The inactive cell volume for the Jurkat cell obtained in this study (~$0.52V_o$) is comparable to a published value of $0.48V_o$ (Reuss et al., 2004). However, there is significant difference between the measured value of inactive cell volume of HeLa cells (~$0.45V_o$) in our experiment and the published value of $V_b = 0.21V_i$ by Morrill and Robbins (Morrill and Robbins 1984). These variations in cell size and hence the inactive cell volumes might be due to the growth conditions employed for HeLa cells at different laboratories (Masters 2002).

There was a significant increase in the measured values of reference membrane permeability, L_{pg} *(or* L_{pg} *[cpa])* and activation energies E_{Lp} *(or* E_{Lp} *[cpa])* obtained in the presence NPs when compared with the corresponding values obtained in their absence for both HeLa and Jurkat cells (see Table 4.1). Interestingly, there are no significant differences in the permeability values obtained in the presence of DMSO and in the absence of DMSO and NPs for both HeLa and Jurkat cells (Table 4.1). However**,** there was a considerable increase in the measured activation energy values in the presence of DMSO and in the absence of DMSO and

NPs. For both HeLa and Jurkat cells, the time of incubation (either 5 min or 3 hr) with NPs did not show any marked effect on the water transport behavior and thus, there are no significant differences (<17%) in the L_{pg} *(or* L_{pg} *[cpa])* and E_{Lp} *(or* E_{Lp} *[cpa])* values in the presence and absence of NPs (Table 4.1).

As stated earlier, the best-fit permeability parameters and the measured $\left(\frac{A_c}{V_o - V_b}\right)$ values were incorporated into Eq. (4) to predict the optimal rates of freezing for both HeLa and Jurkat cells (Table 1). It should be noted that, in the development of Eq. (4) the dynamics and kinetics of IIF have not been included (Toner 1993). Thus, if IIF occurs between –5 and –20 ºC, then potentially even more water will be trapped in the HeLa and Jurkat cells than predicted by water transport alone and the optimal cooling rates obtained using Eq. (4) are overestimated. An examination of the optimal cooling rates reveals that despite significant differences in the water transport behavior and hence the permeability parameters obtained in the presence of NPs versus DMSO, the optimal cooling rates are statistically similar, if not exactly the same**,** for both HeLa and Jurkat cells. However, for both cell types, the optimal cooling rate measured in the absence of NPs or DMSO is significantly higher (30-40%). This is somewhat surprising, as the presence of CPAs are expected to increase the ability of the cell membrane to dehydrate at faster cooling rates (Smith et al., 1998). However a similar decrease in the predicted optimal cooling rates in the presence of CPAs was observed in canine spermatozoa (Thirumala et al., 2003), adipose tissue derived adult stem cells (Thirumala et al., 2005) and in striped bass sperm cells (Thirumala et al., 2006).

An interesting phenomenon observed in this study was the atypical behavior of lymphocytic Jurkat cells adhering to the culture plate when they were incubated in Opti-MEM and treated with NPs or DMSO. Results from MTT viability assays suggest that these cells are metabolizing and thus alive (data not shown). There are no published reports of Jurkat cells adhering to substrates other than specific ligands (e.g., fibronectin) or stimulated endothelial cells. A distinct possibility for the adherent behavior of Jurkat cells could be due to possible stimulating factors present in Opti-MEM and the surface treatment of the culture plate. This is somewhat supported by the observed behavior of Jurkat cells frozen and incubated in the absence of CPAs. However, there are several published reports of Jurkat cells cultured in Opti-MEM that do not exhibit this adherent behavior (Fatok at al., 2000; Sanders et al., 2000; Cui et al., 2003; Bischof 2006). Further understanding is needed to evaluate the Jurkat cell adhesion observed here and to distinguish between competing or complementary modes of the substrate-media in stimulating adhesion.

As shown in Fig 4.7 and described earlier, NPs do not seem to provide any significant cryoprotective function to HeLa cells at the concentrations and freeze-thaw rates investigated in the present study. We have postulated several likely reasons for NPs not showing any cryoprotection. Firstly, the concentration of the NPs used in this study was lower than necessary to achieve some measurable cryoprotective effect. A thorough review of the literature suggests that cryoprotection by high molecular mass materials like polymers, is feasible only at very high concentrations. These non-permeable polymeric CPA solutions act on a colligative basis and tend to have increasingly high viscosities at lower temperatures and form glasses readily at high temperatures by kinetically slowing down the ice crystal growth to zero

(Connor and Ashwood-Smith 1973; Farrant 1969). Moreover, all CPAs showing some cryoprotection do share a common characteristic of freezing-point depression (FPD) (Fuller 2004; Bischof 2006). FPD of polymers show a marked deviation from the linear relationship and increase dramatically at high concentrations. In our experiments with 10% NPs we observed essentially zero FPD, and the NP solution behaved like an isotonic solution. Conversely, a recent study suggested that the use of 10% polyvinylpyrrolidone (PVP) as CPA dramatically increased post-thaw survival of porcine primary adipocytes more than that could be achieved with 10% DMSO as the sole CPA (Li et al., 2006). Further studies are clearly needed to reconcile these disparate observations.

A second explanation for the minimal cryopreservative effect from NPs is that the water transport model for determining optimal cooling rates may not accurately predict the water transport across the cell membrane when the freezing medium contains NPs. This suggests that further modifications and corrections might be needed to the water transport model (Eqns. 1 and 2), to enable it to accurately reflect cell freezing behavior in the presence of NPs. For the purposes of this study, the use of the standard water transport model (Eqns. 1 and 2) was deemed to be sufficient. However, efforts are currently underway in our laboratory to elucidate the necessary modifications to the water model and to further it's use in the presence of NPs.

And finally, the palmitoyl NPs might not posses any cryoprotective action at lower temperatures and in fact might be having the opposite effect. For example, the post-thaw apoptotic response of HeLa cells indicates that the presence of NPs induces a significant increase in apoptosis at low freezing rates (1 ˚C/min) when compared to higher freezing rates

(Fig 4.7). As stated earlier, an increase in the cooling rate from 1 ˚C/min to 22 ˚C/min was accompanied with a significant increase in % necrotic HeLa cells treated and frozen with NPs. This striking result does suggest that NPs could be effective as an adjuvant to cryodestructive procedures. Interestingly, the presence of NPs significantly increased the percentage of apoptotic cells cooled at 1 ˚C/min (Fig 4.7), a cooling rate that is similar to those experienced at the outer edges of a cryosurgical iceball where cell survival is typically the highest. However, it is important to note that a comparison of the % of apoptotic cells found when HeLa cells are frozen in the absence of CPAs and NPs is comparable to that obtained for HeLa cells frozen in the presence of NPs (Fig 4.7) at the three cooling rates investigated and the volume fraction of NPs. As shown in Table 4.2, in the absence of freezing temperatures, the presence of NPs during incubation was not cytotoxic and further encourages the use of palmitoyl NPs for *in vivo* applications. Similar non-cytotoxic nature of gold nanoparticles, when incubated with human fibroblasts**,** was also reported by de la Fuente et al. (de la Fuente et al., 2006).

Our observations suggest that the gold NPs used in our study are interacting with HeLa cells by some physiochemical means and are inducing apoptosis during the freeze-thaw process. This encourages the possibility of using gold NPs in a cryodestruction procedure and is supported by recent studies demonstrating that nanoparticles can potentially enhance and control thermal therapy outcomes through adjuvant (drug) delivery, tomographic visualization and inductive heating within the body (Bischof 2006). Since maximizing the killing effect of cryosurgery has been an important task both for clinical practice and for fundamental research, the association of apoptosis with NPs at low temperatures observed in the present study is of direct relevance for cryosurgical applications.

4.6 CONCLUSIONS

The aim of this study was to evaluate the freezing response of HeLa and Jurkat cells in the presence of commercially available nanoparticles, NPs (Palmitoyl Nanogold®, Nanoprobes) and a commonly used cryoprotective agent, DMSO. By fitting a model of water transport to the experimentally determined volumetric shrinkage data, the membrane permeability parameters were obtained. A generic optimal cooling rate equation was then used to predict the optimal rates of freezing HeLa and Jurkat cells in the presence and absence of DMSO and NPs. To further investigate the predicted optimal cooling rates, the cells were cooled at three controlled freezing rates in the presence and absence of DMSO and NPs using a commercially available controlled rate freezer. The post-thaw viability and apoptotic response of treated HeLa cells were evaluated after 18 hr post-thaw incubation time. Jurkat cells demonstrated an increase in their adhesive properties after treatment and remain adhered to the culture plate, preventing their flow cytometric analysis. For HeLa cells**,** the post-thaw results show that the presence of NPs increased the measured post-freeze apoptotic response at 1 ˚C/min when compared to higher cooling rates and suggests a possible therapeutic use of NPs in cryodestructive procedures.

CHAPTER 5
EVALUATION OF POLYVINYLPYROLLIDONE (PVP) AS A CRYOPROTECTANT FOR ADIPOSE DERIVED STEM CELLS (ASCs)

5.1 INTRODUCTION

Human adipose tissue provides a uniquely abundant and accessible source of adult stem cells. In response to chemical, hormonal or structural stimuli, these adipose-derived adult stem cells (ASCs) can differentiate along multiple lineage pathways, including adipocytes, chondrocytes and osteoblasts (Vogel 2000; Gimble et al., 2003; Gimble et al., 2004). Successful cryopreservation of scientifically and commercially important ASCs could revolutionize tissue engineering and regenerative medicine industry. In general, freezing storage requires the addition of a class of chemicals denoted as cryoprotective agents (CPAs) and their extensive use is based on the serendipitous observation by Polge and co-workers (Polge 1969) that sperm cells were able to survive freezing in the presence of a chemical (glycerol) and did not survive the freezing process in its absence. There is considerable divergence across the classes of organic molecules that possess some CPA activity, ranging from low molecular weight solutes (permeating chemicals) like dimethyl sulfoxide (DMSO) and glycerol, to sugars like sucrose, and trehalose, to high molecular weight polymers (non-permeating) like polyvinylpyrollidone (PVP) and hydroxyl-ethyl-starch (HES) (Lovelock 1954; Connor and Ashwood-Smith 1973). However majority of these CPAs possess relatively low efficiencies and very few of them are effective in preserving nucleated cells[7]. Moreover, many of the permeating CPAs are chemicals, and though they are widely used in cryopreservation procedures, the associated osmotic damage and toxicity during their addition and removal limits the safe (allowable) amount, and therefore

limits the cryoprotective efficiency of the freezing media. These drawbacks associated with permeating CPAs led us to investigate alternative freezing media for the cryopreservation of ASCs, i.e. develop or test the efficacy of freezing media without permeating CPAs such as DMSO.

A systematic study on the use of HES in erythrocyte freezing has been conducted by Sputtek and colleagues (Sputtek and Sputtek, 2004) and showed them to be highly effective. However, Conner and Ashwood-Smith (Conner and Ashwood-Smith 1973) showed that these high molecular weight CPAs, although found to be most effective in red blood cell cryopreservation, in fact possess limited efficacy when used as the sole CPA with nucleated cells. Intriguingly, when used in combination with other permeating CPAs such as DMSO, these high molecular weight CPAs have been shown to make a significant positive contribution to the success of a freezing protocol (Sputtek, and Sputtek 2004). Farrant (1969) advocated that these high molecular weight polymers, such as PVP, exhibit enhanced colligative properties at higher concentrations and hence protect cells by lowering the external salt concentrations in a manner similar to low molecular cryoprotectants. Mazur (1970) proposed that polymeric CPAs prevent denaturing of the membranes due to high solute (salt) solutions at low temperatures either by preventing seeding (nucleation) of the super-cooled water inside the cells or by coating the temperature/salt concentration sensitive plasma membranes. In yet another study, Williams (1983) suggested that the cryoprotective efficiency of polymers resides in their ability to alter the physical properties of solutions during freezing rather than directly protecting and altering the cell membrane characteristics.

Unfortunately, it is still a common practice to add animal serum to the culture media as a source of nutrients and other ill-defined factors – a practice that exists to this day, despite scientific and technical disadvantages to its inclusion, its high cost, and the increasing availability of serum-free alternatives. Obviously, for *in vivo* clinical use, the elimination of animal serum proteins and all possible sources of infectious diseases such as hepatitis, human immunodeficiency virus (HIV) and bovine spongiform encephalopathy (BSE) is a prerequisite (van der Valk et al., 2004). Therefore, it is necessary to replace serum as a supplement in culture/freezing media used for cryopreserving ASCs[12]. In contrast to animal sera, the use of an autologous serum for supplementation eliminates the risk of infectious diseases completely. A disadvantage, however, is that the production of autologous serum is a costly process and requires a preoperative blood donation by the patient (van der Valk et al., 2004). As a replacement for animal serum and to overcome the disadvantages of autologous serum, it is also possible to use human serum albumin in cryopreservation of human tissue. However, the risk of transmission of infectious diseases is not completely eliminated and the production of human serum albumin implies a major capital outlay (Reuther et al., 2006). Therefore efforts need to be made to reduce, and preferably remove, serum (animal and human) in freezing (cryopreservation) media.

The objective of this study was to test the hypothesis that ASCs can be effectively cryopreserved and stored in liquid nitrogen using a freezing medium containing (PVP) as the CPA instead of DMSO. To this end we investigated the post-freeze/thaw viability and apoptotic behavior of Passage 1 (P1) ASCs cryopreserved in fifteen different media: (i) the traditional media containing Dulbecco's Modified Eagle Medium (DMEM) with 80% Fetal Calf Serum (FCS)

and 10% DMSO, (ii) DMEM with 80% Human Serum (HS) and 10% DMSO, (iii) DMEM with various concentrations (1, 5, 10, 20 and 40%) of PVP as the sole CPA; (iv) DMEM with PVP (5, 10 and 20%) and HS (10%); (v) DMEM with PVP (5, 10 and 20%) and FCS (10%); and (vi) DMEM with PVP (10%) and FCS (40 and 80%). The thawed samples were analyzed by brightfield microscopy and flow cytometry to determine the % of viable, necrotic and apoptotic cells. Adipogenic and osteogenic differentiation behavior of the frozen thawed cells was also assessed using histochemical staining and optical density measurements and the expression of adipogenic, osteogenic associated genes was analyzed using reverse-transcription polymerase chain reaction (RT-PCR). Our results suggest that post-thaw ASC cell viability, adipogenic and osteogenic differentiability can be maintained even when they are frozen in the absence of serum and with 10% PVP in DMEM.

5.2 MATERIALS AND METHODS

5.2.1: Isolation, Collection and Culture of ASCs

All human protocols were reviewed and approved by the Pennington Biomedical Research Centre Institutional Review Board. Unless otherwise stated, all reagents were obtained from Sigma Chemicals (St. Louis, MO). Subcutaneous adipose tissue liposuction aspirates from three patients were provided by plastic surgeons in Baton Rouge, LA. These, tissue samples (100 to 200 ml) were washed 3-4 times in phosphate buffered saline (PBS) pre-warmed to 37˚C, suspended in PBS supplemented with 1% bovine serum albumin and 0.1% collagenase (Type I, Worthington Biochemicals, Lakewood, NJ), and digested with gentle rocking for 45-60 min at 37˚C. The digests were centrifuged for 5 min at 1200 rpm (300x g) at room temperature, re-suspended, and the centrifugation step repeated. The supernatant was

aspirated and the pellet re-suspended in stromal medium (DMEM high glucose, 10% fetal bovine serum, 100 units penicillin/ml, 100µg streptomycin/ml, and 25µg amphotericin/ml). The cell suspension was plated at a density equivalent to 0.125 ml of liposuction tissue per sq cm of surface area, using a 35 ml volume of stromal medium per T225 flask. Cells were cultured for 48 hrs in a 5% CO_2, humidified, 37˚C incubator. At which time, the adherent cells were rinsed once with pre-warmed PBS and the cells fed with fresh Stromal Medium. The cells were fed with fresh stromal medium every 2-3 days until they reached approximately 75-80% confluence. The medium was then aspirated; the cells were rinsed with pre-warmed PBS, and harvested by digestion with 0.05% trypsin solution (5-8 ml per T225 flask) for 3 to 5 min at 37˚C. The cells were suspended in Stromal Medium, centrifuged for 5 min at 1200 rpm (300x g), the pellet re-suspended in a volume of 10 ml of stromal medium, and the viable cell count determined by trypan blue exclusion. These cells were identified as Passage 0 (P0). The remaining cells were seeded in T225 flasks at a density of 5 x 10^3 cells per sq cm. The cells were maintained in culture and passaged as described above to obtain Passage 1 (P1) ASCs, and are the cells used in this study.

5.2.2: Preparation of Freezing Solutions and Freezing (& Thawing) Experiments

The CPAs used were: PVP (average molecular weight: 40,000) and DMSO (average molecular weight: 78.14). The PVP was autoclaved at 121˚C for 30 min before being added to DMEM. The DMEM-PVP solutions (PVP concentration ranging from 1 to 40%) were prepared by dissolving weighted PVP in DMEM at room temperature and the solutions were then stored overnight at 4˚C to obtain a homogeneous preparation. PVP concentrations above 40% were

not used as the DMEM-PVP solutions become highly viscous and impossible to handle/transfer. Thus, PVP concentrations above 40% could not be (and were not) investigated.

For the freezing experiments, P1 ASCs were suspended at a concentration of 10^6 cells/mL and equilibrated for ~10 min in the appropriate freezing media. The cell preservation fluid along with the cells was then dispensed in 2ml cryovials and frozen overnight to –80°C in an ethanol-jacketed closed container, and subsequently stored in liquid nitrogen for further two weeks. Prior to the brightfield microscopy and the flow cytometric analysis, individual cryovials of cells were rapidly thawed in a 37˚C water bath (1 to 2 minutes of agitation), re-suspended in the stromal culture media and seeded into the separate wells of a 6-well plate for a 24h incubation period at 37˚C.

5.2.3: Cell Viability and Apoptosis/Necrosis Assessment

A well-established annexin V apoptosis assay was analyzed by quantitative flow cytometry (Pena et al., 2003). As a chemically-induced apoptotic control, ASCs were incubated in fresh medium enriched with 40µM Etoposide. For a necrotic control, ASCs were incubated for 24 hours in fresh medium with 5mM hydrogen peroxide (H_2O_2). The no-treatment control consisted of ASCs treated in fresh medium, free from inducing agents. For each treatment, detached and attached cells were pooled, harvested by trypsinization (0.25% trypsin), washed with 200µL of culture medium, and re-suspended in 100µL of 1x annexin-binding buffer (included in annexin V-FITC/PI kit). Approximately 100µL of the cell suspension was mixed with 8µL of annexin-V-FITC and 8µL of 100 µg/mL propidium iodide (PI) and incubated in the dark at room temperature for 15 minutes. Liquid volume was removed by centrifugation and aspiration, and the cells were re-suspended by gentle vortexing in 300µL of 1X annexin-binding

buffer to be analyzed on the flow cytometer. Apoptotic analyses for ASCs were performed on a FACS Caliber flow cytometer (BD Biosciences, San Jose, CA) utilizing 488-nm laser excitation and fluorescence emission at 530 nm (FL1) and >575nm (FL3). Forward and side scatter measurements were made using linear amplification, and all fluorescence measurements were made with logarithmic amplification. A total of 20,000 cells per sample were acquired using Cell Quest software (BD Biosciences, San Jose, CA).

Apoptosis is characterized by phosphatidylserine (PS) translocation from the inner leaflet to the outer leaflet of the lipid bilayer, while the cell membrane remains intact. Annexin V-positive cells correspond to cells that have experienced PS translocation. PI staining of the cells indicates that the integrity of the cell membrane has been compromised and is used to distinguish living and early apoptotic cells from necrotic cells. The fluorescent dotplots show three cell populations: live (annexin V-FITC-negative and PI-negative; annexin V^- and PI^-) necrotic (annexin V-FITC-positive and PI-positive; annexin V^+ and PI^+), and apoptotic (annexin V-FITC-positive and PI-negative; annexin V^+ and PI^-). Quadrant analysis was performed on the gated fluorescence dotplot to quantify the percentage of live, necrotic, and apoptotic cell populations. The quadrants positions were placed according to the no treatment control and 5 mM H_2O_2 necrotic control.

5.2.4: In vitro Multilineage Differentiation

Frozen/thawed ASCs were analyzed for their capacity to differentiate along the adipogenic and osteogenic lineage using the methods described below. Cell cultures of ASCs cryopreserved in 80% serum (either human serum or animal serum) with 10%DMSO in DMEM were used as controls. For adipogenic differentiation, frozen thawed ASCs were cultured in

stromal media to at least 90% confluence. Adipogenesis was induced by adipogenic induction media consisting of stromal media supplemented with 1% antibiotic/antimycotic, 33µM Biotin, 17µM Pantothenate, 1µM Insulin, 1µM Dexamethasone, 0.5mM IBMX, 5 µM Rosiglitazone (AK Scientific, Mountain View, CA). After 3 days of induction, media was converted to adipogenesis maintenance media (identical to the induction media except for the omission IBMX and Rosiglitazone) and cells were fed 3times per week (Halvorsen et al., 2001). After 14 days of maintenance, the adipogenic differentiation was confirmed histologically using the Oil Red O stain as an indicator of intracellular lipid accumulation. Briefly, the differentiated cells were washed with PBS for 3-4 times and fixed for 10min in 10% formalin and stained with 30% Oil Red O reagent for 60 min at room temperature. Excess stain was removed by washing with distilled water and photographs were taken of a representative field for each condition. In order to quantify the adipogenesis, Oil Red O staining was eluted by 100% isopropanol and the spectrophotometric absorbance of the elution was quantified at 510 nm (Bunnell et al., 2008). Blank wells (without cells) were stained with dye and rinsed in the same manner; these values were subtracted from the experimental data points to control for the stain retention by the walls of the well.

For osteogenesis, the differentiation was induced after culturing frozen thawed ASCs for 3 weeks in osteogenic media consisting of stromal media supplemented with 10mM dexamethasone, 50mg/mL ascorbate-2-phosphate, 10mM 1,25 $(OH)_2$ vitamin D3 and 1M ß-glycerophosphate (Bunnell et al 2008). To determine the osteogenic potential of frozen-thawed ASCs to mineralize ECM, cells were fixed in 70% ice-cold ethanol and stained with 2% Alizarin Red solution (pH adjusted to 4.1-4.3) for 60min at room temperature. To quantify the calcium

content deposited in ECM, the stain was eluted with 10% cetylpyridinium chloride for 30 min at room temperature[16] and the optical density of the solubilized stain was measured at 540 nm using a micro spectrophotometer .

5.2.5: Extraction of Total RNA and RT-PCR Analysis

Total RNA was extracted from cells using TRI-Reagent according to the manufacturer's instructions (Molecular Research Center, Cincinnati, OH). Cells cultured in adipogenic media were harvested 14 days after induction and cells cultured in osteogenic media were harvested 21 days after induction. Cell cultures of ASCs cryopreserved in 80% serum (either animal or human) with 10% DMSO in DMEM were used as controls. Four osteoblastic-associated genes (Osteonectin (OSN), Osteocalcin (OCN), Osteopontin (OPN), and ALP) and four adipogenic associated genes (Adiponectin, aP2, PPARγ2, LPL, and PGC1a) were analyzed in this study (see Table 1). Real time PCR was performed in a final reaction volume of 10µl, including forward and reverse primers (0.1mM), 1.5µg reverse-transcribed RNA, and 5µl SYBR green master mix (Applied Biosystems, Warrington, UK) using an ABI Prism 7900 instrument (Applied Biosystems, Foster City, CA). Each assay was performed in triplicate.

5.2.6: Statistical Analysis

All values are indicated as mean ± SEM. Student's t-test was employed, with $p \leq 0.05$ considered to be significant. ASCs derived from separate individuals were used for each replicate. Cryopreservation experiments and flow cytometry analysis were repeated six times. For flow cytometry analysis, each "n" replicate was composed of a single well and treatment in which ~20,000 cell events were analyzed and each experiment was conducted in triplicate. For

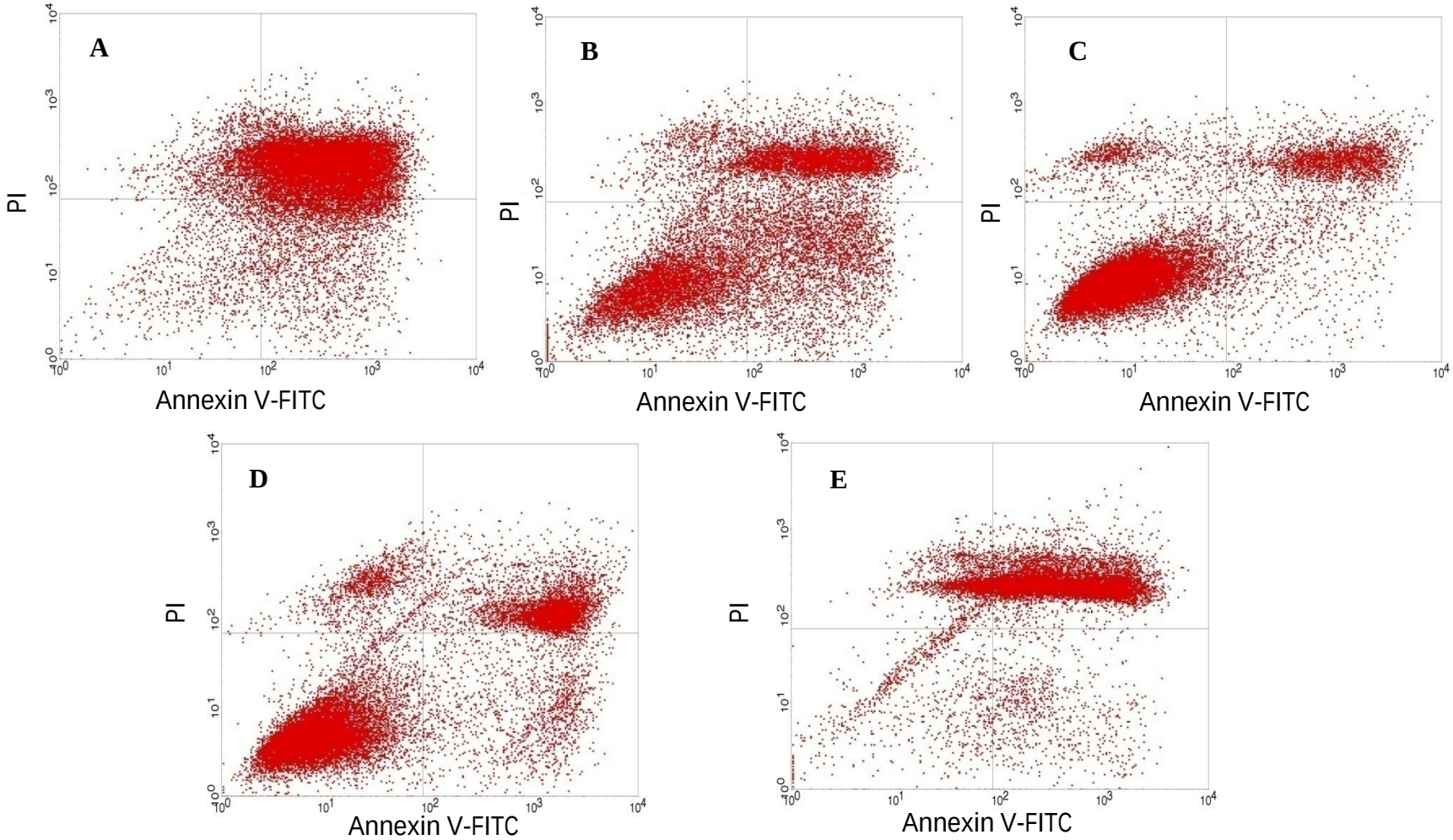

Figure 5.1: Characteristic flow cytometer fluorescence dotplots showing Fluorescence-Activated Cell Sorting (FACS) analysis of ASCs frozen/thawed in the presence various concentrations (1, 5, 10, 20 and 40%) of PVP in DMEM. Figures 5.1A, 5.1B, 5.1C, 5.1D, and 5.1E represent 1, 5, 10, 20 and 40% PVP in DMEM, respectively. The fluorescent dotplots show three cell populations: live (annexin V-FITC-negative and PI-negative; annexin V^- and PI^-) necrotic (annexin V-FITC-positive and PI-positive; annexin V^+ and PI^+), and apoptotic (annexin V-FITC-positive and PI-negative; annexin V^+ and PI^-). The quadrants positions were placed according to the no treatment control and 5 mM H_2O_2 necrotic control (see text for further details).

Table 5.1: The % of viable, apoptotic, and necrotic ASCs obtained using Fluorescence-Activated Cell Sorting (FACS) analysis for cells frozen in 10% DMSO in DMEM media with either 80% Fetal Calf Serum (FCS) or 80% (Human Serum, HS). The % of viable, apoptotic, and necrotic ASCs obtained FACS analysis are also shown for untreated (unfrozen, controls), apoptotic control (treated with 40 µM of Etoposide per ml of cell culture media) and necrotic control (5 mM of hydrogen pereoxide, H_2O_2).

	%Viable (± stdev)	%Apoptotic (± stdev)	%Necrotic (± stdev)
Media with Serum			
80% HS with 10% DMSO in DMEM	82.5 (± 8.3)	5.8 (± 3.9)	8.3 (± 3.3)
80% FCS with 10% DMSO in DMEM	84.1 (± 7.7)	5.7 (± 2.8)	7.5 (± 3.7)
Assay Controls			
Live (Untreated, unfrozen control)	80.2 (± 2.2)	7.3 (± 0.4)	8.6 (± 0.8)
Apoptotic (Etoposide treated)	56.1 (± 8.5)	18.2 (± 1.4)	20.7 (± 3.5)
Necrotic (H_2O_2 treated)	8.8 (± 2.8)	14.5 (± 6.2)	75.0 (± 3.4)

adipogenic and osteogenic differentiation analysis, the staining and gene marker analysis were performed with three replicates.

5.3 RESULTS

As described earlier, the use of PVP with concentrations ranging from 1 to 40% as the sole CPA in DMEM on the post-freeze/thaw viability, apoptotic and necrotic response of ASCs was assessed using flow cytometry. Characteristic flow cytometer fluorescence dotplots for ASCs frozen-thawed with different concentrations of PVP as determined by annexin V staining and PI-uptake are shown in Fig. 5.1. The fluorescence dotplots for cells frozen in the presence

of 1% and 40% PVP (Figs. 5.1A and 5.1E) show a majority of the cells are in the upper right quadrant (annexin V^+ and PI^+) which corresponds to necrotic cell population. Between 1 and 40% PVP, the number of cells present in the lower left quadrant (annexin V^- and PI^-), which corresponds to live cell population, initially increases and then decreases with maximum number of live cells at 10% PVP (Figs. 5.1B, 5.1C and 5.1D). Similar population quadrant analysis was performed on all other experimental treatments to obtain quantitative information on the condition of the cells following the freeze–thaw process (See Tables 5.1 to 5.3).

The post-thaw results obtained from the most routinely used cryopreservation media, either 80% fetal calf serum (FCS) with 10%DMSO in DMEM or 80% human serum (HS) with 10% DMSO in DMEM, were used as controls. The post-thaw behavior of cells frozen obtained using this traditional cryopreservation media is shown in Table 5.1. The viability of ASCs cryopreserved in the control media containing 80% serum with 10%DMSO in DMEM was ~83±8% (Table 5.1). Presumably, this routinely used cryopreservation media produces maximum viability; therefore, this data was used as a control to compare with the data obtained from the freezing media supplemented with PVP. The control data also suggests that the choice of the serum (human or animal) does not alter the ASC survival when frozen/thawed in DMSO and DMEM (Table 5.1). Additional data from assay experiments (unfrozen cells, apoptotic control treated with Epotoside, necrotic cells treated with H_2O_2) are also shown in Table 5.1.

As shown in Table 5.2 and Fig 5.2, the viability of ASCs frozen in PVP and DMEM resembles an inverted U-shape (with 10% PVP being optimal). The use of 1% and 40% PVP in

Table 5.2: The % of viable, apoptotic, and necrotic ASCs obtained using Fluorescence-Activated Cell Sorting (FACS) analysis for cells frozen in DMEM media with varying concentrations (1, 5, 10, 20 and 40%) of PVP.

% of PVP in DMEM	%Viable (± stdev)	%Apoptotic (± stdev)	%Necrotic (± stdev)
1	5.7 (± 0.5)	23.2 (± 1.7)	64.5 (± 8.5)
5	49.3 (± 8.0)	21.0 (± 0.7)	22.6 (± 6.3)
10	64.9 (± 9.6)	12.7 (± 2.6)	15.3 (± 5.7)
20	55.5 (± 11.0)	9.4 (± 2.3)	26.6 (± 4.7)
40	4.6 (± 1.3)	5.0 (± 2.2)	75.0 (± 6.8)

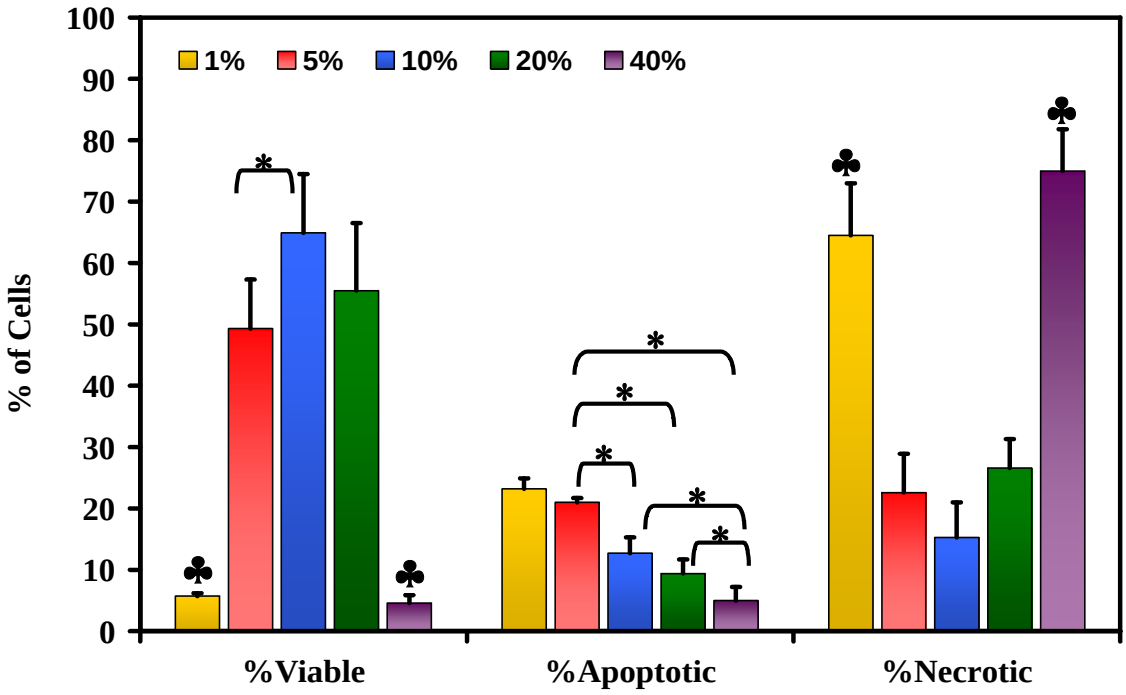

Figure 5.2: 24-hour post-thaw comparison of the percentage of live, necrotic and apoptotic ASCs are shown for various PVP treatments investigated. The error bars represent the standard error in the data. The horizontal bars denoted with asterisks (*) represent statistically significant differences between similar treatments. The symbol above the bar (♣) represents a significant difference from the corresponding data obtained for the other three PVP treatments. For example, in case of % viability, the 1% and 40% PVP treatments are significantly connected with 5, 10 and 20 but not mutually.

DMEM caused a dramatic loss in cell viability (~5%) where as the use of 10% PVP produced a maximum viability of ~65% (Table 5.2). Although the viability of ASCs decreased when the % of PVP was increased from 10 to 20, the data analysis revealed that this increase is statistically not significant (95% confidence level). A similar but opposite trend was observed for the % of cells exhibiting necrosis. As expected, based on the viability response, the % of necrotic ASCs showed a U-shaped response with increasing concentration of PVP. ASCs treated with 1 and 40% PVP treatments were found to have a significant amount of necrotic cells (~65 to 75%) when compared to other treatments (~15 to 27%). Intriguingly, the percentage of apoptotic cells decreased from ~23% to ~5% as the concentration of PVP in DMEM was increased from 1 to 40%.

Table 5.3 and Fig 5.3 show the post-freeze response of ASCs frozen at three concentrations (5, 10 and 20%) of PVP supplemented with either 10% FCS or 10% HS in DMEM. The addition of serum to the freezing media increased the % of viable ASCs by ~4 to 9% when compared with the values obtained in their absence (see Tables 5.2 and 5.3 and Fig 5.3). However, a closer examination of the data revealed that this improvement in the post-thaw cell viability was not statistically significant (95% confidence level). Similarly, the variations in the measured values of apoptotic and necrotic cells obtained in the presence of HS or FCS with PVP and DMEM when compared with the values obtained with just PVP in DMEM are also not statistically significant (95% confidence level).

To further analyze the effect of increasing the % of serum in the media with PVP, we have repeated the cryopreservation experiments with 10% PVP as CPA in the presence of 40% and 80% fetal calf serum (FCS). Fig. 4 shows the viability, apoptotic and necrotic response of P1

Table 5.3: The % of viable, apoptotic, and necrotic ASCs obtained using Fluorescence-Activated Cell Sorting (FACS) analysis for cells frozen in DMEM media with varying concentrations (5, 10 and 20%) of PVP with either 10% of Human Serum (HS) or with 10% Fetal Calf Serum (FCS).

Freezing Media	%Viable Cells (± stdev)	%Apoptotic Cells (± stdev)	%Necrotic Cells (± stdev)
Human Serum (HS)			
85% DMEM +10% HS + 5% PVP	53.2 (± 8.7)	17.6 (± 2.6)	25.5 (± 5.7)
80% DMEM +10% HS + 10% PVP	72.1 (± 8.1)	9.2 (± 0.5)	11.1 (± 5.2)
70% DMEM +10% HS + 20% PVP	61.8 (± 12.5)	10.8 (± 4.2)	24.5 (± 6.0)
Fetal Calf Serum (CS)			
85% DMEM +10% FCS + 5% PVP	55.4 (± 11.0)	15.4 (± 2.1)	19.3 (± 2.6)
80% DMEM +10% FCS + 10% PVP	69.2 (± 6.7)	9.3 (± 1.6)	15.0 (± 2.3)
70% DMEM +10% FCS + 20% PVP	64.3 (± 6.4)	13.2 (± 4.7)	19.6 (± 2.3)

ASCs when cryopreserved in the presence of 10% PVP and DMEM with either 0, or 10, or 40, or 80% FCS. As seen in Fig 5.3, increasing the % of FCS from 10% to 80% did not significantly increase the % of viable cells nor did it significantly decrease the % of necrotic or apoptotic cells. These observations (Tables 5.2 and 5.3; Fig 5.4) indicate that the presence of serum may not be vital to the post-thaw viability and apoptotic, necrotic response of P1 ASCs frozen in PVP and DMEM (and in the absence of DMSO). To address whether the presence of PVP and the absence of serum and DMSO during cryopreservation affects post-thaw adipogenic and osteogenic differentiation in ASCs, we utilized Toluidine blue, Oil Red O and Alizarin Red to stain the undifferentiated ASCs, adipocytes and osteoblasts respectively.

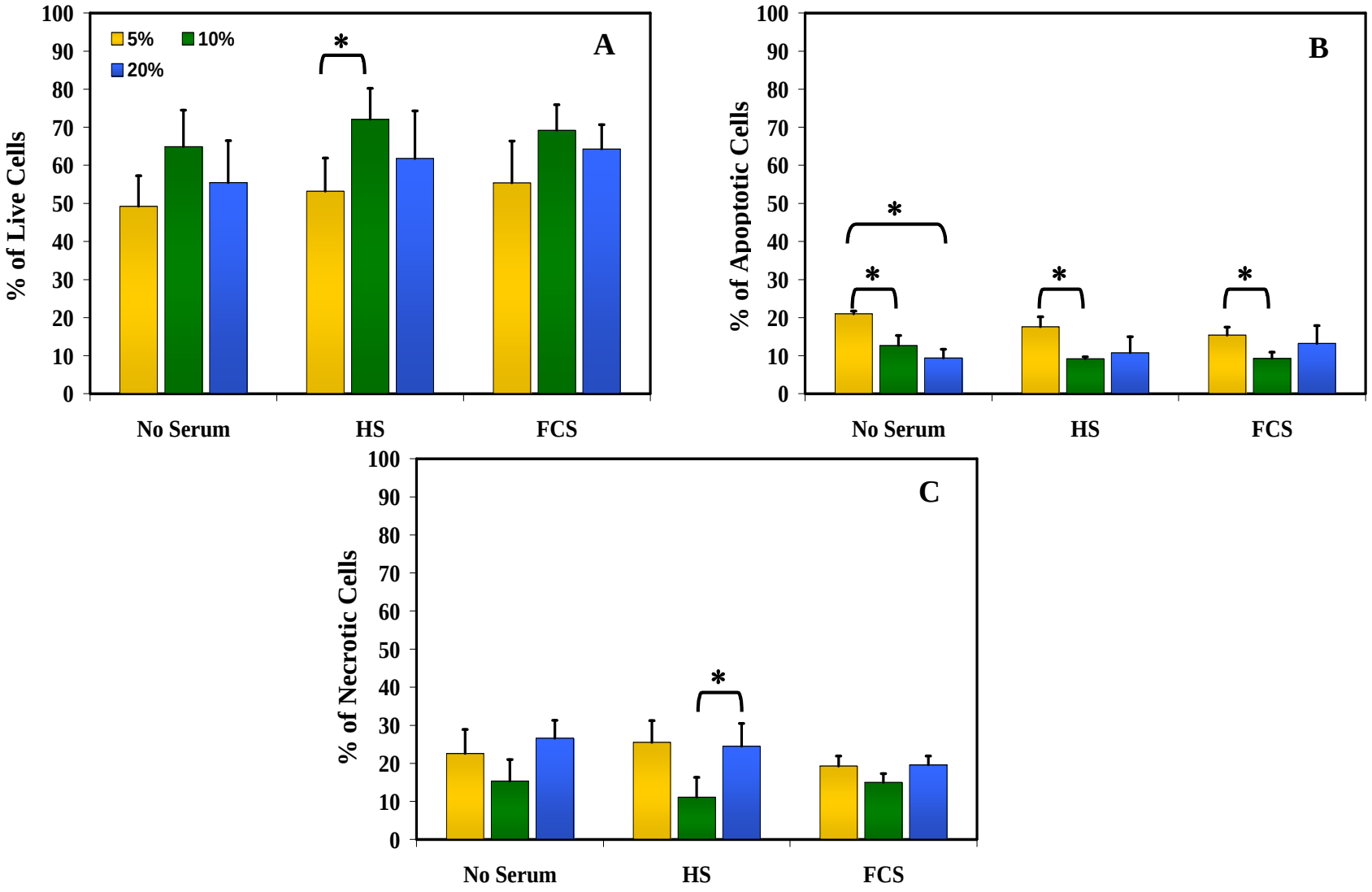

Figure 5.3: 24-hour post-thaw comparison of the percentage of live, necrotic and apoptotic ASCs are shown for various PVP treatments investigated in the presence of 10% serum: live (Fig 5.3A), apoptotic (Fig 5.3B) and necrotic (Fig 5.3C). The error bars represent the standard error in the data. The horizontal bars denoted with asterisks (*) represent statistically significant differences between similar treatments

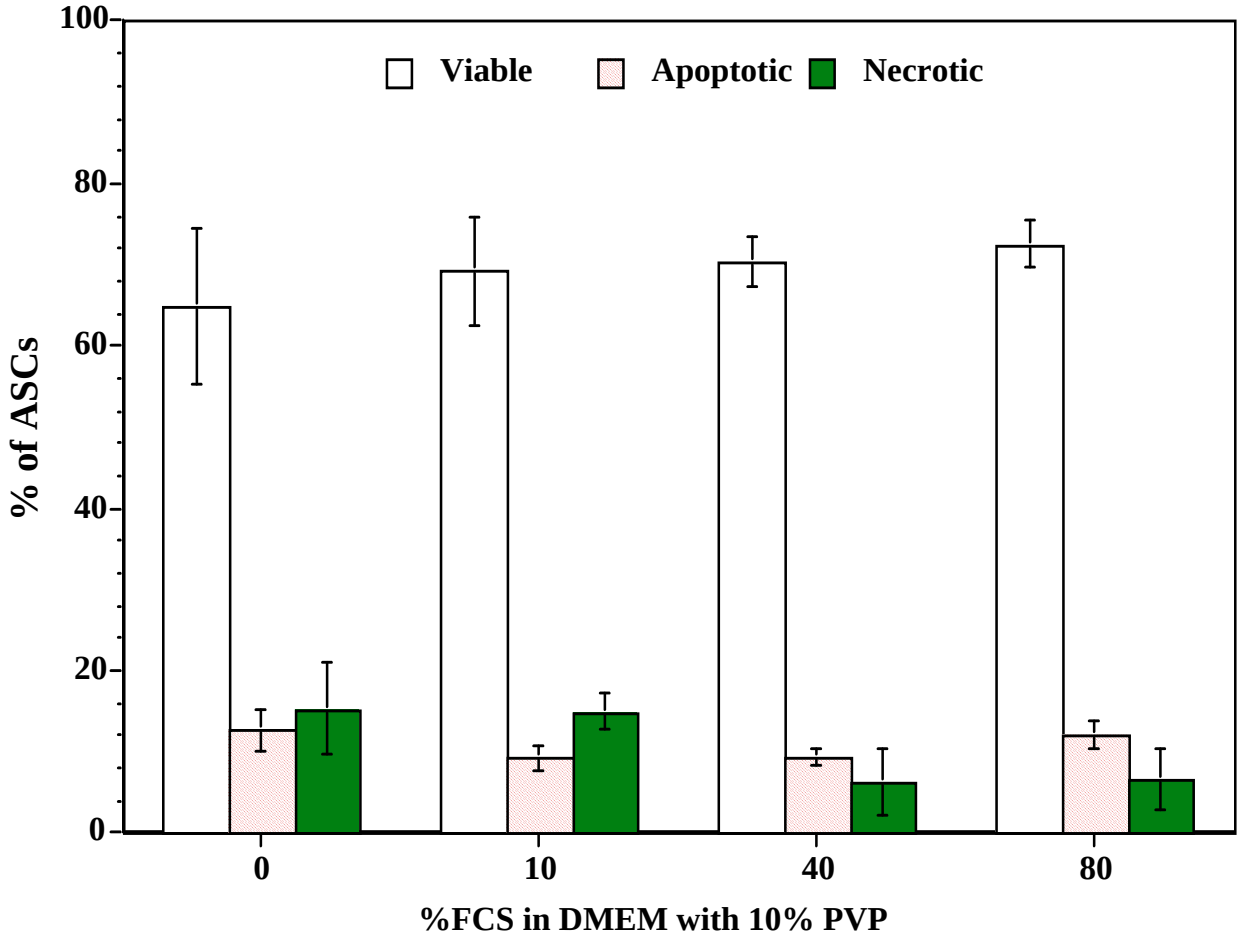

Figure 5.4: 24-hour post-thaw comparison of the percentage of live, necrotic and apoptotic ASCs are shown for various PVP treatments investigated. The error bars represent the standard error in the data. The horizontal bars denoted with asterisks (*) represent statistically significant differences between similar treatments. The symbol above the bar (♣) represents a significant difference from the corresponding data obtained for the other three PVP treatments. For example, in case of % viability, the 1% and 40% PVP treatments are significantly connected with 5, 10 and 20 but not mutually.

As described earlier, the staining was then extracted from the differentiated cells and the optical density (OD) at the appropriate wavelength was determined. The P1 ASCs after 14 days of adipogenic induction and 21 days of osteogenic induction displayed morphological features consistent with adipogenesis or osteogenesis from control (unfrozen) cells (data not shown).

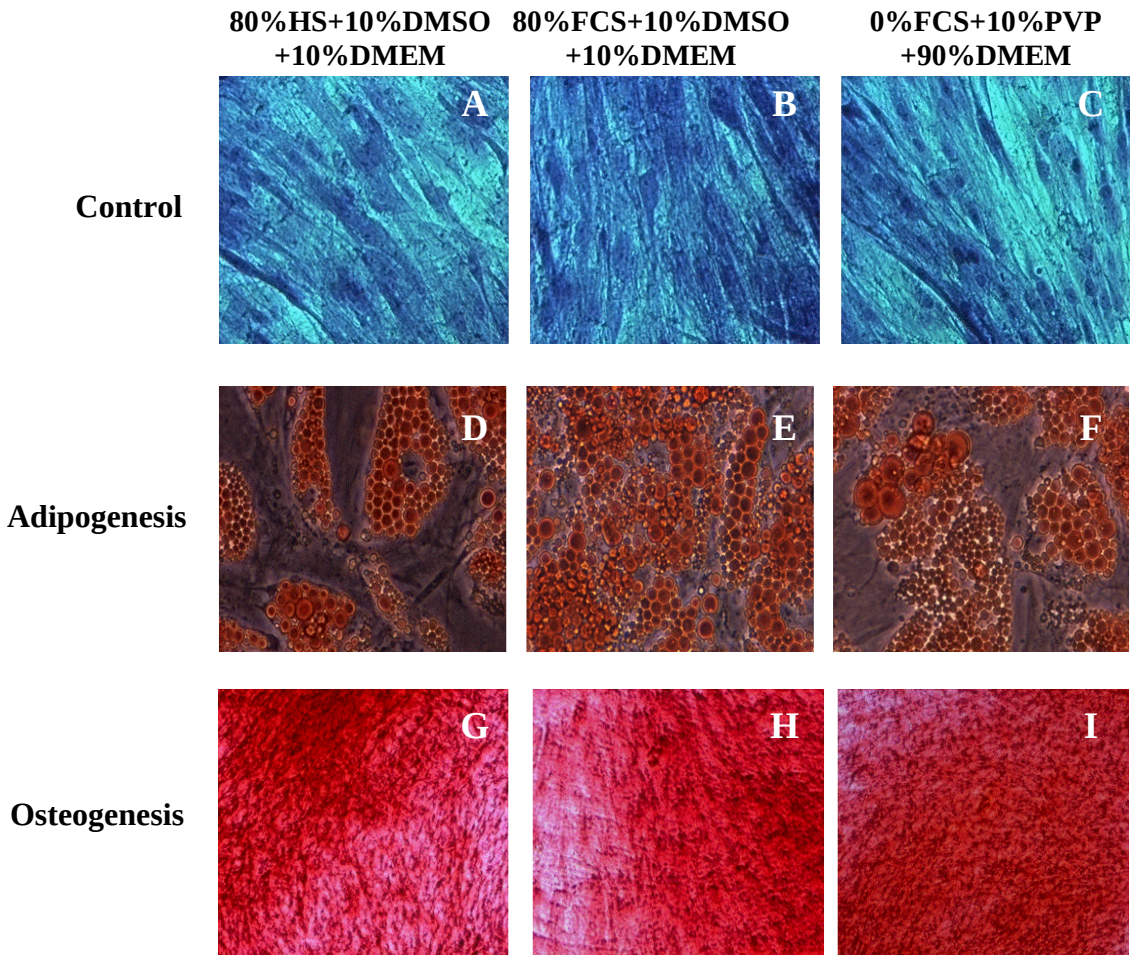

Figure 5.5: Representative phase contrast photomicrographs of P1 ASCs cultured under untreated (Figs 5.5A, 5.5B and 5.5C), adipogenic (Figs 5.5D, 5.5E and 5.5F), or osteogenic (Figs 5.5G, 5.5H and 5.5I) conditions. Adipogenic cultures were stained with oil red O 14 days after induction while osteogenic cultures were stained with alizarin red after 21 days of culture. Figs. 5.5A, 5.5D, 5.5G represent cells that were cryopreserved in media containing 80% HS with 10% DMSO in DMEM. Figs. 5.5B, 5.5E, 5.5H represent cells that were cryopreserved in media containing 80% FCS with 10% DMSO in DMEM. Figs. 4C, 4F, 4I represent cells that were cryopreserved in media containing 0% FCS with 10% PVP in DMEM.

Representative photomicrographs in Fig. 5.5, show undifferentiated ASCs stained positive with toluidine blue (Figs. 5.5A, 5.5B, 5.5C), adipocytes stained positive with Oil Red O (Figs. 5.5D, 5.5E, 5.5F) and mineralized (osteoblast) cultures stained positive with Alizarin Red (Figs. 5.5G, 5.5H, 5.5I). Our experiments showed no significant morphological differences

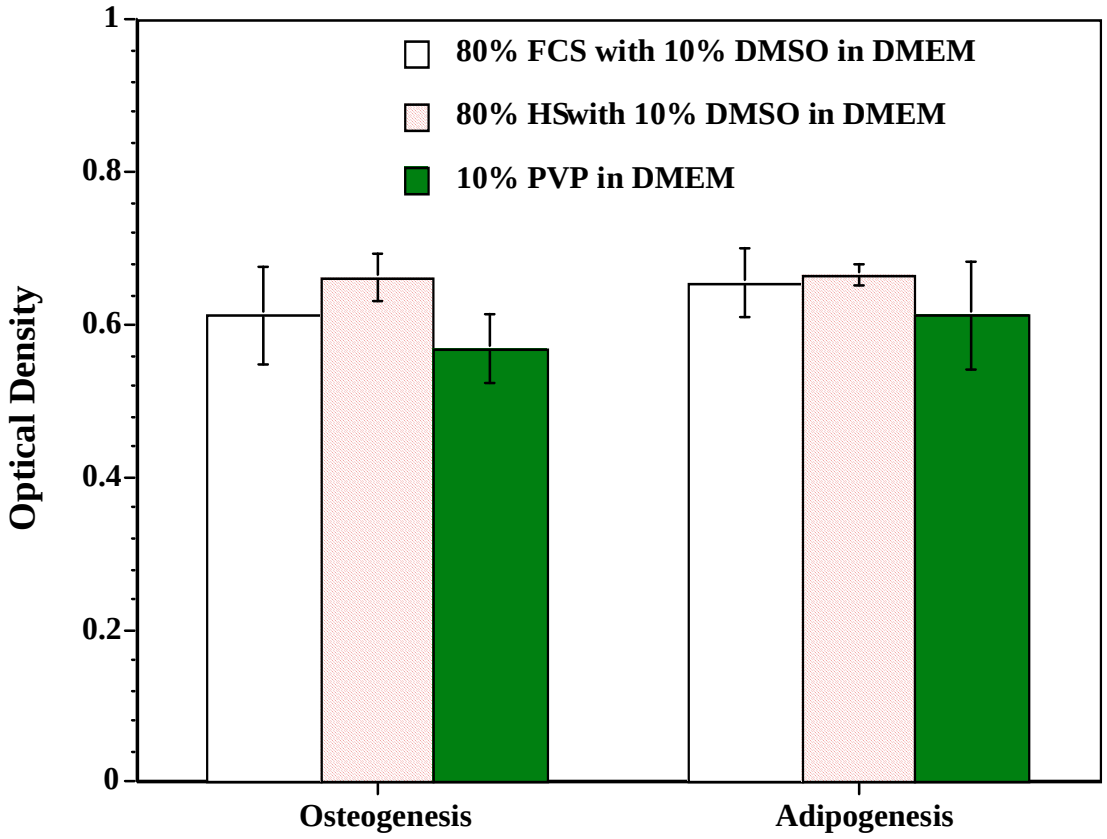

Figure 5.6: Optical density of the extracted dye of ASCs cryopreserved in DMEM containing 80% FCS and 10% DMSO (unshaded columns), in DMEM containing 80% HS and 10% DMSO (partially shaded columns), and in DMEM containing 10% PVP (shaded columns). As stated in the text, we utilized Toluidine blue, Alizarin Red and Oil Red O to stain the undifferentiated ASCs, differentiated osteoblasts, and differentiated adipocytes, respectively. The staining was then extracted from the differentiated cells and the optical density (OD) at the appropriate wavelength was determined (see text for further details).

between the cells cryopreserved in the presence of either 80% HS with 10% DMSO in DMEM (Figs. 5.5A, 5.5D, 5.5G) or 80% FCS with 10% DMSO in DMEM (Figs. 5.5B, 5.5E, 5.5H). More importantly, the results indicated that the adipogenic or osteogenic morphology of the cells cryopreserved in the presence of 10% PVP in DMEM and without any serum (Figs. 5.5C, 5.5F, 5.5I) is consistent with, and no different from, the control experiments with HS (Figs. 5.5A, 5.5D, 5.5G) and with FCS (Figs. 5.5B, 5.5E, 5.5H). The quantitative optical density (OD) measurements from the eluted stains indicated a slight decrease in the differentiation potential

of the ASCs when cryopreserved in the presence of 10% PVP in DMEM (and in the absence of FCS and DMSO) when compared with that obtained from cells frozen with 80% FCS and 10% DMSO in DMEM and with cells frozen with 80% HS and 10% DMSO in DMEM (Fig. 5.6). However, the decrease in the optical density measurement (or as it correlates to the decrease in the differentiation ability) was statistically not significant (95% confidence level).

5.4 DISCUSSION

Prior published work has shown that serum free solutions could be designed that would support cells and tissues at cryopreservation temperatures (Reuther et al., 2006; Merten et al., 1995; Corsini et al., 2004; Sasaki et al., 2005). PVP has been added to slow-cooling, rapid-cooling and vitrification solutions for several cellular systems (El-Shewy et al., 2004; Li et al., 2006; Gómez-Lechón et al., 2006). However, few studies report the use of PVP as the sole component in the cryopreservation media; but it is more commonly used as an additive, and in conjunction, with permeating cryoprotectants like DMSO (Fuller 2004). Solutions containing large amounts of polymers have also been used for corneal cryopreservation (Madden 1993). Despite its widespread use as an additive in cryopreservation media, some studies do report that PVP causes toxic damage during addition and removal (Fuller 2004; Kuleshova 2001). Suzuki et al (2005) determined that 5% PVP had a beneficial effect compared with 10% or 20% PVP for slow freezing of germinal vesicle stage bovine oocytes. A recent study by Li et al (2006) showed that the use fo 10% PVP as a sole cryoprotectant produced maximum survival (~95%), as evidenced by trypan blue dye exclusion, for porcine pre-adipocytes. In our experiments, extremely low (1%) and extremely high (40%) concentrations of PVP caused significant reduction in the % of viable ASCs post-freeze/thaw. Obviously, this suggests that: (i) a minimal

% of PVP is needed before it can act as a cryoprotectant; and (ii) increasing the concentration of PVP beyond an optimum value, causes toxic damage to the cells.

Increasing the serum concentration in the cryopreservation medium has often been shown to increase the post-thaw survival rate of cells that are difficult to preserve; serum concentrations as high as 90% have been reportedly used (Gómez-Lechón 2006; Stevenson 2004; Freshney 2000). Our results demonstrate that the choice of serum (either animal or human) did not alter the phenotype characteristics of frozen/thawed P1 ASCs. This valuable observation, if found to be valid for other cells as well, should allow researchers to shift to allogeneic serum, rather than using xenogenic serum which may contain anomalous and infectious particles, in future cell cryopreservation experiments. However, the use of allogeneic serum does not completely eliminate the risk of bacterial toxins and microorganisms such as viruses, bacteria and fungi (Reuther et al., 2006). Autologous serum could be an alternative for ASCs cryopreservation and culture. However, production of autologous serum is a painstaking and time consuming process and the amount of autologous serum necessary for storage and sufficient expansion of ASCs would exceed the amount a patient could safely provide (Lange et al., 2007). Therefore complete elimination of unhealthy serum products is the best alternative for cryopreservation storage of ASCs for future clinical applications.

The mechanism by which PVP is able to protect cells is not well known. Since the probability of ice formation during cryopreservation plays a major role in the cell survival, the possibility of achieving low temperature storage which avoids ice formation has been a long time research goal. Avoiding damaging ice crystals and achieving glass transition at relatively high temperatures is one way to improve the post-thaw cell survival (Thirumala et al., 2007). In

our experiments the ASCs were cryopreserved by placing them overnight at –80˚C in an ethanol jacketed container, before being transferred to liquid nitrogen. The temperature/time history experienced by the ASCs during the freezing process as well as the associated cooling rates (CRs) measured using a temperature data logger indicated that the ASCs experienced different cooling rates at different time points when frozen in a media consisting of DMEM and PVP when compared with media consisting of DMEM with DMSO and serum (data not shown). Additionally, the cells frozen with PVP experienced significant super-cooling of the extracellular media. Briefly, based on the measured osmolality the phase change temperature of DMEM media containing 10% PVP is –0.6˚C. However, in our freezing experiments the phase change of the extracellular medium in the presence of PVP occurred at –15˚C, i.e., with a significant super-cooling (data not shown). This super-cooling might have resulted in the formation of damaging ice crystals and hence the observed lower post-thaw viability of ASCs frozen with PVP and DMEM when compared with cells frozen with serum and DMSO in DMEM (see Tables 5.1 and 5.2). This possibly deleterious super-cooling associated with the presence of PVP in the freezing media could not be eliminated even with the addition of ice nucleating agents like *Pseudomonas Syringae* (data not shown).

There are several hypothesis reported in the literature concerning polymer cryoprotection but none are widely accepted. These hypothesis include: (i) the possibility that high molecular weight polymers such as PVP could act colligatively and protect cells during freezing (Fuller 2004); (ii) the coating of cell membranes by PVP has been suggested as an alternative mechanism of polymer cryoprotection (Fuller 2004; Nash, 1966); (iii) at high concentrations, PVP exerts considerable effects on freezing point depression of the system, in

excess of that predicted from its molar concentrations (Fuller 2004; Farrant 1969).. Thus, the protection offered by PVP is possibly linked to its non-ideal behavior at high concentrations in aqueous solutions. Further work is clearly needed to elucidate the cryoprotective mechanism of PVP and to mechanistically (biophysically) develop and optimize cryopreservation media for ASCs as well as other cell types.

5.5 CONCLUSIONS

To the best of our knowledge, this is the first attempt to develop serum free, DMSO free solutions for cryopreservation of ASCs. Towards this goal, we have investigated a range of PVP concentrations on the post-thaw behavior and differentiation ability of ASCs in the absence of any serum and DMSO. The results of this study demonstrate that the presence or absence of serum did not significantly alter the viability of ASCs frozen with 10% PVP in DMEM. Although the data indicates some decrease in post-thaw cell viability of ASCs cryopreserved in PVP when compared with the values obtained for cells cryopreserved in 80% serum with 10% DMSO in DMEM. More importantly, the ASCs frozen/thawed in the presence of PVP (and in the absence of both DMSO and serum) displayed similar phenotype and expression patterns of surface markers (morphology and growth/differentiation characteristics) when compared to the ASCs cryopreserved in 80% serum with 10% DMSO in DMEM. We could, thus, hope that serum free cryopreservation is a distinct possibility for adipose stem cell lines, in the near future; and believe that using PVP as the sole cryoprotectant for freezing storage of ASCs could enhance and encourage their use in a wide range of tissue engineering and regenerative medicine problems.

CHAPTER 6
FABRICATION OF MULTIDIMENSIONAL CELLS SHEETS USING ADIPOSE DERIVED STEM CELLS

6.1 INTRODUCTION

While tissue engineering has long been thought to possess enormous potential, conventional applications using biodegradable scaffolds have limited the field's progress, demonstrating a need for new methods (Yang et al., 2005). Most natural tissues are multidimensional in construction that plays a significant role in the mechanical and physiological functions of these tissues. In order to generate tissue with intrinsic functions suitable for *in vivo* applications, it is primarily decisive to develop a method to fabricate 3D tissue in an in vitro or in vivo environment. Traditional tissue engineering methods have generally focused on one of two strategies: either the injection of isolated cell suspensions or the use of biodegradable scaffolds to support tissue formation. There has been considerable progress in developing 3 dimensional cellularized scaffolds to fabricate various tissues including bone, cartilage, blood vessel, nerve, liver, myocardium and many other tissues (Hubbell et al., 1991); (Sikavitsas et al., 2002; Sittinger et al., 1996). However, most of the conventional scaffolds do not allow sufficient cell migration to establish adequate cell–extracellular matrix (ECM) and cell–cell interaction.

Cell seeding plays a crucial role in determining the progression of tissue formation to establish 3 dimensional cell cultures. High density cell seeding in static and dynamic cultures inside bioreactors are methods to improve cell seeding in scaffolds (Sistino, 2003; Martin, 2004). Since the cells located in the interior of the scaffold rely on diffusion for solute transport, the current methods of seeding are compromised by the diminution of nutrients.

To overcome some of the drawbacks associated with traditional scaffold based tissue engineering, cell sheet engineering has been developed as an alternative approach for tissue engineering by Okano's group (Matsuda 2007; Shimizu et al., 2006; Yang et al., 2005). Cell sheet engineering has the advantage of eliminating the use of biodegradable scaffolds. Using temperature-responsive PIPAAm coated TCPS dishes, cultured cells were successfully harvested as intact sheets by simple temperature changes, thereby avoiding the use of proteolytic enzymes (Matsuda 2007; Shimizu et al., 2006; Yang et al., 2005). In a more recent study, a novel method, using a thermoresponsive hydrogel coated on TCPS dishes, was developed for harvesting living cell sheets (Chen et al., 2006). The hydrogel was prepared by pouring aqueous methylcellulose blended with distinct salts on TCPS dishes at room temperature and subsequently gelled at 37 ^{o}C for cell culture. MC with a viscosity of 4000cP at 2% solution was used to form gels at physiological temperatures (Chen et al., 2006). However, the method developed was complicate as MC was too viscous to manipulate with and 50% drying of the hydrogel system to achieve a gel formation temperature below 37 ^{o}C was not practical in a routine cell culture lab. In addition, the procedure described results in a non-uniform coating and is not practicable in a standard cell culture facility. Further, the MC systems generated were not consistently stable as the time of culture is increased.

To overcome the shortcomings associated with the earlier cell sheet engineering technologies (N. Matsuda 2007; Shimizu et al., 2006; Yang et al., 2005; Chen et al 2006) we have developed a modified MC-collagen hydrogel method to create cell sheets, specifically tailored to work with ASCs. By using the method developed by Chen et al., (2006) and by undertaking a systematic study of the thermal (gelation, degradation and swelling) properties

of MC solutions of varying molecular weights, salt concentration, polymer concentration, we were able to discover the optimal composition of MC-aqueous solutions that will form gels at experimentally viable temperatures of ~32 ˚C. A brief description of our experiments in developing/characterizing/fabricating a hydrogel system that is suitable for cell culture and bench-top lab experiments is provided below.

6.2 MATERIALS AND METHODS

6.2.1: Materials

Methylcellulose (MC), with the trade names of M7140, M0262 and M0512 were obtained from Sigma Chemicals. According to the product specifications, the number-average molecular weights of M7140, M0262 and M0512 are 15000, 41000 and 88000 respectively (Table 5.1). Type I collagen solution (3mg/ml Ultra Pure bovine) was purchased from Sigma-Aldrich (Sigma Chemical Company, USA).

6.2.2: Preparation of Aqueous MC

MC solutions were formed by a dispersion technique. Briefly, approximately 1/2 of the required volume of solvent was heated above 90 ºC. The MC powder was mixed with heated solvent and agitated until all polymer particles were thoroughly wetted. The remainder of the solvent volume, a specific dilution of stock 10X phosphate-buffered saline (PBS; Gibco Life Technologies, USA) or H_2O was added cold and the mixture was gently stirred. As the temperature was lowered to 0°C, the polymer became water-soluble, forming a clear solution. Once the entire polymer solution was brought to 0°C, light agitation was continued for 30min and the solutions were allowed to equilibrate at 4°C overnight. The following compositions of

Table 6.1: Commercial names, molecular weights and maneagable aqueous concentrations of methylcellulose (MC)

Methylcellulose (MC)	Molecular Weight	Manageable Concentrations for Spin Coating
M0512	88,000	4%
M0262	41,000	8%
M7140	15,000	16%

MC polymer solutions were formed. For M0512: 1, 2, 3, 4, 5 and 6% of MC in H_2O, 0.5X, 1X, 2X, 4X and 6X PBS; for M0262: 2, 4, 6, and 8% MC in H_2O, 0.5X and 1.0X PBS; and finally for M7140: 2, 4, 6, 8, 10, 12, 14 and 16% MC in H_2O, 0.5X and 1X PBS. For the cell-culture experiments, the prepared MC solutions were autoclaved for 30min at 121°C, 100 kPa.

6.2.3: Calorimetric Characterization of Aqueous MC Solutions

The physical gelation phenomena of aqueous MC solutions with temperature were measured by a differential scanning calorimeter (DSC, Pyris Diamond, Perkin-Elmer, Shelton, CT). The DSC was used to determine the transition temperatures of the prepared aqueous MC solutions heating from 10 to 90 °C. A sample weight of 15-20µg was used for analysis and the reference cell was filled with deionized water. A heating rate of 10°C/min was used for all test samples.

6.2.4: Preparation of the MC Hydrogel Coated TCPS Dish

The prepared aqueous MC solutions that had a gelation temperature below 37 °C were used to coat TCPS dishes (Falcon 3653, diameter 35 mm, Becton Dickinson Labware, Franklin Lakes, NJ). An amount of 400µl of test MC solution was poured into the center of each TCPS

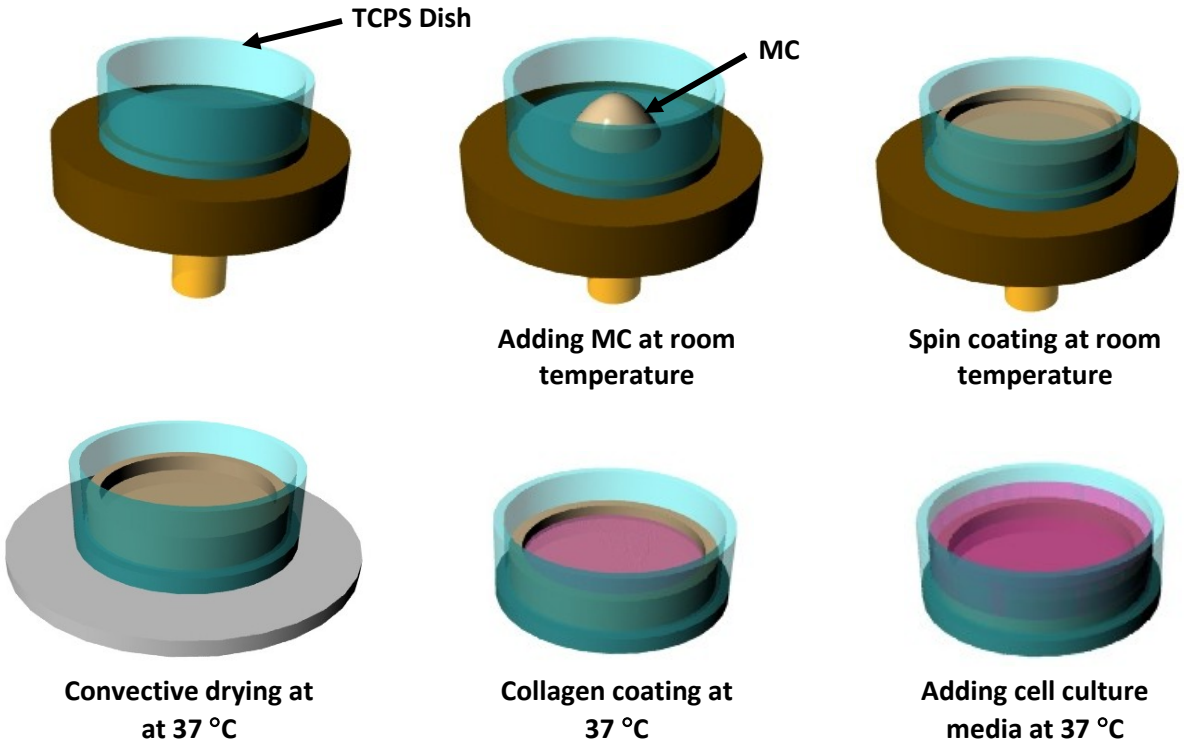

Figure 6.1: Methylcellulose coating procedure for MC-collagen hydrogel system. 300-400µl of MC was placed at the center of the dish before spin coated at a predetermined RPM for each type of MC. High RPM was required for high molecular weight MC.

dish at room temperature (~20°C). Spin coating was employed to evenly spread a thin transparent layer of MC on the TCPS dish. Subsequently, the dish was preincubated at 37°C for 1 h, and a gelled opaque MC hydrogel layer was formed on the dish.

6.2.5: In vitro Degradation, Swelling and Stability of MC Gels

The gels were constructed by spin coating 400µl of MC polymer solution to TCPS dishes, where they were allowed to equilibrate at 37°C for one hour (See Fig 6.1). 2ml of incubation media, consisting of DMEM-F12 and 10% calf serum was added to the dishes containing gels to

study degradation and swelling behavior. At 1, 4, 7, and 10 days of incubation, the media was removed from the dishes and the weight of the wet gel was recorded (n=4 for each gel/media combination). The polymer samples were then dried over night in a convective heater at 70 ^{o}C, and the remaining polymer mass was weighted. Swelling and degradation as a function of time were quantified using the following relationships.

$$\%\text{Swelling (t)} = \frac{\text{Gelweigth(t)}/\text{Polymerweight(t)}}{\text{Gelweight(0)}/\text{Polymerweigth(0)}} \times 100$$

$$\%\text{Degradation (t)} = \frac{\text{Polymerweight(0)} - \text{Polymerweight(t)}}{\text{Polymerweigth(0)}} \times 100$$

Swelling values are normalized to polymer weight to account for lost polymer mass during the swelling study. Further, to evaluate whether the salts blended in the MC hydrogel would leach out with time during in vitro culture, the coated TCPS dish was loaded with cell culture media and the osmolality of the loaded media was monitored with time using an osmometer (Model 3300, Advanced Instruments, Inc., Norwood, MA, USA). An uncoated TCPS dish loaded with the same media was used as a control.

6.2.6: Culture of ASCs on MC Coated TCPS Dishes

To improve the cell adhesion properties the MC hydrogel surface was further coated with collagen (100-150µL of aqueous type I collagen (0.5 mg/mL, bovine dermis collagen, Sigma Chemical Co, USA). Since, only alkaline collagen forms gel net work at physiological temperatures, the collagen solution was adjusted to pH 7.5 using NaOH and HCl. For dilutions 10X PBS (Sigma Chemical Company, USA) was used. Adipose stem cells were isolated from human fat tissue as described in previous chapters. Passage 0 (P0) cells were used in this study. The ASCs were added to the MC coated dish along with the stromal media containing 90%

DMEM/F-12, 10% fetal bovine serum and 1% penicillin-streptomycin. Care must be taken to add media at 37 ^{o}C. Cell attachment and growth were observed daily using a light microscope (E600, Nikon, Tokyo, Japan). A collagen-coated TCPS dish was used as a control.

6.3 RESULTS AND DISCUSSION

6.3.1: Thermal Characterization of Aqueous MC Solutions

A typical example of calorimetric thermogram determined using diamond DSC is shown in Fig 6.2 for a 2% solution of M7140 in 1X PBS. In the heating process, a sharp endothermic peak was observed at around 47 °C indicating the incipient gel formation temperature (IGT). DSC has been routinely used to detect endothermic heat of dehydration of polymeric materials (Sarkar and Walker 1995). Thermal gelation of MC is caused by hydrophobic interactions between molecules containing methoxyl groups. At low temperatures, the cellulose molecules

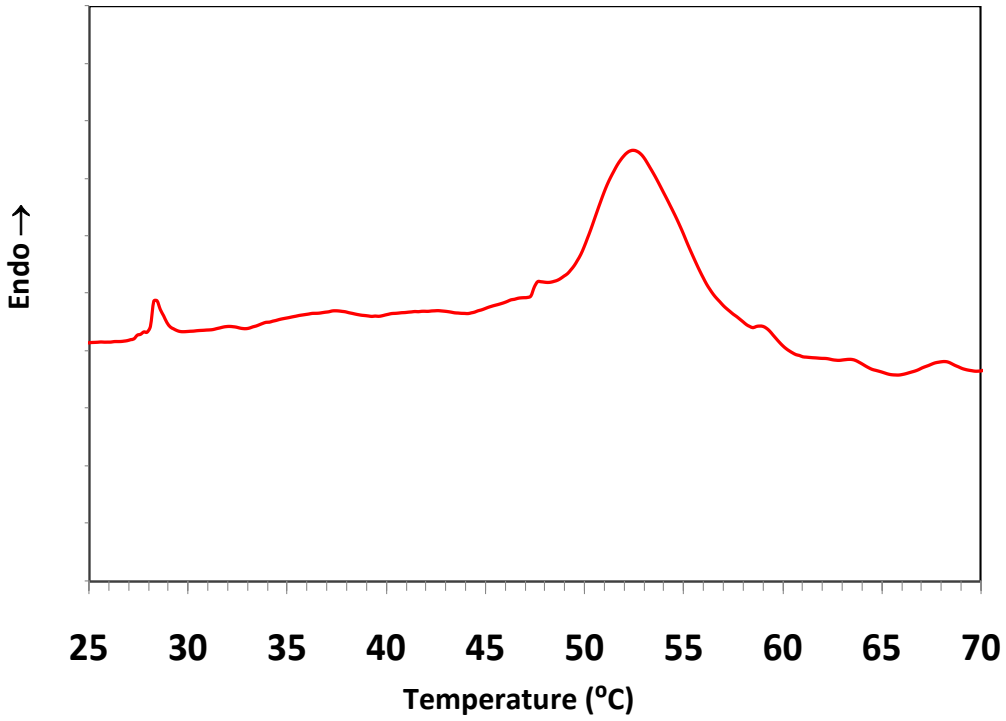

Figure 6.2: A calorimetric thermogram showing the incipient gelation temperature of M0512 at 2% in 1X PBS solution.

are hydrated and there is little polymer–polymer interaction apart from entanglement. As the temperature rises the solutions become less viscous and their viscosity decreases. Before dehydration is complete, polymer–polymer association occurs leading to an increase in viscosity (Sarkar 1979). As the temperature is increased, molecules absorb translational energy and gradually lose their water of hydration, resulting in lowering of viscosity. Eventually, a polymer-polymer association takes place, due to hydrophobic interactions, causing cloudiness in solution and an infinite network structure which results in a sharp rise in viscosity and turbidity as long as the concentration is relatively high. To further prove if the endothermic peaks from DSC thermogram correlated with the gelation, MC gelation was also

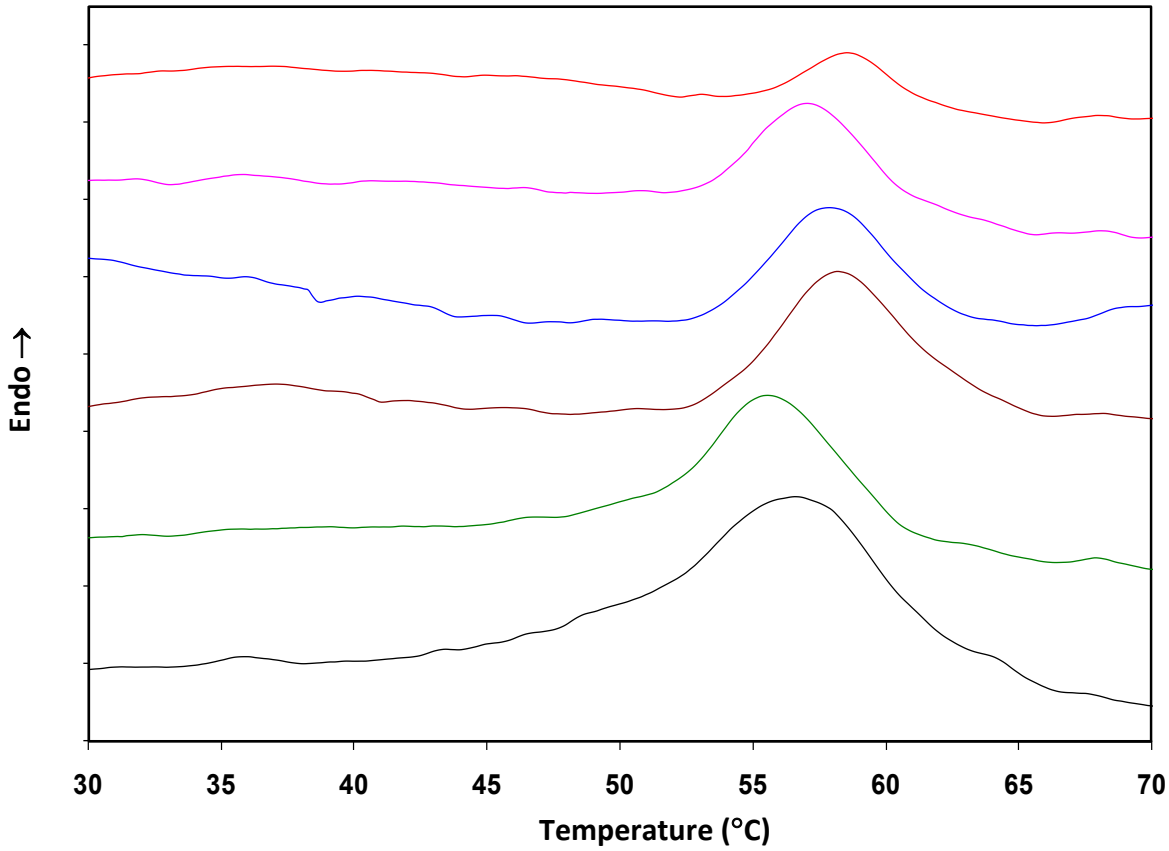

Figure 6.3: DSC thermograms of aqueous M0512 MC solutions at various concentrations. From top curve to bottom curve: 1%, 2%, 3%, 4%, 5% and 6%. The aqueous MC solutions were prepared as described in the methods section of this chapter.

assessed using the qualitative tube inversion method (data not shown). In this method it was assumed that a sample having a yield stress (gel) will not flow whereas a viscous but inelastic sample (sol) will show appreciable flow (Macosko 1994). Gel formation temperature values for the MC concentration series obtained from both DSC and tube inversion measurements were found to be statistically equivalent indicating the DSC endothermic peak was the representation of gel formation during heating.

Fig. 6.3 shows the effects of polymer concentration on heating thermograms for M0512. For the ease of visualization, the thermogram curves for all the concentrations were vertically lifted by a stepwise amount to prevent the curves from overlapping. As shown in Fig 6.3, as the concentration increases endothermic peak increases in height with increasing MC concentration but the peak temperature remains almost the same for up to 4% at around 53 ^{o}C. In addition, the endothermic peak becomes broader with increasing MC concentration suggesting the total energy absorbed by the MC solution increases with concentration. However, For M0512, the solutions above 4% are highly viscous and are extremely difficult to manipulate for TCPS dish coatings.

It was reported that the addition of salts lowers the gelation temperature of the aqueous MC solution (Grignon 1980; Li et al., 2003; Xu et al., 2004; Chen et al., 2006). Upon the addition of salts, water molecules are placed themselves around the salts as water has high affinity to salts than polymer. Therefore, it reduces the intermolecular hydrogen-bond formations between water molecules and the hydroxyl groups of MC. This can increase the hydrophobic interaction between MC molecules and lead to a decrease in their gelation temperature (Chen et al., 2006; Xu et al., 2004).

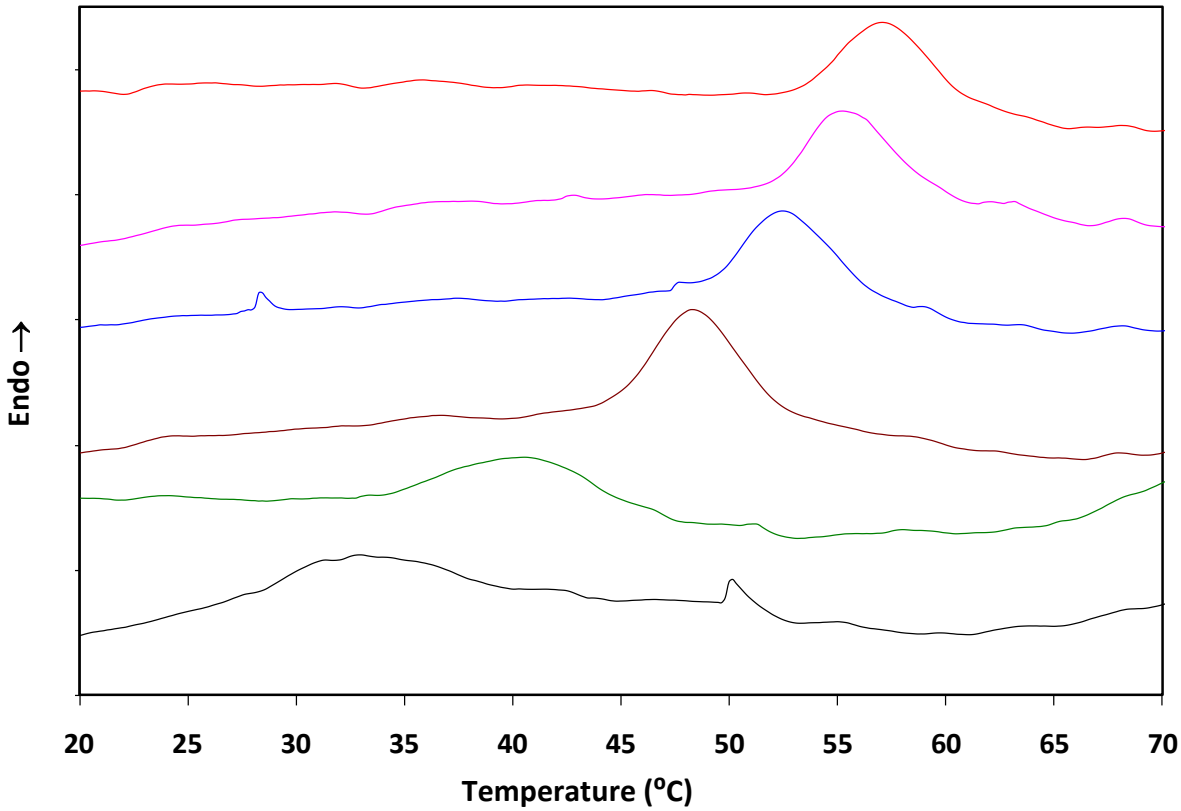

Figure 6.4: DSC thermograms of aqueous M0512 MC solutions (2% w/v) blended with different concentrations of PBS. From top curve to bottom curve: 0.0X, 0.5X, 1.0X, 2.0X, 4.0X and 6.0X. The aqueous MC + Salt solutions were prepared as described in the methods section of this chapter.

Fig 6.4 shows the effects of PBS concentration on the heating thermograms for M0512. As shown, the endothermic peak shifted to the left with increasing PBS concentration. This indicated that the addition of PBS in the aqueous MC solution reduced its sol gel transition temperature. Additionally, as higher concentration of PBS was used, then a lower temperature in its sol gel transition was observed. This fact was also observed in the measurements using tube inversion method.

Effects of salts and ions on the sol-gel transformation of polymers have been extensively studied (Heymann 1935; Sarkar 1979; Sarkar and Walker 1995; Xu et al., 2006; Xu et al., 2004). In general, salts may either enhance or reduce the hydrophobicity of a solute in water. It is

known that the salts mixed usually have a greater attraction for water molecules than polymer molecules, resulting in the removal of water of hydration from polymer chains and thus dehydrating or 'salting out' the polymeric molecules (Chen et al., 2006; Xu et al., 2004). It is well known that the molecules of a certain substance will accelerate its moving rate when giving a heating supply. Because the polymer molecule size and the water molecule size differ from each other greatly, they will behave quite differently when receiving such a heating supply. The smaller ones turn to move quickly while the bigger ones turn to move slowly. Such a difference in moving velocity will dispatch them from each other. Therefore the presence of any salts or electrolytes will promote this reduction in water polymer interaction because of the competing of the water by salts which reveal to us a decrease of the gel formation point.

6.3.2: Osmotic Response of Salt Blended MC Hydrogels

The osmolalities of aqueous MC solutions, used to prepare the MC hydrogels, increases nearly linearly with increasing the concentrations of the salt blended and MC (Chen et al., 2006). The osmolality of the cell culture media is normally maintained at ~300 mOsm/kg. At higher PBS concentrations due to the large difference in osmolality between the coated MC hydrogel and the cell culture media, the salts leak out from the hydrogel and join the cell culture media by significantly increasing its osmolality. This restricts the addition of large amounts of salts to MC solutions in order to reduce their gel formation temperature below the physiological temperature. For example as shown in Fig 6.4, the gel formation temperature of M0512 drops to below 37°C for 2% aqueous solution with the addition of 4X or 6X PBS. However, as shown by Chen et al., (2006), the osmolality of the culture solution significantly increases at high salt concentrations due to the increased osmotic difference between

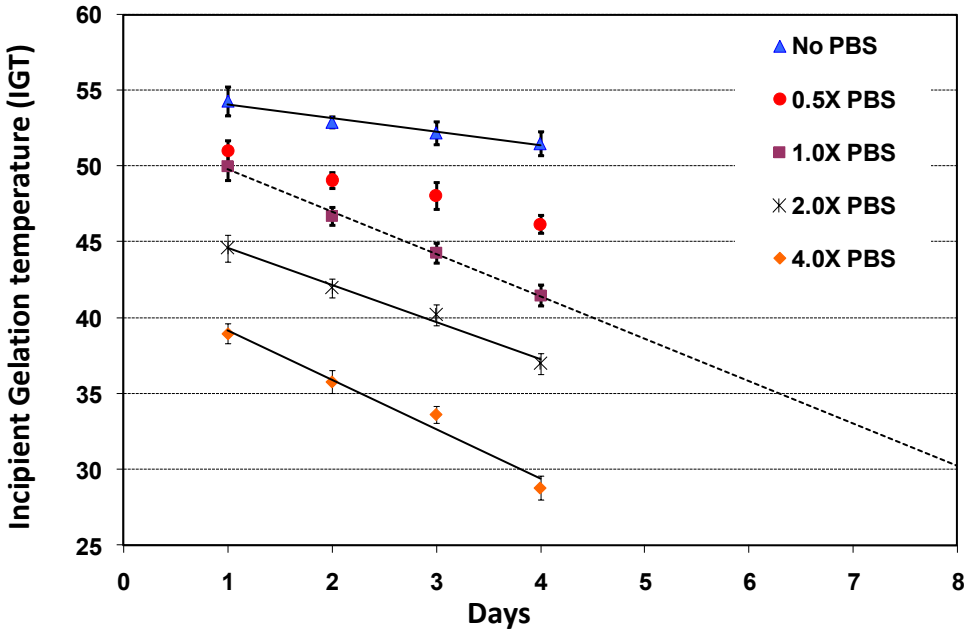

Figure 6.5: Effect of the concentrations of M0512 and PBS on the gelation temperature. The aqueous MC + Salt solutions were prepared as described in the methods section of this chapter.

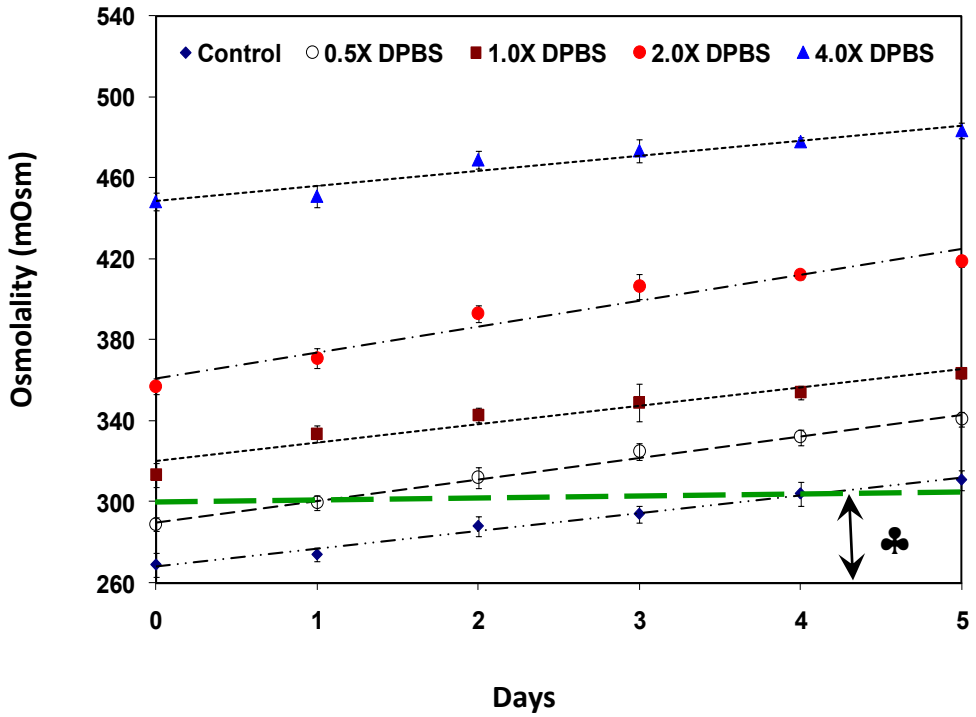

Figure 6.6: Changes in the osmolality of the stromal media loaded in the M0512 coated TCPS dish. The final concentration of the coating after 50% drying is 8% of M0512 + PBS. The ♣ symbol signifies the permissible osmolality during cell culture

the hydrogel coating and the cell culture media (Fig 6.5). To evaluate the stability of the coated M0512 hydrogels after 50% drying under fume hood, a stromal cell culture solution with an osmolality of ~280 mOsm/kg at 37 °C was loaded onto the coated TCPS dishes. An uncoated TCPS dish loaded with the same culture solution was used as a control. Changes in osmolality of the loaded PBS solution with time were monitored by an osmometer and the data is shown in Fig 6.6 (Chen et al., 2006).

There were several shortcomings with MC hydrogels generated from M0512. It was not convenient to dry the coated MC gel for 50% under fume hood. Due to the uneven drying, the obtained hydrogel systems were not stable and degraded with time and more often disintegrated as soon as the media was added (more discussion in the next sections). Moreover, our experiments suggest that by 50% drying of 4% M0512 with 0.5X PBS could not yield a gel formation temperature below 37 ^{o}C (see the Fig 5.4, filled red circles) as was the case with Chen et al., 2006. Our data indicate that 50% drying of 4% M0512 with 1.0X PBS generate a gel formation temperature of ~ 30 ^{o}C. However after drying 4% M0512 with 1.0X PBS the concentration of salts in hydrogel may have become twice and due to which there was a significant increase in osmolality of the stromal media with time as shown in Fig 6.5.

6.3.3: Effect of Molecular Weight on the Gelation of MC Solutions

In order to develop a more convenient method to coat MC onto TCPS dishes, the thermal properties of two more commercially available MCs with different molecular weights (M0262, Mw=41000 and M7140, Mw=15000) were thoroughly investigated in this study. Due to their low molecular weights as compared to M0512 (Mw=88000), highly concentrated and manageable MC solutions, up to 8% for M0262 and up to 16% for M7140, could be prepared. In

further analysis, only lower concentrations of salts (0.5X and 1.0X PBS) were analysed as the experiments with M0512 suggested that high concentrations of salts produce significant increase in osmolality of the culture media. Table 6.2 shows the incipient gelation temperatures (IGTs) of the MC solutions as function of molecular weight. It is interesting to note that within the molecular weight range studied there is no noticeable difference in the IGT. This is contrary to the classical polymer chemistry where one expects an increase in precipitation temperature with decrease in molecular weight. This anomalous behavior of methylcellulose solution can however be explained if one takes into account the molecular weight distribution and the state of aggregation of the polymer in solution (Li et al., 2003; Sarkar 1979; Wang and Li 2005). All the methylcellulose samples have a wide molecular weight distribution where the ratio of weight to number-average molecular weight may vary from 3 to as high as 10 depending on the type of pulp used and the processing conditions (Sarkar 1979). The incipient gelation

Table 6.2: Gelation temperatures of MC-water solutions

MC Concentration (%)	**Gel Point from Calorimetry Experiments (˚C)**		
	M0512 (mol. wt. = 88,000)	M0262 (mol. wt. = 41,000)	M7140 (mol. wt. = 15,000)
2	53.1 (±0.8)	52.5 (±0.3)	50.8 (±0.7)
4	52.2 (±1.3)	48.2 (±1.1)	46.4 (±1.9)
6	48.2 (±1.0)	45.8 (±1.4)	44.9 (±1.5)
8	—	43.2 (±1.4)	44.1 (±0.9)
10	—	41.7 (±2.0)	40.1 (±1.2)
12	—	—	37.6 (±0.8)
14	—	—	34.6 (±1.9)
16	—	—	31.1 (±1.5)

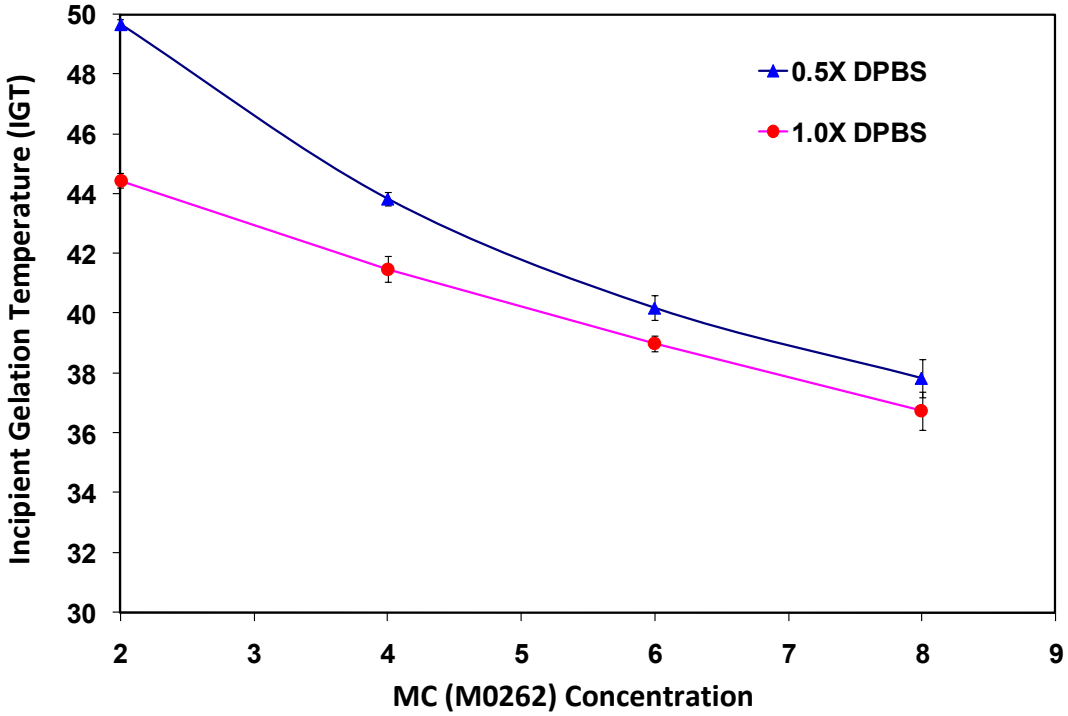

Figure 6.7: Thermal gelation of M0262 (Mw: 44000 and a viscosity of 400cp for 2%MC in water at room temperature and pressure) as a function of concentration in 0.5X and 1X PBS

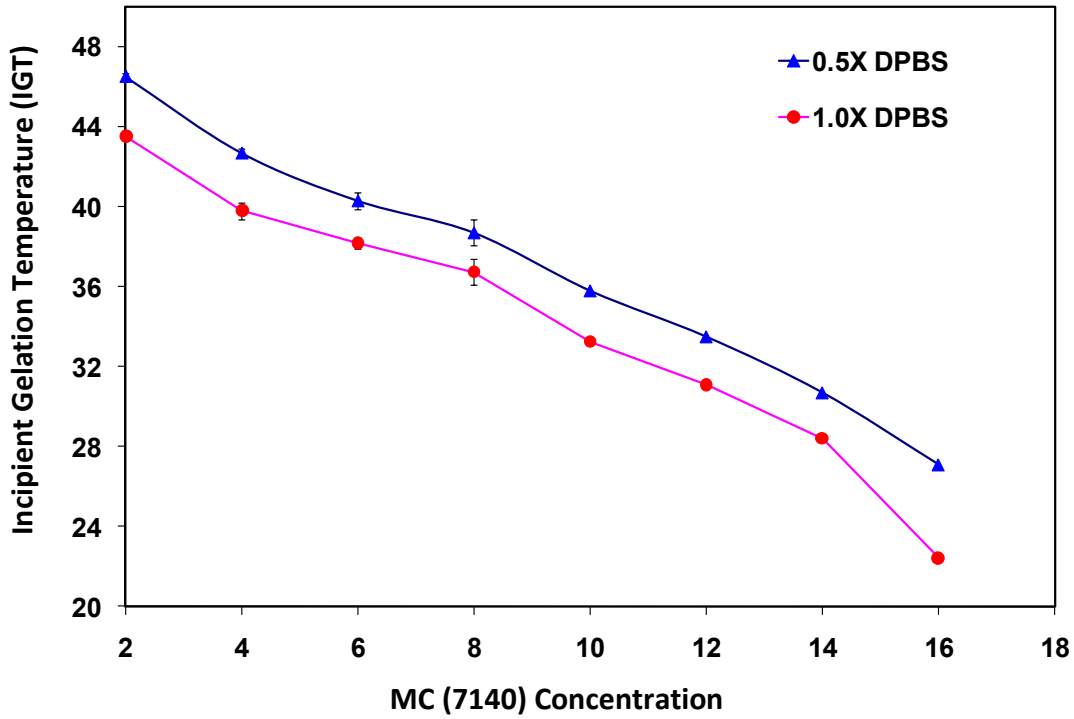

Figure 6.8: Thermal gelation of M07140 (Mw: 15000 and a viscosity of 15cp for 2%MC in water at room temperature) as a function of concentration in 0.5X and 1X PBS.

temperatures actually reflect the influence of the high molecular weight fraction of the sample, which precipitates out first. All the samples of varying average molecular weight contain similar high molecular weight fractions, although of varying amounts. This is the reason why all these samples are exhibiting similar gelation temperatures. As the gelation temperature was independent of the molecular weights investigated, the IGTs of low molecular weight MCs (M0262 and M7140) at high concentration aqueous solutions were further investigated using DSC.

Fig 6.7 and Fig 6.8 show the effects of polymer concentrations of M0262 and M7140 respectively with 0.5X and 1.0X PBS. The data indicates that 8% of M0262 with 1X PBS has a gelation temperature of ~ 37 ^{o}C (See Fig 6.7). However for M7140 a gelation temperature as low as ~25^{o}C could be achieved with 16%MC and 0.5X PBS. Since a lower concentration of M7140 was convenient to manipulate for spin coating the TCPS dish, a concentration of 14% with 0.5X PBS was used for hydrogel formation. We found that this specific aqueous MC underwent a sol-gel reversible transition upon heating or cooling at approximately 32^{o}C (See Fig 6.8).

To evaluate the stability of the MC hydrogel coated on TCPS dishes, a stromal solution with an osmolality of ~ 280 mOsm/kg at 37 °C was loaded in the coated dish. An uncoated dish loaded with the same stromal solution was used as a control. Changes in osmolality of the loaded PBS solution with time were monitored by an osmometer (Chen et al., 2006). As shown in Fig 6.9, the osmolality of the PBS loaded in the MC-coated dish was comparable to that of the control one. Additionally, the MC hydrogel coated on the polystyrene dish stayed intact throughout the entire course of the study.

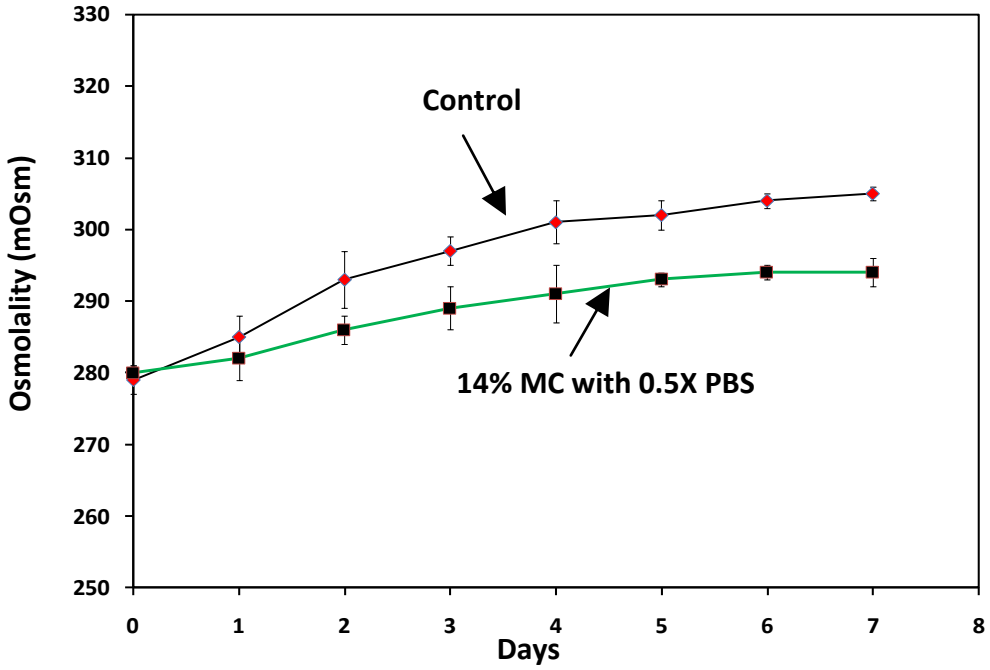

Figure 6.9: Changes in the osmolality of the stromal media loaded in the M7140 coated TCPS dish. Aqueous solution of 14% MC was blended with 0.5X PBS

6.3.4: *In vitro* Degradation and Swelling of MC Hydrogels

The stability of the MC hydrogels generated from all the molecular weights was further investigated by assessing potential polymer degradation and swelling of the hydrogels when subjected to isotonic cell culture. MC hydrogels were constructed using the following concentrations of MC in PBS. For M0515: 8% MC blended with 0.5 and 1.0X PBS (after 50% drying of 4% MC); for M0262: 8% MC blended with 0.5 and 1.0X PBS; for M7140: 14%MC blended with 0.5 and 1.0X PBS. As shown in Fig 6.10, for all the samples investigated the hydrogels reached maximum swollen volume by day 1. Swelling data for low molecular weight polymers differed slightly with M0262 showing more swelling than M7140. However the swelling of M0515 was significantly lower than both M0262 and M7140 (see Fig 6.10A, 6.10C, 6.10E). All the hydrogel systems demonstrated some amount of degradation immediately after

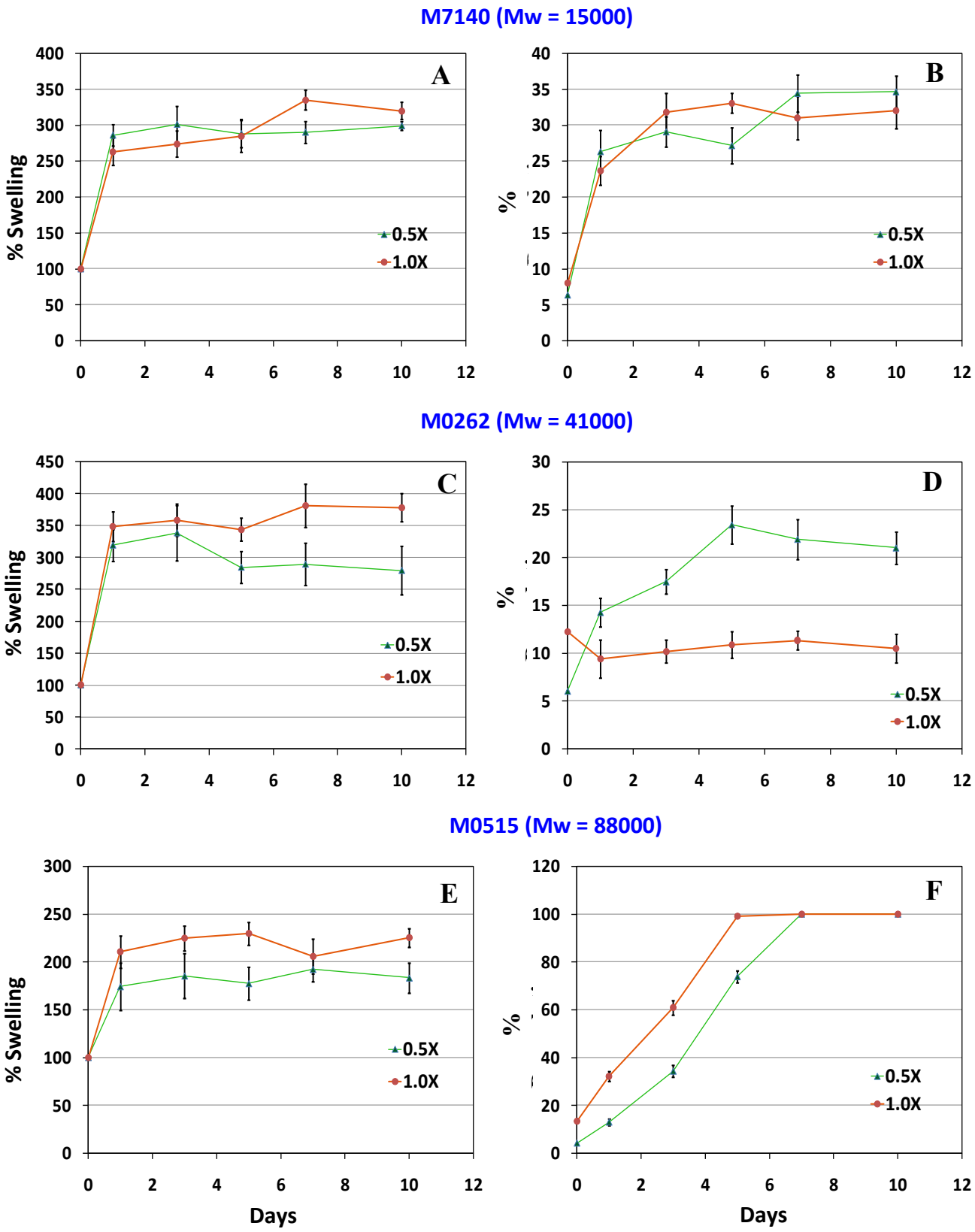

Figure 6.10: Percent swelling and percent degradation values of M7140 (6.10A, 6.10B), M0262 (6.10C, 6.10D), and M 0515 (6.10E, 6.10F)

adding cell culture media (See Fig 6.10B, 6.10D, 6.10F). After this initial loss of polymer mass the degradation profile somewhat leveled off for the duration of the experiment except for M0512. The hydrogel generated was unstable and during the removal of culture media, small patched of hydrogel coating peeled off from the surface. This could be because the hydrogel would have unevenly dried in the fume hood and different regions had different polymer and salts concentrations. This further suggests that using M0252 for cell sheet generation may not be desirable.

6.3.5: Culture of ASCs onto MC Coated Surface and Fabrication of Cell Sheets

For all cell culture experiments, M7140 with 14%MC blended with 0.5X PBS was used to generate the MC coated TCPS dishes. The hydrogel system generated had a thermoresponsive gelation temperature of 32°C. The ASCs cultured on MC coated surface did not attach and formed structures like embroid bodies as shown in Fig 6.11. To improve cell attachments a neutral aqueous bovine collagen type I was evenly spread over the MC coated dish at 37 °C. It was reported that under the influence of increasing temperature, collagen molecules self-assemble into a gel network (Meinel et al., 2004; Pederson et al., 2003; Tianhan et al., 2007, Chen et al., 2006). 100-150µl of 2mg/ml collagen was evenly spread over the MC coated surface. Thermal triggering of collagen gelation was demonstrated at temperatures as low as 20 ^{o}C (Kadler et al., 1996; Pederson et al., 2003). Thus, a thin layer of collagen was formed on the surface of the MC hydrogel gradually (the collagen/MC hydrogel) during incubation for one hour at culture temperature. A scanning electron micrograph of collagen network formed onto the MC coated TCPS dish is shown in Fig 6.12. Collagen coating significantly improved the ASC cell adhesion and proliferation as shown in Fig 6.13A and Fig 6.14.

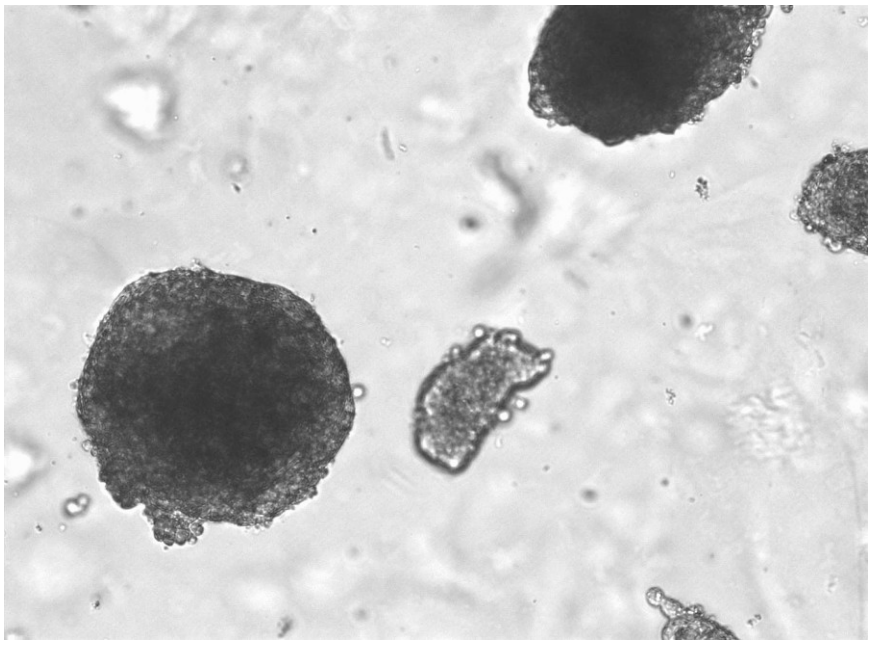

Figure 6.11: ASCs cultured on MC coated TCPS dish. The image shows the unreceptiveness of P1 ASCs when seeded on the MC hydrogel surface and generation embroyd like structures. The cells were cultured for 24 hours.

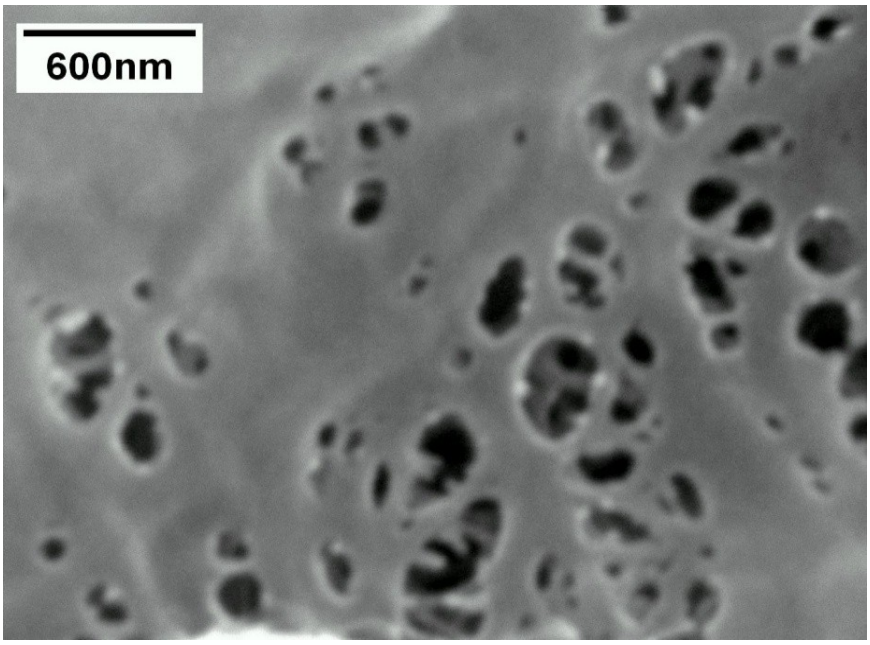

Figure 6.12: SEM image of collagen coating at room temperature. 100-150µl of 2% collagen type 1 is uniformly applied to the MC coated surface and subsequently kept at 37 °C for 1 - 2 hours.

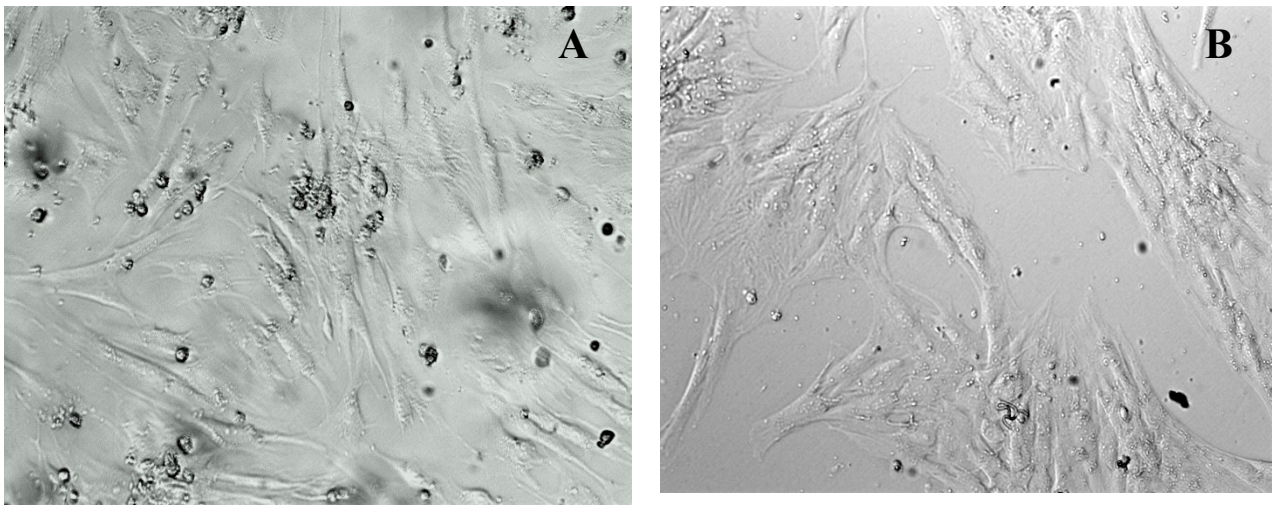

Figure 6.13: A: Passage 1 ASC attachment to MC+Collagen coated surface. B: Cell attached to non-coated TCPS dish (control)

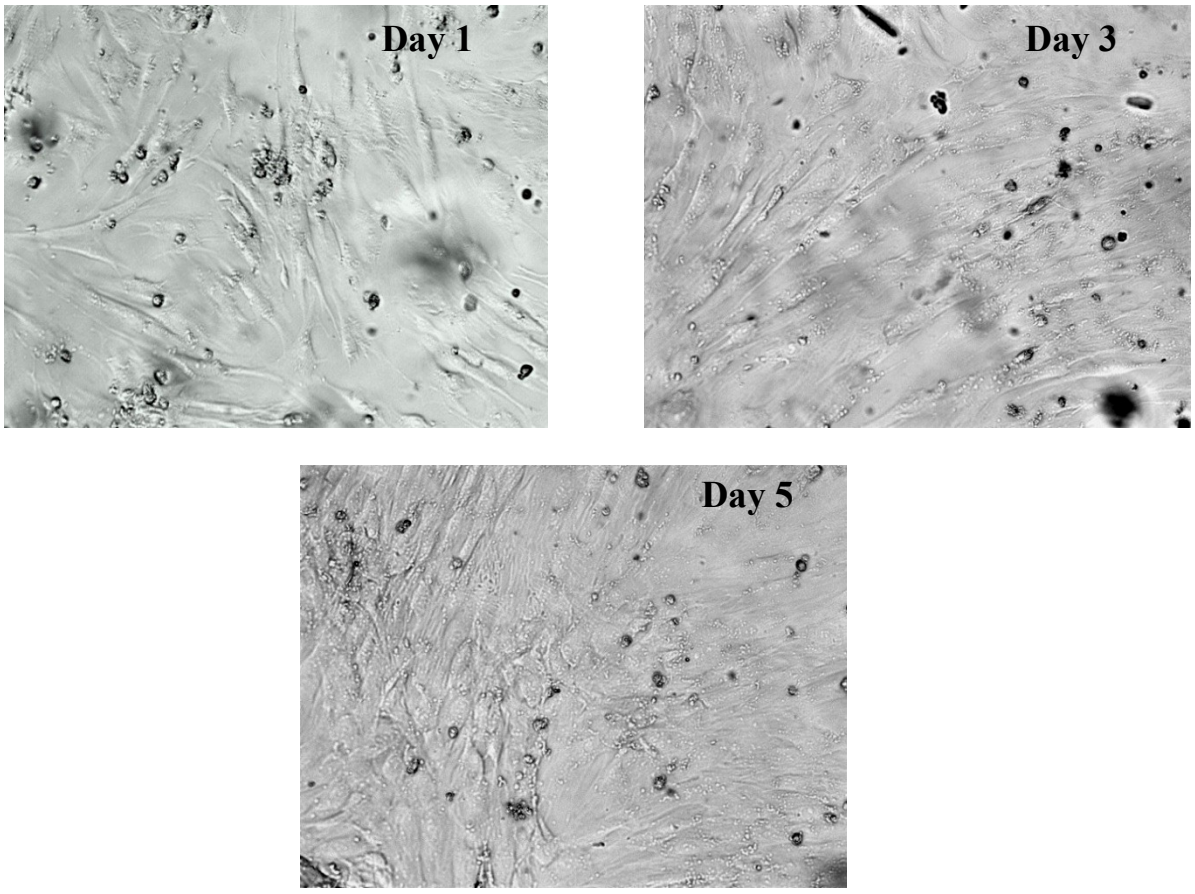

Figure 6.14: Photomicrographs of passage 1 ASCs cultured on the MC + collagen coated TCPS dishes for 1, 3 and 5 days, respectively

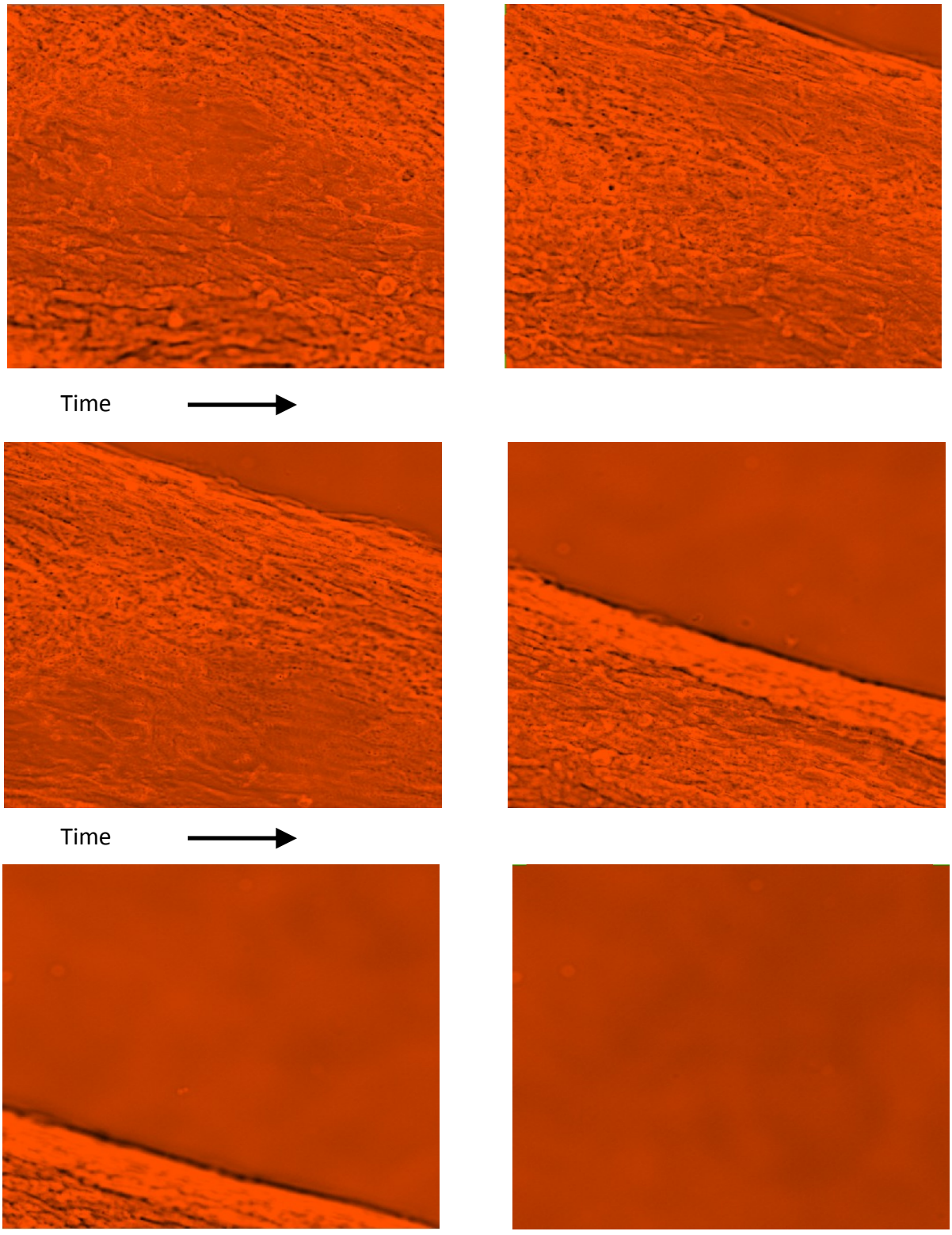

Figure 6.15: Photomicrographs of detaching ASC cell sheet with time (20X)

Upon confluence, a continuous monolayer ASC sheet was formed on the surface of the MC hydrogel (Fig 6.14). When the grown cell sheet was placed outside of the incubator at room temperature, it detached gradually from the surface of the thermo-responsive hydrogel spontaneously, without treating with any enzymes. The grown cell sheet started detaching from its edge at about 2min after cooling at room temperature. Detachment of the entire cell sheet was completed within 3-5min. However, such phenomenon was not observed for the cells cultured on the surface of the collagen-coated TCPS dish. Fig 6.15 shows the continuous detachment of ASC sheet with time.

A multilayer tissue construct was formed by using two or more MC+collagen coated TCPS dishes (Fig 6.16) using a method described by Hayashida et al., (2006). P1 ASC sheets were transferred from one MC grafted culture dish as a monolayer onto another MC+collagen coated culture dish using a PVDF membrane support by lowering the temperature below 32°C. When the monolayer on MC + collagen coated dishes was incubated at a lower temperature with a donut shaped PVDF membrane over it, the polymer MC dissolved and which in turn resulted in weak adhesion between the cell monolayer and the surface. The membrane together with cells was peeled off and transferred to a monolayer on another MC + collagen coated dish at 37^{o}C. Upon reincubation at 37^{o}C, cells from the membrane adhered to the monolayer as an intact cell sheet. The third cell layer was overlaid onto the double layered construct to get a three cell thick multilayered cell construct. After lowering the temperature, the multilayer cell sheet was detached generating a multidimensional cell sheet.

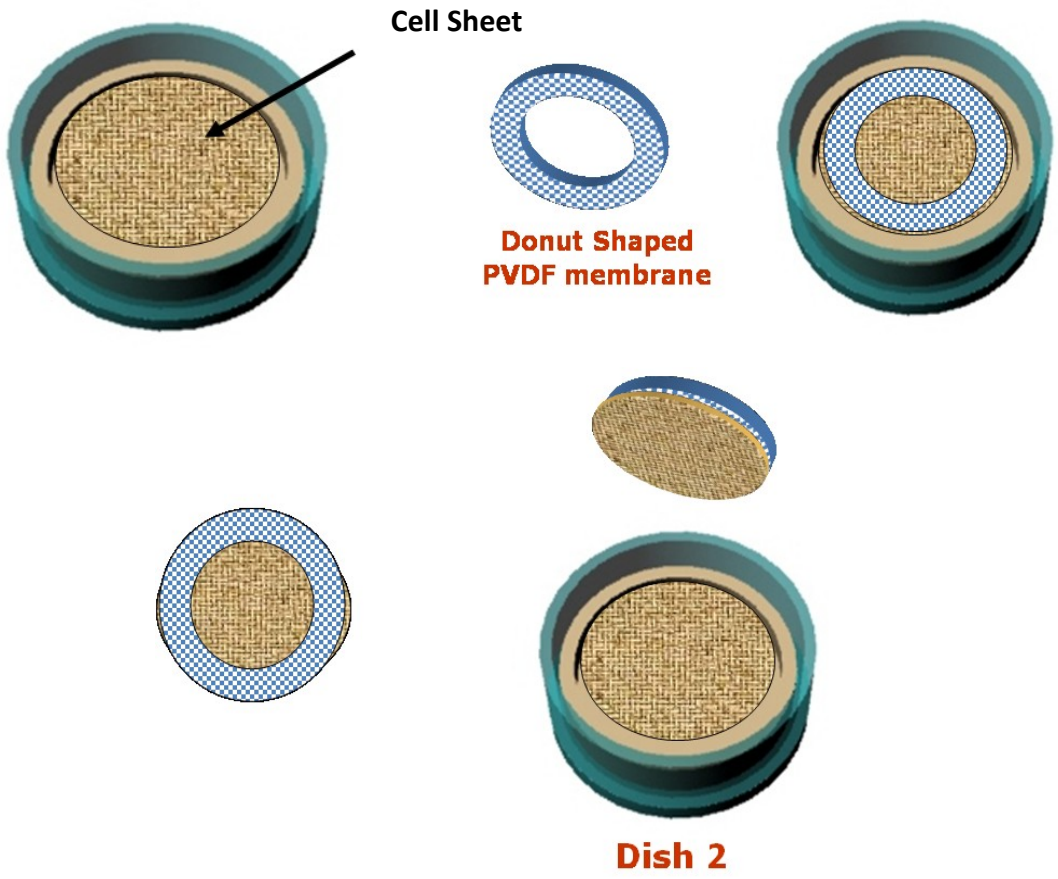

Figure 6.16**:** Steps involved in generating multi-layered ASCs tissue construct. The cell sheet harvested from one TCPS dish was transferred to another TCPS dish by using a polyvinylidene difluoride (PVDF) donut-shaped support membrane and placed directly onto the second cell sheet growing in a separate TCPS dish.

The single or multilayer cell sheets may be used in the applications to tissue reconstructions. Single cell sheets can be transplanted directly to host in the case of skin (Yamato et al., 2001) corneal epithelium (Nishida et al., 2004), and periodontal ligament (Hasegawa et al., 2005). By Layering homotypic cell sheets in a three dimensional tissue structures and by using differentiation ability of ASCs we can create three-dimensional structures such as cardiac muscle. Using heterotypic sratification, laminar structures such as

kidney glomeruli, and liver lobules can be successfully constructed. Using cell sheet engineering, we can thus altogether avoid the need for conventional tissue engineering approaches using isolated cell injections and scaffold based technologies, whose applicability is often limited.

6.4 CONCLUSIONS

In this study a method, using a thermoreversible methylcellulose (MC) hydrogel coated on the TCPS dish, was developed for harvesting a living ASC sheet for tissue engineering applications. The thermal gelation properties of three commercially available MC were systematically investigated for their gel formation, swelling and degradation phenomenon at physiological temperatures. This non-invasive method of cell retrieval using MC coated TCPS dishes allows creation of single and multilayered cell sheet constructs preserving cell-cell and cell–extracellular matrices. The obtained living cell sheets may be used for ASCs tissue reconstructions.

REFERENCES

Akiyama Y; Kikuchi A; Yamato M; Okano T. 2004. Ultrathin poly (N-isopropylacrylamide) grafted layer on polystyrene surfaces for cell adhesion/detachment control. Langmuir. 20(13):5506-5511.

Alapati R; Goff K; Kubisch HM; Devireddy RV. 2008. Water transport in epididymal and ejaculated rhesus monkey (Macaca mulatta) sperm during freezing. Cryobiology 57(2): 182-185

Anchordoguy TJ; Rudolph AS; Carpenter JF; Crowe JH. 1987. Modes of interaction of cryoprotectants with membrane phospholipids during freezing. Cryobiology. 24(4):324-331.

Arakawa T and Timasheff SN. 1985. The stabilization of proteins by osmolytes. Biophys J. 47(3): 411–414.

Ashjian PH; Elbarbary AS; Edmonds B; DeUgarte D; Zhu M; Zuk PA; Lorenz HP; Benhaim P; Hedrick MH. 2003. In vitro differentiation of human processed lipoaspirate cells into early neural progenitors. Plast Reconstr Surg. 111(6): 1922-1931.

Ashwood-Smith MJ. 1987. Mechanisms of cryoprotection action. In: Bowler K, Fuller BJ, eds. Temperature and animals Cells. Company of Biologists, Cambridge. p. 395-406.

Ashwood-Smith MJ and Connor KW. 1973. Cryoprotection of mammalian cells in tissue culture with polymers: possible mechanisms. Cryobiology. 10:488-496.

Ashwood-Smith MJ; Warby C; Connor KW; Becker G. 1972. Low-temperature preservation of mammalian cells in tissue culture with polyvinylpyrrolidone (PVP), dextrand and hydroxyethyl starch (HES). Cryobiology. 9:441-449.

Awad HA; Wickham MQ; Leddy HA; Gimble JM; Guilak F. 2004. Chondrogenic differentiation of adipose-derived adult stem cells in agarose, alginate, and gelatin scaffolds. Biomaterials. 25(16): 3211-3222.

Barbosa JN; Barbosa MA; Aguas AP. 2004. Inflammatory responses and cell adhesion to self-assembled monolayers of alkanethiolates on gold. Biomaterials 25(13):2557-2563.

Balakin KV; Saychuk NP; Tetko IV. 2006. In silico approaches to prediction of aqueous and DMSO solubility of drug-like compounds: trends, problems and solutions. Curr. Med. Chem, 13:223–241.

Barnes DWH and Loutit JF. 1955. The radiation recovery factor: Preservation by the Polge–Smith–Parkes technique. J. Natl. Cancer Inst. 15: 901.

Baust JM; Van B; Baust JG. 2000. Cell viability improves following inhibition of cryopreservation-induced apoptosis. In Vitro Cell Dev Biol Anim. 36(4):262-70.

Benson EE and Bremner D. 2004. Oxidative stress in the frozen plant: A free radical point of view. In: Fuller BJ, Lane NJ, Benson EE, eds. Life in the Frozen State. CRC Press, Boca Raton, FL, USA, p 205-242.

Bernard A and Fuller BJ. 1996. Cryopreservation of human Oocytes: a review of current problems and perspectives, Human Reproduction Update . 2(3): 193-207.

Bevington PR and Robinson DK. 1992. Data Reduction and Error Analysis for the Physical Sciences (2nd Ed). New York: McGraw-Hill.

Bischof JC. 2006. Micro and nanoscale phenomenon in bioheat Transfer. Heat and Mass Transfer, 42(10): 955-966.

Bischof JC; Fahssi WM; Smith D; Nagel T; Swanlund DJ. 2001. A parametric study of freezing injury in ELT-3 uterine leiomyoma tumor cells. Human Reprod. 16: 340-348.

Bjornson CRR; Rietze RL; Reynolds BA; Magli MC; Vescovi AL. 1999. Turning brain into blood: a hematopoietic fate adopted by adult neural stem cells in vivo", Science. 283:534-537.

Box GEP; Hunter WG; Hunter JS. 1978. In Statistics for Experimenters; Wiley: New York.

Brewer JB; Pollock KGJ; Tetley L; Russell DG. 2004. Vesicle size influences the trafficking, processing, and presentation of antigens in lipid vesicles. J Immunol 173:6143-6150.

Brickman JM and Thomas GB. 2002. Pluripotency and tumorigenicity. Nat. Genet. 32: 557-558.

Buchanan SS; Gross SA; Acker JP; Toner M; Carpenter JF; Pyatt DW. 2004. Cryopreservation of stem cells using trehalose: evaluation of the method using a human hematopoietic cell line. Stem Cells Dev. 3(3):295-305.

Bunnell BA; Estes BT; Guilak F; Gimble JM. 2008. Differentiation of adipose stem cells. Methods Mol Biol. 456: 155.

Chen G; Chen N; Garner AL; Kolb J; Swanson RJ; Beebe S; Joshi RP; Schoenbach KH. 2004. Conductivity in Jurkat cell suspension after ultrashort electric pulsing (Speech). In

Proceedings of 3rd International workshop on biological effect of EMFs Vol. 1, pp. 56-65: Kos, Greece.

Chen CH; Tsai CC; Chen W; Mi FL; Liang HF; Chen SC; Sung HW. 2006. Novel living cell sheet harvest system composed of thermoreversible methylcellulose hydrogels. Biomacromolecules. 7(3): 736-743.

Chena CH; Changb Y; Wangb CC; Huanga CH; Huangd CC; Yeha YC; Hwange SM; Sunga HW. 2007. Construction and characterization of fragmented mesenchymal-stem-cell sheets for intramuscular injection. Biomaterials. 28: 4653-4651.

Chvapil M. Reconstituted collagen. In: Viidik A., Vuust J, editors.Biology of collagen. London: Academic Press, 1980: 313-325.

Clarke DM; Baust JM; Van Buskirk RG; Baust JG. 2001. Chemo-cryo combination therapy: an adjunctive model for the treatment of prostate cancer. Cryobiology 42(4): 274-85.

Clarke DL; Johansson CB; Wilbertz J; Veress B; Nilsson E; Karlstrom H; Lendahl U; Frisen J. 2000. Generalized potential of adult neural stem cells; Science. 288: 660-663.

Connor W and Ashwood-Smith MJ. 1973. Cryoprotection of mammalian cells in tissue culture with polymers; possible mechanisms. Cryobiology. 10(6): 488–496.

Corsini J;Hacker C; Bare C. 2004. Serum-free cryopreservation of five mammalian cell lines in either a pelleted or suspended state. Biol Proced Online. 6: 61.

Crowe JH; Carpenter JF; Crowe LM; Achordoguy TJ. 1990. Are Freezing and dehydration similar stress vectors? A comparison. of models of interaction of stabilizing solutes with biomolecules. Cryobiology. 27: 219-231.

Daniel MC and Astruc D. 2004. Gold nanoparticles: assembly, supramolecular chemistry, quantum-size-related properties, and applications toward biology, catalysis, and nanotechnology. Chem Rev. 104: 293–346.

Day SH; Nicoll-Griffith DA; Silva J. 1999. M.Cryopreservation of rat and human liver slices by rapid freezing". Cryobiology. 38: pp.154-159.

Debelak-Fehir KM; Catchatourian R; Epstein RB. 1975. Hemopoietic colony-forming units in fresh and cryopreserved peripheral blood cells of canines and man. Exp Hematol. 3: 109–116.

Debelak-Fehir KM and Epstein RB. 1975. Restoration of hematopoiesis in dogs by infusion of cryopreserved autolo- gous peripheral white cells following busulfan-cyclopho sphamide treatment. Transplantation. 20: 63–67.

de la Fuente JM; Berry CC; Riehle MO ; Curtis ASG. 2006. Nanoparticle targeting at cells. Langmuir 22 (7): 3286 -3293.

Deman JJ; Vakaet LC; Bruyneel EA. 1976. Cell size and mutual cell adhesion. I. Increase in mutual adhesiveness of HeLa cells from density-inhibited suspension cultures by hypotonic treatment. J Membr Biol. 26:189-204.

Deman JJ; and Bruyneel EA. 1977. Thermal transitions in the adhesiveness of HeLa cells: Effects of cell growth, trypsin treatments and calcium. J. Cell Sci. 27: 167-181.

Devireddy RV and Bischof JC. 1998. Measurement of water transport during freezing in mammalian liver tissue - Part II: The use of differential scanning calorimetry. ASME Journal of Biomechanical Engineering. 120: pp. 559-569.

Devireddy RV; Raha D; Bischof JC. 1998. Measurement of water transport during freezing in cell suspensions using a differential scanning calorimeter. Cryobiology 36:124-155.

Devireddy RV; Swanlund DJ; Roberts KP; Pryor JL; Bischof JC. 2000. The effect of extracellular ice and cryoprotective agents on the water permeability parameters of human sperm plasma membrane during freezing. Human Reprod. 15:125-1135.

Devireddy RV; Olin T; Swanlund DJ; Vincente W; Troedsson MHT; Bischof JC; Roberts KP. 2002. Cryopreservation of equine spermatozoa: optimal cooling rates in the presence and absence of cryoprotective agents. Biology of Reproduction. 66:222-231.

Devireddy RV; Fahrig B; Godke R; Leibo SP. 2004. Subzero water transport characteristics of boar spermatozoa confirm observed optimal cooling rates. Mol Reprod Dev. 67:446-457.

Devireddy RV. 2005. Permeability parameters of human ovarian tissue cells to various cryoprotectants and water. Mol Reprod Dev. 70:333-343.

Diller KR and Cravalho EG. 1970. A cryomicroscope for the study of freezing and thawing process in biological systems, Cryobiology. 7: 191—199.

Diller KR. 2005. Bioheat and mass transfer as viewed through a microscope. ASME J Biomech Eng. 127:67-84.

English D; Paterson AH; Bone G; McPherson TA.1979. Cryopreservation of canine hematopoietic cells. Clin Invest Med .1979, 2, 67–74.

El-Shewy HM; Kendall WF Jr; Darrabie M; Collins BH; Opara EC. 2004. Polyvinylpyrrolidone: a novel cryoprotectant in islet cell cryopreservation. Cell Transplant. 13(3): 237.

Eggens I; Fenderson BA; Toyokuni T; Dean B; Stroud MR; Hakomori S. 1989. Specific interaction between LeX and LeX determinants: A possible basis for cell recognition in preimplantation embryos and in embryonal carcinoma cells. J Biol Chem. 264: 9476–9484.

Fahy GM. 1986. The relevance of cryoprotectant "toxicity" to cryobiology. Cryobiology. 23(1):1-13.

Farrant J. 1969. Is there a common mechanism of protection of living cells by polyvinylpyrrolidone and glycerol ding freezing? Nature. 222(5199):1175-1176.

Fischer NO; McIntosh CM; Simard JM; Rotello VM. 2002. Inhibition of chymotrypsin through surface binding using nanoparticle-based receptors. Proc Natl Acad Sci U S A. 99(8):5018-5023.

Fleming K, Hubel A. 2007. Cryopreservation of hematopoietic stem cells: emerging science, technology and issues. Trans Med Hemother, 34, 268-275.

Freshney RI. 2000. Culture of Animal Cells: A Manual of Basic Technique. 4th ed., New York, NY, Wiley-Liss.

Fujioka, T; Yasuchika K.; Nakamura Y; Nakatsuji N; Suemori H. 2004. A simple and efficient cryopreservation method for primate embryonic stem cells. Int J Dev Biol. 48(10), 1149-1154.

Fuller BJ. 2004. Cryoprotectants: the essential antifreezes to protect life in the frozen state. Cryo-Letters. 25(6):375-388.

Galli R; Borello U; Gritti A; Minasi M G; Bjornson C; Coletta M; Mora M; De Angelis MG; Fiocco R; Cossu G; Vescovi, AL. 2000. Skeletal myogenic potential of human and mouse neural stem cells. Nat Neurosci. 3: 986-991.

Gimble JM and Guilak F. 2003. Adipose-derived adult stem cells: isolation, characterization, and differentiation potential. Cytotherapy. 5: 362-369.

Gimble JM and Nuttall ME. 2004. Bone and Fat: Old Questions, New Insights. Endocrine. 23: 183-188.

Go H; Sudo Y; Hosoya K; Ikegami T; Tanaka N. 1998. Effects of Mobile-Phase Composition and Temperature on the Selectivity of Poly(*N*-isopropylacrylamide)-Bonded Silica Gel in Reversed-Phase Liquid Chromatography Anal Chem. 70(19): 4086 – 4093.

Goodman CM; McCusker CD; Yilmaz T; Rotello VM. 2004. Toxicity of gold nanoparticles functionalized with cationic and anionic side chains. Bioconjugate Chem 15:897-900.

Gomez-Lechon MJ; Lahoz A; Jimenez N; Vicente Castell J; Donato MT. 2006. Cryopreservation of rat, dog and human hepatocytes: influence of preculture and cryoprotectants on recovery, cytochrome P450 activities and induction upon thawing. Xenobiotica. 36(6):457-72.

Grignon AMS. 1980. Effect of pH and neutral salts upon the swelling of cellulose gels. Journal of Applied Polymer Science. 25(12):2829-2843.

Halvorsen YDC; Franklin D; Bond AL; Hitt DC; Auchter C; Boskey AL; Paschalis EP; Wilkison WO; Gimble JM. 2001. Extracellular matrix mineralization and osteoblast gene expression by human adipose tissue-derived stromal cells. Tissue Eng. 7(6): 729-741.

Hasegawa M; Yamato M; Kikuchi A; Okano T; Ishikawa I. 2005. Human periodontal ligament cell sheets can regenerate periodontal ligament tissue in an athymic rat model. Tissue Eng. 11(3-4):469-78.

Harimoto M; Yamato M; Hirose M; Takahashi C; Isoi Y; Kikuchi A; Okano T. 2002. Novel approach for achieving double-layered cell sheets co-culture: overlaying endothelial cell sheets onto monolayer hepatocytes utilizing temperature-responsive culture dishes. J. Biomed. Mater Res. 62: 464–470.

Hayashida Y; Nishida K; Yamato M; Yang J; Sugiyama H; Watanabe K; et al. 2006. Transplantation of tissue-engineered epithelial cell sheets after excimer laser photoablation reduces postoperative corneal haze. Invest Ophthalmol Vis Sci. 47: 552-7.

Heymann E. 1935. Studies on sol-gel transformations. I. The inverse sol-gel transformation of methylcellulose in water. Transactions of the Faraday Society. 31:846 - 864.

Hicok K; du Laney T; Sheng Zhou Y; Halvorsen YDC; Hitt CD, Cooper LF; Gimble JM. 2004. Human Adipose Derived Adult Stem Cells Produce Osteoid In Vivo. Tissue Eng. 10: 371-380.

Hirose M; Kwon OH; Yamato M; Kikuchi A; Okano T. 2000. Creation of designed shape cell sheets that are non-invasively harvested and moved onto another surface. Biomacromolecule. 1: 377-381.

Hollister WR; Mathew AJ; Baust JG; Van Buskirk RG. 1998. The effects of freezing on cell viability and mechanisms of cell death in an in vitro human prostate cancer cell line. Mol. Urol. 2(1):13–18.

Horb ME; Shen CN; Tosh D; Slack JM. 2003. Experimental conversion of liver to pancreas. Curr Biol.13: 105-115.

Hubbell JA; Massia SP; Desai NP; Drumheller PD. 1991. Endothelial cell-selective materials for tissue engineering in the vascular graft via a new receptor. Biotechnology. (N Y) 9(6):568-72.

Hudson L and Hay FC, eds. 1980. Practical Immunology, 2nd ed. Blackwell Scientific Publications, Oxford.

Hynsjo L; Granberg L; Haurum J; Thiel S; Larson G. 1995. Use of factorial experimental design to delineate the strong calcium and pH – dependent changes in binding of human surfactant protein-A to neutral glycosphingolipids—A model for studies of protein-carbohydrate interactions. Anal. Biochem. 225(2): 305-314.

Inserte J; Garcia-Dorado D; Ruiz-Meana M; Solares J; Soler j. 1997. The role of Na+-H+ exchange occurring during hypoxia in the genesis of reoxygeneration-induced mycordial oedema. J. Mol. Cell. Cardiol. 29(4): 1167-1175.

Ishiguro H and Rubinsky B. 1994. "Influence of hematocrit on behavior of ice crystals and human red blood cells during directional solidification of cell suspensions" Trans. Japan. Soc. of Mech. Eng. 60, 579: 3755-3761.

Ishiguro H and Rubinsky B. 1994. "Microscopic behavior of ice crystals an biological cells during directional solidification of solutions with cells" Trans. Japan. Soc. of Mech. Eng. 60, 572: 1388-1355 (in Japanese).

Jackson J; Kloster T; Welniak L; Damon M; Rehder B; Schmechel B; Ward B; Kessinger A. 1992. Peripheral blood-derived stem cells can be successfully cryopreserved without using controlled-rate freezing. Prog Clin Biol Res. 377: 367– 371.

Jeong B; Bae YH; Lee DS; Kim SW. 1997. Biodegradable block copolymers as injectable drug-delivery systems. Nature. 388(6645): 860-862.

Kadler KE; Holmes DF; Trotter JA; Chapman JA. 1996. Collagen fibril formation. Biochemical Journal. 316: 1-11.

Kuleshova LL; Shaw JM; Trounson AO. 2001. Studies on replacing most of the penetrating cryoprotectant by polymers for embryo cryopreservation. Cryobiology 43(1): 21-31.

Kanazawa H; Yamamoto K; Matsushima Y; Takai N; Kikuchi A; Sakurai Y; Okano T. 1996. Temperature-responsive Chromatography using Poly(N-isopropylacrylamide)-Modified Silica. Anal Chem. 68 (1): 100-105.

Karlsson JOM; Cravalho EG; Toner M. 1994. A model of diffusion-limited ice growth inside biological cells during freezing. J Appl. Phys. 75: 4442–4455.

Kedem O and Katchalsky A. 1958. Thermodynamic Analysis of the Permeability of Biological Membranes to Non-electrolytes. Bioch. Biophys. Acta 27: 229-246.

Kerr JFR; Wyllie AH; Currie AR. 1972. Apoptosis - Basic Biological Phenomenon with Wide-Ranging Implications in Tissue Kinetics. British Journal of Cancer. 26(4): 239-257.

Korber C; Scheiwe MW; Boutron P; Rau G. 1982. The influence of hydroxyethyl starch on ice formation in aqueous solutions. Cryobiology. l9 (5): 478-92.

Kopen G; Prockop D; Phinney D. 1999. Marrow stromal cells migrate throughout forebrain and cerebellum and they differentiate into astrocytes after injection into neonatal mouse brains. Proc Natl Acad Sci USA. 96: 10711–10716.

Koopman G; Reutelingsperger CP; Kuijten GA; Keehnen RM; Pals ST; van Oers H. 1994. Annexin V for flow cytometric detection of phosphatidylserine expression on B cells undergoing apoptosis. Blood. 84(5): 1415-1420.

Kundu M and Kundu PP. 2001. Effect of salts and surfactant and their doses on the gelation of extremely dilute solutions of methyl cellulose. Polymer. 42(5): 2015-2020.

Kushida A; Yamato M; Konno C; Kikuchi A; Sakurai Y; Okano T. 1999. Decrease in culture temperature releases monolayer endothelial cell sheets together with deposited fibronectin matrix from temperature-responsive culture surfaces. J Biomed Mater Res. 45(4): 355–362.

Lange, C., Cakiroglu, F., Spiess, A.N., Cappallo-Obermann, H., Dierlamm, J., and Zander, A.R. Accelerated and safe expansion of human mesenchymal stromal cells in animal serum-free medium for transplantation and regenerative medicine. J Cell Physiol 213, 18, 2007

Langer R and Vacanti JP. 1993. Tissue engineering. Science. 260(5110): 920–926.

Langer R and Vacanti JP. 1995. Artificial organs. Sci Am. 273(3): 130–133.

Lee YM and Shim JK. 1997. Preparation of pH/temperature responsive polymer membrane by plasma polymerization and its riboflavin permeation. Polymer. 38: 1227-1232.

Lee JW; Hua FJ; Lee DS. 2001. Thermoreversible gelation of biodegradable poly (ε caprolactone) and poly (ethylene glycol) multiblock copolymers in aqueous solutions. J. Controlled Release. 73: 315-327.

Levin RL; Cravalho EG; Huggins CG. 1976. A membrane model describing the effect of temperature on the water conductivity of erythrocyte membranes at subzero temperatures. Cryobiology. 13:415-429.

Lendeckel S; Jodicke A; Christophis P; Heidinger K; Wolff J; Fraser JK; Hedrick MH; Berthold L; Howaldt HP. 2004. Autologous stem cells (adipose) and fibrin glue used to treat widespread traumatic calvarial defects: case report. J Craniomaxillofac Surg. 32(6): 370-373.

Li L; Wang Q; Xu Y. 2003. Thermoreversible Association and Gelation of Methylcellulose in Aqueous Solutions. Nihon Reoroji Gakkaishi(Journal of the Society of Rheology, Japan). 31(5):287-296.

Li Y; Lu RH; Luo GF; Pang WJ; Yang GS. 2006. Effects of different cryoprotectants on the viability and biological characteristics of porcine preadipocyte. Cryobiology, 53(2):240-247.

Liang L; Feng X; Rieke PC; Fryxell GE. 1998. Reversible Surface Properties of Glass Plate and Capillary Tube Grafted by Photopolymerization of N-Isopropylacrylamide. Macromolecules. 31: 7845-7850.

Lincz LF. 1998. Deciphering the apoptotic pathway: all roads lead to death. Immunol Cell Biol. 76(1): 1-19.

Lovelock JE. 1953. Haemolysis of human red blood cells by freezing and thawing, Biochim. Biophys. Acta. 10: 414–426.

Lovelock JE. 1954. The protective action of neutral solutes against haemolysis by freezing and thawing. Biochem. J. 56: 265–270.

Lucke B and McCutcheon M. 1932. The living cell as an osmotic system and its permeability to water. Physiol Rev. 12: 68–139.

Macosko CW. 1994. Rheology: Principles, Measurements and Applications, New York: VCH Publishers.

Madden PW; Taylor MJ; Hunt CJ; Pegg DE. 1993. The Effect of Polyvinylpyrrolidone and the Cooling Rate during Corneal Cryopreservation. Cryobiology. 30: 135-157.

Masters JR. 2002. HeLa cells 50 years on: the good, the bad and the ugly. Nat Rev Cancer. 2(4): 315-319.

Matsuda N. TSMYTO. 2007. Tissue Engineering Based on Cell Sheet Technology. Advanced Materials. 19(20): 3089-3099.

Maritz JS; Stanley ER; Yeo GF; Metcalf D. 1972. A model of haemopoietic cell colony formation. Biometrics. 28(3): 801-811.

Martin I; Wendt D; Heberer M. 2004. The role of bioreactors in tissue engineering. Trends Biotechnol. 22(2): 80-86.

Mathew A; Baust JG; Van Buskirk RG. 1997. Optimization of HypoThermosolt for the hypothermic storage of cardiomyocytes—Addition of EDTA. In Vitro Toxicol. 10(4): 407–415.

Mazur P. 1960. Physical factors implicated in the death of microorganisms at subzero temperatures. Ann N Y Acad Sci. 85:610-629.

Mazur P. 1963. Kinetics of water loss from cells at subzero temperatures and the likelihood of intracellular freezing. J Gen Physiol 47:347–369.

Mazur P. 1970. Cryobiology: the freezing of biological systems, Science. 168: 939–949.

Mazur P; Leibo SP; Chu EHY. 1972. A two-factor hypothesis of freezing injury. Exp. Cell Res.71: 345–355.

Mazur P. 1984. Freezing of living cells: Mechanisms and implications. Am J of Physiol. 247: C125-C142.

Mazur P. 1990. Equilibrium, quasi-equilibrium, and nonequilibrium freezing of mammalian embryos. Cell Biophys. 17:53-92.

McGrath JJ; Cravalho EG; Huggins CE. 1975. An experimental comparison of intracellular ice formation and freeze–thaw survival of HeLa S-3 cells. Cryobiology. 12: 540–550

McGrath JJ. 1988. Membrane transport properties. In: McGrath JJ, Diller KR, eds. Low Temperature Biotechnology: Emerging Applications and Engineering Contributions. BED-Vol. 10, HTD-Vol. 98; ASME Press. p 273–330.

Meinel L; Karageorgiou V; Fajardo R; Snyder B; Shinde-Patil V; Zichner L; Kaplan D; Langer R; Vunjak-Novakovic G. 2004. Bone tissue engineering using human mesenchymal stem cells: effects of scaffold material and medium flow. Ann Biomed Eng. 32(1): 112-22.

Merten OW; Petres S; Couve E. 1995. A simple serum-free freezing medium for serum-free cultured cells. . Biologicals. 23(2): 185.

Meryman HT. 1966. Review of biological freezing, In: Cryobiology; Meryman, H.T., Eds.; Academic Press: New York.

Michael JS; Joyce A; Shunping W; Elizabeth MB; John WL; Peter JD; Paul DB; George RH; John DG. 1998. Derivation of pluripotent stem cells from cultured human primordial germ cells. Devel. Biol. 95: 13726-13731.

Milosevic J; Storch A; Schwarz J. 2005. Cryopreservation does not affect proliferation and multipotency of murine neural precursor cells. Stem Cells. 23(5): 681-688.

Mizuno H; Zuk PA; Zhu M; Lorenz HP; Benhaim P; Hedrick MH. 2001. Myogenic differentiation of human processed lipoaspirate cells. Plastic Reconstr Surg. 109: 199–209

Moffat RJ. 1985. Planning experimental programs-Lecture notes. Stanford Univ. Stanford, CA.

Montgomery DC and Runger GC. 1994. Applied Statistics and Probability for Engineers. John Wiley and Sons.

Moore DS and McCabe GP. 1993. Introduction to the practice of the statistics. Freeman, New York.

Nair CN. 1981. Monovalent Cation Metabolism and Cytopathic Effects ofPoliovirus-Infected HeLa Cells. Journal of Virology. 37(1): 268-273.

Nash T. 1966. Chemical constitution and physical properties of compounds able to protect living cells against damage due to freezing and thawing. In: Meryman HT, eds. Cryobiology. Academic Press, Inc., New York. p 179-211.

Nishida K; Yamato M; Hayashida Y; Watanabe K; Maeda N; Watanabe H, et al. 2004. Functional bioengineered corneal epithelial sheet grafts from corneal stem cells expanded ex vivo on a temperature-responsive cell culture surface. Transplantation. 77(3): 379–85.

Oegema TR; Deloria LB; Fedewa M; Bischof JC; Lewis JL. 1999. “A simple cryopreservation method for the maintenance of cell viability and mechanical integrity of cultured cartilage analog”, Cryobiology. 40: 370-375.

Okano T; Yamada N; Okuhara M; Sakai H; Sakurai Y. 1995. Mechanism of cell detachment from temperature-modulated, hydrophilic-hydrophobic polymer surfaces. Biomaterials. 16(4): 297-303.

Okano T; Yamada N; Sakai H; Sakurai Y. 1993. A novel recovery system for cultured cells using plasma-treated polystyrene dishes grafted with poly(iV-isopropylacrylamide). J Biomed Mater Res. 27: 1243-1251.

Pan YV; Wesley RA; Luginbuhl R; Denton DD; Ratner BD. 2001. Plasma polymerized N-isopropylacrylamide: synthesis and characterization of a smart thermally responsive coating. Biomacromolecules. 2(1): 32-36.

Park YS; Ito Y; Imanishi Y. 1998. Permeation control through porous membranes immobilized with thermosensitive polymer. Langmuir 14: 910-914.

Pazhayannur P and Bischof JC. 1997. Measurement and Simulation of Water Transport During Freezing in Mammalian Liver Tissue. ASME Journal of Biomechanical Engineering. 119 (3), 269-277.

Pederson AW; Ruberti JW; Messersmith PB. 2003. Thermal assembly of a biomimetic mineral/collagen composite. Biomaterials. 24(26): 4881-90.

Pena FJ; Johannisson A; Wallgren M; Rodriguez-Martinez H. 2003. Assessment of fresh and frozen-thawed boar semen using an Annexin-V assay: a new method of evaluating sperm membrane integrity. Theriogenology. 60(4): 677-89.

Pissuwan D; Valenzuela SM; Cortie MB. 2006. Therapeutic possibilities of plasmonically heated gold nanoparticles. Trends Biotechnol. 24: 62-67.

Pittenger MF; Mackay AM; Beck SC; Jaiswal RK; Douglas R; Mosca JD; Moorman MA; Simonetti DW; Craig S; Marshak DR. 1999. Multilineage potential of adult human mesenchymal stem cells. Science. 284: 143-147.

Polge C; Smith AU; A.S P. 1949. Revival of Spermatozoa After vitrification and dehydration at low temperatures. Nature. 164: 666.

Puelacher WC; Vacanti JP; Ferraro NF; Schloo B; Vacanti CA. 1996. Femoral shaft reconstruction using tissue-engineered growth of bone. Int J Oral Maxillofac Surg. 25(3): 223–8.

Rao KP and Joseph T. 1988. Collagen graft copolymers and their biomedical applications. In: Nimni ME, editor. Collagen, vol. III. Biotechnology.Boca Raton, FL: CRC Press Inc :63-86.

Reubinoff BE; Pera MF; Vajta G; Trounson AO. 2001. Effective cryopreservation of human embryonic stem cells by the open pulled straw vitrification method. Hum Reprod. 16(10): 2187-2194.

Reuss R; Ludwig J; Shirakashi R; Ehrhart1 F; Zimmermann H; Schneider S; Weber MM; Zimmermann U; Schneider H; Sukhorukov VL. 2004. Intracellular delivery of carbohydrates into mammalian cells through swelling-activated pathways J. Membrane Biol. 200: 67–81.

Reuther T; Kettmann C; Scheer M; Kochel M; Iida S; Kubler AC. 2006. Cryopreservation of osteoblast-like cells: viability and differentiation with replacement of fetal bovine serum in vitro. Cells Tissues Organs. 183(1): 32-40.

Robertson EJ. Embryo derived stem cell lines. In: Tetracarcinomas and embryonic stem cells: a practical approach; Robertson, E. J., Eds.; IRL press: Oxford, 1987; pp. 71-112.

Rosenbluth MJ; Lam WA; Fletcher DA. 2006. Force microscopy of nonadherent cells: a comparison of leukemia cell deformability. Biophys J. 90(8): 2994-3003.

Rudolph AS and Crowe JH. 1985. Membrane stabilization during freezing: the role of two natural cryoprotectants, trehalose and proline. Cryobiology 22: 367–377.

Safford KM; Hicok KC; Safford SD; Halvorsen YD; Wilkison WO; Gimble JM; Rice HE. 2002. Neurogenic differentiation of murine and human adipose-derived stromal cells. Biochem. Biophys. Res. Commun. 294(2): 371-379.

Safford KM; Safford SD; Gimble JM; Shetty AK; Rice HE. 2004. Characterization of neuronal/glial differentiation of murine adipose-derived adult stromal cells. Exp Neurol. 187(2): 319-328.

Sampathkumar SG; Li V; Jones MB; Sun Z; Yarema KJ. 2006. Metabolic installation of thiols into sialic acid modulates adhesion and stem cell biology. Nat. Chem. Biol. 2: 149-152.

Sanchez-Ramos J; Song S; Cardozo-Pelaez F; Hazzi C; Stedeford T; Willing A; Freeman TB; SaportaS; Janssen W; Patel N; Cooper DR; Sanberg PR. 2000. Adult bone marrow stromal cells differentiate into neural cells in vitro. Exp Neurol. 164: 247-256.

Sarkar N. 1979. Thermal Gelation Properties of Methyl and Hydroxypropyl Methylcellulos. Journal of Applied Polymer Science. 24: 1073-1087.

Sarkar N and Walker LC. 1995. Hydration-dehydration properties of methylcellulose and hydroxypropylmethylcellulose. Carbohydrate polymers. 27(3): 177-185.

Sasaki M; Kato Y; Yamada H; Terada S. 2005. Development of a novel serum-free freezing medium for mammalian cells using the silk protein sericin. Biotechnol Appl Biochem. 42(Pt 2): 183-188.

Sedzik J. 1995. Regression analysis of factorially designed trials—A logical approach to protein crystallization. Biochim. Biophys. Acta. 1251(2): 177-185.

Sen A; Lea-Currie YR; Sujkowska D; Franklin DM; Wilkison WO; Halvorsen YD; Gimble JM. 2001. Adipogenic potential of human adipose derived stromal cells from multiple donors is heterogeneous. J Cell Biochem. 81(2): 312-319.

Shim H; Gutierrez-Adan A; Chen LR; BonDurant RH; Behboodi E; Anderson GB. 1997. Isolation of pluripotent stem cells from cultured porcine primordial germ cells. Biol. Reprod. 57(5): 1089-1095.

Shimizu T; Sekine H; Yang J; Isoi Y; Yamato M; Kikuchi A; Kobayashi E; Okano T. 2006. Polysurgery of cell sheet grafts overcomes diffusion limits to produce thick, vascularized myocardial tissues. FASEB J. 20(6): 708-710.

Shimizu T; Yamato M; Isoi Y; Akutsu T; Setomaru T; Abe K; Kikuchi A; Umezu M; Okano T. 2002. Fabrication of Pulsatile Cardiac Tissue Grafts Using a Novel 3-Dimensional Cell Sheet Manipulation Technique and Temperature-Responsive Cell Culture Surfaces Circ. Res. 90. p. e40.

Shinoka T ; Breuer CK ; Tanel RE ; Zund G; Miura T ; Ma PX, et al. 1995. Tissue engineering heart valves: valve leaflet replacement study in a lamb model. Ann Thorac Surg. 60(6 Suppl): S513–6.

Shiroyanagi Y; Yamato M; Yamazaki Y; Toma H; Okano T. 2004. Urothelium regeneration using viable cultured urothelial cell sheets grafted on demucosalized gastric flaps. BJU Int. 93(7): 1069–75.

Sikavitsas VI; Bancroft GN; Mikos AG. 2002. Formation of three-dimensional cell/polymer constructs for bone tissue engineering in a spinner flask and a rotating wall vessel bioreactor. J Biomed Mater Res. 62(1): 136-48.

Sistino JJ. 2003. Bioreactors for tissue engineering--a new role for perfusionists? J Extra Corpor Technol. 35(3): 200-2.

Sittinger M; Reitzel D; Dauner M; Hierlemann H; Hammer C; Kastenbauer E; Planck H; Burmester GR; Bujia J. 1996. Resorbable polyesters in cartilage engineering: affinity and biocompatibility of polymer fiber structures to chondrocytes. J Biomed Mater Res. 33(2): 57-63

Smith DJ; Schulte M; Bischof JC. 1998. The effect of dimethylsulfoxide on the water transport response of rat hepatocytes during freezing. ASME J Biomech Eng. 120:549-558.

Smith DJ; Fahssi WM; Swanlund DJ; Bischof JC. 1999. A parametric study of freezing injury in AT-1 rat prostate tumor cells. Cryobiology. 39(1): 13-28.

Smith AL and Smith HV. 1989. A comparison of fluorescein diacetate and propidium iodide staining and in vitro excystation for determining Giardia intestinalis cyst viability. Parasitology. 99:329-331..

Sputtek A and Sputtek R, editors. 2004. Life in the Frozen State. Boca Raton: CRC Press. 483-504 p.

Stevenson DJ; Morgan C; Goldie E; Connel G; Grant MH. 2004. Cryopreservation of viable hepatocyte monolayers in cryoprotectant media with high serum content:

metabolism of testosterone and kaempherol post-cryopreservation. Cryobiology. 49: 97-113.

Stiff PJ; Koester AR; Weidner MK; Dvorak K; Risher RI. 1987. Autologous bone marrow transplantation using unfractionated cells cryopreserved in dimethylsulfoxid e and hydroxyethyl starch without controlled-rate freezing. Blood. 70: 974–978.

Suzuki T; Boediono A; Takagi M; Saha S; Sumantri C. 1996. Fertilization and Development of Frozen-Thawed Germinal Vesicle Bovine Oocytes by a One-Step Dilution Method in Vitro. Cryobiology. 33(5): 515-524.

Tatsutani K; Rubinsky B; Onik G; Dahiya R. 1996. Effect of thermal variables on frozen human primary prostatic adenocarcinoma cells. Urology. 48(3): 441-447.

Tianhan W; Weijie Q; Shaoping Z; Yue LYL. 2007. Cross-Linking Of Collagen Gel For Making Tissue Engineering Scaffolds.

Thirumala S, Ferrer MS, Al-Jarrah A, Eilts BE, Paccamonti DL, Devireddy RV. 2003. Cryopreservation of canine spermatozoa: theoretical prediction of optimal cooling rates in the presence and absence of cryoprotective agents. Cryobiology. 47: 109-124.

Thirumala S; Campbell WT; Vicknair MR;, Tiersch TR; Devireddy RV. 2006. Freezing response and optimal cooling rates for cryopreserving sperm cells of striped bass, Morone saxatilis. Theriogenology. 66: 964-973.

Thirumala S and Devireddy RV. 2005. A simplified procedure to determine the optimal rate of freezing biological systems. ASME Journal of Biomechanical Engineering. 127: 295-300.

Thirumala S; Gimble JM; Devireddy RV. 2005. Transport phenomena during Freezing of adipose tissue derived adult stem cells. Biotechnology & Bioengineering. 92: 372-383.

Thirumala S; Forman JM; Monroe WT; Devireddy RV. 2007. Freezing and post-thaw apoptotic behaviour of cells in the presence of palmitoyl nanogold particles. Nanotechnology. (19): 195104.

Thirumala s; Huang C; Dong Q; Tiersch TR and Devireddy RV. 2005. A theoretically estimated cooling rate for the cryopreservation of sperm cells from a live bearing fish, the green swordtail Xiphophorus Helleri, Theriogenology, 63:2395-2415

Thomson J A and Odorico J S. 2000. Human embryonic stem cell and germ cell lines. Trends Biotech. 18: 59-63.

Thomson JA; Joseph IE; Sander SS; Michelle AW; Jennifer JS; Vivienne SM; Jeffery MJ. 1998. Embryonic stem cell lines derived from human blastocysts. Science. 282: 1145-1147.

Toner M. 1993. Nucleation of ice crystals in biological cells. In: Steponkus PL, Ed. Advances in Low-temperature Biology, London; JAI Press. p. 1–52.

Turner N; Armitage M; Butler R; Ireland G. 2004. An in vitro model to evaluate cell adhesion to metals used in implantation shows significant differences between palladium and gold or platinum. Cell Biol Int. 28(7): 541-547.

Vacanti JP. Beyond transplantation. 1998. Third annual Samuel Jason Mixter lecture. Arch Surg. 123(5): 545–9.

Vacanti CA and Vacanti JP. 2000. The science of tissue engineering. Orthop Clin North Am 2000;31(3):351–6.

Vacanti CA; Langer R; Schloo B; Vacanti JP. 1991. Synthetic polymers seeded with chondrocytes provide a template for new cartilage formation. Plast Reconstr Surg. 88(5): 753–9.

van der Valk J; Mellor D; Brands R; Fischer R; Gruber F; Gstraunthaler G; Hellebrekers L; Hyllner J; Jonker FH; Prieto P; Thalen M; Baumans V. 2004. The humane collection of fetal bovine serum and possibilities for serum-free cell and tissue culture. Toxicol In Vitro. 18(1): 1-12.

Visaria RK; Griffin RJ; Williams BW; Ebbini ES; Paciotti GF; Song CW; Bischof JC. 2006. Enhancement of tumor thermal therapy using gold nanoparticle-assisted tumor necrosis factor-alpha delivery. Mol Cancer Ther, 5(4):1014-1020.

Vogel G. 2000. Can old cells learn new tricks? Science. 287: 1418–1419.

von Recum H; Okano T; Wan Kim S. 1998. Growth factor release from thermally reversible tissue culture substrates. J of Controlled Release. 55: 121-130.

Wakitaniv S; Takaoka K; Hattori T; Miyazawa N; Iwanaga T; Takeda S; Watanabe TK; Tanigami A. 2003. Embryonic stem cells injected into the mouse knee joint form teratomas and subsequently destroy the joint. Rheumatology. 42: 162-165.

Walsh JR. “Modeling and design of algal cryopreservation protocols”, Ph.D. Dissertation, The University of Texas at Austin, Austin, Texas

Wang F. 2006. Culture of animal cells: A manual of basic technique, fifth edition: by R. Ian Freshney John Wiley and Sons, Inc., Hoboken, New Jersey, 2005 672 pages, $79.95. In Vitro Cellular & Developmental Biology - Animal 42:169-169.

Wang Q and Li L. 2005. Effects of molecular weight on thermoreversible gelation and gel elasticity of methylcellulose in aqueous solution. Carbohydrate Polymers 62(3):232–238.

Warkentin PI; Jackson JD; Letheby B; Kessinger A. 1994. Effective cryopreservation of cytokine-mobil ized autologous peripheral blood stem cells using non-controlled rate freezing. Prog. Clin. Biol. Res. 389: 643– 647.

Wehner F; Olsen H; Tinel H; Kinne-Saffran E; Kinne RK. 2003. Cell volume regulation: osmolytes, osmolyte transport, and signal transduction. Rev Physiol Biochem Pharmacol, 148:1-80.

Williams RJ. 1983. The surface activity of PVP and other polymers and their antihemolytic capacity. Cryobiology. 20(5): 521-526.

Wickham MQ; Erickson GR; Gimble JM; Vail TP; Guilak F. 2003. Multipotent stromal cells derived from the infrapatellar fat pad of the knee. Clin Orthop. 412: 196-212.

Woodbury D; Schwarz EJ; Prockop DJ; Black IB. 2000. Adult rat and human bone marrow stromal cells differentiate into neurons. J Neurosci Res. 61: 364-370.

Xu XM; Song YM; Ping QN; Wang Y; Liu XY. 2006. Effect of ionic strength on the temperature-dependent behavior of hydroxypropyl methylcellulose solution and matrix tablet. Journal of Applied Polymer Science. 102(4): 4066-4074.

Xu Y; Wang C; Tam KC; Li L. 2004. Salt-Assisted and Salt-Suppressed Sol-Gel Transitions of Methylcellulose in Water. Langmuir. 20(3): 646-652.

Yamada N; Okano T; Sakai H; Karikusa F; Sawasaki Y; Sakurai Y. 1990. Thermo-responsive polymeric surfaces; control of attachment and detachment of cultured cells. Makromol Chem Rapid Commun. 11: 571–6.

Yamato M; Okuhara M; Karikusa F; Kikuchi A; Sakurai Y; Okano T. 1999. Signal transduction and cytoskeletal reorganization are required for cell detachment from cell culture surfaces grafted with a temperature-responsive polymer. J Biomed Mater Res. 44(1): 44-52

Yamada N; Okano T; Sakai H; Karikusa F; Sawasaki Y; Sakurai Y. 1990. Thermo-responsive polymeric surfaces: Control of attachment and detachment of cultured cells. Makromol Chem, Rapid Commun. 11: 571-576.

Yamato M; Utsumi M; Kushida A; Konno C; Kikuchi A; OkanoT. 2001. Thermo-responsive culture dishes allowthe intact harvest of multilayered keratinocyte sheets without dispase by reducing temperature. Tissue Eng. 7(4): 473–80.

Yang L; Li S; Hatch H; Ahrens K; Cornelius JG; Petersen BE; Peck AB. 2002. In vitro trans-differentiation of adult hepatic stem cells into pancreatic endocrine hormone-producing cells. Proc Natl Acad Sci U S A. 99: 8078-8083.

Yanga J; Yamatoa M; Shiizua T; Sekine H; Ohashi K; Kanzaki M; Ohki T; Nishidad K; Okano T. 2007. Reconstruction of functional tissues with cell sheet engineering. Biomaterials. 28(34) :5033-5043.

Yuan S and Diller KR. 2001. Study of freezing biological systems using optical differential scanning calorimeter. ASME Summer BED Conf Proc 50:117-118.

Yu TH; Liu J; Zhou YX. 2005. Selective freezing of target biological tissues after injection of solutions with specific thermal properties. Cryobiology. 50(2): 174-182.

Zuk PA; Zhu M; Mizuno H; Huang JI; Futrell WJ; Katz AJ; Benhaim P; Lorenz HP; Hedrick MH. 2001. Multi-lineage cells from human adipose tissue: implications for cell-based therapies. Tissue. Eng. 7: 211-226.

Zuk PA; Zhu M; Ashjian P; De Ugarte DA; Huang JI; Mizuno H; Alfonso ZC; John K; Fraser JK; Benhaim P; Hedrick MH. 2002. Human adipose tissue as a source of multipotent stem cells. Mol Biol Cell. 13: 4279-4295.

Vogel, G. Can old cells learn new tricks? Science 2000, 287, 1418–1419.

APPENDIX: PERMISSIONS TO USE PUBLISHED ARTICLES

Permission 1:

Permissions/IOPP
Sent by: Jill Membrey

08/04/2009 09:29

To Sreedhar Thirumala <sthiru1@tigers.lsu.edu>
cc
bcc
Subject Re: Permission to the reprint of article

Sreedhar Thirumala <sthiru1@tigers.lsu.edu>

Sreedhar Thirumala
<sthiru1@tigers.lsu.edu>
Sent by:
sreedhar1010@gmail.com

05/04/2009 19:39

To permissions@iop.org
cc
Subject Permission to the reprint of article

Dear Sir/Madam,

I am writing to request permission to reprint the following IOP Journal article that I intend to include as a part of my PhD dissertation. I am the first author and I will include an appropriate credit line referencing to the original article.

S. Thirumala, J.M Forman, W.T. Monroe and R.V. Devireddy. Freezing and Post-Thaw Apoptotic Behavior of Cells in The Presence of Palmitoyl Nanogold Particles. Nanotechnology. 18: 195104 (2007).

.

Thank you.

Sreedhar Thirumala
PhD Student
Dept of Mechanical Engineering
Louisiana State University, LA
http://me.lsu.edu/~devireddy/Bioheatlab/sreedhar.html

PERMISSION TO REPRODUCE AS REQUESTED
IS GIVEN PROVIDED THAT:

~~(a) the consent of the author(s) is obtained.~~
(b) the source of the material including author/editor, title, date and publisher is acknowledged.*

IOP Publishing Ltd
Dirac House
Temple Back
BRISTOL
BS1 6BE

8/4/09
Date

Rights & Permissions

*Please include the IOP Copyright line, mention the journal's homepage at:

www.iop.org/journals/nano

and provide a link back to the article's abstract on our website from the electronic version of your thesis (if applicable).

Thank you.

Permission 2

Re: ASME PUBLICATIONS PERMISSION REQUEST FORM SUBMISSION

Beth Darchi <DarchiB@asme.org> **Mon, Apr 6, 2009 at 11:46 AM**
To: sreedhar1010@gmail.com

Dear Mr. Thirumala:
It is our pleasure to grant you permission to use ASME paper "Cellular Response of Adipose Derived Passage-4 Adult Stem Cells to Freezing Stress," by R.V. Devireddy, S. Thirumala and J.M. Gimble, Journal of Biomechanical Engineering, Vol. 127, 2005, cited in your letter for inclusion in a Doctoral Thesis entitled Cryopreservation of Adult Stem Cells (ASCs) in Suspension and Multi-Dimensional Cell Sheets to be published by Louisiana State University.

As is customary, we ask that you ensure full acknowledgment of this material, the author(s), source and ASME as original publisher on all printed copies being distributed.
Many thanks for your interest in ASME publications.

Sincerely,
Beth Darchi
Permissions & Copyrights
ASME, 3 Park Avenue
New York, NY 10016
T: 212-591-7700
F: 212-591-7841
E: darchib@asme.org

>>> <webmaster@asme.org> 4/5/2009 3:21 PM >>>

ASME PUBLICATIONS PERMISSION REQUEST FORM HAS BEEN SUBMITTED:

ASME Publication Title: Journal of Biomechanical Engineering
Complete List of Authors: R.V. Devireddy, S. Thirumala and J.M. Gimble
Paper Title (Conference/Journal): Cellular Response of Adipose Derived Passage-4 Adult Stem Cells to Freezing Stress
Paper Number (Conference):
Volume Number (Journal): 127
Page(s) in the publication of
the permission request:
Year of Publication: 2005
I would like to... Republish in a Doctoral Thesis
Portion to be used: Entire Article
List Figure Numbers: 0
List Table Numbers: 0
Number of Copies:
Usage: Both
Title of outside publication: Cryopreservation of Adult Stem Cells (ASCs) in Suspension and Multi-Dimensional Cell Sheets
Publisher: Louisiana State University
Comments: I need to submit the permission letter to graduate school by 17th April 2009. It would be glad if you can provide permission before April 17th.
Author: yes

First Name: Sreedhar
Last Name: Thirumala
Address Line 1: 2220 Patrick F Taylor Hall
Address Line 2: Louisiana State University
City: Baton Rouge
State: LA
Zip:
Phone: 225-223-2583
Fax:
Email: sreedhar1010@gmail.com

VITA

Sreedhar Thirumala was born in Amerchintha, AP-India. He received his Bachelor of Technology from Jawaharlal Nehru Technological University, AP, India, in mechanical engineering in 2000. Upon completion, he worked in industry for 2 years in India. He moved to United States in 2002 to pursue a masters' degree in the Department of Mechanical Engineering at Louisiana State University, Louisiana. After completing masters' degree in 2004 he then joined in doctoral program in the department and started working at Stem Cell Laboratory, Pennington Biomedical Research Center, Louisiana, for his doctoral research. He has been awarded with prestigious Economic Development Assistantship (EDA) for 2004-2007 and Dissertation Fellowship for 2007-2008. He was prized with Outstanding Research Assistant Award in the Department of Mechanical Engineering for 2008. He is the candidate for degree of Doctor of Philosophy (PhD) in mechanical engineering to be awarded at the commencement of SPRING 2009. He is looking forward to starting his career in industry and may come back to academia in the distant future.